

UNIVERSIDADE FEDERAL DO RIO GRANDE DO SUL
INSTITUTO DE QUÍMICA
PROGRAMA DE PÓS-GRADUAÇÃO EM QUÍMICA

ELISABETH CUERVO LUMBAQUE

**Degradation of pharmaceuticals in hospital wastewater by solar
photo-Fenton processes**

Thesis presented as a partial requirement for the
obtaining a Doctor of Chemistry degree

Prof. Dr. Carla Sirtori
Advisor

Prof. Dr. Elaine R. L. Tiburtius
Co-advisor

Porto Alegre, November 2020

I believe in social equality, where women and men have the same rights and opportunities in political, economic, social, and environmental decision making.

This is the result of teamwork, support, trust, and friendship.

Gratitude family, friends, and universe!

THESIS FRAMEWORK



The present PhD Thesis, titled “Degradation of pharmaceuticals in hospital wastewater by solar photo-Fenton processes”, was been developed in the *Universidade Federal do Rio Grande do Sul* (Porto Alegre, Brazil) between August 2016 and October, 2020.

The author, MSc. Elisabeth Cuervo Lumbaque, is extremely grateful to CAPES (Finance Code 001) and CNPq for her PhD. research grant (*Processo*: 158197/2019-4). She would additionally like to express her indebtedness to HCPA (*Hospital de Clínicas de Porto Alegre*) for the hospital wastewater samples in addition to the support of their workers (engineers and maintenance personnel). This thesis was carried out within the planned activities of the “Universal project - CNPq” (*Processo*: 403051/2016-9) and, for this reason, we are grateful to CNPq for the public funding obtained.

The PhD candidate held a doctoral internship at the Laboratory of Separation and Reaction Engineering - Laboratory of Catalysis and Materials (LSRE-LCM) at Faculty of Engineering of the University of Port (Portugal) between May-July 2019 under supervision of Prof. Dr. Vitor J.P. Vilar. She was granted a scholarship by ELAP in the University of Manitoba (Canada) in which she engaged in research activities in the Environmental Engineering Department headed by Dr. Qiuyan Yuan (January 2nd to June 12th, 2020).

This thesis is the product of the teamwork of all members of the GMAPs, a research group headed by Dr. Carla Sirtori, in addition to GDMIT group collaboration led by Dr. Elaine R. L. Tiburtius and Dr. Sérgio Toshio Fujiwara (R. I. P) along with assistance from different national and international collaborations.

ABSTRACT

The presence of pharmaceuticals in wastewater represents a serious environmental issue that can contribute toward sanitary and health problems. One of the main points behind this matter, is the low efficiency of degradation in conventional wastewater treatment plants (WWTP), or the direct discharge of untreated effluents into water bodies. To overcome this concern, Advanced Oxidation Processes (AOPs) have been widely used due to their generation of highly reactive hydroxyl radicals (HO^\bullet), which oxidize the abundant organic contents present in wastewaters. Within AOPs, the Fenton process is widely recognized for its versatility, as there are different ways to produce HO^\bullet , facilitating compliance with the specific treatment requirements. The Fenton process is based on the use of iron and hydrogen peroxide for the production of HO^\bullet and other radical oxygen species. This process is of particular interest, as sunlight can be used to improve its efficiency in removing emerging pollutants. Despite this, more research is still needed for its application in large scale wastewater treatment. This study was subsequently developed to evaluate different operational strategies of solar photo-Fenton to remove pharmaceuticals in hospital wastewater.

To achieve this goal, the solar photo-Fenton processes were studied using Fe^0 , $\text{Fe}^{2+/3+}$ -alginate and Fe^{3+} :EDDS under optimized experimental conditions. In addition, analytical monitoring of treatment processes, identification of transformation products (TPs) using LC-QTOF MS, coupled with the use of a purpose-designed database and toxicological/biodegradable predictions using (Q)SAR tools were performed in this research.

A batch reactor (1L) and a *raceway pond* reactor (10 L) made with low-cost materials were operated at pH close to neutrality. Additionally, three types of wastewater were worked on: distilled water (DW), simulated wastewater (SWW) and raw hospital wastewater (RHWW) fortified with a mixture of pharmaceuticals (Dipyron-DIP, Diazepam-DZP, Fluoxetine-FXT, Furosemide-FRS, Gemfibrozil-GFZ, Nimesulide-NMD and Progesterone-PRG) as a model of micropollutants with different initial concentrations ($500 \mu\text{g L}^{-1}$ and $50 \mu\text{g L}^{-1}$), then treated by the solar processes mentioned above. The experiments being carried out on sunny days at noon, the measured solar UV radiation was used to calculate t_{30W} , which allows the comparison of solar experiments carried out on different days, months and seasons throughout the year.

The systems with Fe^0 and Fe^{3+} :EDDS showed rapid degradation of the pharmaceuticals in a reaction time of less than 60 minutes. Fe^{3+} immobilized in alginate was the most efficient strategy for a constant supply of iron into the solution with a consecutive reuse capacity of 3 times. The total consumption of H_2O_2 was observed in SWW and RHW for all systems, and the final concentrations of dissolved iron are in accordance with the maximum level allowed by Brazilian legislation ($<15 \text{ mg L}^{-1}$).

The *raceway pond* reactor was used with Fe^{3+} :EDDS on a larger scale (10L), with the results demonstrating the best efficacy in Fe^{3+} :EDDS (1:2) for the degradation of pharmaceuticals within a short time-frame. Moreover, a more specific study of the TPs generated and degradation pathway proposals, using different proportions of iron and complexing agent, was performed.

Furthermore, in an additional study, the use of an App (PhotoMetrix PRO[®]) for the quantification of H_2O_2 and Fe species, *in loco*, was successfully validated.

Finally, the use of different operational strategies of solar photo-Fenton proved to be efficient in the removal of pharmaceuticals and, in some cases, also that of their transformation products at circumneutral pH in simulated and hospital wastewater. In most cases, during the solar treatments, TPs showed high to moderate toxicity and persistence, but throughout the process(es), these TPs are converted to simpler and less harmful structures. At the same time, the treatments tested presented advantages and disadvantages, such as environmental or economic issues related to the reagents used and the TPs generated, among others. Nevertheless, this research highlights the need for further studies in the area of wastewater treatment using sunlight and real wastewater matrices.

Keywords: hospital wastewater, pharmaceuticals, solar photo-Fenton, transformation products, and (Q)SAR tools.

RESUMO

A presença de fármacos em águas residuais representa um grave problema ambiental que pode contribuir como um dos fatores de problemas sanitários e de saúde pública. Um dos principais fatores, além da frequência dos fármacos no meio ambiente, é a baixa eficiência de degradação destes em sistemas de tratamento convencionalmente empregados para águas residuais. Para superar esse problema, muitos estudos têm focado sua atenção no uso dos Processos Avançados de Oxidação (PAOs) para alcançar a oxidação de diferentes microcontaminantes mediante a geração, majoritariamente, de radicais hidroxila (HO^\bullet), os quais são espécies altamente reativas. Dentro dos PAOs, o processo Fenton é amplamente reconhecido por sua versatilidade, pois existem diferentes formas de produção de HO^\bullet , facilitando o cumprimento dos requisitos específicos de tratamento. O processo Fenton é baseado na utilização de ferro e peróxido de hidrogênio para a produção de HO^\bullet e outras espécies de oxigênio radicais. Este processo é de particularmente interessante, pois a luz solar pode ser usada para melhorar sua eficiência na remoção de contaminantes emergentes. No entanto, ainda são necessários mais estudos para sua aplicação no tratamento de águas residuais em larga escala. Este estudo foi desenvolvido para avaliar diferentes estratégias operacionais do processo foto-Fenton solar para viabilizar a remoção de fármacos em matrizes como é o caso de efluentes hospitalares.

Para este fim, os processos foto-Fenton solares foram estudados usando Fe^0 , $\text{Fe}^{2+/3+}$ -alginato e Fe^{3+} :EDDS em condições experimentais otimizadas. Da mesma forma, o acompanhamento analítico dos processos, a identificação de produtos de transformação (TPs) mediante LC-QTOF MS e o uso de uma base de dados especialmente elaborada para essa finalidade acoplado com a predição toxicológica e da biodegradabilidade empregando ferramentas de análise de risco *in silico* ((Q)SAR) foram empregados nesta tese.

Um reator de batelada em escala de laboratório (1L) e um reator “*raceway pond*” (10 L) feito com materiais de baixo custo foram operados na maioria das experiências em pH próximo à neutralidade. Adicionalmente, foram avaliadas três matrizes aquosas: água destilada (DW), efluente simulado (SWW) e efluente hospitalar real (RHWW) fortificadas com uma mistura de fármacos (Dipirona-DIP, Diazepam-DZP, Fluoxetina-FXT, Furosemida-FRS, Genfibrozila-GFZ, Nimesulida-NMD e Progesterona-PRG),

como micropoluentes modelo, em diferentes concentrações iniciais ($500 \mu\text{g L}^{-1}$ e $50 \mu\text{g L}^{-1}$). Em seguida, tais soluções foram tratadas pelos processos destacados anteriormente.

Os experimentos foram realizados em dias de sol ao meio-dia, a radiação UV medida foi utilizada para calcular t_{30W} , a qual permite a comparação de experimentos solares realizados em diferentes dias, meses e estações ao longo do ano.

Os sistemas com Fe^0 e Fe^{3+} :EDDS apresentaram rápida degradação dos fármacos em um tempo de reação inferior a 60 minutos. Fe^{3+} imobilizado em alginato foi a estratégia mais eficiente para um fornecimento constante de ferro na solução com uma capacidade de reutilização consecutiva de 3 vezes. O consumo total do H_2O_2 foi atingido para matrizes como SWW e RHWW em todos os processos, e os níveis finais de ferro dissolvido estão em acordo com o nível máximo permitido pela legislação Brasileira ($< 15 \text{ mg L}^{-1}$).

O reator do tipo “*raceway pond*” foi utilizado com Fe^{3+} :EDDS em escala superior (10 L). Os resultados demonstram a eficácia do complexo de Fe^{3+} :EDDS (1:2) para a degradação de fármacos em um pequeno tempo de tratamento, bem como, um estudo mais específico dos TPs gerados usando diferentes proporções de ferro e agente complexante.

Adicionalmente, foi validado com sucesso o uso de um aplicativo (PhotoMetrix PRO) para a quantificação, *in loco*, de H_2O_2 e Fe.

Finalmente, as diferentes estratégias operacionais do foto-Fenton solar mostraram-se eficientes na remoção de fármacos e, em alguns casos, também para seus TPs empregando pH próximo à neutralidade, tanto em SWW quanto em RHWW. Na maioria dos casos, os TPs apresentaram toxicidade classificada como alta a moderada e persistência no ambiente. Porém, ao longo do(s) processo(s), tais TPs são convertidos a estruturas mais simples e menos nocivas. Ao mesmo tempo, os diferentes tipos de tratamentos testados apresentaram vantagens e desvantagens, como questões ambientais ou econômicas relacionadas aos reagentes utilizados e aos TPs gerados, dentre outros fatores. Por outro lado, ressalta-se a necessidade de estudos adicionais na área de tratamento de efluentes usando luz solar e matrizes reais.

Palavras-chave: efluente hospitalar, fármacos, foto-Fenton solar, produtos de transformação e (Q)SAR.

Table of Contents

CHAPTER 1: INTRODUCTION	10
1.1 Hospital wastewater treatment and its importance: a pharmaceutical approach	11
1.2 Legislation: regulatory framework	12
1.2.1 Brazilian legislation	13
1.3 Advanced Oxidation Processes and improvements for treatments of wastewaters	14
1.3.1 Fenton	15
1.3.2 Solar photo-Fenton	17
1.3.2.1 Fenton oxidation at circumneutral pH: iron complexes	19
1.3.3 Matrix effect	20
1.4 Database of transformation products	21
1.5 (Q)SAR models	23
CHAPTER 2: OBJECTIVES	26
CHAPTER 3: METHODOLOGY	29
3.1 Reagents, solutions and water matrices	30
3.2 Natural sunlight radiation	33
3.3 Photocatalytic reactors	34
3.3.1 Batch reactor	34
3.3.2 Homemade raceway pond using low-cost materials	35
3.4 General analytical methods	36
3.5 Kinetic studies	36
3.6 Transformation products generated by AOPs	37
3.7 (Q)SAR software programmes	38
CHAPTER 4: RESULT AND DISCUSSION	40
4.1 Solar photo-Fenton process	41
4.1.1 Solar photo-Fenton process: Zero Valent Iron (ZVI)	41
4.1.2 Solar photo-Fenton process: immobilized iron in alginate	87
4.1.3 Solar photo-Fenton process: Fe ³⁺ :EDDS	124
4.1.4 Homemade raceway pond reactor: pharmaceutical degradation, TPs identification and degradation pathways assessment	151
4.1.5 PhotoMetrix PRO®	196
CHAPTER 5: CONCLUSIONS AND FUTURES PERSPECTIVES	215

5.1 Final disposal of wastes	220
List of works developed during the PhD	221
Oral presentations in conferences	223
REFERENCES	225
ANNEXES	232



CHAPTER 1

In this Chapter, the environmental problem intended to be clarified throughout the PhD thesis is presented, relating it in terms of causes, consequences, and treatment of complex wastewaters, especially hospital effluents. Likewise, the identification of transformation products and quantitative structure–activity relationship ((Q)SAR) models for the estimation of toxicity and biodegradability are addressed.

We must share responsibility for meeting the problems like climate change, depletion of natural resources and expanding population that affect us all. To limit our concern to our own nation alone is out of date.

Dalai Lama



INTRODUCTION

1.1 Hospital wastewater treatment and its importance: a pharmaceutical approach

Nowadays, pharmaceuticals (PHCs) are located in different environmental matrices. Hospital wastewaters (RHWW) are one of the main sources of these micropollutants emissions¹. Generally, in a health center or hospital, RHWW are composed of the effluents from different services: kitchen, internal laundry, heating and cooling systems, laboratories, radiology departments, outpatients' departments, transfusion centers and wards. Due to the nature and quantity of the micropollutants, RHWW harbor active substances of medicines and their metabolites, chemicals, heavy metals, disinfectants, sterilizers, and radioactive markers. This wastewater has an extra supply of organic matter; it favors high Chemical Oxygen Demand (COD) associated with a medium or reduced Biochemical Oxygen Demand (BOD₅). Subsequently, conventionally used biological processes are not suitable for wastewater treatment of this type². In general, the wastewater treatment plant (WWTP) are not designed to remove complex compounds such as PHCs. Usually, WWTPs comprise a primary system of physic-chemical treatments and a secondary system of a biological reactor, it formed more frequently by active sludge. These conventional plants have a limited capacity to remove PHCs from urban wastewaters, since most of the compounds cannot be metabolized by microorganisms and may even inhibit the activity of the microorganisms or produce their bioaccumulation in the food chain³. Although some PHCs incoming WWTPs are removed in a low percentage (e.g. biodegradation or adsorption onto sludge), a considerable amount is still released into the environment¹.

Verlicchi et al.⁴ investigated the occurrence of 73 common PHCs from 12 different therapeutic classes of effluents from two hospitals (medium and large-sized) in conjunction with influents and effluents of the local municipal WWTP, which also receives and treats the wastewater from the larger hospital. The study revealed that PHCs are found in consistently higher concentrations in hospital than in urban wastewater,

particularly those commonly used PHCs such as analgesics and antibiotics. The characteristics of the hospital effluent seem to be influenced by the size of the structure and season (concentrations tended to be higher in winter than in summer). Furthermore, RHHW also play an important role in the introduction of pathogens into public wastewaters, particularly multi-resistant bacteria, which contribute to the spread of antibiotic resistance in the environment⁵.

PHCs are classified as one of the most important emerging concern groups due to i) the increase in life expectancy of the world population, ii) the substances not being completely metabolized by the human body, leading to the formation of metabolites conjugated to their native form⁵; iii) continuous introduction into the environment potentially affecting water quality and impacting drinking water supplies; iv) a lack of regulation (or pending regularization processes)³; v) effects in aquatic organisms⁶. At the same time, great progress in analytical detection techniques in recent years have increased PHCs and metabolite detection limits⁷. In this context, important advances in analytical techniques for monitoring of diverse environmental microcontaminants, such as PHCs and their transformation products (TPs) (present at trace and ultra-trace levels) can also be considered.

Current studies have detected more than 80 compounds with pharmacological activity in different aqueous matrices in concentrations from ng L^{-1} to $\mu\text{g L}^{-1}$ ^{5,8-10} with most of them presenting a relevant ecotoxicological potential. In this sense, the PHCs sold without prescriptions, such as analgesic and anti-inflammatory drugs are detected more frequently and in higher concentrations in the environment. Notwithstanding this, antibiotics are the most studied PHCs due to i) the possibility of bacterial resistance phenomena, and ii) low percentage of elimination in the WWTP¹¹.

1.2 Legislation: regulatory framework

Despite growing evidence regarding PHCs in the environment, more information is still needed to understand and evaluate certain PHCs as environmental concerns and fate risks¹². Nevertheless, it is important to emphasize that these micropollutants could limit the potential reuse of treated wastewater and pose a threat to public health and the environment¹³.

The United States Environmental Protection Agency (USEPA; <https://www.epa.gov>) has included six veterinary and human pharmaceuticals in their recent contaminant candidate list (CCL-4) together with other synthetic

hormones, disinfection by-products and pesticides. Similarly, in 2012, the European Commission proposed the setting of environmental quality standards for some pharmaceuticals of emerging concern: diclofenac, estrone (E1), 17- β -estradiol (E2) and 17- α -ethinylestradiol (EE2), clarithromycin, ciprofloxacin, erythromycin, azithromycin, and amoxicillin¹⁴. Nonetheless, most of the PHCs with toxicological evidence remain unregulated, although the European Union (EU), United States of America (USA), World Health Organization (WHO), UNESCO, among others, have shown great interest in mitigating the presence of PHCs in the environment.

This has resulted in several directives and frameworks such as European Directives 2013/39/EU, EU 2015/495, the Water Framework Directive (Commission Implementing Decision 2018/840) and an endocrine disruptor screening program (EDSP) (<https://www.epa.gov/endocrine-disruption/endocrine-disruptor-screening-program-edsp-overview>) by the USEPA.

Based on the precautionary principle, the European Union Water Framework Directive produces an updated list of priority substances every four years (2000/60/EC) and has identified compounds from pharmaceuticals to be potential pollutants. Additionally, NORMAN (Network of reference laboratories, research centers and related organizations for monitoring of emerging environmental substances) (<https://www.norman-network.com/nds/>) has developed a rational and holistic prioritization approach. These efforts clearly indicate that PHCs are an environmental threat for the future and consequently methods for their removal from the environment require immediate attention.

As a consequence, the WHO (https://www.who.int/water_sanitation_health/water-quality/en/) highlight the importance of the water safety plan approaches as the most effective means of considering risk assessment and risk management in the: i) prevention or minimization of contamination of source water contamination; ii) decrease of contamination through treatment processes, and iii) prevention of contamination during storage, distribution and handling of drinking-water.

1.2.1 Brazilian legislation

Through the National Environment Council (CONAMA), the Environmental Ministry is responsible for legal provisions that impact the environmental quality of water in Brazil. A series of resolutions (normally based on the environmental standards set by

USEPA) are established with mandatory nationwide compliance, to maintain the quality of water resources in the country. An important provision is CONAMA Resolution n. 357 of 2005¹⁵, updated in 2011 by CONAMA Resolution n. 430¹⁶ and CONAMA Resolution n. 396 of 2008¹⁷. These resolutions provide instruction on the classification of bodies of surface water and the respective environmental standards, in addition to establishing the conditions and standards for disposing of effluents, including those for direct or indirect human use.

These provisions define various physical and chemical parameters, organic and inorganic chemicals, algae, and microorganisms in monitoring water quality according to the classification of the respective body of water¹⁸. Brazil has the ordinance N° 5.472 of 2005¹⁹, which arose from the Stockholm Convention on Persistent Organic Pollutants, proposes to reduce and eliminate pollutants released by the population through public awareness and education, in addition to stimulating research, development and monitoring.

In 2011, the Ministry of Health published Ruling n. 2.914, the prevailing legislation that sets water quality standards for human consumption which are upheld by the Division of Environmental Health Surveillance. This Ruling sets standards for microorganisms, cyanotoxins, radioactive nucleotides, as well as various organic and inorganic chemical compounds such as pesticides, disinfectants, and disinfection by-products²⁰, but does not include pharmaceuticals or other potential endocrine disruptor microcontaminants.

In the Brazilian context, water pollution involves more than the legal provisions and standards, given important provisions in the country's existing legislation have still not been enforced satisfactorily¹⁸. According to the national sanitation information system 2017 report²¹, only 46% of collected sewage is treated before being dumped into water bodies⁸, which makes it more difficult to control and implement treatment systems for emerging contaminants.

1.3 Advanced Oxidation Processes and improvements for treatments of wastewaters

The low removal efficiency in WWTP could be attributed to many factors, such as the characteristics of the activated sludge (mixed liquor suspended solid and the microbial communities) and wastewater composition²². Considering the limitation of

conventional treatment processes for the total degradation of PHCs and their derivatives with high chemical stability and/or low biodegradability, studies that aim to evaluate the potential of employing new technologies, such as Advanced Oxidation Processes (AOPs) for the treatment of different wastewaters². AOPs operate at ambient temperature and pressure while generating radical oxygen species (ROS) for degradation of organic content, in which PHCs are just a part of that total organic content.

ROS are atoms or molecules containing at least one unpaired electron such as the hydroxyl radical (HO^{\bullet}), superoxide anion radical ($\text{O}_2^{\bullet-}$), hydroperoxyl radical (HO_2^{\bullet}) or alkoxy radical (RO^{\bullet}); the HO^{\bullet} radical has had the most attention in this area due to the strong standard oxidation potential [$E^0(\text{HO}^{\bullet}/\text{H}_2\text{O}) = +2.8 \text{ V NHE}$], high bimolecular reaction rate constants ($10^8\text{--}10^{11} \text{ M}^{-1} \text{ s}^{-1}$) and non-selective reactivity^{23,24}.

AOPs are classified according to the reactive phase (homogeneous and heterogeneous) or hydroxyl radical generation methods (chemical, electro-chemical, sono-chemical and photochemical)²⁵.

In this context photo-Fenton and their modifications have recently shown high efficiency of PHCs degradation in different wastewaters²⁶. In photo-Fenton process the degradation depends on the radiation wavelength (λ), compound molar absorption capacity (ϵ), and quantum yield (ϕ). The most widely used radiation for photolysis has a λ of 200–400 nm, i.e. in the ultraviolet spectrum region. Several studies have demonstrated that numerous PHCs can be photodegraded^{27–29}. Generally, these PHCs contain aromatic rings, heteroatoms, and other functional groups that allow absorption of solar radiation or produce reactions with photosensitizing species that induce their photodegradation in natural water. If compounds are not degraded by direct photolysis, they may be indirectly degraded by radical generation³.

1.3.1 Fenton

The Fenton reaction was discovered by H.J.H. Fenton in 1894. He reported that H_2O_2 could be activated by ferrous (Fe^{2+}) salts to oxidize tartaric acid. This reaction implies the oxidation of ferrous to ferric ions to decompose H_2O_2 into HO^{\bullet} and other transitory species (HO_2^{\bullet} and $\text{O}_2^{\bullet-}$) that can oxidize a wide range of organic compounds. The generated ferric ions can be reduced (slow reaction) with excess hydrogen peroxide to form again ferrous ion and more radicals²⁵. The classic Fenton process has traditionally been carried out at acid pH (between 2.5–3.0)³⁰.

The main reasons for the huge popularity and widespread applicability of Fenton oxidation processes are (i) ROS are generated at ambient pressure and temperature; (ii) easy implementation as a stand-alone or hybrid system, and are also facilitated in integration in existing water treatment processes; (iii) rapid reaction between iron and H₂O₂; (iv) use of cheap and easy-to-handle reagents; and (v) efficiency of mineralization²³.

The rapid decomposition of pollutants is attributed to the rapid production of hydroxyl radicals, due to the presence of Fe²⁺ species in the solution ($k=40-80 \text{ M}^{-1} \text{ sec}^{-1}$)³¹ (Fig. 1). In the second stage, due to the consumption of Fe²⁺ ions and generation of Fe³⁺, the rate of reaction will decrease ($k=2 \times 10^{-3} \text{ M}^{-1} \text{ sec}^{-1}$)³¹. This is because the reaction of Fe³⁺ and H₂O₂ leads to the production of HO₂[•] radicals (E⁰1.50 - 1.65 V) which are weaker oxidants compared to the HO[•] radicals (E⁰2.59 - 2.80 V) and have a lower rate of production^{31,32}.

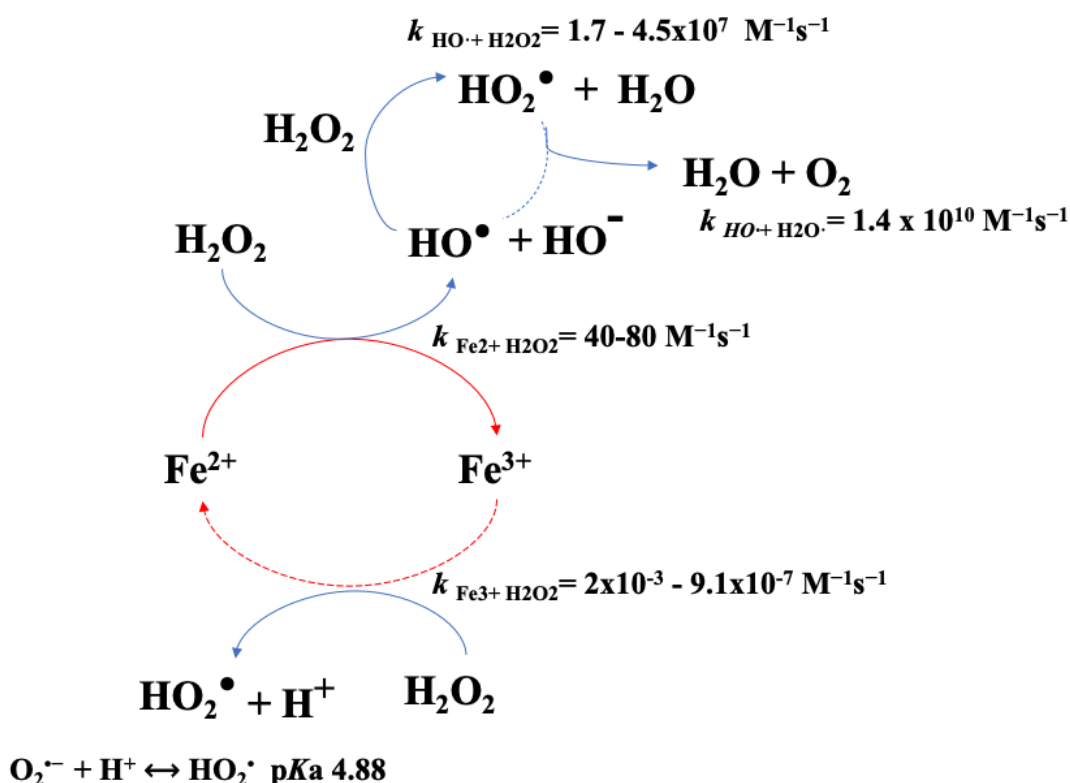


Fig. 1. Fenton reaction mechanism. Source: Adapted by the author.

The use of catalytic iron has major advantages including: (i) high abundance (fourth most abundant element in earth's crust and second-largest product in Brazil³³); (ii) environmental compatibility and low-toxicity; (iii) high reactivity; and (iv) low

commercial cost. Notwithstanding this, the chemical reactivity of iron is strictly dependent upon the pH-dependent speciation of Fe^{2+} , Fe^{3+} and ferric hydroxides (Fig. 2), which determine the type, suitability and practical requirements for each different Fenton-based AOP²³.

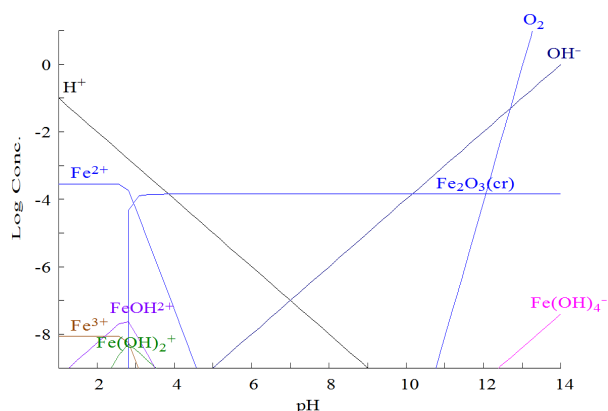


Fig. 2. Predicted iron speciation in water as a function of pH; $[\text{Fe}^{3+}] = 15 \text{ mg L}^{-1}$.

Source: Medusa software v. 3.2.1.

On the whole, the Fenton system is homogeneous if the iron (catalyst) is solubilized in the aqueous matrix or heterogeneous if the iron is immobilized or present as a solid phase material³², as such, it offers a more ecological approach³⁴. Be that as it may, the main drawbacks of Fenton have been identified: i) depletion of oxidants due to the radical scavenging effect of H_2O_2 ; ii) self-decomposition; iii) continuous loss of iron ions and the formation of solidsludge²⁵ and; iv) acidic pH mainly due to iron speciation factors (more solubility). Nonetheless, some studies have demonstrated the possibility of working with almost neutral pHs for practical applications of these treatment processes^{35,36}.

The operating costs of AOPs for the complete oxidation of toxic organic compounds are high, when compared to usually used biological treatment system³⁷. The main cost is related to the use of chemical reactants (for example, H_2O_2) and energy consumption (generation of UVC radiation when lamps are used). For this reason, solar photo-Fenton process are of special interest since they can use solar radiation to generate HO^\bullet ³⁸.

1.3.2 Solar photo-Fenton

A combination of hydrogen peroxide and UV radiation with Fe^{2+} or Fe^{3+} ions (photo-Fenton process) produces more hydroxyl radicals compared to conventional Fenton method or photolysis of H_2O_2 . In the last 20 years, the use of solar energy for the treatment of emerging pollutants in real wastewater has increased through AOPs (Fig. 3a) with solar photo-Fenton processes being the most widely applied, looking for the viability of any large scale effluent treatment technology³⁹. Geographically speaking, Spain and Brazil lead the investigations in this area (Fig. 3b).

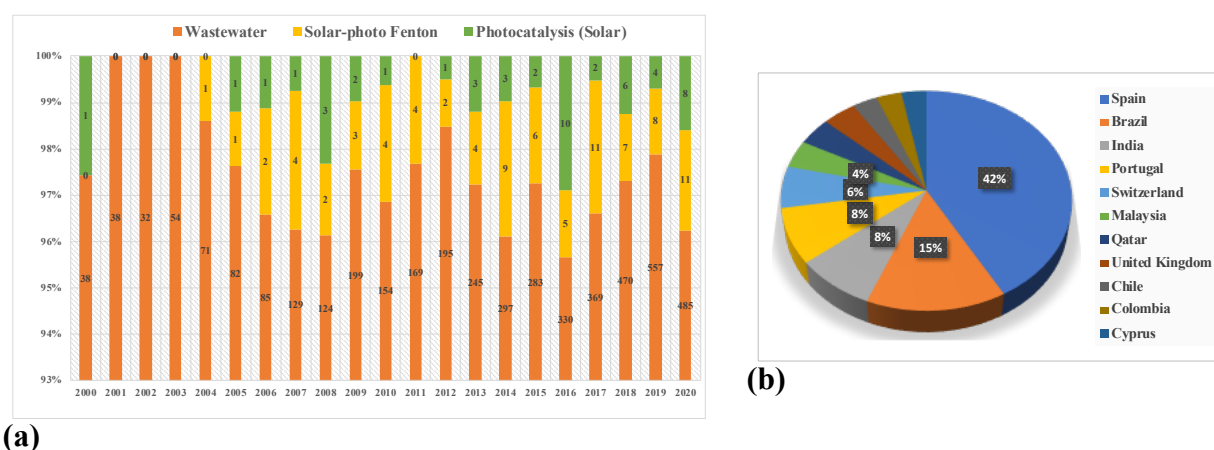


Fig. 3. Trends in the use of solar-driven AOPs for wastewater treatment (TITLE-ABS-KEY (advanced AND oxidation AND process) AND TITLE-ABS-KEY (wastewater) AND TITLE-ABS-KEY (solar AND photo-Fenton)). Source: Adapted from Scopus July 29th, 2020.

In the photo-Fenton process, the photo-reduction of Fe^{3+} to Fe^{2+} occurs by visible light irradiation²³, increasing the rate of organic pollutant degradation in turn²⁵. Notwithstanding this, at acidic range of pH the hydroxy- Fe^{3+} complexes are more soluble and $\text{Fe}(\text{OH})^{2+}$ is the most photoactive monomeric species, it is known to yield HO^\bullet with a quantum yield of 0.075 at 360 nm^{40,41}. In this way, the use of sunlight instead of UVC irradiation reduces costs.

In order to improve the working pH range and the efficiency of the photo-Fenton treatment, chelating agents such as aminopolycarboxylic acids (APCAs) have been used to keep iron in solution^{42,43}. Among the APCAs, ethylenediamine-N, N'-disuccinic acid (EDDS), with high biodegradability and toxicity under environmental conditions, has been used for the solubilization of iron species^{44,45} with high efficiency in the pH range 3-9^{43,46} (Fig. 4). The Fe^{3+} -EDDS complex offers greater photo-absorption compared to

iron aquo-complexes⁴⁷. Photochemical activity is associated with ligand-metal charge transfer (LMCT) transitions³⁶, with rapid photochemical reactions taking place under UV solar radiation (UV-B, 280-315 nm and UV-A, 315-400 nm)^{48,49}. The high efficiency of the photo-Fenton process, associated with the operational versatility that this process allows using chelating agents thereby make the photo-Fenton process an interesting solution that allows the degradation of emerging pollutants⁵⁰ like PHCs.

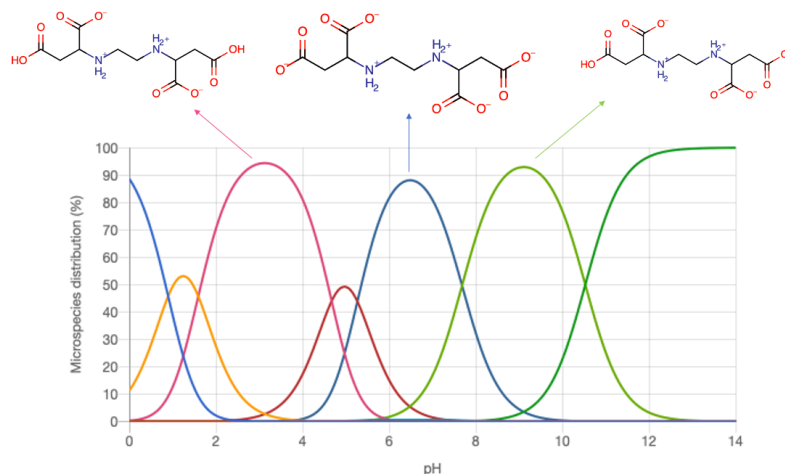


Fig. 4. Distribution of EDDS microspecies as visualized with Chemicalize. Each color in the microspecies distribution diagram represents the protonation states that can be checked on the online platform. Source: <https://chemicalize.com/app/calculation/20846-91-7>.

Being highly viable due to its low cost and reusability, recent studies have suggested the use of zero valence iron (Fe^0 or ZVI) facilitates the removal of different types of pollutants⁵¹. Fenton process using Fe^0 or iron-based materials include: i) the homogeneous Fenton reaction driven by surface-leached iron; ii) the heterogeneous reaction that occurs at the surface of the catalyst and; iii) the physical interaction through adsorption at the surface of the heterogeneous catalyst¹³.

1.3.2.1 Fenton oxidation at circumneutral pH: iron complexes

As previously mentioned, the acidic range of operational pH (usually 2.8–3.5) is necessary to ensure the effectiveness of iron catalyst and to avoid its precipitation as ferric hydroxides. Despite this, working in acidic pH involves the addition of large amount of acid and the subsequent neutralization of the treated matrix⁵². The acidification of treated matrix and subsequently neutralization increase treatment cost, salinity of the solution,

and sludge formation². Besides this, acidification might lead to the release of some gases into the environment in the presence of sulfides or cyanides and potential mobilization of toxic metals may occur at low pH values⁵³. Therefore, significant effort is devoted toward developing strategies to conduct homogeneous Fenton oxidation at higher pH values¹³.

The compounds that can form complexes with iron can be added into the solution to form stable Fe³⁺-complexes. Nevertheless, the formed Fe³⁺ complexes must be able to undergo some form of reduction that can lead to the generation of ferrous ions through ligand-to-metal charge transfer (LCMT) and the consequent production of HO•^{13,54}. Various chelating agents have been used to promote homogeneous Fenton at circumneutral pH⁵⁵⁻⁵⁸. Although natural chelating agents such as humic acid are used, the most commonly reported are the synthetic chelating agents such as ethylenediaminetetraacetic acid (EDTA), ethylenediamine-N,N'-disuccinic acid (EDDS), oxalate, citrate, and nitrilotriacetic acid (NTA). These chelators can form soluble complexes with Fe³⁺ and maintain catalytic ability at circumneutral pH, achieving excellent degradation percentages^{46,59,60}.

1.3.3 Matrix effect

The degradation of PHCs is largely influenced by the quality of the water matrix, and the usefulness results from the impact of the dissolved components, which can have neutral, inhibitory or promotive effects⁶¹. The nature of the reaction matrix is an important consideration since the presence of inorganic compounds in different concentrations such as NaCl, Na₂CO₃ and Na₂SO₃ and organic carbon (carbonate and bicarbonate) in wastewater can result in a scavenging effect on the HO•, decreasing their availability^{13,62,63}. Table 1 presents the main scavenger reactions of the hydroxyl and sulfate radicals.

Humic substances may act as an inner filter and severely decrease removal efficiencies³². They may also cause the formation of i) less active complexes with iron species in Fenton-based processes; ii) competition for catalytic active sites or fouling of the surface area of the catalysts in heterogeneous catalytic processes; and iii) the modification of the electrical surface charge due to the pH or ionic strength. Moreover, the water matrix can play an essential role in the yield of photo-degradation reactions, depending on the presence of promotive and inhibitory substances.

The presence of chloride and sulfates in the aqueous matrix containing the ferric ions results in the formation of less reactive [Fe(Cl)]²⁺, [Fe(Cl₂)]⁺ and FeSO₄⁺ complexes,

leading to the generation of the less reactive inorganic species like $\text{Cl}_2^{\bullet-}$ and $\text{SO}_4^{\bullet-64}$, which decrease the photo-Fenton reaction rate⁶¹.

Conversely, the following factors have a positive impact on Fenton-based processes: (i) the iron ions naturally found in the water matrix may act as an additional source of catalyst source for the Fenton reaction; (ii) inherent reductants present in the water matrix (e.g., phenolic compounds) might reduce Fe^{3+} to Fe^{2+} , increasing the regeneration rate of the catalyst; (iii) Fe^{3+} can react with compounds containing $-\text{COOH}$ and $-\text{OH}$ groups, creating complexes with higher quantum yield, which might undergo photo-reduction through a ligand-to-metal charge transfer to Fe^{2+} ; and (iv) NO_3^- is able to produce HO^\bullet and NO_2^\bullet radical species, promoting the photodegradation of PHCs⁶¹.

Table 1. Scavenger reactions of the hydroxyl and sulfate radicals by components in the matrix.

Reaction	Rate constant ($\text{M}^{-1} \text{s}^{-1}$)
$\text{HO}^\bullet + \text{NO}_2^- \rightarrow \text{NO}_2^\bullet + \text{HO}^-$	8.0×10^9
$\text{SO}_4^{\bullet-} + \text{NO}_2^- \rightarrow \text{NO}_2^\bullet + \text{SO}_4^{2-}$	8.0×10^8
$\text{HO}^\bullet + \text{Cl}^- \rightarrow \text{HClO}^{\bullet-}$	4.3×10^9
$\text{SO}_4^{\bullet-} + \text{Cl}^- \rightarrow \text{Cl}^\bullet + \text{SO}_4^{2-}$	6.6×10^8
$\text{HO}^\bullet + \text{HCO}_3^- \rightarrow \text{CO}_3^{\bullet-} + \text{H}_2\text{O}$	8.5×10^6
$\text{SO}_4^{\bullet-} + \text{HCO}_3^- \rightarrow \text{CO}_3^{\bullet-} + \text{SO}_4^{2-} + \text{H}^+$	9.1×10^6
$\text{HO}^\bullet + \text{NOM} \rightarrow \text{Products}$	$2.23 \times 10^8 \text{ L (mol C)}^{-1} \text{ s}^{-1}$
$\text{SO}_4^{\bullet-} + \text{NOM} \rightarrow \text{Products}$	$>6 \times 10^6 \text{ L (mol C)}^{-1} \text{ s}^{-1}$
$\text{HO}^\bullet + \text{SO}_4^{2-} \rightarrow \text{SO}_4^{\bullet-} + \text{HO}^-$	3.5×10^5

Source: Adapted from Shah *et al.*⁶⁵

1.4 Database of transformation products

Wastewater treatment evaluation has been used frequently in relation to DOC values to evaluate the process, however, false conclusions may be drawn as seen from previously studied treatment processes. In most instances, contaminants are frequently not completely mineralized, favoring the generation of transformation products (TPs)⁶⁶. The formed TPs can present numerous chemical structures, as there is no preferential path given that radical species are not selective.

The challenge to structurally elucidate the TPs is being greatly facilitated by recent developments in liquid chromatography techniques coupled with High Resolution Mass Spectrometry (LC-HRMS), such as Time-of-Flight (TOF) analysers⁶⁷. TOF

technology uses high sensitivity in full-scan MS analysis and Hybrid Q-TOF analyzer, allowing the determination of the chemical formula of precursor and product ions, and they are being employed for characterizing unknowns compounds, such as TPs⁶⁸. Moreover, the use of QTOF simultaneously permits the collection of fragmentation information of an unlimited number of compounds in a simple way⁶⁹ by “broadband collision-induced dissociation” (bbCID) (Fig 5).

Target screening methods based on the use of accurate-mass databases have been recently developed and successfully applied for target compounds (analytes that have commercially available analytical standards), in food and environmental samples allowing a rapid and automatic identification of target analytes⁷⁰. Despite this, most TPs are chemical compounds that do not currently have a commercial analytical standard available.

Using traditional methods, TPs identification can be performed by a method in which following LC-HRMS analysis, TPs are sought manually for the appearance of new chromatographic peaks. Once found, MS and MS/MS spectrum (bbCID data) of the new chromatographic peak are carefully evaluated for the identification of possible molecular ions of the TP and its fragments. It is an approach that requires a great deal of processing time and can only be performed by studying of isolated initial compound. It is thereby essential to know the technician performing the analysis of the process or reaction that takes place in order to assess the viability of these potential TPs⁷¹.

By way of an alternative, if a database is created and used to identify TPs, there will be a crucial gain in time. Processing the data analysis using the compound database yields results from the software in just a few minutes. One example for TPs suspected screening identification using a purpose built-database is shown in Fig. 5. It is a rapid and automatized method of identifying TPs and could be used in real samples such as hospital wastewater. It is important to note that using the database to identify TPs during AOPs is only possible because of the evolution of analytical techniques like LC-QTOF MS, that provide accurate masses of the compounds and its fragments, in addition to fast and efficient data processing through the modern software available^{70,71}.

It is important to observe that, following the initial description in the laboratory analysis, information about each compound found is inserted into the database. In this sense, the database constructed can be specific to each research task. Moreover, it would also be possible to use this tool when different chromatography methods are used. Later,

TPs identification may indicate the main degradation pathway(s) during AOPs treatments.

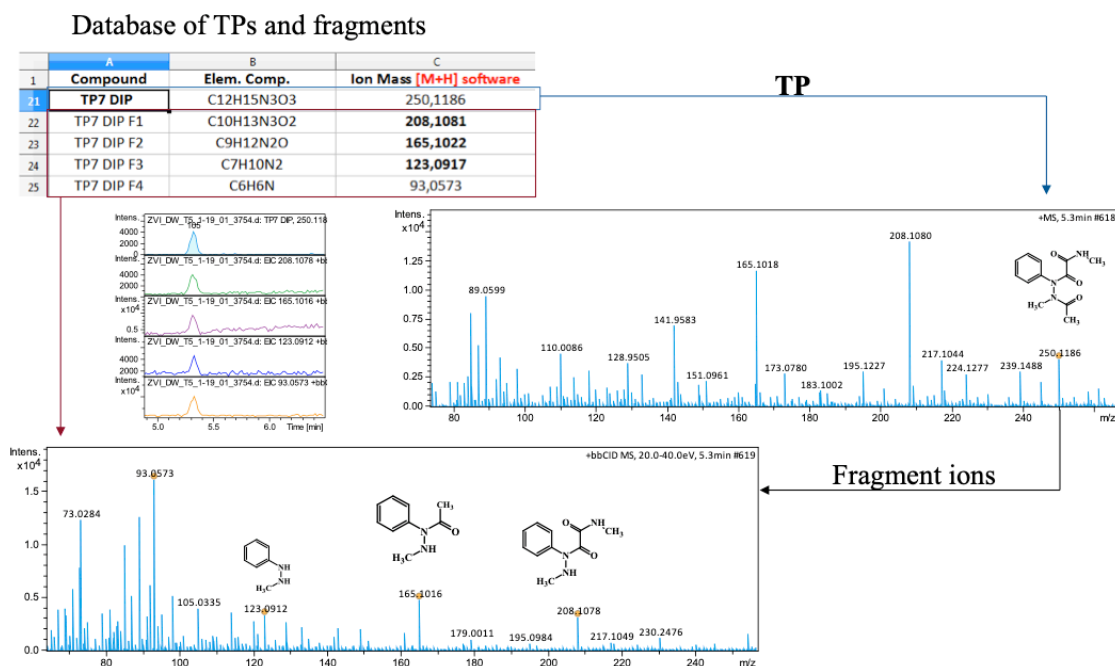


Fig. 5. TPs suspected screening identification using a purpose built-database (full-scan MS and bbCID-MS/MS). Source: Adapted by the author.

1.5 (Q)SAR models

As can be expected, in general, a wide range of TPs end up being generated simultaneously in the reaction medium. In addition, in research using real matrices are used, there may be a synergistic or antagonistic effect or from the mix of TPs, making it very difficult to associate ecotoxicity, toxicity or biodegradability data distinctly with one of the TPs present. In this sense, it is understood that the use of bioassays has limited viability in such conditions.

The limitations of the *in vivo* and *in vitro* approaches for determining the biological activity of chemicals have encouraged the development of *in silico* analysis. The structure-activity relationship (SAR) and quantitative structure-activity relationship ((Q)SAR) models are mathematical models that can predict a relationship between the chemical structure of molecules which is encoded (*e.g.* SMILES - Simplified Molecular-Input Line-Entry System) and their activity against a specific biological target⁷².

(Q)SAR techniques are well suited to dealing with large quantities of data, which allow researchers to discern trends in existing data of environmental relevance and then

extrapolate trends to untested compounds⁷³. The use of *in silico* predictions is based on a chosen property (for example, toxicity) that can be described in relation to a chemical or fragment⁷⁴, which is simultaneously described using certain parameters (e.g, acute and chronic toxicity values). Conversely, the accuracy of these models depends on the correct analysis and selection of computed descriptors as independent variables for the (Q)SAR model definition. The use of (Q)SAR models must be validated and the compounds of study must fall within the model's applicability domain, as reported in several investigations⁷⁵.

Due to concerns about toxicity and effects of TPs to the ecosystem balance⁷⁶, food security and human health, researchers have recently developed (Q)SAR models to investigate the chemical risk assessments, providing faster, more economical and animal-free tools⁷⁷.

Predictions are generated using a range of software tools, including a tool based on expert rules (TOXTREE) and tools based on statistical methodologies (ECOSAR, T.E.S.T and EPI-SUITE). In each case, the predictive performances of the individual software tools are assessed using the internal datasets⁷⁸.

TOXTREE is a flexible and easy-to-use open-source application that classifies chemicals into categories and predicts various types of toxic effects by applying decision tree approaches. Toxtree applies different QSAR models to query chemicals belonging to the classes of aromatic amines, alpha aldehydes, the beta-unsaturated aldehydes and sulfonic group on the aromatic ring⁷⁸.

EPI Suite™ provided the quantitative or qualitative results for each endpoint. Additionally, the user will be given additional information regarding the derivation of the prediction including the fragments or equations identified which are relevant to the endpoint, coefficient values, corrections factors, etc. The mathematical algorithms and fragment-based formulas in the EPI Suite™ modules use experimental data if they are available in the software Database.

The Ecological Structure Activity Relationships Program (ECOSAR) and Toxicity Estimation Software Tool (T.E.S.T.) area is a frequently used (Q)SAR tool developed by USEPA to predict a chemical's acute (short-term) toxicity and chronic (long-term or delayed) toxicity to aquatic organisms, such as fish, aquatic invertebrates, and aquatic plants⁷⁹, bioconcentration factor and mutagenicity⁸⁰.

ECOSAR contains a library of class based QSARs for predicting aquatic toxicity, overlaid with an expert decision tree to select the appropriate chemical class based on

chemical structure. For a complex chemical substance with multiple functional groups (esters, ketones), multiple (Q)SAR classes may be chosen by ECOSAR⁸¹ (Fig. 6). In turn, T.E.S.T uses several advanced QSAR methodologies that provide greater confidence in predicted toxicities. Moreover, this information could be compared and supplemented by different (Q)SAR softwares.

SMILES Class-specific estimations

O=C(C(NC)=O)N(C1=CC=CC=C1)N(C)C(C)=O

Chemical Name:

CAS:

Log Kow: -0.9711

Water Solubility (mg/L): 7894.0

Organic Module Result Experimental Data Physical Properties K_{ow} Estimate Report

Hydrazines

Organism	Duration	End Point	Concentration (mg/L)	Max Log Kow	Flags
Fish	96h	LC50	13.7	5.0	
Daphnid	48h	LC50	11.5	5.0	
Green Algae	96h	EC50	4.06	6.4	
Fish		ChV	47.9	8.0	
Daphnid		ChV	6.89	8.0	
Green Algae		ChV	0.390	8.0	
Mysid	96h	LC50	8.56E+3	5.0	▲
Fish (SW)		ChV	577	8.0	
Mysid		ChV	9.19E+3	8.0	▲

Amides

Organism	Duration	End Point	Concentration (mg/L)	Max Log Kow	Flags
Fish	96h	LC50	1.45E+4	5.0	▲
Daphnid	48h	LC50	2.21E+4	5.0	▲
Green Algae	96h	EC50	596	6.4	
Fish		ChV	51.4	8.0	
Daphnid		ChV	1.23E+3	8.0	
Green Algae		ChV	102	8.0	
Fish (SW)	96h	LC50	8.50E+3	5.0	▲
Mysid (SW)	96h	LC50	211	5.0	
Mysid (SW)		ChV	335	8.0	

Fig. 6. ECOSAR software for toxicity predictions. Source: Adapted by the author.



CHAPTER 2

"We forget that the water cycle and the life cycle are one."

Jacques Yves Cousteau



OBJECTIVES

As discussed in the introduction, the development of efficient methods to remove PHCs from water and wastewater is vital. Nonetheless, processes must be focused on reducing the toxic impact of the TPs formed throughout the process, decreasing costs and using renewable energies.

Having said that, the use of advanced analytical techniques for PHCs monitoring and identification of new compounds will provide improved and more accurate data on the concentration of PHCs in their TPs in waters and wastewaters after the treatment. In addition, TPs information can be used to estimate potential risks associated with individual compounds to the environment or human health.

Considering this, the main objective of this PhD Thesis is to evaluate different solar photo-Fenton processes in pH close to neutrality, for the degradation of pharmaceuticals in different water matrices with an emphasis on hospital wastewater.

With this aim, solar photo-Fenton (heterogeneous and homogeneous) were used combining optimization of the best experimental conditions to increase pharmaceutical degradation rates, kinetics studies, and TPs identification. This thesis will also make proposals for TPs identification, pathway propositions and environmental effect predictions.

In addition to the main objective, this PhD Thesis also includes the following specific aims, which can be divided into three blocks, depending on the solar photo-Fenton system(s) evaluated, analytical tools, and (Q)SAR models. These specific objectives are:

Solar photo-Fenton process:

- To characterize hospital wastewater by some macroparameters, such as: COD, BOD, COD, TOC, Cl⁻, PO₄³⁻, among others;
- To optimize and study pharmaceutical degradation in distilled water, simulated and real hospital wastewater using a batch reactor for solar-photo-Fenton;

- To scale up the process through best performance in the previous stage by means of the construction and use of a low-cost *raceway pond* reactor.

Analytical tools:

- To develop, adapt and validate analytical methods to control the main parameters (such as, iron and H₂O₂ concentrations) during the solar experiments;
- To develop analytical methodology based on LC-QTOFMS for the confirmation and quantification of pharmaceuticals in different matrices;
- To elaborate and employ properly constructed TPs databases to identify a high range of TPs from pharmaceuticals by solar experiments;
- To understand how the degradation mechanism(s) take place through oxidative species by TPs identification during treatment.

(Q)SAR models

- To predict TPs toxicity and biodegradability with *in silico* (Q)SAR tools to identify any possible impact on the environment and human health.



CHAPTER 3

"You cannot hope to build a better world without improving the individuals. To that end, each of us must work for our own improvement"

Marie Curie



METHODOLOGY

3.1 Reagents, solutions and water matrices

The reagents used for chromatographic analysis were of the LC-MS grade. Acetonitrile (ACN), methanol (MeOH) and formic acid (purity = 98%) were purchased from Merck while ammonium acetate LC-MS was purchased from Fluka. The pharmaceuticals included in this thesis were purchased from different suppliers and have an analytical grade (purity > 98.99%). The Fenton and solar photo-Fenton experiments were carried out using iron salts such as $(\text{FeSO}_4 \cdot 7\text{H}_2\text{O})$ and $(\text{Fe}_2(\text{SO}_4)_3 \cdot 5\text{H}_2\text{O})$; and, hydrogen peroxide (H_2O_2 - 39% w/v). To adjust the pH, solutions (0.5 mol L^{-1}) of sulfuric acid (98%, w/v), hydrochloric acid (36%, w/v) and sodium hydroxide were used.

Nine pharmaceuticals (nimesulide (NMD), furosemide (FRS), paracetamol (PCT), propranolol (PPN), dipyron (DIP), fluoxetine (FXT), progesterone (PRG), diazepam (DZP) and gemfibrozil (GFZ)) were selected for use in different combinations in varying initial concentrations ($500 \mu\text{g L}^{-1}$ and $50 \mu\text{g L}^{-1}$) and in several matrices in each study. The stock solution of the pharmaceuticals ($\text{DOC}: 14 \text{ g L}^{-1}$) was prepared in the ratio MeOH:ACN (1:2, v/v) to guarantee its total solubilization. The choice of pharmaceuticals was based on the fact that the majority of them are consumed continuously and, in some circumstances, without a prescription. In addition, the existence of national regulations in Brazil over the control, acquisition and manipulation of many pharmaceuticals (antibiotics and psychiatric drugs) led to the selection of the previously mentioned compounds.

The experiments were carried out in different water matrices: distilled water (DW), simulated hospital wastewater (SWW) and real hospital wastewater (RHW). The composition of the SW was adapted from the method described by OECD⁸² to simulate the organic content of hospital wastewater (Composition for 1L of SW: peptone 160 mg L^{-1} , meat extract 110 mg L^{-1} , urea 30 mg L^{-1} , $\text{Mg}_2\text{SO}_4 \cdot 7\text{H}_2\text{O}$ 2 mg L^{-1} , $\text{CaCl}_2 \cdot 2\text{H}_2\text{O}$ 4 mg L^{-1}). The RHW matrix involves the hospital wastewater from a public hospital located in the city of Porto Alegre (Brazil). The doctoral project related to this

work was presented and approved by the Ethics Committees at UFRGS and the hospital that supplied the effluent under study.

Collections of hospital effluents (Fig.7) have been carried out from 2017 until 2020, monthly (first year) and bi-monthly (second to four year), the sample collection time was in the morning (8 am to 9 am). The sampling bottles were properly cleaned before taking the samples. The bottles were tightly closed by stopper as soon, as they are filled up. The contained wastewater samples were thereafter kept in a cool dry place before taken to the laboratory at the *Universidade Federal do Rio Grande do Sul* (UFRGS).

These samples were characterized by the main physico-chemical parameters, such as: pH, conductivity, chemical oxygen demand (COD), five-daybiological oxygen demand (BOD), total organic carbon (TOC), total chloride (Cl^-), total phosphate (PO_4^{3-}), total suspended solids (TSS), total solids (TS) and biodegradability rate (BOD/COD)⁸³. The values collected are in accordance with the values reported in other studies of hospital wastewater^{84,85}. The average value of each parameter can be seen in Fig. 8(a) and the detailed values in Annex 1.

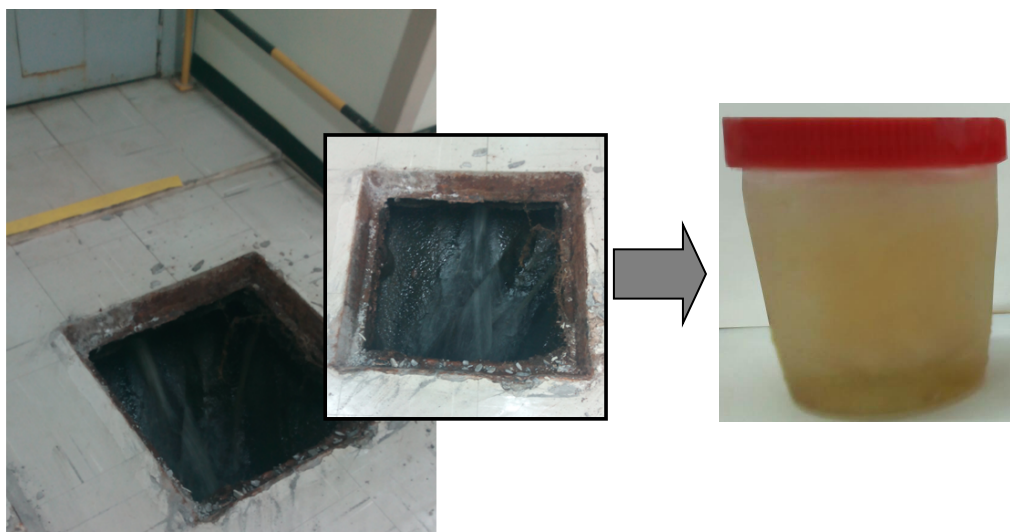


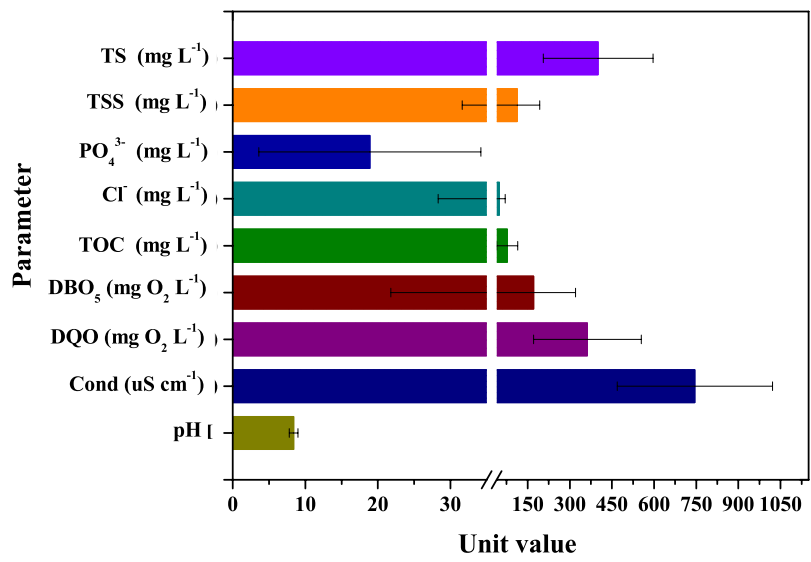
Fig. 7. Wastewater collection in the hospital center. Source: Author.

The hospital where the samples were taken is one of the main ones in the city of Porto Alegre (Brazil). It has 831 beds, 29 operating rooms, and 188 outpatient consultation rooms, an experimental and clinical research center (information taken from the hospital's website).

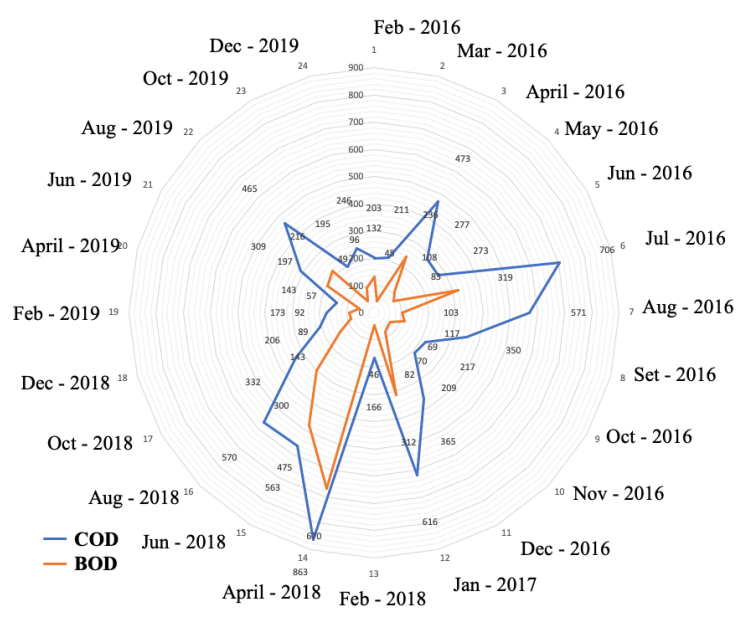
The RHW collection point receives effluent from different areas of the hospital (patient rooms, kitchen, research activities). The main physicochemical characteristics show variations throughout the years (2016-2019) were characterized with the main physicochemical parameters in accordance with Standard Methods for the Examination of Water and Wastewater (APHA)⁸⁶, such as: conductivity, chemical oxygen demand (COD), five-day biological oxygen demand (BOD), total organic carbon (TOC), total chloride (Cl⁻), total phosphate (PO₄³⁻), total suspended solids (TSS), total solids (TS) and biodegradability rate (BOD/COD)⁸³. For further information see Annex I.

The RHW has basic characteristics with pH values within the range 7.9–9.0; an average conductivity of (745.13 μS cm⁻¹). In relation to COD (143 - 863 mg O₂ L⁻¹) and BOD (45-670 mg O₂ L⁻¹), there is no trend of higher or lower biodegradability with respect to the season of the year (Fig.8(b)). In some months, the BOD/COD is less than 0.5, which makes these effluents unsuitable to undergo biological degradation and, therefore, the option of AOPs as initial treatment

The effluent had organic matter content (TOC ~ 78 mg L⁻¹), total solids (~ 400 mg L⁻¹), and total suspended solids (~112.4 mg L⁻¹). Comparing the organic load of domestic wastewater (DOC~20 mg L⁻¹)^{87,88} to organic load of RHW, it can be concluded that the organic load generated by the hospital is between 2 to 42 times greater than a load of domestic wastewater, with an additional greater volume of effluent generated. The concentration of chloride (≈49 mg L⁻¹) and phosphate (≈18mg L⁻¹) may indicate some scavenger or complexing effect from phosphate to iron.



(a)



(b)

Fig. 8 (a) Some physicochemical parameters, and **(b)** COD and BOD measures' for RHW samples. Source: Author.

3.2 Natural sunlight radiation

The natural sunlight was used in the works carried out in this Ph.D. thesis, the experiments being carried out at the *Universidade Federal do Rio Grande do Sul* (UFRGS) on sunny days at noon and under preferable conditions in the summer season (November-February). Information on the location of the solar experiments and the characterization of the actual wastewater from the hospital is provided below (Fig. 9).



Fig. 9. Solar experiments details. Source: Author.

Solar UV radiation was measured by a solar energy meter (ICEL SP-2000), which provided data in terms of the incident irradiation (W m^{-2}). All these data were used to calculate $t_{30\text{W}}$ ⁸⁹ (Eq 1), which is the normalization of the real-time for the UV radiation incident in the reactor; this normalization is called reaction time and allows the comparison of solar experiments carried out on different days, months and seasons throughout the year. Where t_n is the experimental time for each sample, UV is the average solar ultraviolet radiation measured during Δt_n , and $t_{30\text{W}}$ is a “normalized illumination time”^{90,91}. In this equation, time refers to a constant solar UV power of 30 Wm^2 (typical solar UV power on a perfectly sunny day around noon).

$$t_{30\text{W},n} = t_{30} + \Delta t_n \cdot \frac{UV}{30} \frac{V_i}{V_T}; \quad \Delta t_n = t_n - t_{n-1} \quad (\text{Eq. 1})$$

3.3 Photocatalytic reactors

3.3.1 Batch reactor

A 1L Pyrex glass vessel was used as the reactor (Fig. 10). Intensive mixing was used throughout using a mechanical stirrer at approximately 400 rpm. The reactor was covered by aluminum sheet that has a total area of 0.09165 m^2 .



Fig. 10. Batch reactor. Source: Author

3.3.2 Homemade *raceway pond* using low-cost materials

Experiments were carried out in a homemade raceway pond reactor (RPR) with low cost materials (Fig. 11), with a length of 97cm and width of 48cm. It is divided into two separate channels. The RPR includes a paddle wheel connected to an engine to obtain a well-mixed and homogeneous flow. The engine is linked to a variable frequency drive to control the paddle's speed. The photoreactor was filled with 10 L of RHW matrix, resulting in a liquid depth of 4 cm. Thus, the area occupied by the effluent in the RPR was 0.1799m². The RPR was used with a model pharmaceutical mixture (500 and 50 µg L⁻¹ of each) in RHW matrix with different values of Fe³⁺:EDDS (1:1 and 1:2), concentration of iron (5 and 15 mg L⁻¹) and H₂O₂ (200 and 50 mg L⁻¹).



Fig. 11. Low-cost, homemade *raceway pond* reactor. Source: Author.

3.4 General analytical methods

To measure hydrogen peroxide and iron concentrations, samples were taken from the reactors. The ammonium metavanadate method used for the determination of hydrogen peroxide was adapted from Nogueira *et al.*⁹², the absorbance was measured at 410 nm with a LOQ of 2.18 mg L⁻¹.

The iron concentration was spectrophotometrically measured at 510 nm according to the o-phenanthroline adapted procedure (ISO 6332)⁹³. The LOQ was 0.11 mg L⁻¹. Another variant utilized to determine the total dissolved iron was the hydroquinone method⁹⁴; which enabled the identification of the speciation of iron throughout the process. The LOQ was 0.021 mg L⁻¹.

In order to determine mineralization, the analysis was carried out in AnalytikJena AG multi N/C 2100S (at the UFRGS) for TOC determination (LOQ 3.99 mg L⁻¹) and Shimadzu TOC-L CSH analyzer (at the UEPG) with direct injection of the filtered samples (0.45 µm PVDF membrane) for DOC determination (LOQ was 1 mg L⁻¹). Depending on the investigation, one of these analyzers was used, meticulously following the protocols stipulated by each institution.

The characterization of the catalyst was carried out by optical microscopy (Olympus BX41), X-ray diffraction-XRD (Siemens D500), ATR-IR (Bruker Alpha FTIR spectrometer) and zeta potential (Malvern Instruments ZEN3500) (**Paper I and Paper III**).

Scanning electron microscopy images were obtained using a Tescan Vega3 LMU microscope and EDS mapping was performed using an Oxford Instruments system operated at 15 kV and equipped with a backscattered electron detector (**Paper I**). Autolab PGSTAT302N potentiostat with a conventional three-electrode cell setup was used by Fe³⁺:EDDS analysis (**Paper IV**).

3.5 Kinetic studies

The degradation behavior of the pharmaceuticals was evaluated as first and second-order kinetics. For situations in which the degradations were not represented by such kinetics, the kinetic method described by Chan and Chu⁹⁵ was used. This method is applied when a high rate of degradation is observed in the first minutes of the reaction, followed by a slow degradation until the end of the treatment process. The authors derived the mathematical model (Eq. 2) below to simulate the reaction kinetics:

$$\frac{t}{1-(C/C_0)} = \rho + \sigma t \leftrightarrow \frac{d(C/C_0)}{dt} = \frac{-\rho}{(\rho + \sigma t)^2} \quad (\text{Eq. 2})$$

Where C is the concentration of the pharmaceutical remaining in the system after a reaction time t (min), C₀ is the initial concentration, and the parameters ρ (min) and σ (without dimension) are two constant characteristics related to the reaction kinetics and capacity degradation. Therefore, a higher value for 1/ρ indicates a faster initial degradation rate of the pharmaceutical. When t is high and approaches infinity, the reciprocal of the constant σ is the maximum theoretical fraction of pharmaceutical removal.

3.6 Transformation products generated by AOPs

To identify the presence of possible TPs formed throughout the process, samples at scheduled minutes from each experiment were analyzed by LC-QTOF MS operating in positive and negative ionization modes. To allow the identification of the generated TPs, a database was properly developed with information on TPs and all their fragments previously reported in the literature. The purpose built-database includes the elementary composition of the TPs, as well as information on the characteristic fragments. Data processing was adapted from other previous studies that used this tool to qualitatively identify the presence of different compounds (such as drugs, pesticides, metabolites, among others, with or without an available analytical standard)^{96,97}.

The LC was equipped with reverse-phase Luna[®]Omega C18 analytical column (2.1 mm × 50 mm × 1.6 μm) (**Paper III and IV**) and a reverse-phase Hypersil Gold C18 analytical column (2.1 mm × 150 mm × 3 μm) (**from Paper I and V**). For both columns, the mobile phase was a mixture of MeOH acidified with 0.1% formic acid (A) and H₂O acidified with 0.1% formic acid (B) at a flow rate of 0.5 mL/min. In these instances, the gradient was increased from 10% A (initial conditions) to 90% A in 10 min, and then maintained for 2 min. The QTOF mass spectrometer was operated in positive ionization under the following conditions: capillary 4000 V, nebulizer 40 psi, drying gas 9 L/min, gas temperature 200 °C. In all analyses, the injection volume was 5 μL.

The samples injected were previously filtered through a 0.22 μm PVDF filter. The QTOF MS system was operated in broadband collision-induced dissociation (bbCID) acquisition mode that provided MS and MS/MS spectra at the same time. All MS information was recorded over the *m/z* range of 50-1000 with a scan rate of 2Hz. The

bbCID mode enabled work with two different collision energies: one Low Collision Energy (LE) of 10 eV, and a second that applied a High Collision Energy (HE) of 70 eV to obtain MS/MS spectra. TargetAnalysis and DataAnalysis 4.2 software were used for analyses and ions with a deviation of ± 5 ppm of error were assigned possible elemental compositions and double-bond equivalent (RDB).

3.7 (Q)SAR software programmes

A diverse range of (Q)SAR methodologies (statistical and tool based) were applied in pharmaceuticals and their TPs. Toxtree v. 1.3.0⁹⁸, EPI Suite™ software⁹⁹ and T.E.S.T v 4.2.1 were used to estimate biodegradability, mutagenicity, persistence and oral toxicity. While acute and chronic toxicities were estimated using ECOSAR v. 2.0 software¹⁰⁰, the LC₅₀ ratio (mg L⁻¹) was calculated dividing LC₅₀ or EC₅₀ (fish (96 h), *Daphnid* (48 h), and *Green algae* (96 h)) of each TP for the respective values of its parent compound.

Following, Table 2 contains information on the software version, model, analysis characteristics, and the endpoint in relation to the structures of the TPs and pharmaceuticals analyzed in different studies. The endpoints were estimated by entering SMILES (Simplified Molecular Input Line Entry System).

Table 2.(Q)SAR models use in different research studies performed.

Software	Model	Description	Endpoint						
EPI Suite v. 4.11	BIOWIN™	Estimates aerobic and anaerobic biodegradability of organic chemicals using 7 different models. Two of these are the original Biodegradation Probability Program (BPP™). The seventh estimates anaerobic biodegradation potential	Biodegradability						
	AOPWIN™	Estimates the gas-phase reaction rate for the reaction between the hydroxyl radicals and a target structure.	Rate for the reaction						
TOXTREE v. 3.1.0		Determines the Cramer class of a target structure and estimate its relative toxic hazard							
		<table border="1"> <thead> <tr> <th>Class I</th> <th>Class II</th> <th>Class III</th> </tr> </thead> <tbody> <tr> <td>Substances of simple chemical structure with known metabolic pathways</td> <td>Substances that are intermediate. They possess structures that are less innocuous than those in Class I</td> <td>Substances with chemical structures which suggest a significant toxicity</td> </tr> </tbody> </table>	Class I	Class II	Class III	Substances of simple chemical structure with known metabolic pathways	Substances that are intermediate. They possess structures that are less innocuous than those in Class I	Substances with chemical structures which suggest a significant toxicity	Oral toxicity
	Class I	Class II	Class III						
	Substances of simple chemical structure with known metabolic pathways	Substances that are intermediate. They possess structures that are less innocuous than those in Class I	Substances with chemical structures which suggest a significant toxicity						
START biodegradation	Structural alerts for environmental persistence and biodegradability	Readybiodegradability							
In vitro mutagenicity	A decision tree for estimating in vitro mutagenicity	Mutagenic							
ECOSAR v. 2.0	ECOSAR	Classification of substances into defined classes of aquatic toxicity according to rules of EU regulation in relation with ecotoxicity classification, fish, Daphnia and algae with prediction classes such as “not harmful”, “harmful”, “toxic” and “very toxic”.	Toxicity						
T.E.S.T. v.4.2.1	Oral rat LD ₅₀ data set	The final oral rat LD ₅₀ data set contained 7413 chemicals. The modeled endpoint is $-\text{Log}_{10}(\text{LD}_{50} \text{ mol/kg})$.	Oral rat 50 percent lethal dose						
	Bioconcentration factor data set	Ratio of the chemical concentration in biota as a result of absorption via the respiratory surface to that in water at steady state	Bioconcentration Factor						
	Developmental toxicity data set	Developmental toxicity includes any effect interfering with normal development, both before and after birth.	Toxicity						
	Ames Mutagenicity	Ames test, frame-shift mutations of Salmonella typhimurium to a test compound.	Mutagenicity						

Source: Adapted by the author.



CHAPTER 4

“Education, if it means anything, should not take people away from the land, but instill in them even more respect for it, because educated people are in a position to understand what is being lost. The future of the planet concerns all of us, and all of us should do what we can to protect it”

Wangari Maathai



RESULTS AND DISCUSSION

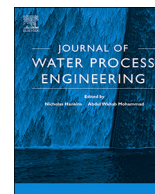
Different operational strategies of solar photo-Fenton were evaluated for the removal of the tested pharmaceuticals from the hospital wastewater: in the first strategy, waste from the metallurgical industry as a source of zero valence iron was used to evaluate the efficiency of this type of material at acid pH (**Paper I**), this first research was supported by the publication of a review article on the different treatments with zero valent iron (**Paper II**). To overcome certain disadvantages of waste material in relation to the use of acidic pH in the paper I, we proceeded to carried out experiments at a pH closer to neutrality. For this purpose, dosage of iron immobilized in alginate spheres was evaluated for pharmaceutical degradation at pH 5.0 (**Paper III**) and Fe^{3+} :EDDS complex was performed at a pH 7.0 (**Paper IV**). Both processes present high percentages of degradation of pharmaceutical, however, Fe^{3+} :EDDS presented higher percentage of degradation in lower reaction times, the main reason for choosing this process for the scale-up stage via homemade *raceway pond* reactor (**Paper V**). As a complement to the solar photo-Fenton processes, the use of an application (PhotoMetrix PRO[®]) for the quantification of H_2O_2 and Fe species, *in loco*, was developed and validated (**Paper VI**).

4.1 Solar photo-Fenton process

4.1.1 Solar photo-Fenton process: Zero Valent Iron (ZVI)

Due to the wide variety of iron materials that can be found in nature and industrial waste, these products have also promoted catalyst research¹⁰¹. The choice of iron-based materials is a major parameter that influences heterogeneous Fenton processes due to the difference in reaction activity in each system. Iron oxide minerals are especially interesting, because they are widespread in the natural environment and can be applied to remediation processes¹⁰². The ZVI induced molecular oxygen activation process to generate H_2O_2 *via* a two-electron molecular oxygen reduction, accompanying the Fe^{2+} release, can be used to degrade organic pollutants for wastewater treatment. The *in-situ* generated H_2O_2 , in turn, reacts with Fe^{2+} to produce HO^\bullet . Despite this, the application of ZVI to numerous matrices are rather poorly recognized¹⁰³.

Based on the above facts, this subsection presents two studies focused on the use of ZVI. The **Paper I**¹⁰⁴ is an application of industrial waste as a source of ZVI and dissolved iron for solar photo-Fenton treatment. The second study (**Paper II**)¹⁰⁵ is a review of the different applications and advances in the use of ZVI in pharmaceutical degradation, with insights on TPs identification and real matrices evaluated thus far.



Degradation of a mixture of pharmaceuticals in hospital wastewater by a zero-valent scrap iron (ZVSI) combined reduction-oxidation process



Elisabeth Cuervo Lumbaque^a, Marcelo Luís Wilde^a, Fabricio Abella Lopes^a,
Ellen de Souza Almeida Duarte^b, Elaine Regina Lopes Tiburtius^c, Marcio Barreto Rodrigues^b,
Carla Sirtori^{a,*}

^a Instituto de Química- Universidade Federal do Rio Grande do Sul, Av. Bento Gonçalves, 9500, Porto Alegre, RS, Brazil

^b Universidade Tecnológica Federal do Paraná. Via do Conhecimento, km 1 s/n, Pato Branco, PR, Brazil

^c Universidade Estadual de Ponta Grossa, Av. General Carlos Cavalcanti, 4748, Ponta Grossa, PR, Brazil

ARTICLE INFO

Keywords:

Reduction-oxidation process
Pharmaceuticals degradation
Transformation products
Toxicity
Biodegradability

ABSTRACT

Zero-valent scrap iron (ZVSI) combined with Fenton-based oxidation reaction (reduction-oxidation process) was studied under natural sunlight conditions to degrade a mixture of six pharmaceuticals. ZVSI is a waste product from metalworking industries, which present excellent reactivity. The morphological and structural properties of ZVSI were evaluated using different techniques. The parent compounds and their transformation products (TPs) were monitored using Liquid Chromatographic coupled with Quadrupole-Time of Flight mass spectrometer (LC-QTOF MS). The *in silico* (quantitative) structure-activity relationship ((Q)SAR) predictions of toxicity and biodegradability were predicted for each TP by using different freely available models. According to the characterization ZVSI consisted mainly of carbon (48.5 %) and iron (43.6 %) with 0.6922 m²/g of surface area. Hematite and magnetite were the main crystalline phases ZVSI. Doehlert design and desirability profile were used to select the experimental conditions. Higher degradation rates were achieved at pH 3.0, 32.5 mg L⁻¹ H₂O₂ and 2 g L⁻¹ ZVSI. Under the optimal conditions, pharmaceuticals removal was as high as 87 % in all matrixes evaluated, following a pseudo-first order kinetic model behavior. Three reuse cycles were performed using real hospital wastewater (RHWW) achieving degradation percentages > 70% and no substantial variation in the crystalline phases of the ZVSI was observed. Twenty-three TPs were detected. According to *in silico* (Q)SAR predictions, the integrated system decreased the toxicity of TPs. Moreover, most of TPs were predicted as persistent compounds. The results indicated that ZVSI combined with solar Fenton-based oxidation is an interesting alternative for the degradation of pharmaceuticals in RHWW allowing the reuse of catalyst.

1. Introduction

Brazil is one of the countries that has substantial iron ore reserves [1]. Zero-valent scrap iron (ZVSI), a waste product from metalworking industries, possesses excellent reactivity, similar to Zero-valent iron (ZVI), but is available at a very low price. The replacement of ZVI by ZVSI in processes can decrease the overall costs and also provide a use for scrap iron [2], however, few studies have explored the advantages of this material [2–4].

ZVI has been successfully applied for the treatment of water and wastewater contain pharmaceuticals [5]. ZVI is a reactive metal with standard redox potential ($E^0 = -0.44$ V). Therefore, it is an effective reducer when it reacts with contaminants containing carbonyl, nitro, and azo groups such as pharmaceuticals. The mechanism of elimination

of contaminants by ZVI *via* reduction refers to the directional transfer of electrons from ZVI to the contaminants (Eq. (1)) [6]. Reduction of carbonyl compounds generates alcohol derivatives, whereas nitro and azo reductions lead to amino derivatives. Sometimes, the hydroxyl and amino moieties are much more susceptible to degradation than other functional groups commonly present in some parent compounds [5]. Meanwhile, when the system is in the presence of dissolved oxygen (DO), there can be corrosion of ZVI and *in situ* generation of H₂O₂ (Eq. (2)) [5]. Moreover, ZVI is oxidized by two-electron transfer in the presence of H₂O₂, under the acidic conditions (Eq. (3)) [7]. The release of Fe²⁺ ions in ZVI/H₂O₂ systems is known as the Fenton reaction, which can produce hydroxyl radicals (HO[•]) that have a strong oxidizing capacity ($E^0 = 2.8$ V) [8] towards a variety of organic compounds. This oxidation of contaminants can be through i) a homogeneous Fenton

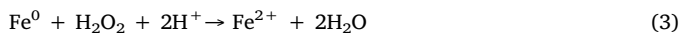
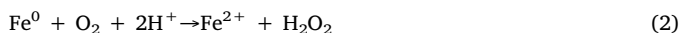
* Corresponding author.

E-mail address: carla.sirtori@ufrgs.br (C. Sirtori).

<https://doi.org/10.1016/j.jwpe.2020.101410>

Received 27 April 2020; Received in revised form 29 May 2020; Accepted 31 May 2020
2214-7144/ © 2020 Elsevier Ltd. All rights reserved.

mechanism; ii) heterogeneous reaction-induced or iii) the synergic action of both mechanisms. [9].



On the other hand, most of the studies using ZVI for the degradation of pharmaceuticals analyzed the degradation of a single compound in water or simulated effluents [5]. However, complex matrixes like raw hospital wastewater (RHWW) or wastewater treatment plants (WWTP) are known to contain a large variety of pharmaceuticals [10] in different concentrations [11], consequently, the study of mixtures of pharmaceutical compounds in real matrixes is necessary to have greater precision regarding the effectiveness of the treatment.

When ZVI is used for degradation of pharmaceuticals, which are present as complex mixtures in wastewater different degradation pathways are generated, leading to the formation of intermediates called transformation products (TPs), whose presence and amounts can vary, depending on the matrix and the treatment employed [12]. The presence of pharmaceuticals and TPs can lead to synergistic and/or antagonistic effects [13], it has, in turn, an environmental outcome. The assessment of environmental fate and effects could to avoid or reduce their environmental and human health impacts. Combining analytical techniques such as LC-QTOF MS and *in silico* (quantitative) structure-activity relationship ((Q)SAR) predictions tools are powerful approaches for a proactive assessment of environmental fate and toxicity. This combination can provide a strong indication about the TPs that may have adverse effects, enabling the proposal of the most appropriate conditions and the types of treatment that could provide total removal of TPs [14,15].

The goal of this work was to evaluate the degradation of a mixture of pharmaceuticals in real hospital wastewater (RHWW), employing ZVSI as a source of the iron species required in a combined reduction-oxidation process. Degradation pathways were proposed for pharmaceutical degradation, together with *in silico* (Q)SAR predictions of the toxicities and biodegradabilities of the proposed TPs.

2. Materials and methods

2.1. Chemicals and aqueous matrixes

Standards of paracetamol (PCT), propranolol (PPN), dipyron (DIP), fluoxetine (FXT), diazepam (DZP), and progesterone (PRG) (analytical grade; purity > 90 %) were used for the degradation study. A mixed stock solution was prepared at a concentration of 14 g L⁻¹ of each of target compounds in acetonitrile:methanol (2:1 v/v). Dilutions of the stock solution were prepared at the initial concentrations of 500 µg L⁻¹ of each pharmaceutical compounds for the degradation experiments.

The three aqueous matrixes employed were distilled water (DW), simulated wastewater (SWW), and raw hospital wastewater (RHWW). The composition of the SWW was adapted from the OECD recommendation [16], consisted of peptone 160 mg L⁻¹, beef extract 110 mg L⁻¹, urea 30 mg L⁻¹, Mg₂SO₄·7H₂O 2 mg L⁻¹ and CaCl₂·2H₂O 4 mg L⁻¹. The characteristics of the RHWW can be seen in the Table 1. The RHWW employed in the degradation studies was used as collected (without filtration). The pharmaceutical compounds were spiked into the different aqueous matrixes, prior to pH adjustment.

2.2. Characterization of the ZVSI

Granulometric, Powder X-ray diffraction (XRD), Scanning electron microscopy (SEM), EDS mapping, Brunauer–Emmett–Teller (BET) surface area (S_{BET}) and the point of zero charge were analyzed. More information about the characterization can be seen in Text S.1

Table 1
Main physicochemical characteristics of the RHWW matrix.

Parameters (units)	Value	Method	LOD	LOQ
pH	9.9	SMWW# 4500-H ⁺ B		
Conductivity (µS cm ⁻¹)	1132	SMWW 2510 B	1	0.2
Dissolved organic carbon (mg L ⁻¹)	67.6	SMWW 5310	1.68	3.99
Chemical oxygen demand (mg L ⁻¹ O ₂)	173	SMWW 5220 B	5	0.8
Biological oxygen demand (mg L ⁻¹ O ₂)	92	SMWW 5210 B	2	0.6
Total solids (mg L ⁻¹)	415	SMWW 2540 B	10	5
Total suspended solids (mg L ⁻¹)	156	SMWW 2540 D	10	5
Chloride – Cl ⁻ (mg L ⁻¹)	69.2	SMWW 4110 B	0.5	0.02
Total phosphate – PO ₄ ³⁻ (mg L ⁻¹)	22.27	SMWW 4500 P E	0.03	0.006

SMWW – Standard Methods for the examination of water and wastewater (American Public Health Association et al., 1998).

(supplementary material).

2.3. Experimental design of the reduction-oxidation process

Doehlert design was used for optimization of the variables in the reduction-oxidation (Table S.2.1, supplementary material). Batch experiments were performed using a solar photo-reactor (1 L) equipped with an aeration system providing agitation. The ZVSI was added to the photo-reactor containing the initial mixture of pharmaceuticals, in the dark, and was left for 15 min. After this time, H₂O₂ (39% w/v) was added to the photo-reactor, which was then exposed to sunlight. The initial pH was adjusted to 3.0 using H₂SO₄ (0.5 mol L⁻¹). The experiment was carried out at Chemistry Institute of *Universidade Federal do Rio Grande do Sul*, RS Brazil (latitude 30° 4' 21.0864" S, longitude 51° 7' 11.838" W) using natural sunlight irradiation on a sunny day around noon. Natural solar UV radiation was measured using a solar energy meter (SP-2000, ICCEL), which provides data in terms of incident radiation (W m⁻²). To facilitate the comparison with other photocatalytic experiments the “normalized illumination time” (t_{30W}) [17] was used instead of exposition time (t).

2.4. Reuse experiments

The reuse experiments of ZVSI were performed in RHWW matrix under the same experimental conditions. After the first set of experiments, the ZVSI was separated by centrifugation, washed at least three times with ultrapure water, and dried at 60 °C for 2 h. The washed material was employed in three successive experiments.

2.5. Analytical determinations

The iron speciation and H₂O₂ residual were determined by 1,10-phenanthroline and hydroquinone [18] and NH₄VO₃ [19] methods using a Cary 50 UV–vis spectrophotometer. Mineralization was monitored by measuring the DOC of the RHWW samples, with direct injection of the filtered (0.45 µm PVDF membrane) samples into a Shimadzu TOC-L CSH analyzer.

2.6. LC-QTOF MS instrumentation

The pharmaceuticals and their TPs were monitored and quantified using a liquid chromatograph (Nexera X2, Shimadzu) connected to a QTOF mass spectrometer (Impact II, Bruker Daltonics). Further details are provided in Text S.3 (supplementary material). Identification of the TPs was carried out by constructing a purpose-built database with TPs reported in the literature, including over 175 compounds. This database was updated from previous work [20]. Each TP was assigned with a number and the acronym of the pharmaceutical from which it

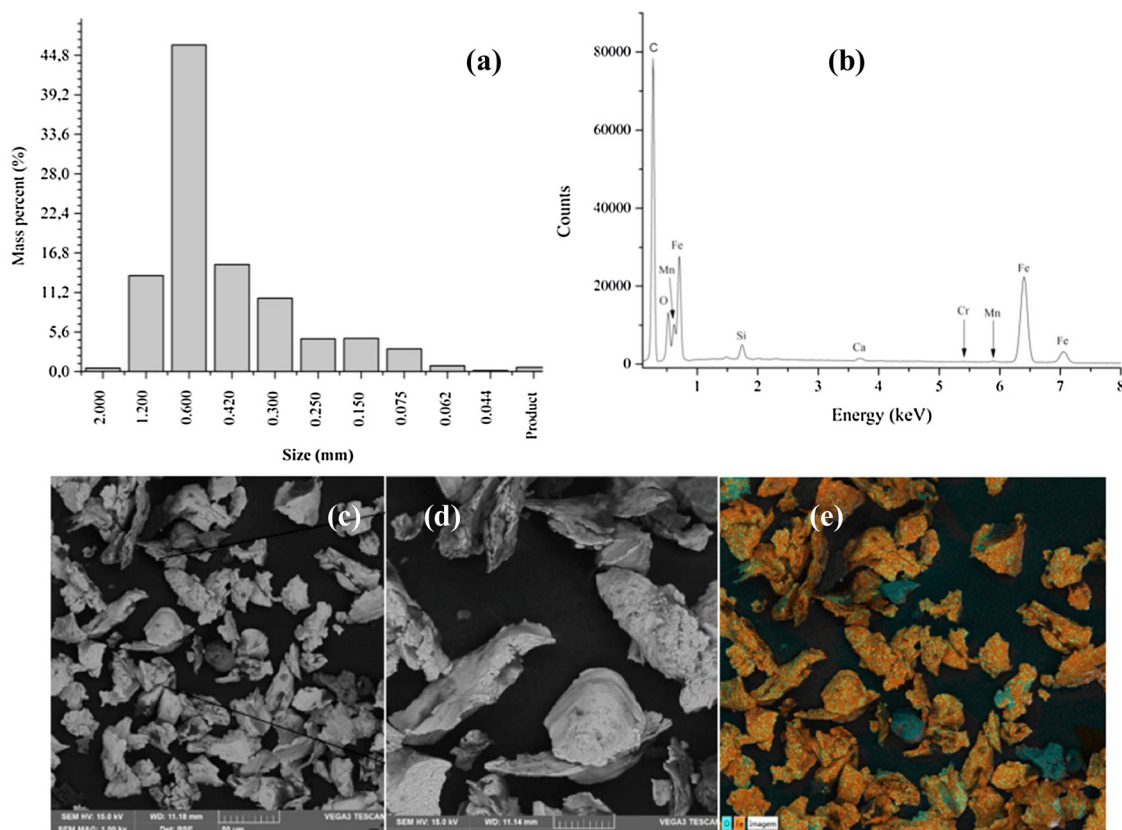


Fig. 1. Characterization of ZVSI, simple granulometric distribution (a); X-Ray Diffractogram (b), SEM image (c–d); EDS image (d).

originated.

2.7. *In silico* predictions of biodegradability and toxicological risk of the TPs

Predictions of biodegradability and ecotoxicity of pharmaceuticals and their TPs were made by *in silico* (Q)SAR tools. Toxtree v. 13.0 [21] and EPI Suite™ (BIOWIN 1-7) software from US EPA [22] were used to estimate biodegradability, persistence and oral toxicity. While acute and chronic toxicities were estimated using Ecological Structure Activity Relationships (ECOSAR v. 2.0 software) from US EPA [23]. The LC₅₀ ratio (mg L⁻¹) was calculated dividing LC₅₀ or EC₅₀ (fish (96 h), *Daphnid* (48 h), and *Green algae* (96 h)) of each TP for the respective values of its parent compound.

3. Results and discussion

3.1. Characterization of the ZVSI

Fig. 1a shows a histogram of the ZVSI particle size distribution (~85% in the size range 1.2–0.3 mm, and 47% corresponding to Tyler mesh size 28 (0.6 mm)), for more information Table S.1.1 (supplementary material). According with BET surface area analysis, the ZVSI has a 0.6922 m²/g, with a micropore volume of 2.39 × 10³ cm³/g and 4.13 nm of micropore width. The XRD of the ZVSI (Fig. 1b) showed peaks at 20° of 27, 45, 55, 65, and 83°. The narrow and intense peaks located at 27° and 45° evidenced the crystalline character of the material. The XRD crystallographic library data enabled the identification of two phases. According to ICSD (Inorganic Crystal Structure Database) card 31829, the peaks at 27° and 55° were of graphitic carbon, while based on ICSD card 64999 the peaks at 45°, 65°, and 83° corresponded to ZVI. Similar results were obtained by Shaibani and Ghambari (2011) [24]. The average crystallite size was calculated using the Scherrer equation (Eq. (3)).

$$d = \frac{k \cdot \lambda}{\beta \cdot \cos \theta} \quad (3)$$

Where k is the Scherrer constant (0.91), β is the width at half height, λ is the wavelength of the radiation (0.15406 nm), and θ is the Bragg angle. Values of 56.2 and 25.1 nm were obtained for the graphitic carbon and metallic iron, respectively.

The layered image obtained using SEM (Fig. 1c) showed a little of surface oxidation onto the material. The particles presented irregular edges, rough surfaces, and were deformed because mechanical machining processes generated them. At higher magnification (Fig. 1d), small pores could be seen onto surface, indicating that the material could act as an adsorbent.

The energy dispersive spectrometry (EDS) technique showed the presence of the elements Fe, C, O, Si, Cr, Mn, and Ca (Fig. 1e). Carbon and iron presented the highest percentages, 48.5% and 43.6%, respectively.

The hydrated surface of ZVSI in aqueous solution could be pH-dependent. The effect of pH on the surface charge is characterized by the isoelectric point (IEP). Fig. S.4.1 (supplementary material) shows the zeta potential of the ZVSI particles, as a function of solution pH. The IEP was found to be near pH 7.0, while increasing the pH the ZVSI particles acquired an outer layer of iron oxide at the surface, where ligands could be adsorbed. The adsorption of anions decreases the IEP, once more protons are needed to neutralize the negative charges of the adsorbed anionic species [25]. At pH 3.0, the ZVSI presented a positive surface charge of 16.63 mV, which could be explained by transfer of Fe²⁺/Fe³⁺ to the solution and the formation of dimers of Fe₂O₃·nH₂O on the surface. As the pH was changed, the species formed on the surface of the ZVSI also changed, as shown by charge variations.

3.2. Optimization of the experimental conditions using a Doehlert design

Preliminary studies were carried out in the dark using the ZVSI,

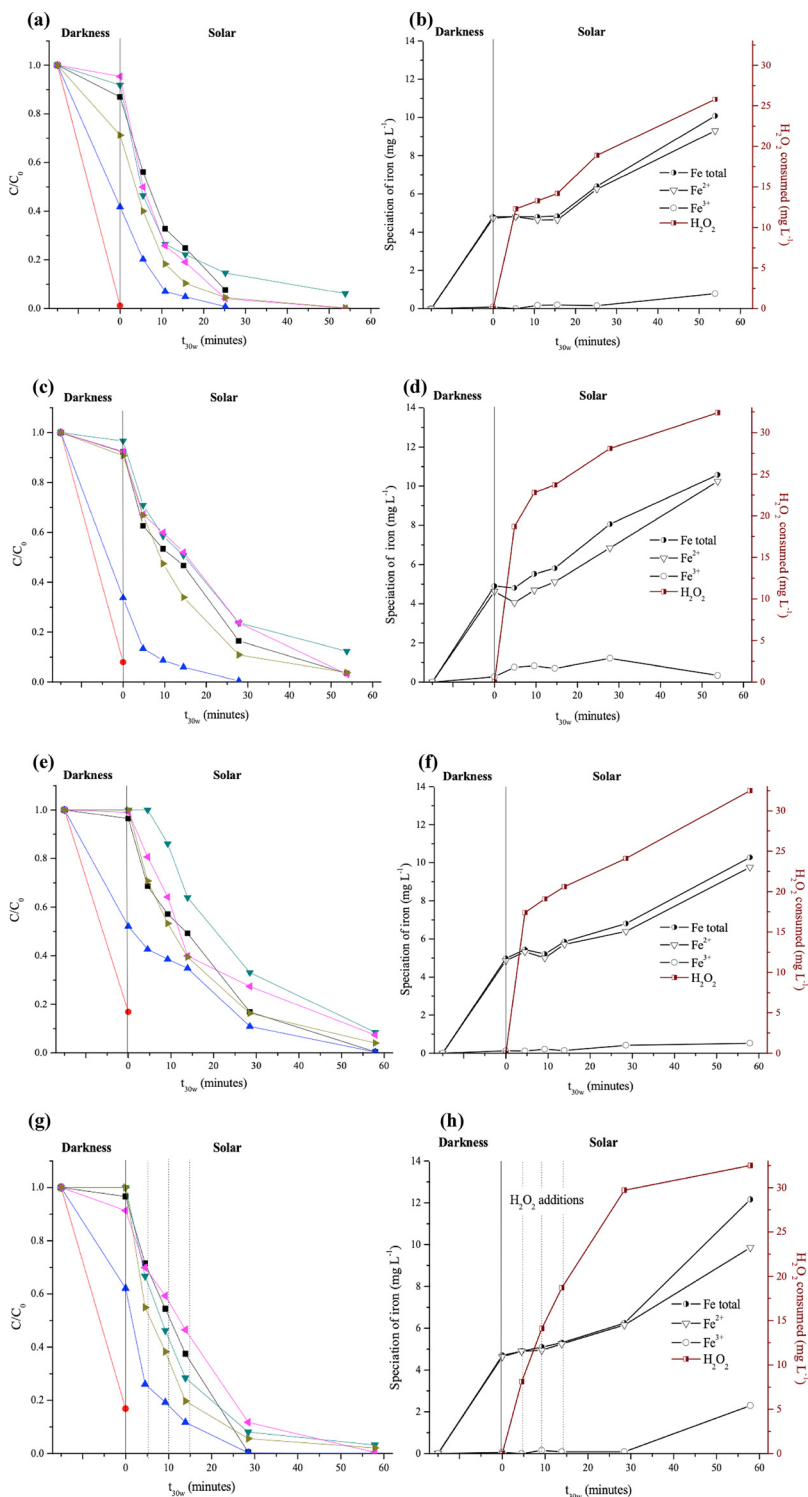


Fig. 2. Pharmaceutical degradation and H₂O₂ consumed employed ZVSI in DW matrix (a–b) SWW matrix (c–d) and RHWW with unique addition of H₂O₂ (e–f), \bullet PCT, \blacktriangle DIP, \blacktriangle PPN, \blacktriangle FXT, \blacktriangle DZP and \blacktriangle PRG. Pharmaceutical degradation employed ZVSI in RHWW with successive additions of H₂O₂ (g–h). (Conditions: 2 g L⁻¹ ZVSI, 32.5 mg L⁻¹ H₂O₂ at pH 3.0).

with agitation for 60 min using an aeration system (Fig. S.4.2, supplementary material). The results revealed greater degradation of the pharmaceuticals in the system when aeration was applied (ZVI + air). ZVI + air promotes the coexistence of reduction, adsorption, and oxidation reactions due to H₂O₂ formation in an acidic medium by the reaction of ZVI with O₂ [26]. This result is in accordance with Xiong et al (2015) [27], who indicated the degradation capacity of ZVI could be improved by air aeration.

According to the core-shell model [28], the shell consists of iron oxides/hydroxides formed by the oxidation of ZVSI, and the oxide film

provides sites for chemical reactions. ZVSI can serve as an electron donor (Eq. (1)), and pharmaceuticals accept the electrons and undergo reducing reaction. First, the pharmaceutical according to its charge is easily adsorbed in ZVSI to a favorable reaction site and then, the electrons are then transferred from the ZVSI to the molecule of pharmaceutical.

Although the reduction of pharmaceuticals occurs on the surface of ZVSI, H₂O₂ can also be generated *in situ* from ZVSI and initiate oxidative degradation of pharmaceuticals under acidic conditions (Eq. (2)) [29].

While reaction presented in Eq. (1) is dominant in Fe^{2+} generation, the reaction presented in Eq. (2) controls the generation of Fe^{2+} ions in the presence of dissolved oxygen (DO) [30] and promotes the Fenton reaction in the ZVSI /air/water matrix in the darkness. Yuan et al. (2016) [31] proved that ZVI could intensify Fenton process.

The highest primary elimination of pharmaceuticals occurred in the first 15 min, so this time was established as the contact time of ZVSI with the pharmaceuticals solution in the dark, after which the solar photo-Fenton process was immediately started with addition of H_2O_2 .

Doehlert design (quadratic model) was applied to optimize the experimental conditions of ZVSI (g L^{-1}) and H_2O_2 (mg L^{-1}) at pH 3.0 in a DW matrix. Nine experiments were performed and the analytical response was reported as the percentage decrease of the summed peak areas of the pharmaceuticals ($(1 - \sum(A_t/A_0)) * 100$), after $t_{30W} = 25.2$ min (Table S.2.1).

The highest degradations rates were found in the experiments 5 (98.36%) and 6 (99.06%). Analysis of variance (ANOVA) (Table S.2.2, supplementary material) and the F-test provided the statistical significance (within a 95% confidence interval), confirming that the quadratic model could explain 97.57% of the variance. The Pareto chart of the effects (Fig. S.2.2) shows that the variables (ZVSI and H_2O_2) and the square of the ZVSI are considered statistically important for treatment. Furthermore, the Pareto chart of effects shows that although ZVSI and H_2O_2 have a positive effect on treatment, the quadratic interaction term has an antagonist effect, confirming the results shown in the desirability profile (Fig. S.2.1, supplementary material). The desirability profile from 0.0 (undesirable) to 1.0 (very desirable) provided indication of the optimum experimental conditions, the H_2O_2 concentration showed desirability value of 1.0 in the range from 32.5 to 64 mg L^{-1} (intermediate concentration level), whereas for ZVSI was 2 g (maximum amount evaluated). Accordingly, pH 3.0, 32.5 mg L^{-1} of H_2O_2 and 2 g ZVSI were selected for the subsequent experiments.

In order to confirm the effectiveness of these conditions, experiments 5 and 6 were performed in SWW matrix, a matrix containing high organic matter content (similar to the RHWW matrix, and more complex than DW). Higher degradation rates were achieved in experiment 6, compared to experiment 5, with values of 94.59% and 87.48%, respectively, confirming the correct selection of the experimental conditions.

3.3. Degradation of pharmaceutical compounds in different aqueous matrixes

The solar driven ZVSI oxidation process was carried out for $t_{30W} = 53.9$ min, using the DW, SWW, and RHWW matrixes under the optimized conditions described above. The results showed that DIP presented the highest degradation rates in the three matrixes in the darkness step. Furthermore, FXT, DZP, and PRG were more persistent throughout the process in DW (Fig. 2a). However, it can be mentioned that acidic conditions mainly remove most pharmaceuticals through an oxidation reaction.

To analyze the interaction of the pharmaceuticals with the ZVSI, the distribution of each pharmaceutical microspecies in function of pH was calculated using Chemicalize.org by ChemAxon [32] (Fig. S.5.1, Supplementary material). The pharmaceuticals studied were calculated neutrally charged at pH 3.0, with the exception of DIP (negatively charged), influencing the adsorption onto ZVSI compared to other pharmaceuticals. Adsorption favors the transfer of electrons from the ZVSI to the DIP, therefore producing reduction reactions [30]. The alkene moiety present in the pyrazolone ring and the substituents from DIP is more susceptible to protonation. The structure of the products is determined by the site of protonation of the radical anion intermediate formed after the first electron transfer step [34]. Subsequently, the generated HO^\cdot , iron corrosion products represent the oxidation and adsorption ability, which is influenced by solution pH [35]. In oxidation process the molecules can undergo aromatic ring openings and

hydroxylation, for more information see Section 3.6.

Preliminary studies were performed considering desorption of DIP in acidic and basic solutions, as well as in organic solvents such as methanol and ethanol. However, due to the strong adsorption of DIP and its possible reduction onto ZVSI, it was not possible to calculate the amount of DIP adsorbed.

On the other hand, PCT, FXT, DZP, and PRG were identified at the end of the treatment in both SWW and RHWW matrixes (Fig. 2c and e). Table 1 shows the final concentrations of the pharmaceuticals in the different matrixes studied. The results showed that the complexity of the matrix decreased the efficiency of the solar process. The ZVSI capacity for adsorption of DIP and degradation of pharmaceuticals decreased in SWW and RHWW matrixes, which could be explained by the ionic effects caused by the phosphate, chloride and sulfate ions occupy active sites and form strong complexes onto ZVI surface [36]. This behavior was also observed by Springer et al. (2016) [37], where lower DIP adsorption was associated with increases in the concentrations of ligands such as phosphate or sulfate, suggesting that the DIP adsorption mechanism was influenced by the formation of complexes between the internal sphere and metal ions on the particle surface.

Lai et al. [38] confirmed the formation of a passive film on the surface of ZVI/granular activated carbon consisting of inorganic ions (i.e. FeSO_4 , FePO_4 and $\text{Fe}_3(\text{PO}_4)_2$) in the wastewater treatment, which decreased the degradation efficiency. On the other hand, organic matter adsorbs on the catalyst surfaces providing strong steric repulsive forces that oppose the attractive ZVSI magnetic interactions [39]. Natural organic matter is a common scavenger of reactive radicals and humic acids can significantly restrict the elimination of pharmaceuticals in the ZVSI system [40].

The initial pH 3.0 accelerated corrosion of the ZVSI releasing more Fe^{2+} into the solutions bulk (final concentrations of Fe^{2+} : 9.30 mg L^{-1} in DW; 10.24 mg L^{-1} in SWW; 9.75 mg L^{-1} in RHWW), compared to Fe^{3+} (final concentrations of Fe^{3+} : 0.78 mg L^{-1} in DW; 0.34 mg L^{-1} in SWW; 0.52 mg L^{-1} in RHWW) (Fig. 2b, d, and f). The ZVSI acted as a continuous source of dissolved iron into the solution, with a predominance of Fe^{2+} , which in turn contributed to the homogeneous Fenton reaction. After the treatment, the pH increased to final values of 4.0, 3.8, and 3.6 in the DW, SWW, and RHWW, respectively. The increase in pH could reflect the contribution of Fe^{2+} in a Fenton reaction, forming HO^\cdot and HO^- . Such behavior was reported by Segura et al. (2013) [41], who evaluated the capacity of the ZVI/ H_2O_2 system for the wastewaters treatment with different organic amounts. In the present work, H_2O_2 consumption was 25.8 mg L^{-1} in DW, while in SWW and RHWW H_2O_2 was complete consumed.

Successive H_2O_2 additions were employed to improve the degradation efficiency. For this purpose, H_2O_2 was added for four times (t_{30W} : 0, 4.5, 9.2, and 13.9 min), at a concentration of 8.13 mg L^{-1} . The results obtained (Fig. 2g and 2 h) showed that there remaining concentration of the parent compounds were lower than single addition (Table 2). H_2O_2 was completely consumed and 12.16 mg L^{-1} of total dissolved iron released into the solutions. These results were in agreement with the work of Hinojosa Guerra et al. (2019) [42], who used successive additions of H_2O_2 in a solar photo-Fenton process for the degradation of PCT and amoxicillin in synthetic wastewater and real effluent from a treatment plant, achieving degradation rates of 90% and 80%, respectively.

High mineralization rates were obtained using successive H_2O_2 additions (29.60%), compared to a single addition (19.90%). These results indicate that successive additions of H_2O_2 minimized the effect of hydroxyl radical scavengers and preserved the catalytic activity of ZVSI, decreasing the formation of hydroxides that could inhibit electron transport.

3.4. Degradation kinetics

Usually, photo-Fenton process follows a pseudo-first order kinetic

Table 2
Final concentrations of pharmaceuticals in combined reduction-oxidation process.

Pharm	MATRIX											
	DW			SWW			RHWW					
	C _t ($\mu\text{g L}^{-1}$)	r ²	k _{obs} min ⁻¹	C _t ($\mu\text{g L}^{-1}$)	r ²	k _{obs} min ⁻¹	Unique addition			Successive addition		
C _t ($\mu\text{g L}^{-1}$)							r ²	k _{obs} min ⁻¹	C _t ($\mu\text{g L}^{-1}$)	r ²	k _{obs} min ⁻¹	
PCT	< LD	0.993 (1 st)	0.086	17.02	0.995 (1 st)	0.057	2.05	0.996 (1 st)	0.096	< LD	0.996 (1 st)	0.067
DIP	< LD	i.d		< LD	i.d		< LD	i.d		< LD	i.d	
PPN	0.36	0.996 (1 st)	0.139	< LD	0.996 (1 st)	0.152	1.82	0.982 (1 st)	0.056	0.52	0.993 ^(b)	0.381
FLX	61.68	0.997 ^(b)	0.432	61.72	0.990 (1 st)	-0.338	42.37	0.992 (1 st)	0.045	15.99	0.999 (1 st)	0.086
DZP	0.57	0.997 (1 st)	0.114	15.76	0.993 (1 st)	0.587	35.69	0.993 (1 st)	0.045	2.48	0.986 (1 st)	0.093
PRG	9.91	0.998 ^(b)	0.647	19.89	0.995 (1 st)	0.054	21.72	0.994 (1 st)	0.055	10.45	0.992 (1 st)	0.100

1st Pseudo-first order kinetic model.

^(b)Chan and Chu model.

i.d Insufficient results for analysis.

[43,44]. Most of the experiments were fitted by the linear behavior of $-\ln(C/C_0)$ vs t_{30W} ($r^2 > 0.99$). Due to competitive matrix effects, TPs formed, and changes in pH [45], other kinetic models were used. The model proposed by Chan and Chu (2003) [46] considered two stages of degradation, (i) rapid and indicative of high reactivity, and (ii) slow kinetic characterized by a smaller slope. Table 2 shows the final concentrations (C_t) of the parent compounds, the kinetic models and k_{obs} (min⁻¹). The pseudo first-order model fitted most of the pharmaceutical degradation kinetics. However, some kinetic behaviors were in agreement with Chan and Chu model [46], as well as with the findings of Liu et al., (2017) [47] for the degradation of chloramphenicol by nano-ZVI.

Relating the matrix and the k_{obs} values (Table 2), a considerable decrease in the kinetic of degradation is evident, mainly in PRG, FXT and DZP, while PCT degradation rate showed less variation in relation with the complexity of matrix. The degradations in DW show a higher constant rate due to the greater availability of active sites in ZVSI, the association of k_{obs} was PRG > FXT > PPN > DZP > PCT. In SWW, a decrease in reaction kinetic was substantial in PRG compared to k_{obs} in DW. In RHWW, the presence of ions and organic matter decreases the availability of active sites in ZVSI; besides, the suspended particles could obstruct the passage of UV radiation to the matrix, inhibit the formation of HO[•] radicals to promote the oxidation of pharmaceuticals reducing k_{obs}.

3.5. Reuse experiments

The stability of ZVSI plays an important role for the treatment processes. Such behavior was evaluated by a three-reuse cycles, employing the RHWW matrix (Fig. 3a). The ZVSI still maintained high degradation capability even after the three reuse cycles as indicated by the XRD acquired after each cycle (Fig. 3b). Low intensity peaks were observed (at 21, 23, 36, 40, 60, 63, 74, and 78°), corresponding to the crystalline phase of magnetite. No significant alterations of the crystalline phases were observed by XRD, indicating the structural stability of the catalyst. The degradation rates decreased slowly between the first and the third cycles, with reductions of 10.07% (PCT), 1.75% (PPN), 3.69% (FLX), 6.68% (DZP), and 6.31% (PRG). The total dissolved iron into the solution decreased with from 9.13, to 6.78, and 6.73 mg L⁻¹ in the first, second, and third reuse cycles, respectively. The corresponding consumptions of H₂O₂ were 30.52, 30.12, and 29.38 mg L⁻¹, respectively. As the number of reuse cycles increased, the adsorption of DIP decreased, due to loss of the active sites by the formation of hydroxides during washing. The results showed removal over 89.93% of pharmaceuticals in three cycles of reuse, demonstrating the potential of ZVSI reuse for the degradation of pharmaceuticals.

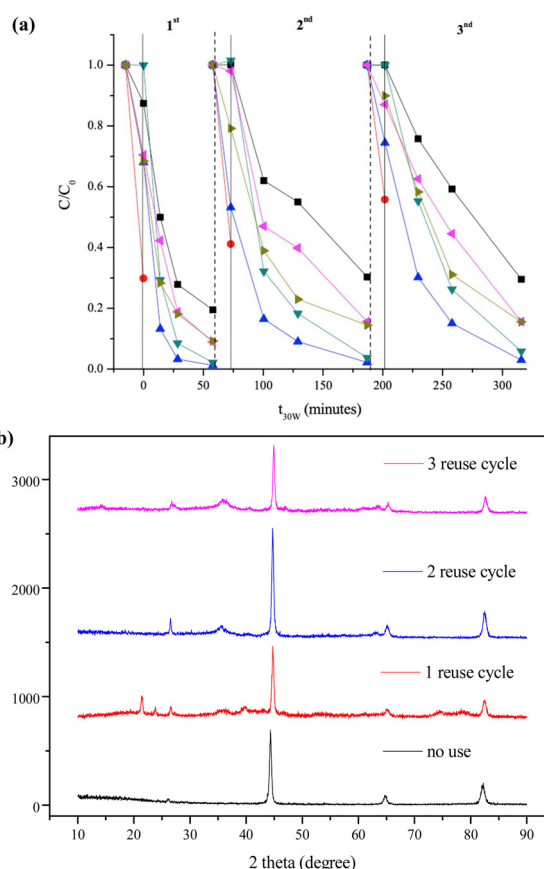


Fig. 3. Reusability tests on ZVSI for pharmaceuticals degradation in RHWW, —■— PCT, —●— DIP, —▲— PPN, —▼— FXT, —◆— DZP and —▶— PRG. (Conditions: 2 g L⁻¹ ZVSI, 32.5 mg L⁻¹ H₂O₂(successive additions) at pH 3.0)(a); X-ray diffractograms acquired after each cycle (b).

3.6. Identification of transformation products

High-resolution mass spectrometry (LC-QTOF MS) in positive ionization mode allowed the detection of 23 TPs in the aqueous matrixes studied. These TPs were identified by the *m/z* values associated with low mass errors (RDB < 5 ppm). The LC-QTOF MS data were based on a purpose-built database containing data for 175 TPs previously reported in different articles in the current literature. The database included the elemental compositions of the TPs, and their fragments, when available (Table S.6.1, supplementary material).

During the first 15 min of the process (in the dark), ZVSI related processes include adsorption, reduction, and oxidation steps, which proceeded onto the surface [33]. The formations of intermediate radical anions (short-lived products) are predominates in reduction reactions [48]; many possible reactions such as the scission of C–C and CN–bonds can be attributed to this. The corrosion of the ZVSI by oxygen (O_2) can produce reactive oxidants capable of oxidize the pharmaceutical compounds, these characterized by the hydroxylation reaction of the aromatic ring, electron abstraction, hydrogen abstraction and double bond addition [42].

According to the reactive oxygen species (ROS) involved in the process. The superoxide anion is generated by the first reduction of oxygen by 1 electron. At low pH, it is protonated and called perhydroxyl radical, with $pK_a (HO_2^-/O_2^{\cdot-}) = 4.8$ [49]. However, the reduction of oxygen by 1 electron is not thermodynamically favored compared to its complete reduction (4 electrons, $E^*(O_2/H_2O) = 0.81$ V) [50]. In contrast, the hydroxyl radical (HO^{\cdot}) is the most powerful oxidant among ROS, with a potential of $E^*(HO^{\cdot}/H_2O) = 2.34$ V [51]. At low pH values, HO^{\cdot} is the predominant species ($pK_a (HO^{\cdot}/O_2^{\cdot-}) = 11.9$ [52]). Therefore, the oxidation of pharmaceuticals at pH 3.0 can be explained by the action of HO^{\cdot} .

Most of the TPs were formed during this stage. The DIP TPs showed an increase in this first part of the process, which is related to the rapid reaction of this pharmaceutical with ZVSI. Though the formation of PPN TPs occurred in the presence of sunlight and H_2O_2 addition.

It is well known that DIP is hydrolyzed to 4-MAA, due to the presence of a water-soluble sulfonate group ($R-SO_3H$). There are four possible pathways for the cleavage of 4-MAA: (i) loss of the methylamine chain, partial aromatic ring reduction (alkene moiety protonation) and subsequent oxidation, confirmed by the identification of TP9 DIP, with and further hydroxylation opening the pyrazolone ring (TP2 DIP). Oxidation of secondary alcohol from TP2 DIP to ketone forming TP3 DIP; (ii) TP7 DIP is generated by pyrazolinone ring opening, leading to loss of the amino-methyl group (TP3 DIP) [53] or formation of TP2 DIP. TP3 FAA, a TP from formyl-amino-antipyrine (FAA), a human metabolite of DIP [54] was also observed; (iii) epoxy compound (TP2 AAA) and N-phenylacetamide (TP9 AAA) originated from acetyl-aminoantipyrine (AAA), another human metabolite of DIP [54]. TP9 AAA was formed by cleavage of the six-membered ring and further N–N bond cleavage of the hydrazine group from TP2 AAA, an unstable intermediate susceptible to oxidation in an acidic medium [55]. The presence of these DIP metabolites in RHW was reported by Becker et al.(2020) [10]; (iv) a hydroxylated derivative of 4-MAA was formed and oxidized forming a quinone-imine intermediate (TP17 DIP) [17] (Fig.4a).

TP1 DZP and TP2 DZP were formed by cleavage of the

benzodiazepinic ring from TP6 DZP, while TP5 DZP was formed by the loss of CH_3 and formation of a five-membered ring [56]. TP1 DZP and TP5 DZP were detected in drinking water samples [57], evidencing their formation in the environment, associated with human metabolism. These TPs are recalcitrant and were not removed by conventional drinking water treatments. TP6 DZP was formed by a hydrolysis reaction of the double bond of DZP during the advanced Fenton process (Fig. 4b). This TP was previously reported to be a product of a chlorination process [58].

PPN contains two types of reactive sites, the naphthalene moiety and the lateral chain. Cleavage and ring opening due to electrophilic hydroxyl radical attack on the naphthalene moiety formed TP7 PPN, TP22 PPN, TP26/27 PPN, and TP45 PPN. Additionally, TP2 PPN and TP3 PPN are side chain derived TPs [59–61]. The CO– bond cleavage and subsequent oxidation of the TP7 PPN formed anphthalic acid (TP37 PPN) [62] (Fig.4c).

The degradation of PCT follow by two hydroxylation steps on the aromatic ring starts forming TP2 PCT and TP 3 PCT which can be in the *ortho* and *meta* positions, TP 3 PCT is tri-hydroxylated intermediate (Fig. 4d), which was previously observed during photo-Fenton treatment [63].

PRG undergo H-abstraction, with the first step of the reaction being electron transfer from oxygen in the enone moiety by ZVSI, followed by the abstraction of hydrogen by HO^{\cdot} , generating TP3 PRG. This TP was identified by Shamsipur et al. (2017) [64] in studies of the electrocatalytic oxidation of PRG.

Finally, cleavage of the C O bond of FLX can produce two types of structures containing and not fluorine atoms. It was possible to identify TP16 FLX (Fig.4e), evidencing the loss of fluoride and formation of a cyanide group. This TP was reported previously by Tisler et al.(2019) [65].

Concerning the single H_2O_2 addition, out of the 23 TPs identified, 9 TPs were persistent throughout the process in the RHW, whereas in the DW and SWW matrixes, none of the TPs identified were detectable at the end of treatment. Of these 9 persistent TPs in the RHW, three TPs were from DIP (TP3 DIP, TP9 AAA, and TP3 FAA), 4 TPs from PPN (TP2 PPN, TP3 PPN, TP22 PPN, and TP37 PPN), and one TP from each DZP and FXT (TP2 DZP and TP16 FXT) (Fig. S.6.1, supplementary material). For the successive H_2O_2 additions, from the 9 TPs above, TP22 PPN, TP3 DIP, and TP2 DZP were not detectable at the end of process. Therefore, the successive H_2O_2 additions strategy improved the degradation of both the pharmaceuticals and the TPs.

3.6.1. *In silico* (Q)SAR predictions of toxicological risk and biodegradability of the TPs

The *in silico* (Q)SAR assessment of toxicity and biodegradability of

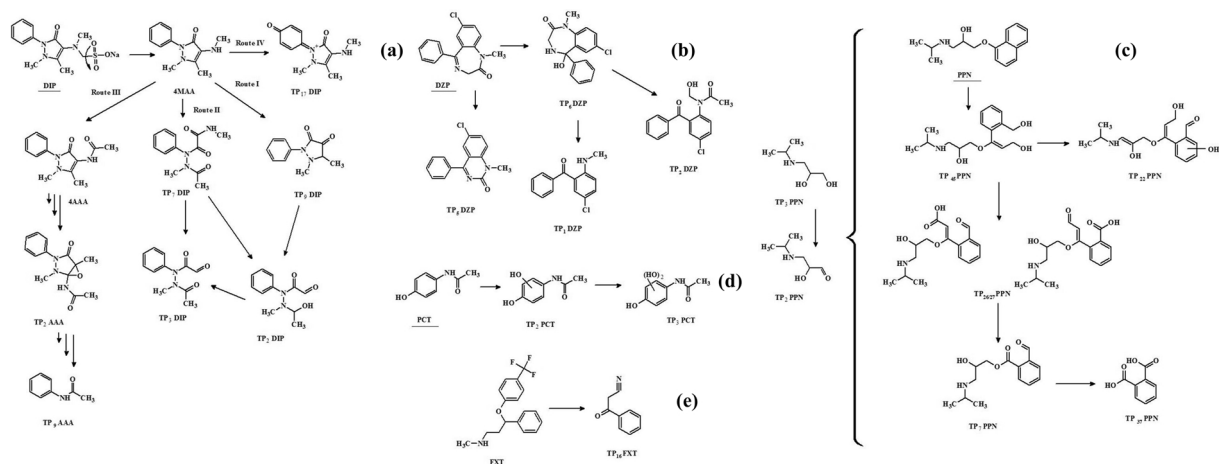


Fig. 4. Proposed degradation pathway during reduction-oxidation process.

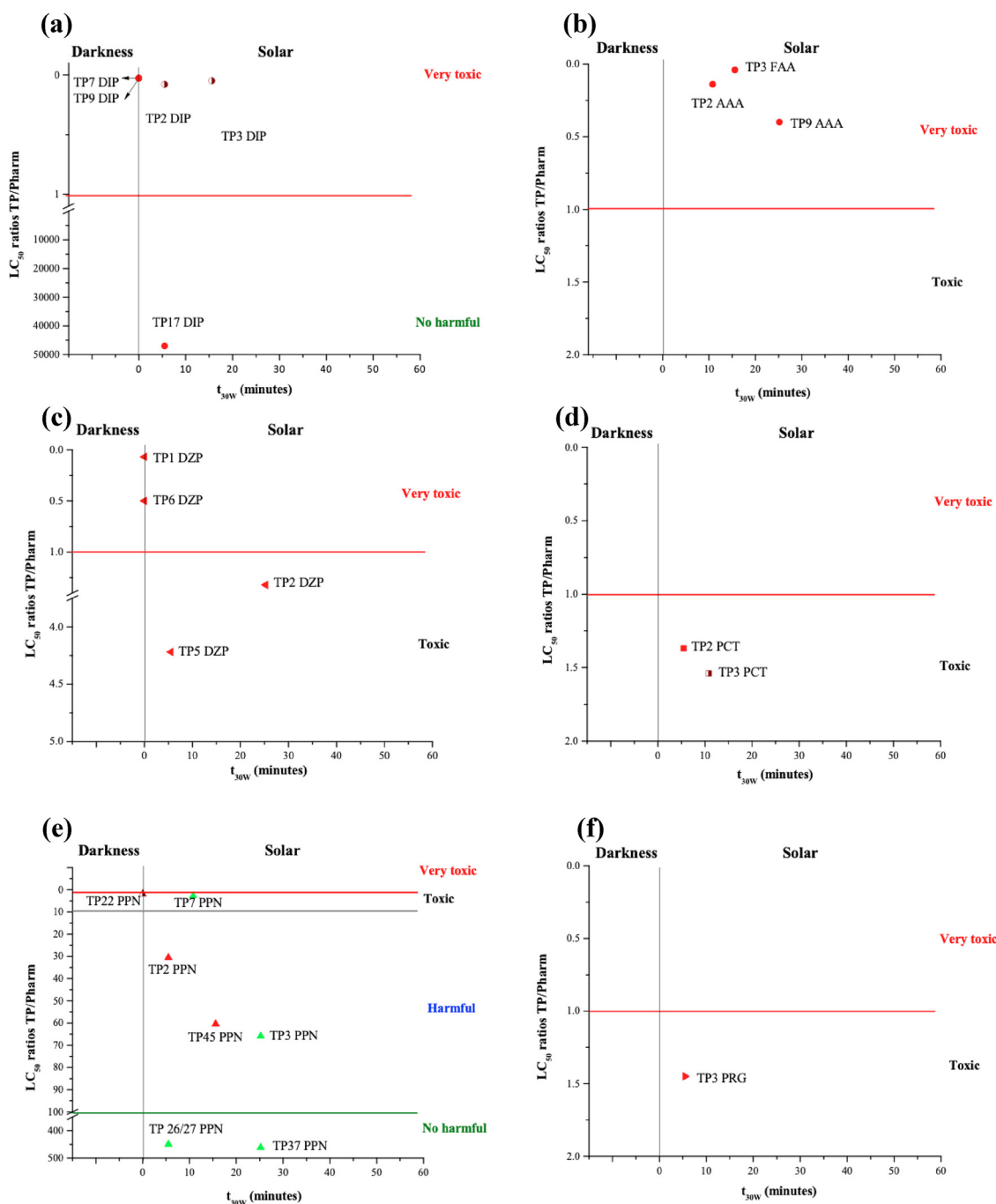


Fig. 5. Acute normalized toxicity (LC_{50} ratios TP/Pharm) and biodegradability of TPs throughout the process. ■ No biodegradable for EPI-suite and TOXTREE, ■ biodegradable for EPI-suite and TOXTREE and ■ only biodegradable for a single software.

pharmaceuticals and their TPs were carried out by using EPI SuiteTM, Toxtree, and ECOSAR software. Table S.6.2 (supplementary material) shows the ECOSAR *in silico* predictions for acute and chronic toxicities towards the aquatic organisms *Fish*, *Daphnid*, and *Green algae*. The $LC_{50}/EC_{50}/ChV$ predicted values were evaluated according to the Globally Harmonized Classification and Labeling System of Chemicals [66]. The predictions indicated that the DIP TPs presented acute toxicity, being harmful to *Fish* and *Daphnid*, and toxic to *Green algae*. DIP TPs presented high chronic toxicity towards *Green algae*. Most of the DZP TPs presented acute toxicity, being harmful to the three organisms tested, whereas TP1 DZP, TP2 DZP, and TP6 DZP presented high chronic toxicity towards *Fish* and *Daphnid*. TP16 FXT presented harmful acute and chronic toxicities. For the PCT TP, the predicted lower chronic

toxicity values towards all three organisms indicated a threat to the aquatic ecosystem. According to the predicted acute and chronic toxicity values for PPN TPs, most TPs could be considered non-harmful. Exception to TP7 PPN and TP22 PPN that showed chronic toxicity towards *Daphnid*. Finally, TP3 PRG indicated that the molecule could be considered harmful to the three organisms.

Fig. 5 depicts a normalization of the LC_{50} and EC_{50} values for *Fish*, *Daphnid*, and *Green algae*, comparing TPs to their parent compounds in order to show their toxicity effects (i.e. $LC_{50TP}/LC_{50Parent}$ Compound). A value > 1 indicated that the TP toxicity was lower than their parent compounds, whereas a value < 1 indicated higher toxicity of the TP. The LC_{50} and EC_{50} ratios showed that the TPs from FXT, PCT, PPN, and PRG exhibited lower toxicity, compared to its parent compounds

(ratios > 1). However, TP2 DIP, TP3 DIP, TP7 DIP, TP9 DIP, TP2 AAA, TP9 AAA, and TP3 FAA exhibited higher toxicities, compared to DIP (ratios < 1). The same behavior was observed for TP1 DZP and TP6 DZP. Considering the normalized values, Fig. 5 also shows the t_{30W} where the highest intensity peaks of the most toxic TPs occurred. As depicted, four TPs (TP7 DIP, TP9 DIP, TP1 DZP, and TP6 DZP) (Fig. 5a and c) had a higher intensity during the dark stage, with a decrease during the solar process. The other TPs were formed during the oxidative (solar) stage, with the highest intensities in the first 30 min of the process, decreasing after. Compared to the other structures identified, DIP and DZP TPs were predicted as more toxic. PCT and PRG TPs presented toxicity and most PPN TPs were predicted as harmful and not harmful (Fig. 5d, e and f).

The Cramer rules were in accordance with most of the ECOSAR estimations for DIP, DZP, and PPN. It should be noted that the Cramer prediction reports toxic effects in terms of oral toxicity, while ECOSAR reports the results in terms of the acute and chronic toxicity values.

The *in silico* (Q)SAR predictions for biodegradability provided by BIOWIN 1-7 and START (Toxtree) can be seen in Table S.6.3 (supplementary material). Comparing the *in silico* (Q)SAR predictions, similar results were pointed out, indicating most of the TPs as non-biodegradable compounds. BIOWIN is fragment-based, while START is based on structural alerts, which are molecular functional groups or substructures linked to environmental persistence or biodegradability. Information about the SMILES, ECOSAR fragment type data, and BIOWIN 1-7 predictions can be seen in Table S.6.3 (supplementary material).

4. Conclusions

Considering that iron scrap can be easily acquired from industrial waste, the use of ZVSI as catalyst can improve the economic viability and can be incorporated in integrated system of reduction-oxidation for the degradation of pharmaceuticals in complex matrixes. Excellent results in terms of elimination of the pharmaceuticals were found for the reuse of ZVSI. The ZVSI provides a continuous release of Fe^{2+} into the solutions bulk. Successive H_2O_2 additions can be used as a strategy improving the pharmaceutical degradation and mineralization ratios. Combining reducing and oxidizing stages was useful for the remediation of pharmaceuticals and degraded most of the persistent TPs that presented toxic characteristics. Besides, ZVSI offers an alternative for the treatment of effluents containing high amounts of salts and organic matter, reducing the release of toxic products, allowing the reuse of industrial waste for the degradation of micropollutants.

Declaration of Competing Interest

The authors declare that they have no known competing financial interests or personal relationships that could have appeared to influence the work reported in this paper.

Acknowledgments

The authors wish to thank CNPq (Processo: 403051/2016-9). Elisabeth Cuervo Lumbaque (Processo: 158197/2019-4) and Dr. Marcelo L. Wilde (Grant No. 155905/2018-0) thank CNPq for their PhD and Research scholarships, respectively. Professor Dr. Vladimir Lavayen is thanked for his support in the characterization analysis.

Appendix A. Supplementary data

Supplementary material related to this article can be found, in the online version, at doi:<https://doi.org/10.1016/j.jwpe.2020.101410>.

References

- [1] M. Yellishetty, G.M. Mudd, Substance flow analysis of steel and long term sustainability of iron ore resources in Australia, Brazil, China and India, *J. Clean. Prod.* 84 (2014) 400–410, <https://doi.org/10.1016/j.jclepro.2014.02.046>.
- [2] G. Zhen, X. Lu, Y.-Y. Li, Y. Liu, Y. Zhao, Influence of zero valent scrap iron (ZVSI) supply on methane production from waste activated sludge, *Chem. Eng. J.* 263 (2015) 461–470, <https://doi.org/10.1016/j.cej.2014.11.003>.
- [3] Y. Liu, Q. Wang, Y. Zhang, B.-J. Ni, Zero valent iron significantly enhances methane production from waste activated sludge by improving biochemical methane potential rather than hydrolysis rate, *Sci. Rep.* 5 (2015) 1–6.
- [4] E. GilPavas, S. Correa-Sánchez, D.A. Acosta, Using scrap zero valent iron to replace dissolved iron in the Fenton process for textile wastewater treatment: Optimization and assessment of toxicity and biodegradability, *Environ. Pollut.* 252 (2019) 1709–1718.
- [5] E. Cuervo Lumbaque, E.R. Lopes Tiburtius, M. Barreto-Rodrigues, C. Sirtori, Current trends in the use of zero-valent iron (Fe⁰) for degradation of pharmaceuticals present in different water matrices, *Trends Environ. Anal. Chem.* 24 (2019) e00069, <https://doi.org/10.1016/j.teac.2019.E00069>.
- [6] F. Fu, D.D. Dionysiou, H. Liu, The use of zero-valent iron for groundwater remediation and wastewater treatment: a review, *J. Hazard. Mater.* 267 (2014) 194–205.
- [7] S. Adityasulindro, C. Julcour, L. Barthe, Heterogeneous Fenton oxidation using Fe-ZSM5 catalyst for removal of ibuprofen in wastewater, *J. Environ. Chem. Eng.* 6 (2018) 5920–5928, <https://doi.org/10.1016/j.jece.2018.09.007>.
- [8] S.G. Huling, B.E. Pivetz, In-situ Chemical Oxidation (No. EPA/600/R-06/072), Washington, DC (2006).
- [9] J. He, X. Yang, B. Men, D. Wang, Interfacial mechanisms of heterogeneous Fenton reactions catalyzed by iron-based materials: a review, *J. Environ. Sci.* 39 (2016) 97–109, <https://doi.org/10.1016/j.jes.2015.12.003>.
- [10] R.W. Becker, M. Ibáñez, E.C. Lumbaque, M.L. Wilde, T.F. da Rosa, F. Hernández, C. Sirtori, Investigation of pharmaceuticals and their metabolites in Brazilian hospital wastewater by LC-QTOF MS screening combined with a preliminary exposure and in silico risk assessment, *Sci. Total Environ.* (2019) 134218, <https://doi.org/10.1016/j.scitotenv.2019.134218>.
- [11] L. Prieto-Rodríguez, S. Miralles-Cuevas, I. Oller, A. Agüera, G.L. Puma, S. Malato, Treatment of emerging contaminants in wastewater treatment plants (WWTP) effluents by solar photocatalysis using low TiO_2 concentrations, *J. Hazard. Mater.* 211 (2012) 131–137.
- [12] L. Kothhoff, J. Keller, D. Lörchner, T.F. Mekonnen, M. Koch, Transformation products of organic contaminants and residues—overview of current simulation methods, *Molecules*. 24 (2019) 753, <https://doi.org/10.3390/molecules24040753>.
- [13] D. Fatta-Kassinos, M.I. Vasquez, K. Kümmerer, Transformation products of pharmaceuticals in surface waters and wastewater formed during photolysis and advanced oxidation processes – degradation, elucidation of byproducts and assessment of their biological potency, *Chemosphere* 85 (2011) 693–709, <https://doi.org/10.1016/j.chemosphere.2011.06.082>.
- [14] E. Cuervo Lumbaque, D. Salmoria Araújo, T. Moreira Klein, E.R. Lopes Tiburtius, J. Argüello, C. Sirtori, Solar photo-Fenton-like process at neutral pH: Fe(III)-EDDS complex formation and optimization of experimental conditions for degradation of pharmaceuticals, *Catal. Today* (2019), <https://doi.org/10.1016/j.cattod.2019.01.006>.
- [15] N.D.H. Khaleel, W.M.M. Mahmoud, O. Olsson, K. Kümmerer, Studying the fate of the drug Chlorprothixene and its photo transformation products in the aquatic environment: identification, assessment and priority setting by application of a combination of experiments and various in silico assessments, *Water Res.* 149 (2019) 467–476.
- [16] Guidelines for Testing of Chemicals, Simulation Test-Aerobic Sewage Treatment 303^a, (1999).
- [17] L.A. Pérez-Estrada, S. Malato, A. Agüera, A.R. Fernández-Alba, Degradation of dipyrone and its main intermediates by solar AOPs, *Catal. Today* 129 (2007) 207–214, <https://doi.org/10.1016/j.cattod.2007.08.008>.
- [18] R.C. Atkins, Colorimetric determination of iron in vitamin supplement tablets. A general chemistry experiment, *J. Chem. Educ.* 52 (1975) 550, <https://doi.org/10.1021/ed052p550>.
- [19] R.F.P. Nogueira, M.C. Oliveira, W.C. Paterlini, Simple and fast spectrophotometric determination of H_2O_2 in photo-Fenton reactions using metavanadate, *Talanta* 66 (2005) 86–91, <https://doi.org/10.1016/j.talanta.2004.10.001>.
- [20] E. Cuervo Lumbaque, R.M. Cardoso, A. Dalleggrave, L.O. dos Santos, M. Ibáñez, F. Hernández, C. Sirtori, Pharmaceutical removal from different water matrixes by Fenton process at near-neutral pH: doehlert design and transformation products identification by UHPLC-QTOF MS using a purpose-built database, *J. Environ. Chem. Eng.* 6 (2018) 3951–3961, <https://doi.org/10.1016/j.jece.2018.05.051>.
- [21] G. Patlewicz, N. Jeliakova, R.J. Safford, A.P. Worth, B. Aleksiev, An evaluation of the implementation of the Cramer classification scheme in the Toxtree software, *SAR QSAR Environ. Res.* 19 (2008) 495–524, <https://doi.org/10.1080/10629360802083871>.
- [22] US EPA, EPI Suite™-Estimation Program Interface, (2019) (Accessed November 3, 2019), <https://www.epa.gov/tsca-screening-tools/epi-suite-estimation-program-interface>.
- [23] US EPA, Ecological Structure Activity Relationships (ECOSAR), (2019) (Accessed October 3, 2019), <https://www.epa.gov/tsca-screening-tools/ecological-structure-activity-relationships-ecosar-predictive-model>.
- [24] M.E. Shaibani, M. Ghambari, Characterization and comparison of gray cast iron powder produced by target jet milling and high energy ball milling of machining

- scraps, Powder Technol. 212 (2011) 278–283, <https://doi.org/10.1016/J.POWTEC.2011.06.002>.
- [25] Y.-P. Sun, X. Li, J. Cao, W. Zhang, H.P. Wang, Characterization of zero-valent iron nanoparticles, Adv. Colloid Interface Sci. 120 (2006) 47–56, <https://doi.org/10.1016/J.CIS.2006.03.001>.
- [26] C. He, J. Yang, L. Zhu, Q. Zhang, W. Liao, S. Liu, Y. Liao, M. Asi, D. Shu, pH-dependent degradation of acid orange II by zero-valent iron in presence of oxygen, Sep. Purif. Technol. 117 (2013) 59–68, <https://doi.org/10.1016/j.seppur.2013.04.028>.
- [27] Z. Xiong, B. Lai, P. Yang, Y. Zhou, J. Wang, S. Fang, Comparative study on the reactivity of Fe/Cu bimetallic particles and zero valent iron (ZVI) under different conditions of N₂, air or without aeration, J. Hazard. Mater. 297 (2015) 261–268.
- [28] W. Yan, A.A. Herzing, C.J. Kiely, W. Zhang, Nanoscale zero-valent iron (nZVI): aspects of the core-shell structure and reactions with inorganic species in water, J. Contam. Hydrol. 118 (2010) 96–104.
- [29] A. Babuponnusami, K. Muthukumar, A review on Fenton and improvements to the Fenton process for wastewater treatment, J. Environ. Chem. Eng. 2 (2014) 557–572, <https://doi.org/10.1016/j.jece.2013.10.011>.
- [30] A. Shimizu, M. Tokumura, K. Nakajima, Y. Kawase, Phenol removal using zero-valent iron powder in the presence of dissolved oxygen: roles of decomposition by the Fenton reaction and adsorption/precipitation, J. Hazard. Mater. 201 (2012) 60–67.
- [31] Y. Yuan, B. Lai, Y.-Y. Tang, Combined Fe⁰/air and Fenton process for the treatment of dinitrodiazophenol (DDNP) industry wastewater, Chem. Eng. J. 283 (2016) 1514–1521.
- [32] Chemicalize.org, www.chemicalize.com, (2019). <https://chemicalize.com> (accessed August 15, 2019).
- [33] N. Fujioka, M. Suzuki, S. Kurosu, Y. Kawase, Linkage of iron elution and dissolved oxygen consumption with removal of organic pollutants by nanoscale zero-valent iron: effects of pH on iron dissolution and formation of iron oxide/hydroxide layer, Chemosphere. 144 (2016) 1738–1746.
- [34] F.A. Carey, R.J. Sundberg, Reduction of Carbon-Carbon Multiple Bonds, Carbonyl Groups, and Other Functional Groups, Adv. Org. Chem., Springer, 2007, pp. 367–471.
- [35] J. Cao, Z. Xiong, B. Lai, Effect of initial pH on the tetracycline (TC) removal by zero-valent iron: adsorption, oxidation and reduction, Chem. Eng. J. 343 (2018) 492–499, <https://doi.org/10.1016/J.CEJ.2018.03.036>.
- [36] A.M.E. Khalil, O. Eljamal, T.W.M. Amen, Y. Sugihara, N. Matsunaga, Optimized nano-scale zero-valent iron supported on treated activated carbon for enhanced nitrate and phosphate removal from water, Chem. Eng. J. 309 (2017) 349–365.
- [37] V. Springer, E. Pecini, M. Avena, Magnetic nickel ferrite nanoparticles for removal of dipyrone from aqueous solutions, J. Environ. Chem. Eng. 4 (2016) 3882–3890, <https://doi.org/10.1016/J.JECE.2016.08.026>.
- [38] B. Lai, Y. Zhou, J. Wang, Y. Zhang, Z. Chen, Passivation process and the mechanism of packing particles in the Fe⁰/GAC system during the treatment of ABS resin wastewater, Environ. Technol. 35 (2014) 973–983.
- [39] J. Vidmar, P. Oprčkal, R. Milačič, A. Mladenović, J. Ščančar, Investigation of the behaviour of zero-valent iron nanoparticles and their interactions with Cd²⁺ in wastewater by single particle ICP-MS, Sci. Total Environ. 634 (2018) 1259–1268.
- [40] P. Xie, L. Zhang, J. Chen, J. Ding, Y. Wan, S. Wang, Z. Wang, A. Zhou, J. Ma, Enhanced degradation of organic contaminants by zero-valent iron/sulfite process under simulated sunlight irradiation, Water Res. 149 (2019) 169–178, <https://doi.org/10.1016/J.WATRES.2018.10.078>.
- [41] Y. Segura, F. Martínez, J.A. Melero, Effective pharmaceutical wastewater degradation by Fenton oxidation with zero-valent iron, Appl. Catal. B Environ. 136–137 (2013) 64–69, <https://doi.org/10.1016/J.APCATB.2013.01.036>.
- [42] M.M. Hinojosa Guerra, I. Oller Alberola, S. Malato Rodríguez, A. Agüera López, A. Acevedo Merino, J.M. Quiroga Alonso, Oxidation mechanisms of amoxicillin and paracetamol in the photo-Fenton solar process, Water Res. 156 (2019) 232–240, <https://doi.org/10.1016/J.WATRES.2019.02.055>.
- [43] A.J. Expósito, J.M. Monteagudo, A. Durán, A. Fernández, Dynamic behavior of hydroxyl radical in sono-photo-Fenton mineralization of synthetic municipal wastewater effluent containing ulipyrine, Ultrason. Sonochem. 35 (2017) 185–195, <https://doi.org/10.1016/j.ultsonch.2016.09.017>.
- [44] M.G. Alalm, A. Tawfik, S. Ookawara, Degradation of four pharmaceuticals by solar photo-Fenton process: kinetics and costs estimation, J. Environ. Chem. Eng. 3 (2015) 46–51, <https://doi.org/10.1016/J.JECE.2014.12.009>.
- [45] I. Michael, E. Hapeshi, C. Michael, A.R. Varela, S. Kyriakou, C.M. Manaia, D. Fatta-Kassinos, Solar photo-Fenton process on the abatement of antibiotics at a pilot scale: degradation kinetics, ecotoxicity and phytotoxicity assessment and removal of antibiotic resistant enterococci, Water Res. 46 (2012) 5621–5634.
- [46] K.H. Chan, W. Chu, Modeling the reaction kinetics of Fenton's process on the removal of atrazine, Chemosphere. 51 (2003) 305–311, [https://doi.org/10.1016/S0045-6535\(02\)00812-3](https://doi.org/10.1016/S0045-6535(02)00812-3).
- [47] X. Liu, Z. Cao, Z. Yuan, J. Zhang, X.-P. Guo, Y. Yang, F. He, Y. Zhao, J. Xu, Insight into the kinetics and mechanism of removal of aqueous chlorinated nitroaromatic antibiotic chloramphenicol by nanoscale zero-valent iron, Chem. Eng. J. 334 (2017) 508–518, <https://doi.org/10.1016/j.cej.2017.10.060>.
- [48] Y. Zhang, L. Zhao, Y. Yang, P. Sun, Degradation of the antibiotic ornidazole in aqueous solution by using nanoscale zero-valent iron particles: kinetics, mechanism, and degradation pathway, RSC Adv. 8 (2018) 35062–35072.
- [49] B.H.J. Bielski, D.E. Cabelli, R.L. Arudi, A.B. Ross, Reactivity of HO₂/O₂⁻ radicals in aqueous solution, J. Phys. Chem. Ref. Data 14 (1985) 1041–1100.
- [50] F. Collin, Chemical basis of reactive oxygen species reactivity and involvement in neurodegenerative diseases, Int. J. Mol. Sci. 20 (2019) 2407.
- [51] P. Wardman, Reduction potentials of one-electron couples involving free radicals in aqueous solution, J. Phys. Chem. Ref. Data 18 (1989) 1637–1755.
- [52] G.V. Buxton, C.L. Greenstock, W.P. Helman, A.B. Ross, Critical review of rate constants for reactions of hydrated electrons, hydrogen atoms and hydroxyl radicals (OH/O₂⁻ in aqueous solution, J. Phys. Chem. Ref. Data 17 (1988) 513–886.
- [53] M.J. Gómez, C. Sirtori, M. Mezcuca, A.R. Fernández-Alba, A. Agüera, Photodegradation study of three dipyrone metabolites in various water systems: identification and toxicity of their photodegradation products, Water Res. 42 (2008) 2698–2706, <https://doi.org/10.1016/j.watres.2008.01.022>.
- [54] M. Favier, R. Dewil, K. Van Eyck, A. Van Schepdael, D. Cabooter, High-resolution MS and MSn investigation of ozone oxidation products from phenazone-type pharmaceuticals and metabolites, Chemosphere. 136 (2015) 32–41, <https://doi.org/10.1016/J.CHEMOSPHERE.2015.04.010>.
- [55] A.S. Giri, A.K. Golder, Fenton, photo-fenton, H₂O₂ photolysis, and TiO₂ photocatalysis for dipyrone oxidation: drug removal, mineralization, biodegradability, and degradation mechanism, Ind. Eng. Chem. Res. 53 (2014) 1351–1358, <https://doi.org/10.1021/ie402279q>.
- [56] I. Carpinteiro, R. Rodil, J.B. Quintana, R. Cela, Reaction of diazepam and related benzodiazepines with chlorine. Kinetics, transformation products and in-silico toxicological assessment, Water Res. 120 (2017) 280–289, <https://doi.org/10.1016/J.WATRES.2017.04.063>.
- [57] X. Zhang, Y. Yang, J. Zhang, Y. Yang, F. Shen, J. Shen, B. Shao, Determination of emerging chlorinated byproducts of diazepam in drinking water, Chemosphere 218 (2019) 223–231, <https://doi.org/10.1016/J.CHEMOSPHERE.2018.11.076>.
- [58] B. Yang, C. Xu, R.S. Kookana, M. Williams, J. Du, G. Ying, F. Gu, Aqueous chlorination of benzodiazepines diazepam and oxazepam: kinetics, transformation products and reaction pathways, Chem. Eng. J. 354 (2018) 1100–1109, <https://doi.org/10.1016/J.CEJ.2018.08.082>.
- [59] J. Santiago-Morales, A. Agüera, Mdel M. Gómez, A.R. Fernández-Alba, J. Giménez, S. Esplugas, R. Rosal, Transformation products and reaction kinetics in simulated solar light photocatalytic degradation of propranolol using Ce-doped TiO₂, Appl. Catal. B Environ. 129 (2013) 13–29, <https://doi.org/10.1016/j.apcatb.2012.09.023>.
- [60] M.L. Wilde, W.M.M. Mahmoud, K. Kümmerer, A.F. Martins, Oxidation-coagulation of β-blockers by K₂Fe^{VI}O₄ in hospital wastewater: assessment of degradation products and biodegradability, Sci. Total Environ. 452–453 (2013) 137–147, <https://doi.org/10.1016/j.scitotenv.2013.01.059>.
- [61] M.L. Wilde, S. Montipó, A.F. Martins, Degradation of β-blockers in hospital wastewater by means of ozonation and Fe²⁺/ozonation, Water Res. 48 (2014) 280–295, <https://doi.org/10.1016/j.watres.2013.09.039>.
- [62] S.O. Ganiyu, N. Oturan, S. Raffy, G. Esposito, E.D. van Hullebusch, M. Cretin, M.A. Oturan, Use of sub-stoichiometric titanium oxide as a ceramic electrode in anodic oxidation and electro-fenton degradation of the beta-blocker propranolol: degradation kinetics and mineralization pathway, Electrochim. Acta 242 (2017) 344–354, <https://doi.org/10.1016/J.ELECTACTA.2017.05.047>.
- [63] A.G. Trovó, R.F.P. Nogueira, A. Agüera, A.R. Fernandez-Alba, S. Malato, Paracetamol degradation intermediates and toxicity during photo-Fenton treatment using different iron species, Water Res. 46 (2012) 5374–5380.
- [64] M. Shamsipur, A. Pashabadi, A.A. Taherpour, K. Bahrami, H. Sharghi, Manganese mediated oxidation of progesterone in alkaline medium: mechanism study and quantitative determination, Electrochim. Acta 225 (2017) 292–302.
- [65] S. Tisler, F. Zindler, F. Freeling, K. Nödler, L. Toelgyesi, T. Braunbeck, C. Zwiener, Transformation products of fluoxetine formed by photodegradation in water and biodegradation in zebrafish embryos (Danio rerio), Environ. Sci. Technol. 53 (2019) 7400–7409.
- [66] United Nations, Economic Commission for Europe, Secretariat, Globally Harmonized System of Classification and Labelling of Chemicals (GHS), United Nations, 2011.

SUPPORTING INFORMATION

Degradation of a mixture of pharmaceuticals in hospital wastewater by a zero-valent scrap iron (ZVSI) combined reduction-oxidation process

*Elisabeth Cuervo Lumbaque^a, Marcelo Luís Wilde^a, Fabricio Abella Lopes^a, Ellen De Souza Almeida Duarte^b, Elaine Regina Lopes Tiburtius^c, Marcio Barreto Rodrigues^b,
Carla Sirtori^{a*}*

^aInstituto de Química- Universidade Federal do Rio Grande do Sul, Av. Bento Gonçalves, 9500, Porto Alegre-RS, Brazil.

^b Universidade Tecnológica Federal do Paraná. Via do Conhecimento, km 1 s/n, Pato Branco –PR, Brazil.

^c Universidade Estadual de Ponta Grossa, Av. General Carlos Cavalcanti, 4748, Ponta Grossa- PR, Brazil.

* To whom all correspondence should be addressed

e-mail: carla.sirtori@ufrgs.br (Prof. Carla Sirtori)

S1. Aqueous matrixes studied

Three aqueous matrixes employed were distilled water (DW), simulated wastewater (SWW), and raw hospital wastewater (RHWW). The composition of the SWW was adapted from the OECD recommendation (OECD, 1999). The characteristics of the RHWW can be seen in the table S.1. The RHWW employed in the degradation studies was used as collected (without filtration). The pharmaceutical compounds were spiked into the different aqueous matrixes, prior to pH adjustment.

Table S.1 Main physicochemical characteristics of the RHWW matrix

Parameters (units)	Value	Method	LOD	LOQ
pH	9.9	SMEWW 4500-H ⁺ B		
Conductivity ($\mu\text{S cm}^{-1}$)	1132	SMEWW 2510 B	1	0.2
Dissolved organic carbon (mg L^{-1})	67.6	SMEWW 5310	1.68	3.99
Chemical oxygen demand ($\text{mg L}^{-1} \text{O}_2$)	173	SMEWW 5220 B	5	0.8
Biological oxygen demand ($\text{mg L}^{-1} \text{O}_2$)	92	SMEWW 5210 B	2	0.6
Total solids (mg L^{-1})	415	SMEWW 2540 B	10	5
Total suspended solids (mg L^{-1})	156	SMEWW 2540 D	10	5
Chloride – Cl ⁻ (mg L^{-1})	69.2	SMEWW 4110 B	0.5	0.02
Total phosphate – PO_4^{3-} (mg L^{-1})	22.27	SMEWW 4500 P E	0.03	0.006

SMEWW – Standard Methods for the examination of water and wastewater (American Public Health Association et al., 1998).

S2. Characterization of the ZVSI

Granulometric analysis was performed according to a standard method [1]. Powder X-ray diffraction analyses employed a Rigaku Miniflex 600 instrument operated with a $\text{CuK}\alpha$ radiation source ($\lambda = 1.5418 \text{ \AA}$), 15 mA current, and 40 kV voltage. Scanning was performed in the 2θ range from 10 to 90° , at a rate of 2° min^{-1} , with a step size of 0.02° . Scanning electron microscopy images were obtained using a Tescan Vega3 LMU microscope. EDS mapping was performed using an Oxford Instruments system operated at 15 kV and equipped with a backscattered electron detector.

For determination of the point of zero charge, 0.1 g amounts of ZVSI were added to Erlenmeyer flasks, together with 50 mL volumes of pharmaceutical solutions containing 0.1 mol L^{-1} NaCl, at different initial pH values in the range from 1 to 11. The mixtures were stirred for 24 h, followed by zeta potential determination using a Zeta Plus instrument (Brookhaven Instruments), at $\lambda = 660 \text{ nm}$.

S.3 Experimental conditions: Doehlert Design

Table S.3.1 Doehlert design for pharmaceuticals degradation through combined reduction-oxidation process.

VARIABLE 1					
Codified value	-1	-0.5	0	0.5	1
[H ₂ O ₂] (mg L ⁻¹)	10	32.5	55	77.5	100
[H ₂ O ₂] (mmol L ⁻¹)	0.29	0.95	1.62	2.28	2.94
VARIABLE 2					
Codified value	-0.866		0	0.866	
ZVISI(g L ⁻¹)	0.5		1.25	2	
QUADRATIC MODEL					
Experiment number	[H ₂ O ₂]	ZVISI	Response (% Decrease Σ area) ^a		
1	1	0	91.35		
2	0.5	0.866	97.95		
3	-1	0	83.37		
4	-0.5	-0.866	88.61		
5	0.5	-0.866	98.36		
6	-0.5	0.866	99.06		
7	0	0	94.33		
8	0	0	92.01		
9	0	0	91.29		

^aSolar photo-Fenton treatment time (t_{30w}):25.2 min.

Table S.3.2 Selected ANOVA parameters.

ANOVA parameters	
Matrixes	DW
Parameter number (p)	6
Experiments number (n)	9
Level number (m)	7
Significance (α)	0.051

Table S.3.3 Analysis of variance for quadratic model in photo-Fenton process for DW and SW matrixes.

Analysis of Variance - Quadratic Model					
VS	QS	DF	QM	F test.	P
Regression	205.23	5	41.045	24.0458 ^b	0.013
Residuals	5.1209	3	1.707		
Lack of fit	0.0719	1	0.0719	0.028471	0.882
Pure error	5.049	2	2.5245		
Total	210.35	8			
<i>% Variance explained</i>				97.57	
<i>% Maximum variance explainable</i>				97.60	

^bSignificant values

VS: variance source, QS: quadratic sums, DF: degrees of freedom, QA: quadratic mean, F test: calculated value of measured test F, p: statistical parameter p.

Table S.3.4 Coefficients for DW and SWW matrixes.

Coefficients	
	DW
x ₀	92.54
x ₁	4.098
x ₂	2.899
x ₁ ²	-5.18
x ₂ ²	6.332
x ₁ x ₂	-6.27

Model equation: $Y = 92.54 + 4.098 \cdot x_1 + 2.899 \cdot x_2 - 5.184 \cdot x_1^2 + 6.332 \cdot x_2^2 - 6.272 \cdot x_1 x_2$

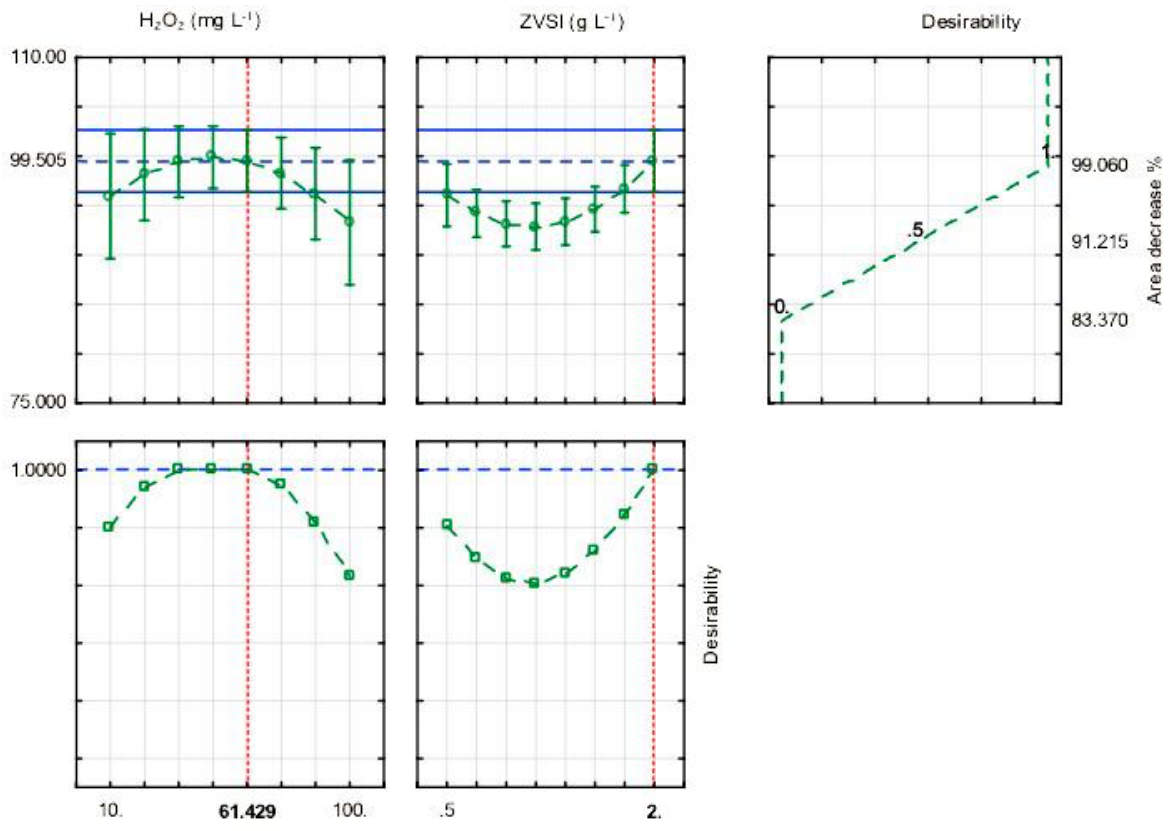
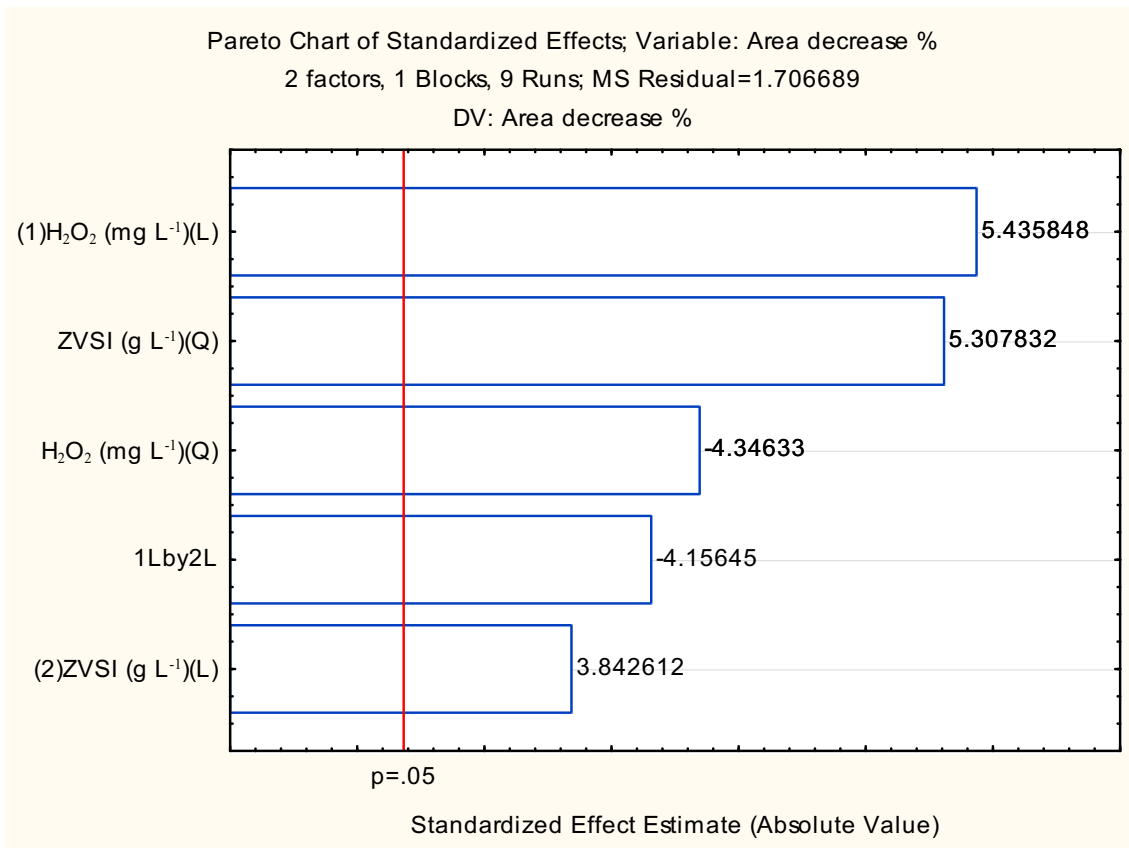


Fig S.3.1 Profiles of predicated values and desirability functions for the pharmaceuticals degradation.



FigS.3.2 Standardized main effect Pareto chart for the Doehlert design of pharmaceutical degradation. The vertical line in the chart defines 95% confidence level.

S.4 LC-QTOF MS analysis

The LC was equipped with a reverse-phase Hypersil Gold C18 analytical column (2.1 mm × 150 mm × 3 μm). When ionization in positive mode was selected, the mobile phase was a mixture of MeOH acidified with 0.1% formic acid (A) and H₂O acidified with 0.1% formic acid (B) at a flow rate of 0.5 mL/min. In this case, the gradient progressed from 10% A (initial conditions) to 90% A in 10 min, and then maintained for 2 min. The QTOF mass spectrometer was operated in positive ionization mode under the following conditions: capillary 4000 V, nebulizer 40 psi, drying gas 9 L/min, gas temperature 200 °C. In all analyses, the injection volume was 5 μL. The samples injected were previously filtered through a 0.22 μm PVDF filter. The QTOF MS system was operated in broadband collision-induced dissociation (bbCID) acquisition mode that provided MS and MS/MS spectra at the same time. All MS information was recorded over the *m/z* range of 50–1000 with a scan rate of 2 Hz. The bbCID mode allowed for work with two different collision energies: one with a Low Collision Energy (LE) of 10 eV, and a second that applies a High Collision Energy (HE) of 70 eV to obtain MS/MS spectra. TargetAnalysis and DataAnalysis 4.2 software's were employed for analyzes and, in most cases, for ions with a deviation of ±5 ppm of error were assigned possible elemental compositions and double-bond equivalent (RDB).

Limit of detection (LOD) and limit of quantification (LOQ) for each pharmaceutical studied, in both water matrixes, were determined for the quantification method developed in this work (see Table S.4.1).

Table S.4.1. Parameters for quantification method used to determine pharmaceuticals in different matrixes studied.

Matrix	DW		SWW		RHWW	
Pharmaceuticals	LOD ($\mu\text{g L}^{-1}$)	LOQ ($\mu\text{g L}^{-1}$)	LOD ($\mu\text{g L}^{-1}$)	LOQ ($\mu\text{g L}^{-1}$)	LOD ($\mu\text{g L}^{-1}$)	LOQ ($\mu\text{g L}^{-1}$)
Paracetamol (PCT)	0.25	0.83	0.47	1.56	0.1	0.33
Propranolol (PPN)	0.03	0.10	0.05	0.18	0.04	0.13
Dipyron (DIP)	0.36	1.19	0.44	1.47	0.88	2.94
Fluoxetine (FXT)	4.29	14.28	1.25	4.16	1.07	3.57
Progesterone (PRG)	0.025	0.08	0.09	0.31	0.23	0.77
Diazepam (DZP)	0.01	0.03	0.01	0.03	0.04	0.13

S.5 Preliminary studies

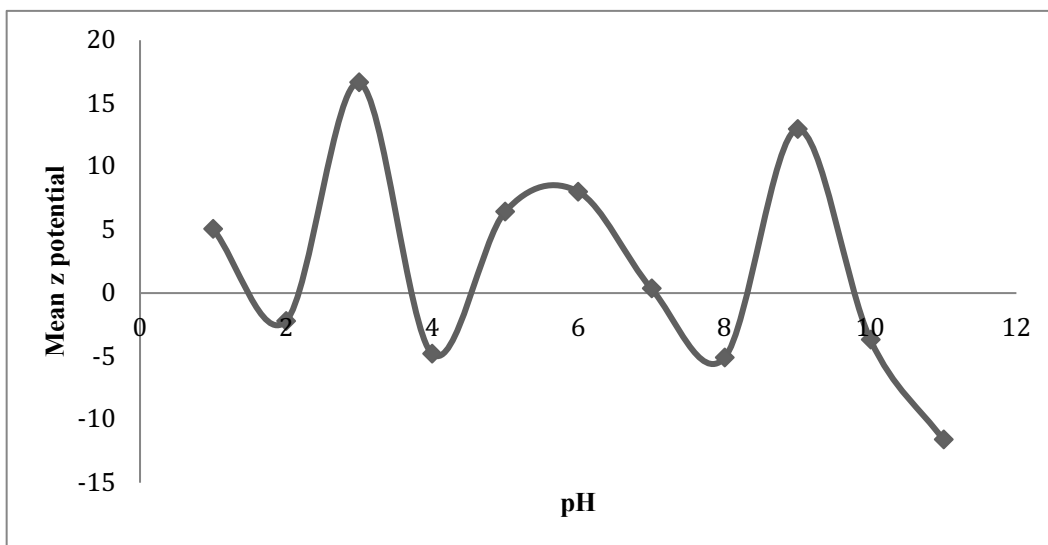


Figure S.5.1 Zeta potential of ZVSI in different pH

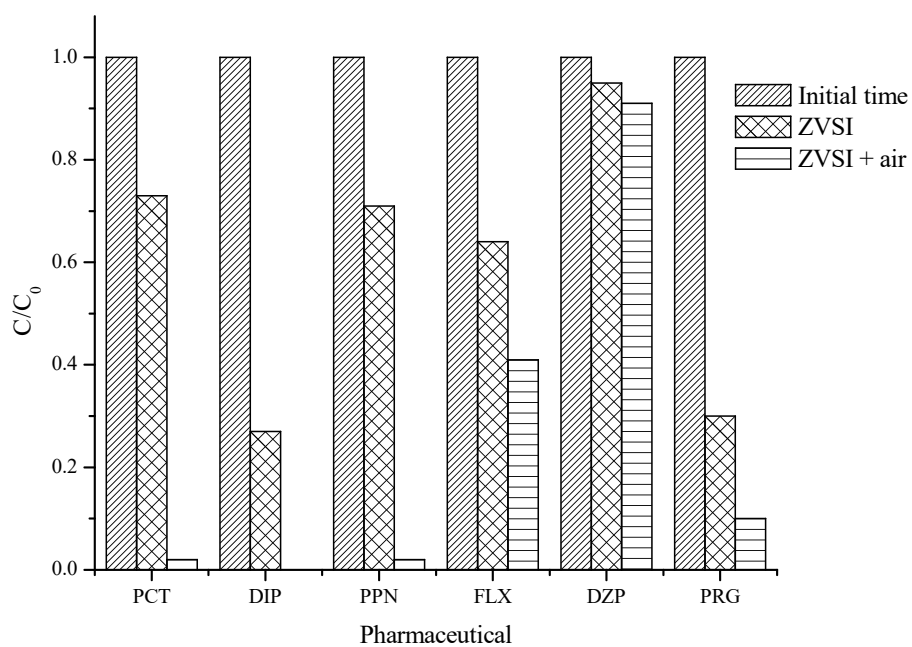


Fig S.5.2 Area decrease of pharmaceuticals with ZVSI and ZVSI with air for 60 minutes in darkness.

S.6 Microspecies distribution according pH values

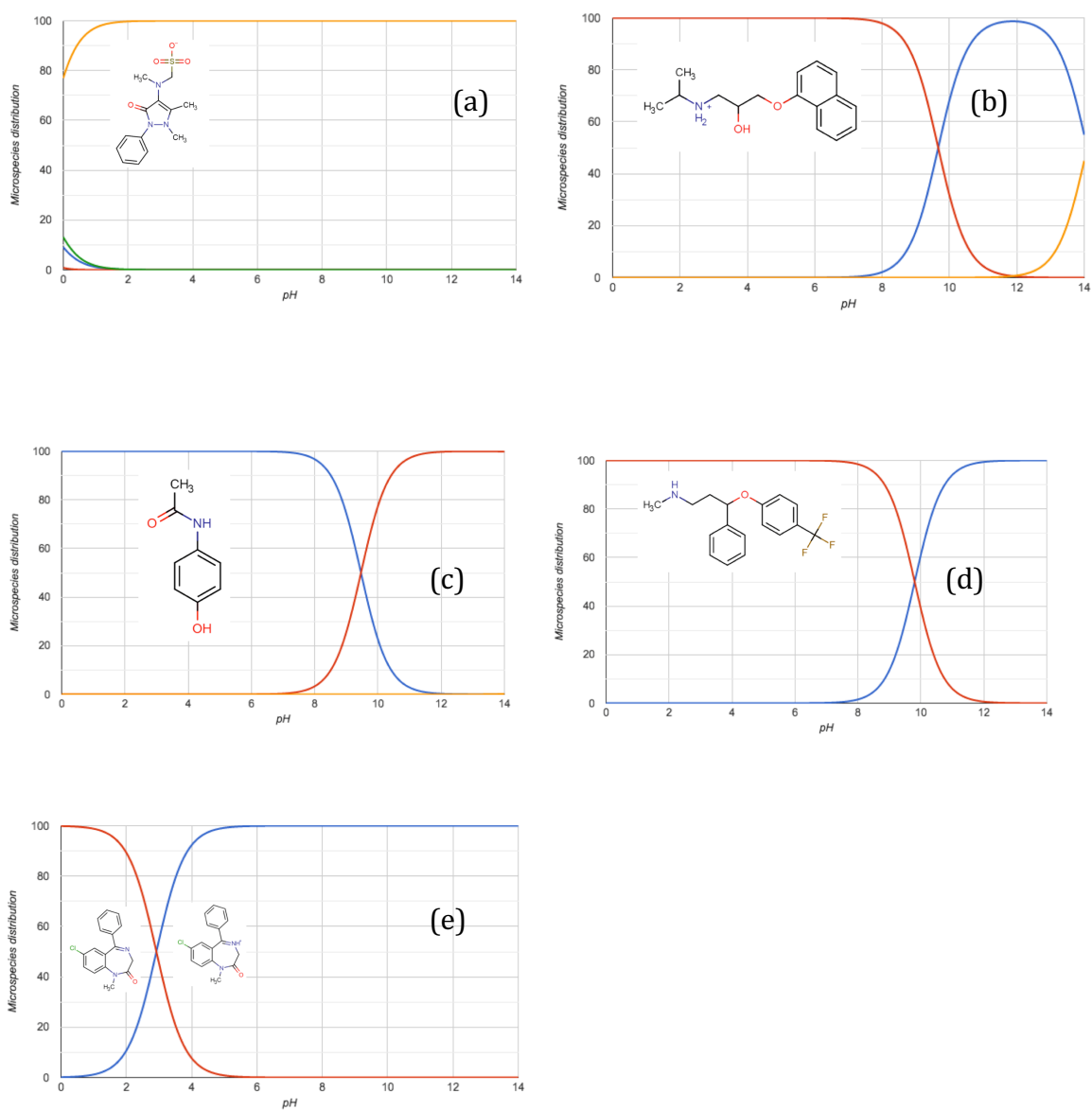


Fig. S.6.1 Micro-species distribution of DIP (a), PPN (b), PCT (c), FLX (d) and DZP

(e). Calculated values using Chemicalize.org by ChemAxon Chemicalize.org.

S.7 Transformation products

Table S.7.1. TPs identified through reductive-oxidative process at pH 3.0 in DW, SWW and RHW matrixes.

Compound	Rt (min)	Ion Mass (<i>m/z</i>)		Error (ppm)	DBE	Matrix			
		Ion Formula [M-H] ⁺	Experimental			Calculated	DW	SWW	RHW
TP2 DIP	3.1	C₁₁H₁₅N₂O₃	223.1075	223.1077	0.9	5.5		X	
		C ₈ H ₁₀ N	120.0808	120.0808	0.2	4.5			
TP3 DIP	2	C₁₁H₁₃N₂O₃	221.0921	221.0921	0	6.5			X
		C ₁₀ H ₁₁ N ₂ O	175.0864	175.0866	0.9	6.5			
		C ₁₀ H ₈ NO	158.0599	158.06	0.6	7.5			
TP7 DIP	5.3	C₁₂H₁₆N₃O₃	250.1186	250.1186	0.1	6.5	X		
		C ₁₀ H ₁₄ N ₃ O ₂	208.1078	208.1081	1.3	5.5			
		C ₉ H ₁₃ N ₂ O	165.1016	165.1022	3.8	4.5			
		C ₇ H ₁₁ N ₂	123.0912	123.0917	3.6	3.5			
TP9 DIP	3.8	C₁₁H₁₃N₂O₂	205.0972	205.0972	-0.3	6.5		X	X
		C ₁₀ H ₁₃ N ₂ O	177.1022	177.1022	0.5	5.5			
		C ₈ H ₁₀ N	120.0806	120.0808	1.5	4.5			
TP17 DIP	4.4	C₁₂H₁₄N₃O₂	232.108	232.1081	0.1	7.5	X		X
		C ₆ H ₁₄ NO	116.1066	116.107	3.4	0.5			
TP2 AAA	5.1	C₁₃H₁₆N₃O₃	262.1189	262.1186	-0.9	7.5			X
		C ₆ H ₁₃ O ₃	133.0861	133.0859	-1	0.5			
		C ₄ H ₉ O ₂	89.0601	89.0597	-4.3	0.5			
TP9 AAA	1.1	C₈H₁₀NO	136.0757	136.0757	0.1	4.5			X
		C ₈ H ₇ O	119.0492	119.0491	-0.1	5.5			
		C ₆ H ₇ O	95.0492	95.0491	-0.9	3.5			
		C ₇ H ₇	91.0543	91.0542	-1.3	4.5			
		C ₄ H ₈ NO	86.0602	86.06	-1.9	1.5			

TP3 FAA	4.6	C₁₁H₁₃N₂O₄	237.0871	237.087	-0.5	6.5			X
		C ₈ H ₁₁ N ₂ O	151.0861	151.0866	2.9	4.5			
		C ₇ H ₆ NO	120.0443	120.0444	0.5	5.5			
		C ₆ H ₈ N	94.0652	94.0651	-0.9	3.5			
TP1 DZP	7.8	C₁₄H₁₃ClNO	246.0681	246.068	-0.2	8.5	X		
		C ₁₄ H ₁₁ ClN	228.0575	228.0575	-0.3	9.5			
		C ₇ H ₅ O	105.0335	105.0335	-0.3	5.5			
TP2 DZP	9.3	C₁₆H₁₅ClNO₃	304.0746	304.0735	-3.7	9.5			X
		C ₁₀ H ₁₁ O ₃	179.0698	179.0703	2.4	5.5			
TP5 DZP	8.3	C₁₅H₁₂ClN₂O	271.063	271.0633	0.8	10.5	X		
		C ₅ H ₁₂ NO	102.0912	102.0913	1.2	0.5			
		C ₄ H ₉	57.0696	57.0699	5.1	0.5			
TP6 DZP	6.9	C₁₆H₁₆ClN₂O₂	303.0902	303.0895	-2.4	9.5		X	X
		C ₁₄ H ₁₁ ClN	228.0574	228.0575	0.2	9.5			
		C ₁₄ H ₁₃ ClNO	246.0681	246.068	-0.4	8.5			
TP16 FXT	1.2	C₉H₈NO	146.06	146.06	0.6	6.5		X	X
TP2 PCT	8	C₆H₆NO₃	140.0349	140.0342	-5	4.5			X
		C ₅ H ₆ NO ₂	112.0393	112.0393	-0.1	3.5			
TP3 PCT	1.6	C₈H₁₀NO₄	184.0602	184.0604	1.3	4.5	X		
		C ₆ H ₆ NO ₂	124.0395	124.0393	-1.4	4.5			
		C ₄ H ₆ N	68.0497	68.0495	-2.6	2.5			
TP2 PPN	1.3	C₆H₁₄NO₂	132.1018	132.1019	0.6	0.5		X	X
		C ₅ H ₁₂ N	86.0965	86.0964	-0.9	0.5			
TP3 PPN	0.9	C₆H₁₆NO₂	134.1174	134.1176	0.9	-0.5	X		X
		C ₃ H ₈ NO	74.06	74.06	0.6	0.5			
		C ₄ H ₁₀ N	72.0806	72.0808	2.3	0.5			
		C ₃ H ₆ N	56.0492	56.0495	4.5	1.5			
TP7 PPN	3.9	C₁₄H₂₀NO₄	266.1389	266.1387	-0.9	5.5	X		X
		C ₁₁ H ₁₄ NO ₄	224.0921	224.0917	-1.8	5.5			
TP22 PPN	4.7	C₁₆H₂₂NO₄	292.155	292.1543	-2.4	3.5	X		

		C ₉ H ₇ O	131.0492	131.0491	-0.3	44.3		
		C ₆ H ₁₄ NO	116.1071	116.107	-0.5	6.8		
TP26/27 PPN	4.9	C₁₆H₂₂NO₅	308.1497	308.1492	-1.4	6.5	X	X
		C ₁₆ H ₂₀ NO ₄	290.1387	290.1387	0.1	7.5		
TP37 PPN	11.4	C₈H₇O₄	167.0338	167.0339	0.3	5.5	X	
		C ₈ H ₅ O ₃	149.0233	149.0233	0.4	6.5		
TP45 PPN	6.7	C₁₆H₂₆NO₄	296.1836	296.1856	6.8	4.5	X	X
		C ₆ H ₁₃ O ₃	133.086	133.0859	-0.4	0.5		
		C ₄ H ₉ O ₂	89.06	89.0597	-3.2	0.5		
TP3 PRG	9	C₂₁H₂₉O₂	313.2158	313.2162	1.3	7.5	X	
		C ₄ H ₉	57.0706	57.0699	-13.1	0.5		

X means that the TPs were found at the aqueous matrix indicated.

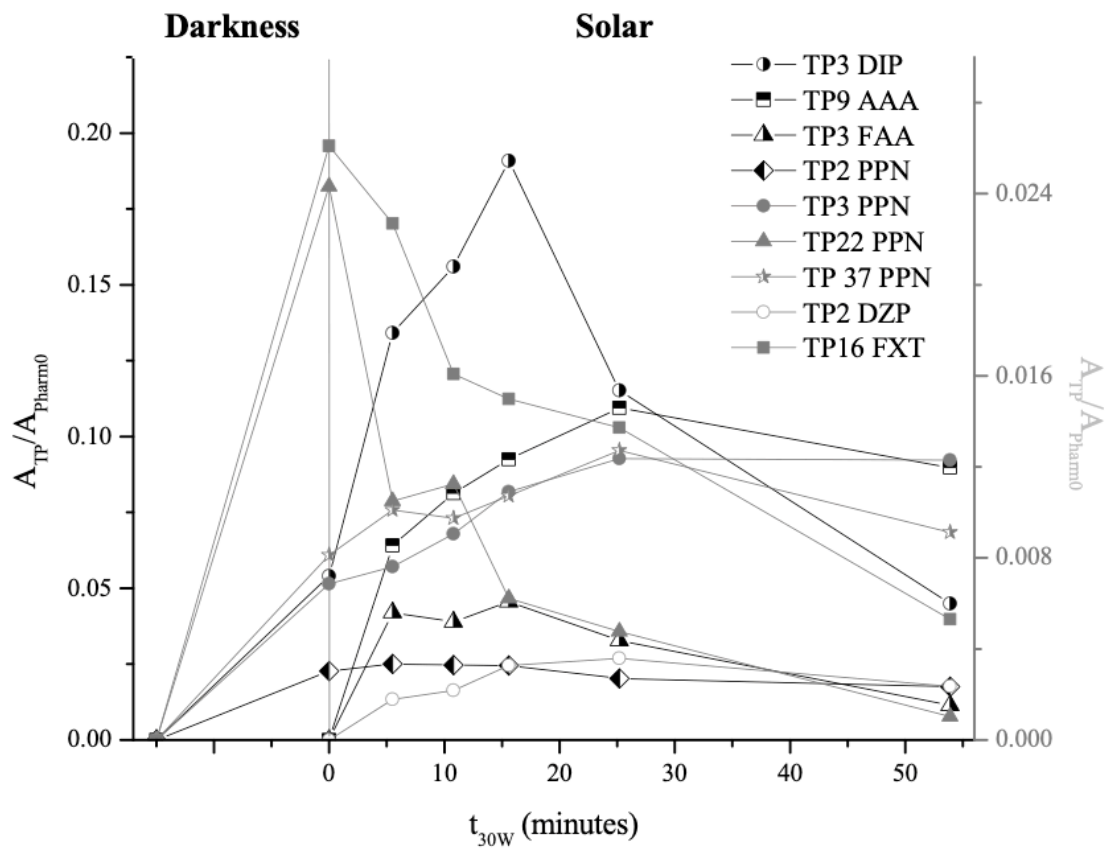


Fig S.7.1 Profile of the most persistent TPs in the reductive-oxidative process.

Table S.7.2. Biodegradability and toxicological Hazard of pharmaceuticals and TPs generated through reduction-oxidation process.

Pharm.	Biodegradability		Toxicity									
	EPI-suite	TOXTREE	TOXTREE	ECOSAR								
			Cramer Toxicity	Acute (mg L ⁻¹) ^a			Chronic (ChV) (mg L ⁻¹) ^a			LC ₅₀ ratios (TP/Pharm)		EC ₅₀ ratios (TP/Pharm)
	BIOWIN	START		Fish 96h-LC ₅₀	Daphnid 48h-LC ₅₀	Green algae 96h-EC ₅₀	Fish 96h-LC ₅₀	Daphnid 48h-LC ₅₀	Green algae 96h-EC ₅₀	Fish 96h	Daphnid 48h	Green algae 96h
DIP	NO	Persistent	High	474.00	46.90	56.00	48.80	3.21	16.30	1.00	1.00	1.00
TP2 DIP	YES	Persistent	High	38.4	20.7	6.93	198	20.7	0.602	0.08	0.44	0.12
TP3 DIP	YES	Persistent	Intermediate	23.1	15.1	5.16	100	12	0.469	0.05	0.32	0.09
TP7 DIP	NO	Persistent	Intermediate	13.70	11.50	4.06	47.90	6.89	0.39	0.03	0.25	0.07
TP9 DIP	NO	Persistent	Intermediate	13.3	10.4	3.65	49	6.73	0.346	0.03	0.22	0.07
TP17 DIP	NO	Persistent	Low	2x10 ⁷	9.69x10 ⁵	5.88x10 ⁶	2.81x10 ⁸	2.99x10 ⁴	9.44x10 ⁵	47046	20660	1.05x10 ⁵
TP2 AAA	NO	Persistent	High	65.30	201.00	264.00	0.03	19.80	138.00	0.14	4.29	4.71
TP9 AAA	NO	Persistent	Low	190.00	212.00	16.60	1.67	25.20	7.14	0.40	4.52	0.30
TP3 FAA	NO	Persistent	Intermediate	19.40	13.90	4.82	77.60	9.98	0.45	0.04	0.30	0.09
DZP	NO	Persistent	High	22.60	19.80	3.55	0.40	4.24	3.08	1.00	1.00	1.00
TP1 DZP	NO	Persistent	High	1.99	1.39	2.42	0.25	0.24	1.00	0.09	0.07	0.68
TP2 DZP	NO	Persistent	High	29.80	26.50	4.47	0.50	5.44	3.69	1.32	1.34	1.26
TP5 DZP	NO	Persistent	High	144.00	83.60	67.50	14.40	8.60	18.40	6.37	4.22	19.01
TP6 DZP	NO	Persistent	High	85.30	9.88	8.64	5.44	0.79	2.81	3.77	0.50	2.43
FXT	NO	Persistent	High	1.08	0.18	0.08	0.03	0.02	0.03	1.00	1.00	1.00
TP 16 FXT	YES	Persistent	High	1350.00	689.00	328.00	116.00	49.70	67.40	1250	3937.14	4151.90
PCT	NO	Persistent	High	320.00	63.30	26.30	26.50	5.12	37.00	1.00	1.00	1.00
TP2 PCT	NO	Persistent	Low	27.7	1.2	3.62	0.201	0.267	0.551	1.79	1.37	1.63
TP3 PCT	YES	Persistent	Low	32.2	1.35	4.16	0.23	0.301	0.63	2.08	1.54	1.87
PPN	NO	Persistent	High	20.20	2.58	1.85	0.95	0.23	0.65	1.00	1.00	1.00

TP2 PPN	NO	Persistent	Low	869.00	78.90	112.00	116.00	4.97	30.40	43.02	30.58	60.54
TP3 PPN	YES	Easily	High	1999.00	170.00	272.00	321.00	10.10	70.90	98.96	65.89	147.03
TP7 PPN	YES	Easily	Low	54.60	55.30	28.80	13.40	0.50	9.51	2.70	21.43	15.57
TP22 PPN	YES	Persistent	Low	38.70	37.60	20.50	7.62	0.37	7.29	1.92	14.57	11.08
TP26 PPN	YES	Easily	Low	12300.00	1160.00	1510.00	1450.00	75.80	425.00	608.91	449.61	816.22
TP37 PPN	YES	Easily	Low	9320.00	4860.00	2540.00	824.00	373.00	549.00	461.39	1883.72	1372.97
TP 45 PPN	NO	Persistent	Low	1220.00	115.00	152.00	146.00	7.52	42.50	60.40	44.57	82.16
PRG	NO	Persistent	High	17.10	6.78	5.57	2.53	1.48	3.63	1.00	1.00	1.00
TP3 PRG	NO	Persistent	High	24.80	10.50	8.27	4.01	2.19	4.92	1.45	1.55	1.48

^aThe predicted toxicity values by ECOSAR were classified according to the system established by the Globally Harmonized System of Classification and Labeling of Chemicals (GHS) (United Nations, 2011): not harmful $LC_{50}/EC_{50}/ChV > 100$; harmful $100 \geq LC_{50}/EC_{50}/ChV > 10$; toxic $10 \geq LC_{50}/EC_{50}/ChV > 1$; very toxic $LC_{50}/EC_{50}/ChV \leq 1$. Biodegradability predictions.

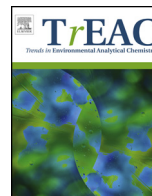
Table S.7.3. TPs identified through reductive-oxidative process: SMILES, BIOWIN data and class-specific estimations employed in toxicity and biodegradability predictions.

Comp	SMILES	Log Kow	BIOWIN	BIOWIN	BIOWIN	BIOWIN	BIOWIN	BIOWIN	BIOWIN	BIOWIN	Class-specific estimations
			1	2	3	4	5	6	7		
			Linear model	Non-linear model	Ultimate survey model (weeks)	Primary survey model (days-weeks)	MITI Linear model	MITI Non-Linear model	Anaerobic linear model		
DIP	<chem>O=C1N(C2=CC=CC=C2)N(C)C(C)=C1NC</chem>	9981	0.9260	0.9444	2.7655	3.5824	0.1414	0.0332	0.5157	NO	Hydrazines
TP2 DIP	<chem>O=C(C=O)N(C1=CC=C(C=C1)N(C)C(O)C</chem>	-2.16	1.2132	1	2.9123	3.8581	0.6147	0.5980	0.5075	YES	Hydrazines
TP3 DIP	<chem>O=C(C=O)N(C1=CC=C(C=C1)N(C)C(C)=O</chem>	7578	1.0554	0.9999	2.7568	3.7315	0.5103	0.3896	0.5405	YES	Hydrazines
TP7 DIP	<chem>O=C(C(NC)=O)N(C1=CC=CC=C1)N(C)C(C)=O</chem>	11.69	0.9671	0.9813	2.6161	3.6984	0.1395	0.0421	-0.2295	NO	Hydrazines
TP9 DIP	<chem>CN1C(C)C(=O)C(=O)N1c1ccccc1</chem>	7.64	0.7784	0.8708	2.7699	3.5580	0.1589	0.0542	0.4574	NO	Hydrazines
TP17 DIP	<chem>O=C1/[N+](N(C)C(C)=C1NC)=C(C=C2)C=CC2=O</chem>	15.326	0.7972	0.5874	2.6856	3.5322	0.1859	0.0380	-0.3490	NO	Aliphatic Amines
TP2 AAA	<chem>CN1N(C2=CC=CC=C2)C(C3(C)OC13NC(C)=O)=O</chem>	10.364	0.2462	0.0437	2.1567	3.3645	0.2405	0.0583	-1.1552	NO	Epoxides
TP9 AAA	<chem>CC(NC1=CC=CC=C1)=O</chem>	7.758	1.0214	0.9962	2.8683	3.8630	0.4781	0.5323	-0.0703	NO	Amides
TP3 FAA	<chem>O=C(C(O)=O)N(C1=CC=CC=C1)N(C)C(C)=O</chem>	9.923	0.8359	0.8906	3.0638	3.8974	0.2324	0.0745	0.6047	NO	Hydrazines
DZP	<chem>C1C1=CC=C2C(C(C3=CC=CC=C3)=NCCC(N2C)=O)=C1</chem>	9.647	0.7678	0.8085	2.3311	3.4819	0.0837	0.0217	-0.8789	NO	Amides
TP1 DZP	<chem>O=C(C1=CC(C1)=CC=C1NC)C2=CC=CC=C2</chem>	11.569	0.3493	0.0449	2.3142	3.2022	0.0135	0.0148	-0.8607	NO	Neutral organics
TP2 DZP	<chem>O=C(C1=CC(C1)=CC=C1N(C(C)=O)CO)C2=CC=CC=C2</chem>	14.578	0.9243	0.8624	2.4266	3.5617	0.3357	0.0888	-0.9920	NO	Amides

TP5 DZP	<chem>C1C1=CC=C(C(C(C2=C C=CC=C2)=N3)=C1)N(C)C3=O</chem>	7.836	0.5643	0.2589	2.4163	3.2967	-0.0209	0.0107	-0.1910	NO	Neutral organics
TP6 DZP	<chem>O=C(CN1)N(C)C(C(C1(O)C2=CC=CC=C2)=C3) =CC=C3C1</chem>	14.178	0.7291	0.6390	2.1036	3.3457	0.1310	0.0145	-1.0358	NO	Aliphatic Amines
FXT	<chem>FC(F)(F)C1=CC=C(OC (CCNC)C2=CC=CC=C 2)C=C1</chem>	9259	0.4937	0.1305	1.9910	3.2523	0.2360	0.0000	0.5562	NO	Aliphatic Amines
TP 16 FXT	<chem>O=C(CC#N)C1=CC=CC =C1</chem>	7749	1.1204	0.9990	2.7955	3.5558	0.5602	0.6065	0.2112	YES	Neutral organics
PCT	<chem>CC(NC1=CC=C(O)C= C1)=O</chem>	11041	1.0015	0.9886	2.8673	3.8748	0.4866	0.5090	-0.1124	NO	Phenol Amines
TP2 PCT	<chem>CC(NC1=CC(O)=CC(O) =C1)=O</chem>	14354	1.1097	0.9942	2.8883	3.8914	0.4950	0.4856	0.0638	NO	Phenol Amines
TP3 PCT	<chem>CC(NC1=CC(O)=C(O)C(O)=C1)=O</chem>	18276	1.2179	0.9971	2.9093	3.9080	0.5034	0.4623	0.2399	YES	Phenol Amines
PPN	<chem>OC(CNC(C)C)COC1=C C=CC2=CC=CC=C21</chem>	13966	1.0685	0.9782	2.7523	3.7234	0.3861	0.2010	0.2173	NO	Aliphatic Amines
TP2 PPN	<chem>CC(O)NCC(O)C=O</chem>	5331	1.2823	1	3.1160	4.0279	0.8766	0.9221	0.8038	NO	Aldehydes
TP3 PPN	<chem>CC(C)NCC(CO)O</chem>	7669	1.1554	0.9886	3.2492	3.9578	0.6698	0.7508	0.8400	YES	Aliphatic Amines
TP7 PPN	<chem>O=CC1=CC=CC=C1C(O CC(CNC(C)C)O)=O</chem>	133932	1.3926	1	2.9598	4.0633	0.9036	0.8760	0.6200	YES	Aldehydes
TP22 PPN	<chem>O/C(CO)C(C1=CC=CC(O)=C1C=O)=C(CO)=C N(C)C</chem>	14547	1.1256	0.9987	2.9344	3.9331	0.7164	0.4297	0.5186	YES	Aldehydes
TP26/27 PPN	<chem>O=C(O)C1=CC=CC=C1/ C(OCC(CNC(C)C)O)=C/ C=O</chem>	17503	1.0279	0.9991	2.8059	3.7717	0.8194/0.6 236	0.6595/0.3 432	0.3829	YES	Aliphatic Amines
TP37 PPN	<chem>O=CC1=CC=CC=C1/C(OCC(CNC(C)C)O)=C/C(O)=O</chem>	16233	0.9237	0.9949	3.0826	4.1495			0.3041	YES	Neutral organics
TP45 PPN	<chem>O=C(O)C1=CC=CC=C1 C(O)=O</chem>	9817	1.0222	0.9959	3.0078	3.6235	1.0047	0.9569	0.9855	YES	Aliphatic Amines
TP 45 PPN	<chem>OC(CNC(C)C)CO/C(C1 =CC=CC=C1CO)=C/CO</chem>		0.8896	0.4621	3.0421	3.8435	0.3826	0.1337	0.2790	NO	Aliphatic Amines
PRG	<chem>O=C1C=C2CCC3C(CC C4C(C)=O)C4(C)CCC3 C2(C)CC1</chem>	9446	0.2436	0.0030	2.0350	3.0427	0.3623	0.0674	-1.7307	NO	Vinyl/Propargyl/K etones
TP3 PRG	<chem>O=C1C=C2C=CC3C(CC C4C(C)=O)C4(C)CCC3 2(C)CC1</chem>	9171	0.2446	0.0031	2.0395	3.0456	0.3412	0.0481	-1.6377	NO	Vinyl/Propargyl/K etones

References

- [1] ABNT 7217, 1987. Aggregates – Determination of particle size composition. (version in portuguese).
- [2] Chemicalize.org, 2019. <https://chemicalize.com> (accessed 8.15.19).
- [3] OECD, Guidelines for Testing of Chemicals, Simulation Test-Aerobic Sewage Treatment 303^a, 1999.
- [4] Standard Methods for the examination of water and wastewater (American Public Health Association) 1998.



Current trends in the use of zero-valent iron (Fe⁰) for degradation of pharmaceuticals present in different water matrices

Elisabeth Cuervo Lumbaque^a, Elaine R. Lopes Tiburtius^b, Márcio Barreto-Rodrigues^c,
Carla Sirtori^{a,*}

^a Instituto de Química- Universidade Federal do Rio Grande do Sul, Av. Bento Gonçalves, 9500, Porto Alegre, RS, Brazil

^b Universidade Estadual de Ponta Grossa, Av. General Carlos Cavalcanti, 4748, Ponta Grossa, PR, Brazil

^c Universidade Tecnológica Federal de Paraná, Via do Conhecimento, km 1 s/n, Pato Branco, PR, Brazil

ARTICLE INFO

Article history:

Received 1 April 2019

Received in revised form 24 June 2019

Accepted 5 July 2019

Keywords:

Zero-valent iron
Pharmaceuticals
Water matrices
Degradation

ABSTRACT

Zero-valent iron (Fe⁰) has recently been proposed as a potential candidate for the degradation of pharmaceuticals, because Fe⁰ can release dissolved iron species, activate molecular oxygen, and react with oxidant species. Additionally, due to its small particle size and large surface area, this catalyst can provide better degradation results, compared to traditional processes. This work focuses on the elimination of pharmaceuticals present in different water matrices, considering the potential harm that these substances can cause in the environment. The mechanisms of pharmaceutical removal using Fe⁰ particles include reduction, adsorption, precipitation, and oxidation processes. Most studies have focused on oxidation processes in the presence of Fe⁰ and radicals derived from oxidants such as hydrogen peroxide (H₂O₂), ozone (O₃), peroxysulfate (SO₅²⁻), peroxydisulfate (S₂O₈²⁻), and oxygen (O₂). Most of the results have shown that high percentages of pharmaceuticals can be removed, degraded, and mineralized. The mechanisms of oxidation and the parameters that influence the degradation of pharmaceuticals, as well as the possible degradation pathways, are discussed here. This review provides information on trends of different processes that use Fe⁰, considering aspects such as particle size, type of matrix, the pharmaceuticals studied, and the results obtained that can improve understanding of new advances in the field of advanced oxidation processes (AOPs) for the degradation and elimination of pharmaceuticals.

© 2019 Elsevier B.V. All rights reserved.

1. Introduction

Zero-valent iron (Fe⁰) has received recent research attention for use in catalysts employed in heterogeneous Fenton and Fenton-like processes. Fe⁰, which has a standard reduction potential (E⁰) of -0.41 V (SHE), is one of the most promising materials for water and wastewater treatment at ambient pressure and temperature. Its advantages include small particle size and high surface area [1], low cost, green synthesis [2], low toxicity [3], easy association with other materials, and suitability for use in bioremediation [4]. It can provide efficient degradation or transformation of hazardous pollutants such as heavy metals [5], halogenated compounds [6], pesticides [7], surfactants [8], dyes [9], and phenolic compounds [10], among others.

The mechanisms of removal of organic contaminants using Fe⁰ particles include reduction, adsorption, precipitation, and

oxidation, with the process being highly pH-dependent. The use of Fe⁰ involves both homogeneous and heterogeneous processes, which may act synergistically. The dissolved iron ions leached from Fe⁰ contribute to homogeneous reactions [11], while Fe⁰ and its oxides on the surface participate in heterogeneous reactions. A lower initial pH accelerates the corrosion of Fe⁰ and releases more electrons, compared to a higher initial pH, while increase of the pH favors the formation of iron hydroxides that precipitate, hence decreasing the efficiency of the process [12]. During the oxidation process, Fe⁰ can release dissolved iron species and activate molecular oxygen [13], making it an effective catalyst for the generation of reactive oxygen species (ROS) from oxidants such as hydrogen peroxide (H₂O₂), peroxydisulfate (HSO₅⁻), peroxysulfate (SO₅²⁻), persulfate (S₂O₈²⁻), ozone (O₃), or oxygen (O₂). As a result, Fe⁰ can be used to remove and mineralize emerging pollutants [14].

In the last decades, pharmaceuticals have become recognized as bioactive chemicals present at different concentration levels (μg L⁻¹ and ng L⁻¹) in the environment. The increased production of these substances by pharmaceutical industries and their use in

* Corresponding author.

E-mail address: carla.sirtori@ufrgs.br (C. Sirtori).

hospitals, households, and veterinary activities has led to their increasing presence in wastewater. These compounds may be considered as emerging pollutants, because they are not yet regulated or are currently in the process of being regulated. Most countries do not yet possess the conditions for the control of these substances in wastewaters or natural waters [15].

Many pharmaceuticals cannot be effectively treated by wastewater treatment plants (WWTP), due to their hydrophilic nature, resistance to biological processes, and relatively long half-life, which causes persistence in aquatic ecosystems. The stability of the active principle in the environment and its transformation in metabolic pathways can lead to variable amounts of transformation products (TPs) and metabolites [16] that may present greater or smaller larger environmental impacts, compared to the parent compound. Although many studies have reported the degradation of pharmaceutical products and their TPs, techniques are still needed to achieve complete mineralization and/or low toxicities. The low concentrations of pharmaceuticals and TPs require the use of advanced chromatography techniques combined with high resolution mass spectrometry for their identification and quantification. The aim of this review is to provide an overview of the use of Fe⁰ in the treatment of pharmaceutical products that are present in different water matrices, focusing on the operational conditions, progress in the development of catalysts, effect of the matrix, and the identification and toxicity of TPs. The latest studies and perspectives for treatments to degrade pharmaceuticals using Fe⁰ are presented.

2. Fe⁰ performance factors

The main factors that affect the performance of Fe⁰ used in processes for contaminant removal are the operational conditions, the catalyst characteristics, and the matrix. It is essential to consider the effects of these factors in the development of techniques employing Fe⁰ for water treatment [13].

2.1. Operational conditions

2.1.1. pH

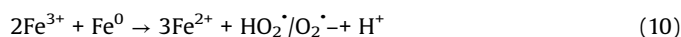
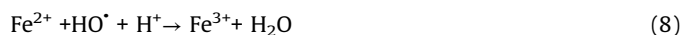
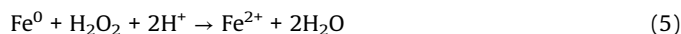
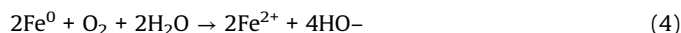
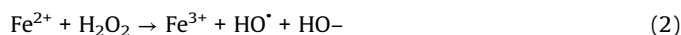
The efficiency of degradation of pharmaceuticals in Fe⁰-mediated processes is strongly affected by pH. The initial pH affects the surface charge of the Fe⁰ catalyst, with a lower pH resulting in a more positive charge that facilitates the contact of the oxidizing reagent and more Fe²⁺ produced by corrosion of Fe⁰, with this the Fe⁰/Fe²⁺ reduction potential increases, resulting in dissolution of the passivated layers, hence promoting the generation of ROS and degradation of the contaminant. Conversely, increasing the pH increases the quantity of negative surface charges on the catalyst, so the formation of repulsive forces inhibits ROS generation [17]. Cao et al [18] studied the degradation of tetracycline by HSO₅⁻ activewith Fe⁰ under acidic conditions (2.0, 4.0, 5.0) and alkaline conditions (9.0, 10.0), pharmaceutical removal efficiency reached a value 76.6%, 72.5%, 58.3%, 69.3%, 63.2%, respectively, these results confirm the best reaction efficiency by acid pH.

In the case of the Fe⁰/H₂O₂ system, the optimum efficiency is also obtained at pH around 3 [19,20], according to studies done by Daneshkhah et al [14] for the removal of metoprolol, solution pH values (3, 5, 7, and 9) were evaluated, the results indicate that the pH of the solution plays an important role in the elimination of metoprolol from aqueous solutions, since under acidic conditions, more than 95% of the pharmaceutical was removed. In systems where chelating agents are used, the best pH values are closer to neutral. Zhou et al [21] studied the degradation of antibiotic norfloxacin by heterogeneous sonochemical Fe⁰/tetrphosphate Fenton-like system at a pH range of 3–9, according with the results

neutral to weak alkaline circumstances were favorable for the pharmaceutical degradation and the maximum k_{obs} was achieved at the system of initial pH 7. In the case of Fe⁰/S₂O₈²⁻, it was demonstrated that the low corrosion rate of Fe⁰ at neutral pH greatly inhibited degradation performance [22]. The optimum pH depends on factors such as the ratio of the reagents, pharmaceutical concentration, and physicochemical characteristics of the solution, at low pH value, the characteristics of the matrix can influence the use of aerobic or anaerobic conditions for the elimination of contaminants in wastewater [23].

2.1.2. Oxidant agents

There are different reaction mechanisms that use Fe⁰ as a catalyst, with the generation of oxidizing radicals depending on the oxidant involved in the process. In acidic solution, Fe⁰ can easily release Fe²⁺ (Eq. (1)), which can activate H₂O₂ to produce hydroxyl free radicals in the Fenton system (Eq. (2)). The oxidation of Fe⁰ by dissolved oxygen produces H₂O₂ via the transfer of two electrons from the particle surface to oxygen (Eq. (3)). The oxidation of Fe²⁺ in a neutral medium generates hydroxyl radicals, hence increasing the pH of the solution (Eq. (4)), in a mechanism known as the advanced Fenton process [24]. The H₂O₂ produced is reduced to water (Eq. (5)) or is converted to HO[•], while reaction with Fe²⁺ leads to Fe⁴⁺ (e.g. FeO²⁺) (Eqs. (2) and (6)). However, the rapid accumulation of HO[•] can enable it to be easily eliminated by H₂O₂ and Fe²⁺ (Eqs. (7) and (8)). Furthermore, the Fe³⁺ generated reacts with H₂O₂ in a Fenton-like process (Eq. (9)), while Fe³⁺ can react sequentially with Fe⁰ to give a sustained supply of Fe²⁺ (Eq. 10) [25]. This generation of ferrous iron and recycling of ferric iron at the Fe⁰ surface can avoid the accumulation of excess ferrous iron and reduce the precipitation of iron hydroxides during the reaction (Eq. (11)). The precipitation of Fe³⁺ ions occurs at pH higher than 4.0, while at pH < 4, there is the formation of oxyhydroxides of Fe³⁺ (Eqs. (12)–(14)) that have low efficiency for the production of radicals [26]. The main mechanism of the Fenton process is represented in Fig. 1.



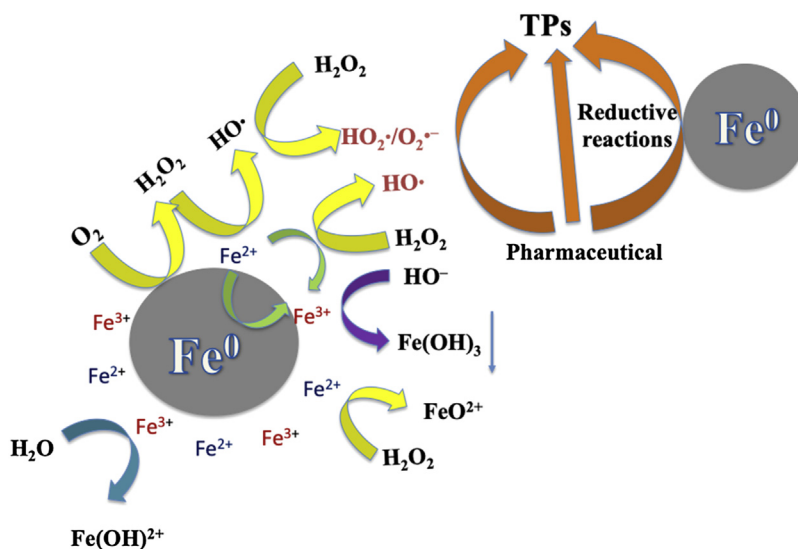
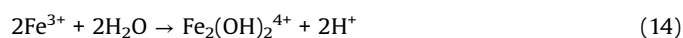


Fig. 1. Schematic diagram of pharmaceuticals degradation using Fe⁰/H₂O₂ system.



Persulfate (S₂O₈²⁻) and peroxymonosulfate (HSO₅⁻) are activated by heat, ultraviolet light, ultrasound, and Fe⁰ or other transition metals, forming the sulfate radical (SO₄^{·-}), which is an efficient strong oxidant for the degradation of emerging pollutants

[27]. The reaction between Fe⁰ and S₂O₈²⁻ is shown in Eq. (15), with the Fe²⁺ formed subsequently reacting with S₂O₈²⁻ to generate SO₄^{·-} (Eq. (16)). Meanwhile, HO[·] can be formed by reaction between SO₄^{·-} and H₂O/OH⁻ (Eqs. (17) and (18)) (Fig. 2) [28].

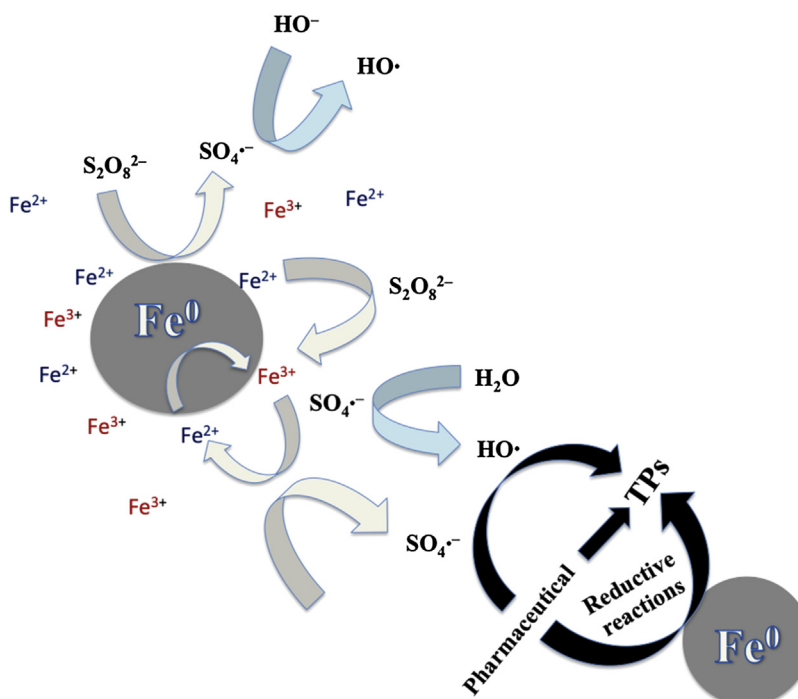
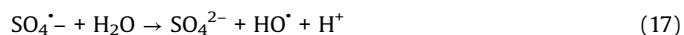
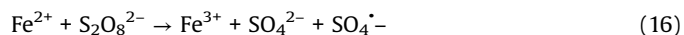
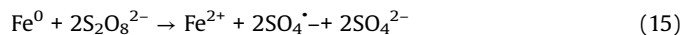


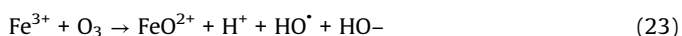
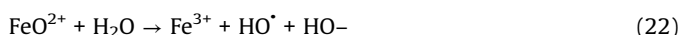
Fig. 2. Schematic diagram of pharmaceuticals degradation using Fe⁰/S₂O₈²⁻ system.

Segura et al. [29] studied the pretreatment of a pharmaceutical wastewater (PWW) by Fenton oxidation with Fe⁰ and H₂O₂, with aeration used to improve degradation of the complex mixture of organic compounds present in the wastewater. The authors demonstrated the efficiency of the aerated system (air/Fe⁰/H₂O₂) for pharmaceutical degradation in a complex matrix, which could be explained by the fact that under oxidizing conditions, oxygen acts as an electron acceptor, generating H₂O₂ and consequently improving the efficiency of degradation. Mineralization can be improved by the successive addition of H₂O₂, as demonstrated by improved elimination of dissolved organic carbon (DOC) in effluent when H₂O₂ was added in two steps [30]. However, it is important to highlight that at higher concentrations, H₂O₂ inhibited the corrosion of iron, so it is essential to employ an optimum hydrogen peroxide concentration [14]. The strong negative effect of a high H₂O₂ concentration on pollutant removal by Fe⁰/H₂O₂ might be due to the scavenging effect of HO• and the inhibition of iron corrosion by H₂O₂ [31].

Tan et al. [32] studied the removal of chloramphenicol in water employing HSO₅⁻, which revealed that the combination of Fe⁰ and HSO₅⁻ at pH 3.0 and 7.0 was extremely effective for chloramphenicol decomposition. This was attributed to the generation of highly reactive radicals such as SO₄^{•-} and HO• in the system, following addition of the catalyst. Gao et al. [33] obtained satisfactory results for the degradation of propranolol by Fe⁰-activated S₂O₈²⁻, under ultrasonic irradiation. This oxidant can be activated using transition metal ions such as Cu²⁺, Ag⁺, and Co²⁺ [34].

2.1.3. Ozonation

Another process that can be employed for the degradation of pharmaceuticals is the coupling of ozonation with a metallic catalyst. The mechanism proceeds by chemisorption on the catalyst surface, leading to the formation of active oxidizing species and redox reactions. The ozonation is accelerated by the addition of catalysts, with the efficiency of the process depending on the type and surface properties of the catalyst, as well as the pH [35]. Study done by Malik et al [36] reported the biodegradability enhancement, COD (Chemical Oxygen Demand), color and toxicity removal via O₃, O₃/Fe²⁺, O₃/Fe⁰ processes. The last process showed the highest biodegradability (BI = BOD₅/COD), COD, color and toxicity removal of 62.3%, 93% and 82%, respectively. One of the advantages of this process is the reduction in the cost of the operation, despite the additional expense associated with catalyst separation. The reaction with ozone leads to the formation of ozonide, oxygen, and hydroxyl radicals (Eqs. (19)–(23)). In some cases, these reactive oxygen species (ROS) are more reactive than ozone for pharmaceutical degradation [35].



2.1.4. Weak magnetic field

The application of a weak magnetic field has recently been employed to improve the performance of Fe⁰, representing an

efficient and environmentally friendly method without any additional energy requirement. The “magnetic memory” of Fe⁰ can induce a heterogeneous magnetic field around the Fe⁰ surface. The presence of a magnetic gradient force in the solution generates paramagnetic ions such as Fe²⁺, which move to the location with the most intense magnetic force flux, resulting in the localized distribution of iron ions. This enhances the generation of Fe²⁺ [37], with the rapid removal of iron oxides, suppression of the negative effects of scavengers such as SO₄²⁻ [38], greater production of ROS and iron oxides, and consequent improved removal of contaminants [39]. Zhou et al [40] demonstrated significant synergistic degradation of antibiotic diclofenac in a novel magnetic field enhanced Fe⁰/EDTA Fenton-like system, this improved the k_{obs} of pharmaceutical and shortening the initial lag degradation period with total degradation of 80% of pharmaceutical in 120 min.

2.1.5. Bioprocesses

There is increasing use of processes that offer sustainable *in situ* production of hydrogen peroxide, with lower energy consumption. These processes are characterized by enzymatic activity related to materials of biological origin, together with the presence of a source of iron ions [41]. The removal of compounds can be improved by the combined use of Fe⁰ and anaerobic microorganisms, where the Fe⁰ is an electron donor for the reduction of sulfate, nitrate, and chlorinated aromatics by microorganisms. The synergetic degradation effect is mainly attributed to the biodegradation capacity of the hydrogenbacteria [42]. Bavandi et al [43] have also shown that n-Fe⁰ can improve the growth of microorganisms and bioproduction. The authors investigated the effect of starch/n-Fe⁰ as a modifier of *Oscillatoria* cyanobacteria in the elimination efficiency of trinitrophenol, with this the bioremoval efficiency increased by more than 10% compared to the use of *Oscillatoria* cyanobacteria alone.

Otherwise, Changotra et al [44] studied the Fenton-biological joint processes, it combines Fenton applications as pretreatment technology and biological treatment, the authors showed COD elimination efficiency of the combined treatment around 84% compared to 60% obtained by solar photo-Fenton and 40% by biological treatment, this strategy providing enhanced biodegradation of pollutants in comparison to single stage oxidation or biological treatment. The proposal of the joint Fenton-biological process is postulated as a new sustainable method from different water matrices [41,45].

2.1.6. Temperature

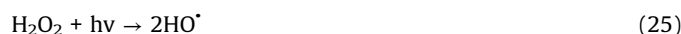
Temperature is another factor that can influence the oxidation process mediated by Fe⁰. According to the Arrhenius law, it is expected that an increase in temperature should lead to faster generation of radicals. On the other hand, it also increases the rates of deleterious reactions, so the temperature effect depends on the respective activation energies. In heterogeneous Fenton oxidation with Fe⁰ catalyst, it was reported that catalytic activity was improved by increasing the temperature from 10 to 80 °C, with no optimum value being observed [46]. Liu et al [47], observed that the removal rate of chloramphenicol by Fe⁰ increased with increasing reaction temperature, the 98% of antibiotic was removed at 40 °C with a linear relationship between ln k_{obs} and 1/T (R² = 0.988).

2.1.7. Irradiation

Solar processes are effective techniques for the degradation of pollutants, employing photo-irradiation in the light absorption range between 290 and 575 nm, which accelerates the reaction rate, reduces sludge production, and improves the degradation efficiency. Xie et al [48] studied the degradation of propranolol with a Fe⁰/sulfite/O₂/photo system, demonstrating that irradiation

and aeration could effectively accelerate the degradation of propranolol (96.7%) by promoting the Fe^0/O_2 reaction to produce HO^\bullet , while additional oxygenation by rapid agitation maintained a supply of the oxygen necessary for the generation of reactive radicals. According to the authors aeration facilitates the transport of electrons of active substances in the reaction solution and increases the utilization of light energy through the detection photons, increasing the elimination rate of propranolol in the system.

Ultraviolet radiation has been widely used for disinfection of drinking water and wastewater treatment. Evaluation of the performance of $\text{Fe}^0/\text{H}_2\text{O}_2/\text{UV}$ and $\text{Fe}^0/\text{S}_2\text{O}_8^{2-}/\text{UV}$ systems showed that UV irradiation could remove contaminants by photolysis and activate the oxidant reagents for generation of ROS (Eqs. (24) and (25)). The use of UV irradiation in degradation processes can help to overcome the activation energy for oxidation of Fe^0 and accelerate the generation and recycling of Fe^{2+} , thereby enhancing the reaction (Eqs. (26) and (27)) [22].



2.2. Iron characteristics

The different oxidation states of iron range from Fe^0 to Fe^{6+} enriched by the number of accessible spin states. Iron cations have applicability and great importance in inorganic, analytical, and environmental chemistry [49]. In advanced oxidation technologies, iron Fe^{2+} and Fe^{3+} salts are commonly used in homogeneous processes (such as Fenton and Fenton-like processes). When Fe^0 is

used in water remediation treatment, the heterogeneous mechanism is considered to mainly involve particle interactions, since the catalyst is in the solid state, although homogeneous and heterogeneous reactions can occur in the solution and/or on the surfaces of the particles of iron and its corrosion products, with ROS production occurring in both phases (Fig. 3). Iron corrosion products including goethite, hematite, lepidocrocite, and maghemite have been studied in remediation processes [50]. In photo-Fenton systems, hematite has significant photoactivity, solid hematite would act as an iron reservoir that would be released and/or activated under irradiation (Fe^{3+} photoreduction to Fe^{2+}) for the Fenton process to take place in solution ($\text{Fe}^{2+} + \text{H}_2\text{O}_2$) [51]. Moreover, some modifications in the structure of iron corrosion products are being studied and successfully applied in the elimination of pharmaceuticals, such as the study carried out by Yang et al [52], where the authors synthesized and studied the effect of hematite-biochar compounds (FOC) and pyrite-biochar compounds (FSC) on the elimination of norfloxacin from the aqueous solution, with the synthesis the average pore width increased the functional groups on the surface of FOC and FSC, which could interact with the pharmaceutical product through hydrogen bonds, action of the π - π electron acceptor donor, complexation and ion exchange interaction. FOC and FSC showed an elimination capacity of 81.63% and 96.34%, respectively.

The dissolved iron ions in solution, generated from Fe^0 , play an important role in determining the efficiency of the degradation system, since the concentrations of ROS including HO^\bullet , $\text{O}_2^{\bullet-}$, $\text{HO}_2^{\bullet-}$, and $\text{SO}_4^{\bullet-}$ are affected by the concentrations of these iron ions [11]. However, an excessive quantity of Fe^0 may cause decomposition of the oxidant to produce unreactive oxygen species, as well as scavenging of the active radical species [29].

2.2.1. Particle size

The particle size also affects pollutant degradation, since it influences the mobility, stability, and reactivity of the components of the system. Ambika et al. [53] studied the effect of particle size on phenol removal, with meso-zero-valent iron (m- Fe^0) particles being quantitatively evaluated in comparison with coarse zero-

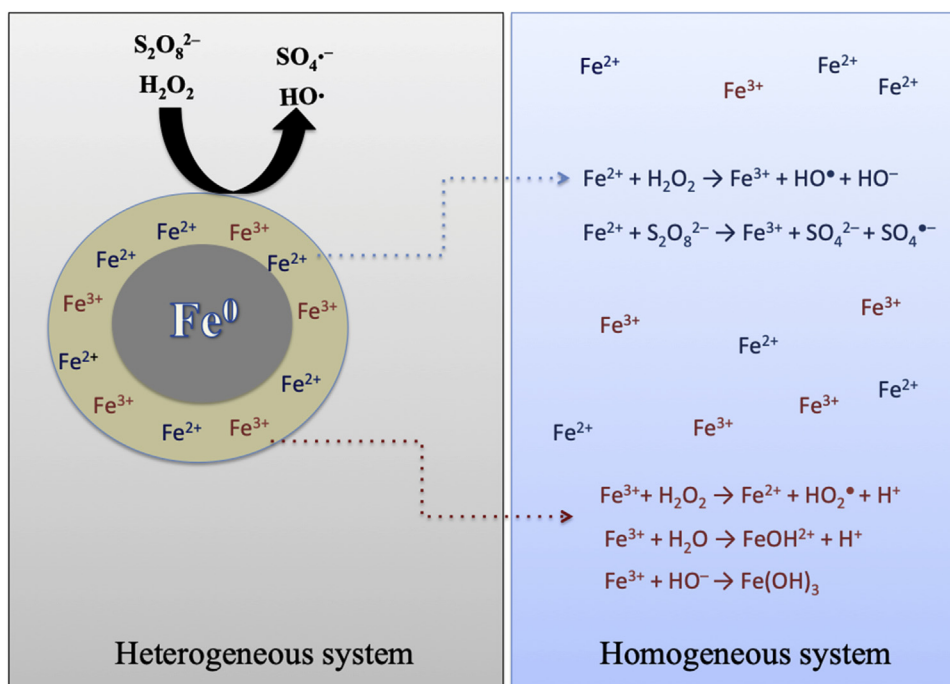


Fig. 3. Schematic diagram of homogeneous/heterogeneous systems using Fe^0 .

valent iron (c-Fe⁰) and nanozero-valent iron (n-Fe⁰) particles. The c-Fe⁰ particle size was between 0.2 and 5 mm, while n-Fe⁰ was typically smaller than 100 nm and m-Fe⁰ presented an intermediate particle size. The experiments were carried out under different pH conditions (pH 3, 4, 6, 7, 8, and 10) and the results showed that the m-Fe⁰ particles provided consistent phenol degradation at neutral pH, with an efficiency of 89% in 20 min, helping to avoid disadvantages such as the agglomeration and low reactivity presented by c-Fe⁰ and n-Fe⁰. In the work of Ma et al. [54], the use of n-Fe⁰ provided greater efficiency in the removal of norfloxacin, which was attributed to higher catalytic activity provided by the high specific surface area and consequent greater availability of active sites, favoring corrosion of the catalyst surface and enhanced formation of HO[•]. Despite high reactivity, n-Fe⁰ has drawbacks related to the preparation process, which in some cases requires an inert atmosphere and expensive reagents, which can hinder scale-up. Depending on their size, the particles may require storage media in order to maintain reactivity, due to the tendency for aggregation and passivation.

The work of De Perini and Nogueira [30] demonstrated the influence of particle size on the efficiency of sertraline degradation. The degradation rate was improved when the quantity of larger particles (20 mesh) was increased, while no significant change was observed in the case of smaller particles (200 mesh).

It has been suggested that m-Fe⁰ particles may be especially suitable for use under field conditions, where a consistent degradation process is necessary. These particles are reactive at slightly higher pH, due to the size of the particles and their resistance to dissolution, being able to transport electrons through the iron oxide formed on the surface at high pH, unlike n-Fe⁰ particles that tend to agglomerate and produce potentially stable larger particles in the long term [53].

2.2.2. Bimetallic systems

Many studies have demonstrated that zero-valent metals (such as Cu, Ni, Pd, Ag, and Bi) show satisfactory performance when H₂O₂ is used for the degradation of organic pollutants [54]. Bimetallic Fe⁰ (Fig. 4a) exhibits super-magnetic properties and can be easily separated from the liquid phase under the influence of an external magnetic field [55]. The added metal can significantly accelerate the rate of corrosion of Fe⁰, increasing its reactivity and the formation of hydrogen species on the surface, which can suppress the oxidation of Fe⁰ [56]. These bimetallic particles have been

shown to present higher activity, compared to monometallic systems. For example, Ni/n-Fe⁰ and Cu/n-Fe⁰ have been used as inexpensive materials to promote highly efficient removal of pharmaceuticals at pH 6.0 [57] and from wastewater at neutral pH [58]. Weng et al [59] examined functional bentonite-supported nanoscale (B-Fe/Ni) for the simultaneous removal of amoxicillin, ampicillin and penicillin, the results showed degradation percentages of 94.6%, 80.6% and 53.7%, respectively. Kinetics studies of mixed antibiotics using B-Fe/Ni confirmed that adsorption and degradation occurred simultaneously as removing of antibiotics in the presence of particles. In other work, Ni has been used as a catalyst that improved the stability of iron-based bimetallic nanoparticles in air, preventing oxidation and providing better corrosion stability, while offering lower costs for on-site remediation [60]. Bi/n-Fe⁰ has gained attention due its low carrier density, high electron distribution, and highly anisotropic Fermi surface, as well as its low cost and environmentally friendly characteristics [61].

2.2.3. Support materials

In order to improve the stability of Fe⁰ in suspensions and during transportation, various materials have been used as supports or for the purpose of encapsulation, including biochar [62], activated carbon [63], magnesium aluminum phyllosilicate [64], vermiculite [65,66], bentonite [1,67], kaolinite [68], zeolite [46], graphene [69], carbon spheres, and carbon polystyrene resin (Fig. 4b). Iron waste has also been used as a source of Fe⁰ for eliminating bacteria and contaminants in municipal wastewater [70]. Additionally, biopolymers such as alginate have been successfully used to immobilize different iron species [58]. For example, the use of alginate [59,71,72] and chitosan to immobilize Fe⁰ led to mechanisms of diffusion of oxidants or ions that were mediated by the pore size of the cross-linked structure. Elsewhere, chitosan was employed for the immobilization of Fe³⁺ and Fe⁰ [34]. This catalyst was used with S₂O₈²⁻, achieving 98.5% degradation of acetaminophen, with minimum leaching of the iron. The material showed excellent stability when used with S₂O₈²⁻ to produce abundant free radicals for the oxidation of pharmaceuticals, and also protected the metal ions from leaching.

Pirsaheb et al. [73] studied the use of n-Fe⁰ encapsulated in carbon for the removal of amoxicillin and ciprofloxacin. The useful characteristics of this eco-friendly catalyst included high surface area, high reactivity, and efficient removal of the compounds at

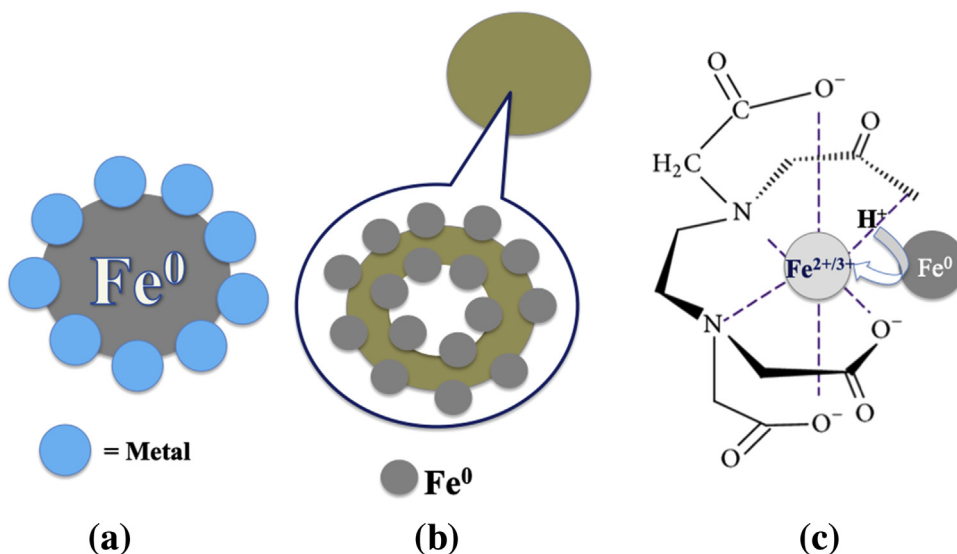


Fig. 4. Representation of Fe⁰ catalyst: (a) bimetallic, (b) supported in other material and (c) complexed.

different pH values. It was found that the removal efficiencies were highly dependent on the properties of the antibiotic and the structure of the catalyst. Otherwise, studies reported that the sepiolite-supported n-Fe⁰ prevent agglomeration and provide a large reactive area with removal percentages for metoprolol higher than 50% in the presence of SO₄²⁻, Cl⁻, HCO₃⁻, and NO₃⁻ ions at pH 3.0 [14]. However, other work using Fe-zeolite as a catalyst found appreciable catalytic activity of this type of catalyst at near-neutral pH (pH 4–6) [46].

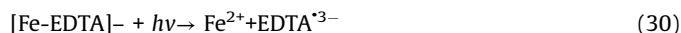
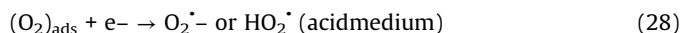
Sulfide-modified zero-valent iron (S-Fe⁰) is a new material based on Fe⁰ that offers enhanced reactivity and selectivity towards different pollutants. Sulfidation, modifies with reduced sulfur (i.e., sodium sulfide, dithionite, and thiosulfate), in such a way the iron sulfides replaced the iron oxide passive layer on the Fe⁰ particles, increasing electron transfer [74] and inhibit nearby adsorption sites for oxygen, consequently lowering the dissociation of O₂ and subsequent growth of iron hydroxide. This has two positive effects, since it enhances the generation of H₂O₂ and HO[•], while preserving a considerable amount of Fe⁰ for subsequent Fe³⁺ reduction. Given the high conductivity of S-Fe⁰, it can act as an electron shuttle in the reduction of surface bound Fe³⁺ to Fe²⁺ by Fe⁰, with the regenerated Fe²⁺ then being used for repeated HO[•] generation [75]. S-Fe⁰ was applied to HSO₅⁻ to degrade sulfamethoxazole, the removal efficiency of pharmaceutical by S-m-Fe⁰/HSO₅⁻ system was increased by 29.4% in comparison with m-Fe⁰/HSO₅⁻ system [74], this result suggests that sulfidation has good potential for the elimination of micropollutants in the aquatic environment.

2.2.4. Chelating agents

The use of chelating agents was recently reported to improve the efficiency of degradation of pollutants by means of an oxidative mechanism [76]. In this technique, Fe⁰ releases dissolved iron species in the presence of chelating agents that enable the operation to be performed at different pH values. In tests using nanoparticles of Fe⁰ in the presence of different chelating agents [77], it was found that EDTA presented the best chelating effect with Fe⁰ with a weight percentage of iron of 91.28%, which could solve the stability problem of Fe⁰ for its applications in environmental remediation and water purification (Fig. 4c).

According with Zhou et al [40], in the Fe⁰-EDTA system, the degradation of pharmaceuticals can be attributed to the activation of O₂ and *in situ* generation of ROS mainly HO[•] in the redox cycle of Fe-EDTA ligands, in this study, a significant synergistic degradation of the diclofenac antibiotic was demonstrated in a Fe⁰/EDTA-Fenton-like system with percentages of degradation greater than 90% for the elimination of antibiotic. Bautitz et al. [19] studied the degradation of diazepam in an homogeneous system using EDTA as a chelating agent. Evaluation was made of parameters such as the concentration and pretreatment of iron, as well as the effect of complexation with EDTA under oxic and anoxic conditions, with the best results achieved under oxic conditions following pretreatment using H₂SO₄.

The role of the complexation agent in an oxygenated system is related to Fe-complex formation after fast oxidation of Fe⁰ to Fe²⁺ and Fe³⁺. The Fe²⁺-EDTA complex is capable of activating dissolved oxygen and generating reactive oxygen species such as O₂ or HO₂, which lead to H₂O₂ formation (Eqs. (28)–(29)) [19]. Fenton reactions performed in the presence of the Fe-EDTA complex are able to oxidize a wide variety of pharmaceuticals (Fig. 5). Chelating agents such as EDTA can undergo a series of coordination reactions with ferrous ions and the main product generated by the photolysis is Fe²⁺ (Eq. (30)), which in the presence of H₂O₂ gives rise to the Fenton reaction.



Another chelating agent that has been widely studied is sodium citrate, because it is an environmentally friendly and readily biodegradable multidentate organic complexing agent. In evaluation of the behavior of acetaminophen degradation with citrate and S₂O₈²⁻, Deng et al. [78] found that when the dosage of sodium citrate was increased, it could compete with the pharmaceutical for SO₄^{•-} radical attack, consequently reducing the degradation efficiency.

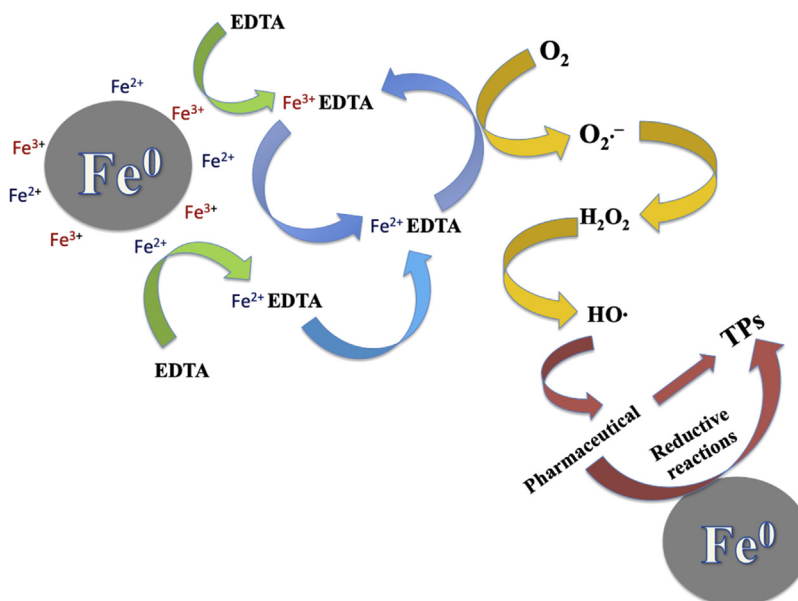


Fig. 5. Schematic diagram of pharmaceuticals degradation using Fe⁰/EDTA system.

2.3. Matrix effects

The elimination of emerging contaminants by AOPs is influenced by the quality of the water matrix, with the efficiency reflecting the interactions of the dissolved components, which may have neutral, inhibitory, or promoter effects. The composition of the water matrix depends on the source (for example, domestic, hospital, agricultural, or industrial) and can also have a significant impact on the inactivation of bacteria in water disinfection processes [79]. The wastewater components include organic compounds such as natural organic matter (NOM) composed of humic and fulvic acids, carbohydrates, proteins, and inorganic species such as carbonate, bicarbonate, nitrite, sulfate, chloride, phosphate, and surfactants, which can be scavengers of HO^\bullet and $\text{SO}_4^{\bullet-}$.

The absorption of light can have an inhibitory effect, due to the substances present in the matrix. It may also result in the formation of less active iron complexes and competition for catalytic active sites. The presence of NOM has been found to cause a significant increase in energy consumption, due to its strong absorption properties and its high reactivity with oxidizing radicals [80]. In the case of Fe^0 , the catalyst may be deactivated by poisoning of the active sites or fouling of the surface area, as well as by modification of the surface electrical charge due to the effects of pH or ionic strength [46,79].

Considering the anions commonly found in aqueous media, it has been found that HCO_3^- has a greater influence than SO_4^{2-} or NO_3^- , with the order of inhibition usually being: $\text{HCO}_3^- > \text{Cl}^- > \text{SO}_4^{2-} > \text{H}_2\text{PO}_4^- > \text{NO}_3^-$ [33]. Studies have shown the inhibitory effects on pharmaceutical degradation of HCO_3^- [34], Cl^- and CO_3^{2-} [32], SO_4^{2-} [35,54], and cations [14]. However, it has been reported that some species can also act as promoters, an example being NO_3^- , which produces HO^\bullet and NO_2^\bullet radical species, hence promoting the photodegradation of pollutants [79]. At low concentrations, chloride ions can have a positive effect on the kinetic constants and the percentage degradation, because they can react with HO^\bullet to generate dichloride ($\text{Cl}_2^{\bullet-}$) and chlorine (Cl^\bullet) radicals that can then react with organic compounds in solution [81]. The presence of chloride ions accelerates the corrosion of Fe^0 by H_2O_2 and the formation of ROS, hence increasing the degradation of organic materials. In contrast, phosphate has been found to inhibit ROS formation and the degradation of organic compounds [82].

As has been noted, the temperature and values lower of pH accelerate the release of ions from surface of Fe^0 to solution, subsequently, the ions can activate the oxidant reagent to generate radicals, which directly participate in the degradation of pharmaceutical, the activation of oxidant reagent can originate from homogeneous (releasing ions from Fe^0 surface) and heterogeneous process (on Fe^0 surface). The most common oxidizing agents used with Fe^0 are H_2O_2 , $\text{S}_2\text{O}_8^{2-}$ and HSO_5^- , the concentration used must be careful, since high concentration causes an elimination effect, the successive addition of oxidizing agent is an alternative to improve the mineralization. The weak magnetic field, bimetallic systems, support materials and chelating agents have recently been used to improve the Fe^0 yield and the efficiency of pharmaceuticals degradation by means of oxidative mechanism.

Besides, the optimum conditions for the degradation of pharmaceutical products using Fe^0 also depend on the proportion of the reagents and total organic matter (TOC) (catalyst/oxidant agent, Fe^0/TOC or oxidant agent/TOC). Segura et al [29] studied the degradation of pharmaceuticals in wastewater, the authors reported a TOC reduction of up to 80%, this value was reached with moderate loads of Fe^0 and H_2O_2 , Fe^0/TOC weight and $\text{H}_2\text{O}_2/\text{TOC}$ molar ratios of 12 and 3.2, respectively.

3. Fe^0 as a potential catalyst in the removal of pharmaceuticals

Pharmaceutical products are continuously introduced into the environment, mainly from hospital wastewater [83], personal care products [84], pharmaceutical industry waste [85], and inappropriate discarding of drugs [86]. Their presence at low concentrations is recognized as being potentially harmful to ecosystems, while the persistence of traces of pharmaceuticals and other xenobiotic compounds in water can lead to public health problems following their ingestion in drinking water or contaminated food [87].

A plausible mechanism for pharmaceuticals degradation using Fe^0 and oxidant involves adsorption, reduction and oxidation. The elimination of pharmaceuticals by Fe^0 is mediated by its surface. The iron oxide/hydroxide layer blocks the active sites and, therefore, inhibits the transfer of electrons from the surface, which promotes the reductive degradation of pharmaceutical, at the same time it increases its absorption and that of its intermediates [88], the electrostatic interaction between iron oxide/ Fe^0 and pharmaceutical play an important role in removal process since it depends on the charge of the compound and the iron surface there may be a greater or lesser interaction. On the other hand, at a pH acid at an acid pH, the best electron transfer is promoted, which means that upon contact with an oxidizing agent, ROS can be generated and, therefore, oxidative degradation can also occur [12].

Karim et al. [20] investigated the degradation of 17α -ethinylestradiol, used as a model steroidal estrogen, by commercially sourced n- Fe^0 at pH 3, 5, and 7, under different oxygen conditions. It was found that the dominant radicals were HO^\bullet at pH 3 and $\text{O}_2^{\bullet-}$ at pH 5. Liu et al. [47] showed that Fe^0 could be employed to efficiently remove chloramphenicol from different natural waters within several minutes, demonstrating that n- Fe^0 is a promising material that can be used to reduce antibiotic selection pressure in the environment. Weng et al. [1] reported that the removal of amoxicillin was based on a combination of adsorption and reductive degradation.

The use of ultrasonic irradiation in advanced oxidation technologies enables the production of highly reactive species such as HO^\bullet , O^\bullet , H^\bullet , and H_2O_2 by thermal fragmentation of water molecules and organic solutes during acoustic cavitation involving the formation, growth, and subsequent implosion of bubbles [35]. This technique has been reported to improve the effectiveness of the Fenton process [54,89].

Considering the kinetics of the degradation processes, Du et al. [31] reported three phases in the sulfamethoxazole degradation curve, with an initial lag phase, a second rapid degradation phase, and finally a stationary phase. The stationary phase was due to saturation of the surface of the material, representing a disadvantage of the process. One way to address such a drawback is to use bimetallic materials that offer greater stability at different pH values.

Table 1 summarizes the main and most recent studies concerning the removal of pharmaceuticals using Fe^0 as a catalyst in different systems, providing information about the nature of the matrix, the principal results obtained, and the TPs identified.

The main groups of pharmaceuticals employed in the studies involving processes with Fe^0 were antibiotics and anti-inflammatory compounds in distilled or deionized water. In the majority of cases, the parent compound removal percentages exceeded 70%, while the identification of TPs and their toxicities are topics that are currently a focus of investigation. The reaction time can vary according to the concentrations of the reagents used, the nature of the matrix, and the physicochemical characteristics of the pharmaceuticals. The shortest time reported was 10 min, while some processes required days. Higher degradation efficiency was

Table 1
Studies reported in the literature concerning the removal of pharmaceuticals using Fe⁰ as catalyst.

Pharmaceutical / initial concentration	Family or function	Experimental conditions	Water matrix	Results	TPs	Ref.
Tetracycline 20 mg L ⁻¹	Antibiotic	[Fe ⁰] = 0.4 g L ⁻¹ Air aeration = 500 mL min ⁻¹ pH = 2.5 Time = 30 min	Deionized water	Fe ⁰ /air process achieved 90% degradation	✓	[12]
Metopropol 3 mg L ⁻¹	β ₁ receptor blocker	[Fe ⁰] = 0.5 g L ⁻¹ [H ₂ O ₂] = 10 mmol L ⁻¹ pH = 3.0 Time = 60 min	Deionized and tap water	Maximum removal rates of 67.24% and 55.16%		[14]
Ciprofloxacin 10 mg L ⁻¹	Antibiotic	[Fe ⁰] = 0.05 mmol L ⁻¹ [S ₂ O ₈ ²⁻] = 1.6 mmol L ⁻¹ pH = 7.0 ± 0.2 Temperature = 25 °C Time = 20 min	Deionized water	99% degradation		[17]
Diazepam 25 mg L ⁻¹	Benzodiazepine family (calming effect)	[Fe ⁰] = 5, 25, and 40 g L ⁻¹ Particle size = 0.85 mm [EDTA] = 119 mg L ⁻¹ pH = 2.5 With presence and absence of O ₂ Time = 120 min	Ultrapure water	96% degradation and 60% mineralization		[19]
17α-ethinylestradiol 0.01 mmol L ⁻¹	Estrogen	[Fe ⁰] = 89.5 mmol L ⁻¹ pH = 3, 5, and 7 under different oxygen conditions 200 rpm Time = 90 min	Distilled water	Maximum removal of 99.4% at pH 3.0 under anaerobic conditions and ambient oxygen, and 85.8% under saturated oxygen conditions	✓	[20]
Sulfamethazine 10 mg L ⁻¹	Antimicrobial	[Fe ⁰ /BC] = 1.2 g L ⁻¹ BC: Biochar [H ₂ O ₂] = 20 mmol L ⁻¹ pH = 3.0 Temperature = 20.0 ± 0.2 °C Time = 12 h	Ultrapure water	74.04% removal efficiency		[25]
Pharmaceutical Wastewater samples TOC = 0.1 g L ⁻¹		[Fe ⁰] = 0.6, 1.2, and 2.4 g L ⁻¹ [H ₂ O ₂] = 0.23 and 0.96 g L ⁻¹ pH = 3.0 Temperature = 22 ± 2 °C Air flow = 5 L min ⁻¹ Time = 60 min	Real industrial wastewater generated from a pharmaceutical manufacturing plant	Air/Fe ⁰ /H ₂ O ₂ system achieved TOC reductions of up to 80%		[29]
Sertraline 72 μmol L ⁻¹	Antidepressant	[Fe ⁰] = 0.5-2.5 g L ⁻¹ Particle size = 74 and 840 μm [H ₂ O ₂] = 5 mmol L ⁻¹ pH = 2.5 Time = 90 min	Ultrapure water and effluent from a sewage treatment plant	Sertraline was totally degraded in water and effluent using the Fe ⁰ /H ₂ O ₂ system		[30]
Cloroamphenicol 10 mg L ⁻¹	Antibiotic	[Fe ⁰] = 0.5 g L ⁻¹ [HSO ₅ ⁻] = 0.2 mmol L ⁻¹ pH = 3.5, 7.0, and 10 Temperature = 20 °C Time = 120 min	Distilled water	97.2% removal at pH 3.5, with small proportion of mineralization		[32]
Propranolol 40 μmol L ⁻¹	β blocker	[Fe ⁰] = 0.15 g L ⁻¹ Particle size = 50 nm [S ₂ O ₈ ²⁻] = 1 mmol L ⁻¹ pH = 3, 4.5, and 7 P = 250 W Time = 30 min	Ultrapure water	Removal rate up to 94.2%	✓	[33]
Acetaminophen 30 mg L ⁻¹	Nonsteroidalanti-inflammatory	[Fe ⁰] = 0.08 g L ⁻¹ [S ₂ O ₈ ²⁻] = 2.0 mmol L ⁻¹ pH = 7.0 Time = 35 min	Deionized water	98.5% removal efficiency, without pH control	✓	[34]
Ibuprofen	Nonsteroidalanti-inflammatory	[Fe ⁰ -graphite] = 5 mg L ⁻¹ Fe equivalent of the catalysts	Ultrapure water	TOC degradation rates of 79% and 41% with Fe ⁰ -graphite;		[35]

Table 1 (Continued)

Pharmaceutical / initial concentration	Family or function	Experimental conditions	Water matrix	Results	TPs	Ref.
10 mg L⁻¹		Particlesize = 20-100 nm		100% ibuprofen elimination was obtained with Fe ⁰ -graphite and ultrasonic irradiation		
Diclofenac 20 mg L⁻¹	Nonsteroidalanti-inflammatory	pH = 6.5 O ₃ flow = 12 mg min ⁻¹ 861 kHz Time = 60 min [Fe ⁰] = 1.0 mmol L ⁻¹	Deionized water	Total removal	✓	[37]
Tetracycline	Antibiotic	[H ₂ O ₂] = 1.0 mmol L ⁻¹ pH = 3-6 Time = 60 min [Fe ⁰] = 0.38 g	Simulated municipal wastewater	Removal rates reached over 90%		[42]
1, 10, 30, 50, 80, 100, and 150 mg L⁻¹		Particle size = 100 nm				
Ibuprofen 20 mg L⁻¹	Nonsteroidalanti-inflammatory	pH = 7.0 Anaerobic biodegradation Time = 25 days [Fe ⁰ -zeolite] = 4.8 g L ⁻¹ [H ₂ O ₂] = 6.4 mmol L ⁻¹	Distilled water and Effluent from a municipal wastewater treatment plant	88% of ibuprofen and 27% of TOC were removed	✓	[46]
Propranolol	β blocker	pH = 4.3 Temperature = 25 °C Time = 3 h [Fe ⁰] = 0.1 mmol L ⁻¹	Ultrapure water	Degradation improved from 68.5% to 98.7% with increased sulfite dose	✓	[48]
20 mmol L⁻¹		Particle size = 46.2 μm [Sulfite] = 0.5 mM pH = 6.0 ± 0.2 Temperature = 25 °C Simulated sunlight irradiation Time = 60 min [Fe ⁰ -Cu] = 0.25 g L ⁻¹	Ultrapure water	Removal efficiencies of 46.68% and 91.5% using n-Fe ⁰ /H ₂ O ₂ and US/n-Fe ⁰ /H ₂ O ₂ systems, respectively		[54]
5 mg L⁻¹		Particle size = nano-sized (625 mesh) [H ₂ O ₂] = 10 mmol L ⁻¹ pH= 3.0 Ultrasound power of 240 W at 20 kHz Time = 30 min [Fe ⁰] = 1 g L ⁻¹	Distilled water	54.0 mg g ⁻¹ removalcapacityofthe material	✓	[55]
100 mg L⁻¹		Particlesize = 12 nm pH = 6.5 Temperature = 40 °C [Ni/n-Fe ⁰] = 200 mg L ⁻¹	Ultrapure water	71.4, 62.3, and 31.1% removal using Cu/n-Fe ⁰ , Ni/n-Fe ⁰ , and Fe ⁰ , respectively		[57]
100 mg L⁻¹		[Cu/n-Fe ⁰] = 200 mg L ⁻¹ Particle size = 20-80 nm pH = 6.0 Time = 240 min [Fe ⁰] = 765 mg L ⁻¹	Distilled water and hospital effluent	Removal of 90% of amoxicillin and 51% of ciprofloxacin from distilled water; removal of 71 and 34%, respectively, from real wastewater		[73]
100 mg L⁻¹		Particle size = 240 nm [H ₂ O ₂] = 20 mmol L ⁻¹ pH = 3.5 Time = 60 min [S-Fe ⁰] = 3g L ⁻¹	Ultrapure water	Removal rates reached 92.5, 84.2, and 73.6% for 1, 5, and 10 mg L ⁻¹ of diclofenac		[75]
10 mg L⁻¹		Particle size = 100 nm pH = 3.0 Temperature = 25 ± 5 °C Oxygen aeration = 800 mL min ⁻¹ Time = 2 h				

Table 1 (Continued)

Pharmaceutical / initial concentration	Family or function	Experimental conditions	Water matrix	Results	TPs	Ref.
Diclofenac 10 mg L ⁻¹	Nonsteroidalanti-inflammatory	[Fe ⁰] = 0.4 g L ⁻¹ [EDTA] = 2 mmol L ⁻¹ pH = 5.0 Temperature = 25 °C With presence and absence of O ₂ Time = 120 min	Distilled water	The system was successful for the degradation of diclofenac		[40]
Acetaminophen 0.066 mmol L ⁻¹	Nonsteroidalanti-inflammatory	[Fe ⁰] = 0.1-1 mmol L ⁻¹	Distilled water	93.19% removal of acetaminophen and 36.81 and 38.92% removal of TOC at pH 3 and 5.5		[78]
Chloramphenicol 0.30 mmol L ⁻¹	Antibiotic	[S ₂ O ₈ ²⁻] = 0.4 mmol L ⁻¹ pH = 1.5-10 Temperature = 80 °C Time = 180 min [Fe ⁰] = 1.8 mmol L ⁻¹	Deionized water, groundwater, river water, seawater, and wastewater	Removal efficiencies of 92.0, 93.7, 96.8, and 87.9% for groundwater, river water, seawater, and wastewater, respectively	✓	[47]
Tinidazol 45, 80, and 100 mg L ⁻¹	Antibiotic	Particle size = nanomaterial pH = 7.0 Temperature = 303 K Time = 30 min [Fe ⁰] = 0.2 g [H ₂ O ₂] = 1 mol L ⁻¹ pH = 3.0 130 kHz radiation frequency Time = 150 min [Fe ⁰] = 0.1% w/w	Not reported	93% removal, with COD removal greater than 50%		[89]
Pharmaceutical and personal care products			Sewage sludge collected from a municipal wastewater treatment plant	Most of the pharmaceuticals and personal care products could be removed		[90]
Sulfamethoxazole 25 μmol L ⁻¹	Antibiotic	Particle size = 160 nm pH = 7.0 Time = 30 days [Fe ⁰] = 25 mg L ⁻¹	Deionized water	97.9% degradation was achieved	✓	[91]
Amoxicillin 10 mg L ⁻¹	Antibiotic	Particle size = 3.9 μm [H ₂ O ₂] = 0.25 mmol L ⁻¹ pH = 3.0 Temperature = 20 ± 1 °C Time = 10 min [Fe ⁰] = 0.027 mmol L ⁻¹	Deionized water and soils	100% amoxicillin removal from aqueous systems and soils		[92]
Ciprofloxacin 20-100 mg L ⁻¹	Antibiotic	Particle size = 20 and 100 nm [H ₂ O ₂] = 0.36 mmol L ⁻¹ pH = 3.0 and 7.0 Time = 15 min [Wheat straw-Fe ⁰] = 0.75 g L ⁻¹	Ultrapure water	More than 85% of the pharmaceutical was removed		[93]
Ciprofloxacin 10 mg L ⁻¹	Antibiotic	pH = 6.0 Temperature = 25 °C Time = 240 min [Fe ⁰] = 5 mmol L ⁻¹	Deionized water	Complete removal of ciprofloxacin with 59.99% TOC removal		[94]
		Particle size = 61.16 nm pH = 7.0 Time = 120 min				

Where: TOC: Total organic carbon; COD: Chemical oxygen demand; ✓: Transformation products (TPs) evaluation was performed.

achieved at acid pH values, although some studies reported removal percentages above 60% at pH near 7.0.

4. Transformation products and toxicity assessment

The formation of TPs in processes involving Fe⁰ and oxidant reagents has been attributed to H-abstraction (reduction reactions), with formation of amine and amide groups [12], as well as deprotonation by electron abstraction, leading to hydrolysis and the loss of methyl and amino groups [20,21].

The degradation pathways involve successive hydroxylation, decarboxylation, loss of some functional groups, open aromatic ring, addition to unsaturated bond reaction of radical and eventually mineralization [18,33,95]. Depending on the structure of the pharmaceutical, the TPs can include several isomers [46] and homo and heterogeneous dimers [47]. The hydroxylation reaction with the electrophilic addition of HO[•] to the aromatic ring can form a resonance-stabilized carbon-centered radical [19]. Hydroquinones can be formed from aromatic rings, while substances such as acetamide and phenol can be produced after the breaking of bonds

by free radicals [34]. Dechlorination or hydroxylation can open benzene rings and generate low molecular weight organic acids such as oxalic, acetic, and formic acids, which can be oxidized to CO₂ and H₂O [37]. In pharmaceuticals containing a sulfonamide group, a hydroxylation of the phenyl ring is produced followed by a radical attack on the S—N bond to generate aminothiazole and sulphanic acid, which is further oxidized to form aniline [96,97]. In another way, fluoride abstraction is an important step in the degradation of fluorinated pharmaceuticals [98], in this case, C—F bond is broken through radical substitution due to its nucleophilicity and instability [99]. These TPs can be identified using chromatographic techniques such as LC-MS/MS [94].

The toxicities of Fe⁰ nanoparticles are a function of their properties, the tolerance presented by organisms, and environmental conditions. The main mechanism of toxicity caused by nanoparticles is oxidative stress induced by reactive oxygen species [100], with negative effects such as disturbances in the functioning of the cell due to the blockage of cellular ducts. In bacteria, Fe⁰ can cause structural changes in the membranes, inhibiting mobility and nutrient intake, consequently leading to cell death. The ROS generated by Fe⁰ can cause lipid peroxidation and DNA damage. Negative effects of nanoparticles on the reproduction and mortality of soil and water organisms have been reported. In plants, there may be blocking of the absorption of water and nutrients by the roots, due to the deposition and accumulation of n-Fe⁰ particles on the root surface. The low solubility of Fe⁰ causes the particles to persist in biological systems, leading to long-term effects that include mutagenic effects in organisms [101]. The TPs generated in processes employing Fe⁰ may be more toxic than the original pollutant, resulting in additional inhibitory and/or toxic effects in certain organisms [102].

5. Conclusions and future prospects

In the search for new and better technologies for water treatment, Fe⁰ is a promising material for the elimination of emerging pollutants. The main disadvantage of using Fe⁰ for degradation of pollutants is the cost of catalyst synthesis, catalyst instability, acidic conditions, high concentrations of iron released in the solution and long reaction times. Advances in terms of new supports and in the immobilization and complexation of Fe⁰ have led to excellent results in the degradation of pharmaceuticals, providing solutions to the aforementioned disadvantages. An important advantage of using Fe⁰ is the possibility of reusing the material, hence generating less waste. This, combined with the *in situ* generation of H₂O₂, makes the process environmentally friendly by reducing of cost and any negative impacts caused by excess of oxidizing agents.

However, further studies are needed to investigate the degradation of pharmaceuticals present in matrices such as hospital, domestic, and industrial wastewaters, as well as the degradation of mixtures of pharmaceuticals. In future studies of n-Fe⁰, improvements are required in terms of particle longevity and the use of environmentally friendly synthesis methods employing inexpensive and biodegradable sources, at the same time integration of Fe⁰ with conventional biological treatment is necessary in order to improve the methods currently employed in WWTPs. It is important to evaluate the use of radiation sources such as LEDs and solar light, as well as other sources of energy, for the degradation of pharmaceuticals using Fe⁰, taking into consideration the costs of developing and operating reactors and scale-up for application in real wastewater treatment and water disinfection. In terms of the different groups of pharmaceuticals, there is a paucity of studies concerning the reaction behaviors and degradation efficiencies for psychiatric and hormonal drugs as well as understand the interactions between the

new Fe⁰-based catalysts and pharmaceuticals, considering the impact of the toxicities of the TPs generated and their mechanisms of degradation, especially when bioprocesses are employed.

Acknowledgments

This study was financed in part by the Coordenação de Aperfeiçoamento de Pessoal de Nível Superior - Brasil (CAPES) - Finance Code 001. The authors wish to thank CNPq (Processo: 403051/2016-9).

References

- [1] X. Weng, W. Cai, S. Lin, Z. Chen, Degradation mechanism of amoxicillin using clay supported nanoscale zero-valent iron, *Appl. Clay Sci.* 147 (2017) 137–142, doi:http://dx.doi.org/10.1016/j.clay.2017.07.023.
- [2] T. Wang, J. Lin, Z. Chen, M. Megharaj, R. Naidu, Green synthesized iron nanoparticles by green tea and eucalyptus leaves extracts used for removal of nitrate in aqueous solution, *J. Clean. Prod.* 83 (2014) 413–419, doi:http://dx.doi.org/10.1016/j.jclepro.2014.07.006.
- [3] Y. Lü, J. Li, Y. Li, L. Liang, H. Dong, K. Chen, C. Yao, Z. Li, J. Li, X. Guan, The roles of pyrite for enhancing reductive removal of nitrobenzene by zero-valent iron, *Appl. Catal. B Environ.* 242 (2018) 9–18, doi:http://dx.doi.org/10.1016/j.apcatb.2018.09.086.
- [4] J. Chen, Z. Xiu, G.V. Lowry, P.J.J. Alvarez, Effect of natural organic matter on toxicity and reactivity of nano-scale zero-valent iron, *Water Res.* 45 (2011) 1995–2001, doi:http://dx.doi.org/10.1016/j.watres.2010.11.036.
- [5] Y. Zou, X. Wang, A. Khan, P. Wang, Y. Liu, A. Alsaedi, T. Hayat, X. Wang, Environmental remediation and application of nanoscale zero-valent iron and its composites for the removal of heavy metal ions: a review, *Environ. Sci. Technol.* 50 (2016) 7290–7304, doi:http://dx.doi.org/10.1021/acs.est.6b01897.
- [6] S. Chen, F. Wang, W. Chu, X. Li, H. Wei, N. Gao, Weak magnetic field accelerates chloroacetamide removal by zero-valent iron in drinking water, *Chem. Eng. J.* 358 (2019) 40–47, doi:http://dx.doi.org/10.1016/j.cej.2018.09.212.
- [7] H. Liu, J. Yao, L. Wang, X. Wang, R. Qu, Z. Wang, Effective degradation of fenitrothion by zero-valent iron powder (Fe⁰) activated persulfate in aqueous solution: kinetic study and product identification, *Chem. Eng. J.* 358 (2019) 1479–1488, doi:http://dx.doi.org/10.1016/j.cej.2018.10.153.
- [8] H.M. Abd El-Lateef, M.M. Khalaf Ali, M.M. Saleh, Adsorption and removal of cationic and anionic surfactants using zero-valent iron nanoparticles, *J. Mol. Liq.* 268 (2018) 497–505, doi:http://dx.doi.org/10.1016/j.molliq.2018.07.093.
- [9] E. Cuervo Lumbaque, M.F. Gomes, V. Da Silva Carvalho, A.M. de Freitas, E.R.L. Tiburtius, Degradation and ecotoxicity of dye reactive black 5 after reductive-oxidative process, *Environ. Sci. Pollut. Res.* 24 (2017) 6126–6134, doi:http://dx.doi.org/10.1007/s11356-016-7150-y.
- [10] M. Kallel, C. Belaid, T. Mechichi, M. Ksibi, B. Elleuch, Removal of organic load and phenolic compounds from olive mill wastewater by Fenton oxidation with zero-valent iron, *Chem. Eng. J.* 150 (2009) 391–395, doi:http://dx.doi.org/10.1016/j.cej.2009.01.017.
- [11] Y. Wu, L. Fan, S. Hu, S. Wang, H. Yao, K. Wang, Role of dissolved iron ions in nanoparticulate zero-valent iron/H₂O₂ Fenton-like system, *Int. J. Environ. Sci. Technol.* (2018) 1–12, doi:http://dx.doi.org/10.1007/s13762-018-2094-z.
- [12] J. Cao, Z. Xiong, B. Lai, Effect of initial pH on the tetracycline (TC) removal by zero-valent iron: adsorption, oxidation and reduction, *Chem. Eng. J.* 343 (2018) 492–499, doi:http://dx.doi.org/10.1016/j.cej.2018.03.036.
- [13] F. Rezaei, D. Vione, Molecules effect of pH on zero valent iron performance in heterogeneous Fenton and fenton-like processes: a review, *Mol.* 23 (2018) 1–18, doi:http://dx.doi.org/10.3390/molecules23123127.
- [14] M. Daneshkhal, H. Hossaini, M. Malakootian, Removal of metoprolol from water by sepiolite-supported nanoscale zero-valent iron, *J. Environ. Chem. Eng.* 5 (2017) 3490–3499, doi:http://dx.doi.org/10.1016/j.jece.2017.06.040.
- [15] M. Al Aukidy, P. Verlicchi, N. Voulvoulis, A framework for the assessment of the environmental risk posed by pharmaceuticals originating from hospital effluents, *Sci. Total Environ.* 493 (2014) 54–64, doi:http://dx.doi.org/10.1016/j.scitotenv.2014.05.128.
- [16] Y. Li, L. Zhang, X. Liu, J. Ding, Ranking and prioritizing pharmaceuticals in the aquatic environment of China, *Sci. Total Environ.* 658 (2019) 333–342, doi:http://dx.doi.org/10.1016/j.scitotenv.2018.12.048.
- [17] S. Zhu, W. Wang, Y. Xu, Z. Zhu, Z. Liu, F. Cui, Iron sludge-derived magnetic Fe⁰/Fe₃C catalyst for oxidation of ciprofloxacin via peroxymonosulfate activation, *Chem. Eng. J.* (2019), doi:http://dx.doi.org/10.1016/j.cej.2019.02.011.
- [18] J. Cao, L. Lai, B. Lai, G. Yao, X. Chen, L. Song, Degradation of tetracycline by peroxymonosulfate activated with zero-valent iron: performance, intermediates, toxicity and mechanism, *Chem. Eng. J.* 364 (2019) 45–56.
- [19] I.R. Bautitz, A.C. Velosa, R.F.P. Nogueira, Zero valent iron mediated degradation of the pharmaceutical diazepam, *Chemosphere* 88 (2012) 688–692, doi:http://dx.doi.org/10.1016/j.chemosphere.2012.03.077.
- [20] S. Karim, S. Bae, D. Greenwood, K. Hanna, N. Singhal, Degradation of 17 α -ethinylestradiol by nano zero valent iron under different pH and dissolved

- oxygen levels, *Water Res.* 125 (2017) 32–41, doi:http://dx.doi.org/10.1016/j.WATRES.2017.08.029.
- [21] T. Zhou, X. Zou, X. Wu, J. Mao, J. Wang, Synergistic degradation of antibiotic norfloxacin in a novel heterogeneous sonochemical Fe⁰/tetrathosphate Fenton-like system, *Ultrason. Sonochem.* (2017), doi:http://dx.doi.org/10.1016/j.ultrsonch.2017.01.015.
- [22] Y. Pan, Y. Zhang, M. Zhou, J. Cai, Y. Tian, Enhanced removal of emerging contaminants using persulfate activated by UV and pre-magnetized Fe⁰, *Chem. Eng. J.* 361 (2019) 908–918, doi:http://dx.doi.org/10.1016/j.CEJ.2018.12.135.
- [23] L. Tang, H. Feng, J. Tang, G. Zeng, Y. Deng, J. Wang, Y. Liu, Y. Zhou, Treatment of arsenic in acid wastewater and river sediment by Fe@Fe₂O₃ nanobunches: the effect of environmental conditions and reaction mechanism, *Water Res.* 117 (2017) 175–186.
- [24] Z. Wang, J. Li, W. Tan, X. Wu, H. Lin, H. Zhang, Removal of COD from landfill leachate by advanced Fenton process combined with electrolysis, *Sep. Purif. Technol.* 208 (2019) 3–11, doi:http://dx.doi.org/10.1016/j.SEPUR.2018.06.048.
- [25] J. Deng, H. Dong, C. Zhang, Z. Jiang, Y. Cheng, K. Hou, L. Zhang, C. Fan, Nanoscale zero-valent iron/biochar composite as an activator for Fenton-like removal of sulfamethazine, *Sep. Purif. Technol.* 202 (2018) 130–137, doi:http://dx.doi.org/10.1016/j.SEPUR.2018.03.048.
- [26] I. Hussain, Y. Zhang, S. Huang, X. Du, Degradation of p-chloroaniline by persulfate activated with zero-valent iron, *Chem. Eng. J.* 203 (2012) 269–276, doi:http://dx.doi.org/10.1016/j.CEJ.2012.06.120.
- [27] J. Wang, S. Wang, Activation of persulfate (PS) and peroxymonosulfate (PMS) and application for the degradation of emerging contaminants, *Chem. Eng. J.* 334 (2018) 1502–1517, doi:http://dx.doi.org/10.1016/j.CEJ.2017.11.059.
- [28] A. Li, Z. Wu, T. Wang, S. Hou, B. Huang, X. Kong, X. Li, Y. Guan, R. Qiu, J. Fang, Kinetics and mechanisms of the degradation of PPCPs by zero-valent iron (Fe⁰) activated peroxydisulfate (PDS) system in groundwater, *J. Hazard. Mater.* 357 (2018) 207–216, doi:http://dx.doi.org/10.1016/j.JHAZMAT.2018.06.008.
- [29] Y. Segura, F. Martínez, J.A. Meleró, Effective pharmaceutical wastewater degradation by Fenton oxidation with zero-valent iron, *Appl. Catal. B Environ.* 136–137 (2013) 64–69, doi:http://dx.doi.org/10.1016/j.APCATB.2013.01.036.
- [30] J.A. de Lima Perini, R. Fernandes Pupo Nogueira, Zero-valent iron mediated degradation of sertraline – effect of H₂O₂ addition and application to sewage treatment plant effluent, *J. Chem. Technol. Biotechnol.* 91 (2016) 276–282, doi:http://dx.doi.org/10.1002/jctb.4705.
- [31] J. Du, W. Guo, X. Li, Q. Li, B. Wang, Y. Huang, N. Ren, Degradation of sulfamethoxazole by a heterogeneous Fenton-like system with microscale zero-valent iron: kinetics, effect factors, and pathways, *J. Taiwan Inst. Chem. Eng.* 81 (2017) 232–238, doi:http://dx.doi.org/10.1016/j.JTICE.2017.10.017.
- [32] C. Tan, Y. Dong, D. Fu, N. Gao, J. Ma, X. Liu, Chloramphenicol removal by zero valent iron activated peroxymonosulfate system: kinetics and mechanism of radical generation, *Chem. Eng. J.* 334 (2018) 1006–1015, doi:http://dx.doi.org/10.1016/j.CEJ.2017.10.020.
- [33] Y. Gao, N. Gao, W. Wang, S. Kang, J. Xu, H. Xiang, D. Yin, Ultrasound-assisted heterogeneous activation of persulfate by nano zero-valent iron (nZVI) for the propranolol degradation in water, *Ultrason. Sonochem.* (2018), doi:http://dx.doi.org/10.1016/j.ULTSONCH.2018.07.001.
- [34] Z. Dong, Q. Zhang, J. Hong, B.-Y. Chen, Q. Xu, Deciphering acetaminophen degradation using novel microporous beads reactor activate persulfate process with minimum Iron leachate for sustainable treatment, *Catal. Lett.* 148 (2018) 2095–2108, doi:http://dx.doi.org/10.1007/s10562-018-2418-0.
- [35] A. Ziyilan, N.H. Ince, Catalytic ozonation of ibuprofen with ultrasound and Fe-based catalysts, *Catal. Today* 240 (2015) 2–8, doi:http://dx.doi.org/10.1016/j.CATTOD.2014.03.002.
- [36] S.N. Malik, S.M. Khan, P.C. Ghosh, A.N. Vaidya, G. Kanade, S.N. Mudliar, Treatment of pharmaceutical industrial wastewater by nano-catalyzed ozonation in a semi-batch reactor for improved biodegradability, *Sci. Total Environ.* 678 (2019) 114–122, doi:http://dx.doi.org/10.1016/j.SCIOTENV.2019.04.097.
- [37] X. Li, M. Zhou, Y. Pan, Degradation of diclofenac by H₂O₂ activated with pre-magnetization Fe⁰: influencing factors and degradation pathways, *Chemosphere* 212 (2018) 853–862, doi:http://dx.doi.org/10.1016/j.CHEMOSPHERE.2018.08.144.
- [38] J. Du, W. Guo, D. Che, N. Ren, Weak magnetic field for enhanced oxidation of sulfamethoxazole by Fe⁰/H₂O₂ and Fe⁰/persulfate: performance, mechanisms, and degradation pathways, *Chem. Eng. J.* 351 (2018) 532–539, doi:http://dx.doi.org/10.1016/j.CEJ.2018.06.094.
- [39] Y. Pan, Y. Zhang, M. Zhou, J. Cai, X. Li, Y. Tian, Synergistic degradation of antibiotic sulfamethazine by novel pre-magnetized Fe⁰/PS process enhanced by ultrasound, *Chem. Eng. J.* 354 (2018) 777–789, doi:http://dx.doi.org/10.1016/j.CEJ.2018.08.084.
- [40] T. Zhou, K. Feng, W. Xiang, Y. Lv, X. Wu, J. Mao, C. He, Rapid decomposition of diclofenac in a magnetic field enhanced zero-valent iron/EDTA Fenton-like system, *Chemosphere* 193 (2018) 968–977, doi:http://dx.doi.org/10.1016/j.CHEMOSPHERE.2017.11.090.
- [41] M. Kahoush, N. Behary, A. Cayla, V. Nierstrasz, Bio-Fenton and Bio-electro-Fenton as sustainable methods for degrading organic pollutants in wastewater, *Process Biochem.* 64 (2018) 237–247, doi:http://dx.doi.org/10.1016/j.procbio.2017.10.003.
- [42] X. Pan, N. Lv, C. Li, J. Ning, T. Wang, R. Wang, M. Zhou, G. Zhu, Impact of nano zero valent iron on tetracycline degradation and microbial community succession during anaerobic digestion, *Chem. Eng. J.* 359 (2019) 662–671, doi:http://dx.doi.org/10.1016/j.CEJ.2018.11.135.
- [43] R. Bavandi, M. Emtyazjoo, H.N. Saravi, F. Yazdian, M. Sheikhpour, Study of capability of nanostructured zero-valent iron and graphene oxide for bioremoval of trinitrophenol from wastewater in a bubble column bioreactor, *Electron. J. Biotechnol.* 39 (2019) 8–14, doi:http://dx.doi.org/10.1016/j.EJBT.2019.02.003.
- [44] R. Changotra, H. Rajput, A. Dhir, Treatment of real pharmaceutical wastewater using combined approach of Fenton applications and aerobic biological treatment, *J. Photochem. Photobiol. A Chem.* 376 (2019) 175–184, doi:http://dx.doi.org/10.1016/j.jphotochem.2019.02.029.
- [45] W. Qian, J. Zhang, Y. Xiong, X. Chen, S. Tian, L. Kong, Y. Guo, Construction and performance of a novel integrative Fenton-like and upward flow biological filter bed, *Chem. Eng. J.* 273 (2015) 166–172, doi:http://dx.doi.org/10.1016/j.CEJ.2015.03.058.
- [46] S. Adityasulindro, C. Julcour, L. Barthe, Heterogeneous Fenton oxidation using Fe-ZSM5 catalyst for removal of ibuprofen in wastewater, *J. Environ. Chem. Eng.* 6 (2018) 5920–5928, doi:http://dx.doi.org/10.1016/j.JECE.2018.09.007.
- [47] X. Liu, Z. Cao, Z. Yuan, J. Zhang, X.-P. Guo, Y. Yang, F. He, Y. Zhao, J. Xu, Insight into the kinetics and mechanism of removal of aqueous chlorinated nitroaromatic antibiotic chloramphenicol by nanoscale zero-valent iron, *Chem. Eng. J.* 334 (2017), doi:http://dx.doi.org/10.1016/j.cej.2017.10.060.
- [48] P. Xie, L. Zhang, J. Chen, J. Ding, Y. Wan, S. Wang, Z. Wang, A. Zhou, J. Ma, Enhanced degradation of organic contaminants by zero-valent iron/sulfite process under simulated sunlight irradiation, *Water Res.* 149 (2016) 169–178, doi:http://dx.doi.org/10.1016/j.WATRES.2016.10.078.
- [49] J. Chen, W.R. Browne, Photochemistry of iron complexes, *Coord. Chem. Rev.* 374 (2018) 15–35, doi:http://dx.doi.org/10.1016/j.CCR.2018.06.008.
- [50] B.D. Yirsaw, M. Megharaj, Z. Chen, R. Naidu, Environmental application and ecological significance of nano-zero valent iron, *J. Environ. Sci.* 44 (2016) 88–98, doi:http://dx.doi.org/10.1016/j.JES.2015.07.016.
- [51] L. Demarchis, M. Minella, R. Nisticò, V. Maurino, C. Minero, D. Vione, Photo-Fenton reaction in the presence of morphologically controlled hematite as iron source, *J. Photochem. Photobiol. A Chem.* 307–308 (2015) 99–107, doi:http://dx.doi.org/10.1016/j.JPHOTOCHEM.2015.04.009.
- [52] X. Yang, X. Zhang, Z. Wang, S. Li, J. Zhao, G. Liang, X. Xie, Mechanistic insights into removal of norfloxacin from water using different natural iron ore – biochar composites: more rich free radicals derived from natural pyrite-biochar composites than hematite-biochar composites, *Appl. Catal. B Environ.* 255 (2019) 117752, doi:http://dx.doi.org/10.1016/j.APCATB.2019.117752.
- [53] S. Ambika, M. Devasena, I.M. Nambi, Synthesis, characterization and performance of high energy ball milled meso-scale zero valent iron in Fenton reaction, *J. Environ. Manage.* 181 (2016) 847–855, doi:http://dx.doi.org/10.1016/j.JENVMAN.2016.06.054.
- [54] X. Ma, Y. Cheng, Y. Ge, H. Wu, Q. Li, N. Gao, J. Deng, Ultrasound-enhanced nanosized zero-valent copper activation of hydrogen peroxide for the degradation of norfloxacin, *Ultrason. Sonochem.* 40 (2018) 763–772, doi:http://dx.doi.org/10.1016/j.ULTSONCH.2017.08.025.
- [55] K.P. Singh, A.K. Singh, S. Gupta, P. Rai, Modeling and optimization of reductive degradation of chloramphenicol in aqueous solution by zero-valent bimetallic nanoparticles, *Environ. Sci. Pollut. Res.* 19 (2012) 2063–2078, doi:http://dx.doi.org/10.1007/s11356-011-0700-4.
- [56] L. Chen, R. Ni, T. Yuan, Q. Yue, B. Gao, Removal of tridecane dicarboxylic acid in water by nanoscale Fe₀/Cu₀ bimetallic composites, *Ecotoxicol. Environ. Saf.* 164 (2018) 219–225, doi:http://dx.doi.org/10.1016/j.ECOENV.2018.08.023.
- [57] Y. Wu, Q. Yue, Y. Gao, Z. Ren, B. Gao, Performance of bimetallic nanoscale zero-valent iron particles for removal of oxytetracycline, *J. Environ. Sci.* 69 (2018) 173–182, doi:http://dx.doi.org/10.1016/j.JES.2017.10.006.
- [58] H. Feng, L. Tang, J. Tang, G. Zeng, H. Dong, Y. Deng, L. Wang, Y. Liu, X. Ren, Y. Zhou, Cu-Doped Fe@Fe₂O₃ core-shell nanoparticle shifted oxygen reduction pathway for high-efficiency arsenic removal in smelting wastewater, *Environ. Sci. Nano* 5 (2018) 1595–1607.
- [59] X. Weng, W. Cai, R. Lan, Q. Sun, Z. Chen, Simultaneous removal of amoxicillin, ampicillin and penicillin by clay supported Fe/Ni bimetallic nanoparticles, *Environ. Pollut.* 236 (2018) 562–569, doi:http://dx.doi.org/10.1016/j.ENVPOL.2018.01.100.
- [60] A.R. Yazdanbakhsh, H. Daraei, M. Rafiee, H. Kamali, Performance of iron nanoparticles and bimetallic Ni/Fe nanoparticles in removal of amoxicillin trihydrate from synthetic wastewater, *Water Sci. Technol.* 73 (2016) 2998–3007, doi:http://dx.doi.org/10.2166/wst.2016.157.
- [61] J. Gong, C.-S. Lee, E.-J. Kim, Y.-Y. Chang, Y.-S. Chang, Enhancing the reactivity of bimetallic Bi/Fe⁰ by citric acid for remediation of polluted water, *J. Hazard. Mater.* 310 (2016) 135–142, doi:http://dx.doi.org/10.1016/j.JHAZMAT.2016.02.027.
- [62] J. Deng, H. Dong, C. Zhang, Z. Jiang, Y. Cheng, K. Hou, L. Zhang, C. Fan, Nanoscale zero-valent iron/biochar composite as an activator for Fenton-like removal of sulfamethazine, *Sep. Purif. Technol.* 202 (2018) 130–137, doi:http://dx.doi.org/10.1016/j.SEPUR.2018.03.048.
- [63] Y. Wu, Q. Yue, Z. Ren, B. Gao, Immobilization of nanoscale zero-valent iron particles (nZVI) with synthesized activated carbon for the adsorption and degradation of Chloramphenicol (CAP), *J. Mol. Liq.* 262 (2018) 19–28, doi:http://dx.doi.org/10.1016/j.MOLLIQ.2018.04.032.
- [64] W. Zhang, L. Qian, D. Ouyang, Y. Chen, L. Han, M. Chen, Effective removal of Cr(VI) by attapulgite-supported nanoscale zero-valent iron from aqueous solution: Enhanced adsorption and crystallization, *Chemosphere* 221 (2019) 683–692, doi:http://dx.doi.org/10.1016/j.CHEMOSPHERE.2019.01.070.

- [65] S. Yang, P. Wu, Q. Ye, W. Li, M. Chen, N. Zhu, Efficient catalytic degradation of bisphenol A by novel Fe⁰-vermiculite composite in photo-Fenton system: mechanism and effect of iron oxide shell, *Chemosphere* 208 (2018) 335–342, doi:http://dx.doi.org/10.1016/j.chemosphere.2018.06.008.
- [66] R. Zhao, Z. Zhou, X. Zhao, G. Jing, Enhanced Cr(VI) removal from simulated electroplating rinse wastewater by amino-functionalized vermiculite-supported nanoscale zero-valent iron, *Chemosphere* 218 (2019) 458–467, doi:http://dx.doi.org/10.1016/j.chemosphere.2018.11.118.
- [67] Z. Li, H. Dong, Y. Zhang, J. Li, Y. Li, Enhanced removal of Ni(II) by nanoscale zero valent iron supported on Na-saturated bentonite, *J. Colloid Interface Sci.* 497 (2017) 43–49, doi:http://dx.doi.org/10.1016/j.jcis.2017.02.058.
- [68] B. Kakavandi, A. Takdastan, S. Pourfadakari, M. Ahmadmoazzam, S. Jorfi, Heterogeneous catalytic degradation of organic compounds using nanoscale zero-valent iron supported on kaolinite: mechanism, kinetic and feasibility studies, *J. Taiwan Inst. Chem. Eng.* (2018), doi:http://dx.doi.org/10.1016/j.jtice.2018.11.027.
- [69] F. Liu, J. Yang, J. Zuo, D. Ma, L. Gan, B. Xie, P. Wang, B. Yang, Graphene-supported nanoscale zero-valent iron: removal of phosphorus from aqueous solution and mechanistic study, *J. Environ. Sci.* 26 (2014) 1751–1762, doi:http://dx.doi.org/10.1016/j.jes.2014.06.016.
- [70] P. Villegas-Guzman, S. Giannakis, S. Rtimi, D. Grandjean, M. Bensimon, L.F. de Alencastro, R. Torres-Palma, C. Pulgarin, A green solar photo-Fenton process for the elimination of bacteria and micropollutants in municipal wastewater treatment using mineral iron and natural organic acids, *Appl. Catal. B Environ.* 219 (2017) 538–549, doi:http://dx.doi.org/10.1016/j.apcatb.2017.07.066.
- [71] K. Yi, Z. Fan, J. Tang, A. Chen, J. Shao, L. Peng, Q. Zeng, S. Luo, The elucidation of surrounding alginate gels on the pollutants degradation by entrapped nanoscale zero-valent iron, *Colloids Surf. B Biointerfaces* 171 (2018) 233–240, doi:http://dx.doi.org/10.1016/j.colsurfb.2018.07.033.
- [72] E. Cuervo Lumbaque, R. Wielens Becker, D. Salmoria Araújo, A. Dalleggrave, T. Ost Fracari, V. Lavayen, C. Sirtori, Degradation of pharmaceuticals in different water matrices by a solar homo/heterogeneous photo-Fenton process over modified alginate spheres, *Environ. Sci. Pollut. Res.* (2019), doi:http://dx.doi.org/10.1007/s11356-018-04092-z.
- [73] M. Pirsahab, S. Moradi, M. Shahlaei, X. Wang, N. Farhadian, A new composite of nano zero-valent iron encapsulated in carbon dots for oxidative removal of bio-refractory antibiotics from water, *J. Clean. Prod.* 209 (2019) 1523–1532, doi:http://dx.doi.org/10.1016/j.jclepro.2018.11.175.
- [74] Y. Li, X. Zhao, Y. Yan, J. Yan, Y. Pan, Y. Zhang, B. Lai, Enhanced sulfamethoxazole degradation by peroxydisulfate activation with sulfide-modified microscale zero-valent iron (S-mFe⁰): performance, mechanisms, and the role of sulfur species, *Chem. Eng. J.* (2019), doi:http://dx.doi.org/10.1016/j.cej.2019.03.178.
- [75] Y. Su, D. Jassby, S. Song, X. Zhou, H. Zhao, J. Filip, E. Petala, Y. Zhang, Enhanced oxidative and adsorptive removal of diclofenac in heterogeneous fenton-like reaction with sulfide modified nanoscale zerovalent Iron, *Environ. Sci. Technol.* 52 (2018) 6466–6475, doi:http://dx.doi.org/10.1021/acs.est.8b00231.
- [76] E. Cuervo Lumbaque, D. Salmoria Araújo, T. Moreira Klein, E.R. Lopes Tiburtius, J. Argüello, C. Sirtori, Solar photo-Fenton-like process at neutral pH: Fe(III)-EDDS complex formation and optimization of experimental conditions for degradation of pharmaceuticals, *Catal. Today* (2019), doi:http://dx.doi.org/10.1016/j.cattod.2019.01.006.
- [77] M.B. Allabaksh, B.K. Mandal, M.K. Kesarla, K.S. Kumar, P.S. Reddy, Preparation of stable zero valent iron nanoparticles using different chelating agents, *J. Chem. Pharm. Res.* 2 (2010) 67–74.
- [78] J. Deng, Y. Shao, N. Gao, Y. Deng, C. Tan, S. Zhou, Zero-valent iron/persulfate (Fe⁰/PS) oxidation acetaminophen in water, *Int. J. Environ. Sci. Technol.* 11 (2014) 881–890, doi:http://dx.doi.org/10.1007/s13762-013-0284-2.
- [79] A.R. Lado Ribeiro, N.F.F. Moreira, G. Li Puma, A.M.T. Silva, Impact of water matrix on the removal of micropollutants by advanced oxidation technologies, *Chem. Eng. J.* 363 (2019) 155–173, doi:http://dx.doi.org/10.1016/j.cej.2019.01.080.
- [80] H. Bang, Y.M. Slokar, G. Ferrero, J.C. Kruithof, M.D. Kennedy, Removal of taste and odor causing compounds by UV/H₂O₂ treatment: effect of the organic and inorganic water matrix, *Desalin. Water Treat.* 57 (2016) 1–10, doi:http://dx.doi.org/10.1080/19443994.2016.1177274.
- [81] J.I. Martínez-Costa, J. Rivera-Utrilla, R. Leyva-Ramos, M. Sánchez-Polo, I. Vello-Gala, A.J. Mota, Individual and simultaneous degradation of the antibiotics sulfamethoxazole and trimethoprim in aqueous solutions by Fenton, Fenton-like and photo-Fenton processes using solar and UV radiations, *J. Photochem. Photobiol. A Chem.* 360 (2018) 95–108, doi:http://dx.doi.org/10.1016/j.jphotochem.2018.04.014.
- [82] R. Ling, J.P. Chen, J. Shao, M. Reinhard, Degradation of organic compounds during the corrosion of ZVI by hydrogen peroxide at neutral pH: kinetics, mechanisms and effect of corrosion promoting and inhibiting ions, *Water Res.* 134 (2018) 44–53, doi:http://dx.doi.org/10.1016/j.watres.2018.01.065.
- [83] L.H.M.L.M. Santos, M. Gros, S. Rodriguez-Mozaz, C. Delerue-Matos, A. Pena, D. Barceló, M.C.B.S.M. Montenegro, Contribution of hospital effluents to the load of pharmaceuticals in urban wastewaters: identification of ecologically relevant pharmaceuticals, *Sci. Total Environ.* 461–462 (2013) 302–316, doi:http://dx.doi.org/10.1016/j.scitotenv.2013.04.077.
- [84] J. Wang, S. Wang, Removal of pharmaceuticals and personal care products (PPCPs) from wastewater: a review, *J. Environ. Manage.* 182 (2016) 620–640, doi:http://dx.doi.org/10.1016/j.jenvman.2016.07.049.
- [85] J. Fick, H. Söderström, R.H. Lindberg, C. Phan, M. Tysklind, D.G.J. Larsson, Contamination of surface, ground, and drinking water from pharmaceutical production, *Environ. Toxicol. Chem.* 28 (2009) 2522–2527, doi:http://dx.doi.org/10.1897/09-073.1.
- [86] S. Chung, B.W. Brooks, Identifying household pharmaceutical waste characteristics and population behaviors in one of the most densely populated global cities, *Resour. Conserv. Recycl.* 140 (2019) 267–277, doi:http://dx.doi.org/10.1016/j.resconrec.2018.09.024.
- [87] J. Rivera-Utrilla, M. Sánchez-Polo, M.Á. Ferro-García, G. Prados-Joya, R. Ocampo-Pérez, Pharmaceuticals as emerging contaminants and their removal from water. A review, *Chemosphere* 93 (2013) 1268–1287, doi:http://dx.doi.org/10.1016/j.chemosphere.2013.07.059.
- [88] N. Fujitoka, M. Suzuki, S. Kurosu, Y. Kawase, Linkage of iron elution and dissolved oxygen consumption with removal of organic pollutants by nanoscale zero-valent iron: effects of pH on iron dissolution and formation of iron oxide/hydroxide layer, *Chemosphere* 144 (2016) 1738–1746.
- [89] H. Rahmani, M. Gholami, A.H. Mahvi, M. Ali-Mohammadi, K. Rahmani, Tinidazol antibiotic degradation in aqueous solution by zero valent iron nanoparticles and hydrogen peroxide in the presence of ultrasound radiation, *J. Water Chem. Technol.* 36 (2014) 317–324, doi:http://dx.doi.org/10.3103/S1063455X14060101.
- [90] F. Suanon, Q. Sun, M. Li, X. Cai, Y. Zhang, Y. Yan, C.-P. Yu, Application of nanoscale zero valent iron and iron powder during sludge anaerobic digestion: impact on methane yield and pharmaceutical and personal care products degradation, *J. Hazard. Mater.* 321 (2017) 47–53, doi:http://dx.doi.org/10.1016/j.jhazmat.2016.08.076.
- [91] J. Du, W. Guo, X. Li, Q. Li, B. Wang, Y. Huang, N. Ren, Degradation of sulfamethoxazole by a heterogeneous Fenton-like system with microscale zero-valent iron: kinetics, effect factors, and pathways, *J. Taiwan Inst. Chem. Eng.* 81 (2017) 232–238, doi:http://dx.doi.org/10.1016/j.jtice.2017.10.017.
- [92] S. Machado, J.G. Pacheco, H.P.A. Nouws, J.T. Albergaria, C. Delerue-Matos, Green zero-valent iron nanoparticles for the degradation of amoxicillin, *Int. J. Environ. Sci. Technol.* 14 (2017) 1109–1118, doi:http://dx.doi.org/10.1007/s13762-016-1197-7.
- [93] Y. Shao, P. Zhao, Q. Yue, Y. Wu, B. Gao, W. Kong, Preparation of wheat straw-supported Nanoscale Zero-Valent Iron and its removal performance on ciprofloxacin, *Ecotoxicol. Environ. Saf.* 158 (2018) 100–107, doi:http://dx.doi.org/10.1016/j.ecoenv.2018.04.020.
- [94] S.K. Mondal, A.K. Saha, A. Sinha, Removal of ciprofloxacin using modified advanced oxidation processes: kinetics, pathways and process optimization, *J. Clean. Prod.* 171 (2018) 1203–1214, doi:http://dx.doi.org/10.1016/j.jclepro.2017.10.091.
- [95] N.S. Shah, J.A. Khan, M. Sayed, Z.U.H. Khan, H.S. Ali, B. Murtaza, H.M. Khan, M. Imran, N. Muhammad, Hydroxyl and sulfate radical mediated degradation of ciprofloxacin using nano zerovalent manganese catalyzed S₂O₈²⁻, *Chem. Eng. J.* 356 (2019) 199–209.
- [96] Y.-P. Chen, L.-M. Yang, J.P. Chen, Y.-M. Zheng, Electrospun spongy zero-valent iron as excellent electro-Fenton catalyst for enhanced sulfathiazole removal by a combination of adsorption and electro-catalytic oxidation, *J. Hazard. Mater.* (2019).
- [97] J. Wu, B. Wang, L. Blaney, G. Peng, P. Chen, Y. Cui, S. Deng, Y. Wang, J. Huang, G. Yu, Degradation of sulfamethazine by persulfate activated with organo-montmorillonite supported nano-zero valent iron, *Chem. Eng. J.* 361 (2019) 99–108.
- [98] L.W. Matzek, K.E. Carter, Sustained persulfate activation using solid iron: kinetics and application to ciprofloxacin degradation, *Chem. Eng. J.* 307 (2017) 650–660.
- [99] J. Deng, M. Xu, Y. Chen, J. Li, C. Qiu, X. Li, S. Zhou, Highly-efficient removal of norfloxacin with nanoscale zero-valent copper activated persulfate at mild temperature, *Chem. Eng. J.* 366 (2019) 491–503.
- [100] C. Lei, Y. Sun, D.C.W. Tsang, D. Lin, Environmental transformations and ecological effects of iron-based nanoparticles, *Environ. Pollut.* 232 (2018) 10–30, doi:http://dx.doi.org/10.1016/j.envpol.2017.09.052.
- [101] M. Stefaniuk, P. Oleszczuk, Y.S. Ok, Review on nano zerovalent iron (nZVI): From synthesis to environmental applications, *Chem. Eng. J.* 287 (2016) 618–632, doi:http://dx.doi.org/10.1016/j.cej.2015.11.046.
- [102] C. Yangin-Gomec, T. Olmez-Hanci, I. Arslan-Alaton, S. Khoei, H. Fakhri, Iopamidol degradation with ZVI- and ZVA-activated chemical oxidation: investigation of toxicity, anaerobic inhibition and microbial communities, *J. Environ. Chem. Eng.* 6 (2018) 7318–7326, doi:http://dx.doi.org/10.1016/j.jece.2018.09.028.

4.1.2 Solar photo-Fenton process: immobilized iron in alginate

As it mentioned above, Fenton processes have been shown to be enhanced by light due to the decomposition of the photoactive $[\text{Fe}(\text{OH})]^{2+}$ species, promoting an additional generation of HO^\bullet radicals in solution¹⁰⁶. Therefore, in order to remove the iron ions from solution, separation techniques are necessary with additional operational costs. For this reason, the development of photo-Fenton processes has been promoted on the basis of heterogeneous catalytic systems, which provide an easy separation-recovery of the catalyst from the treated wastewater.

In this way, research efforts are currently focused on the use of support with high stability and allowing an efficient generation of HO^\bullet . In the literature, different organic and inorganic materials have already been reported as supports for the immobilization of active iron species in heterogeneous photo-Fenton processes^{107–110}.

This subsection therefore presents a study focused on the analysis of the immobilization of iron in alginate as a continuous iron dosing strategy in the solar photo-Fenton process for the degradation of model pharmaceuticals (**Paper III**)¹¹¹. The spheres produced from a biodegradable raw material (alginate) could easily remove from the reaction medium and considered for reuse. In addition, the possible TPs generated during the treatment processes were analyzed.



Degradation of pharmaceuticals in different water matrices by a solar homo/heterogeneous photo-Fenton process over modified alginate spheres

Elisabeth Cuervo Lumbaque¹ · Raquel Wielens Becker¹ · Débora Salmoria Araújo¹ · Alessandro Dallegrave¹ · Tiago Ost Fracari¹ · Vladimir Lavayen¹ · Carla Sirtori¹

Received: 15 August 2018 / Accepted: 27 December 2018
© Springer-Verlag GmbH Germany, part of Springer Nature 2019

Abstract

A solar homo/heterogeneous photo-Fenton process using five materials (Fe(II), Fe(III), mining waste, Fe(II)/mining waste, and Fe(III)/mining waste) supported on sodium alginate was used as a strategy to iron dosage for the degradation of eight pharmaceuticals in three different water matrices (distilled water, simulated wastewater, and hospital wastewater). Experiments were carried out in a photoreactor with a capacity of 1 L, using 3 g of iron-alginate spheres and an initial hydrogen peroxide concentration of 25 mg L⁻¹, at pH 5.0. All the materials prepared were characterized by different techniques. The Fe(III)-alginate spheres presented the best pharmaceutical degradation after a treatment time of 116 min. Nineteen transformation products generated during the solar photo-Fenton process were identified by liquid chromatography coupled to quadrupole time-of-flight mass spectrometry, using a purpose-built database developed for detecting these transformation products. Finally, the transformation products identified were classified according to their toxicity and predicted biodegradability.

Keywords Pharmaceuticals · Solar homo/heterogeneous photo-Fenton process · Hospital wastewater · Neutral pH · Transformation products

Introduction

In recent years, the photo-Fenton process has been widely studied for the removal of persistent pollutants from wastewater, using solar light as the radiation source; looking at the viability of any field-scale water treatment technology, it depends on its efficiency under natural solar irradiation instead of artificial light sources (Bansal et al. 2018). The results of the studies

show a faster removal and mineralization of recalcitrant organic compounds, compared to typical dark Fenton processes, and has the advantage of being able to use solar light for UV irradiation (Alalm et al. 2015). The heterogeneous photo-Fenton reaction has been successfully used for the degradation of pharmaceuticals in water and wastewater (Mirzaei et al. 2017), offering a more environmentally friendly approach, according to life cycle assessment, for the treatment of pharmaceuticals in wastewater, compared to other advanced wastewater treatment processes (Rodríguez et al. 2016). Besides, this system allows to extend the range of viable operative pH.

Recent studies have reported the successful use of iron supported on sodium alginate, a biopolymer (Titouhi and Belgaied 2016; Cruz et al. 2017). This material is derived from algae and can undergo ion exchange with divalent or trivalent cations, producing an “egg-box” type structure (Liu et al. 2016). It can be employed as a catalyst in Fenton reactions, taking advantage of the ability of alginate to form solid gel structures and iron ions to participate in the cation exchange; this strategy represents a new way to maintain iron as an effective catalyst at neutral pH. The reaction of Fe(II) or Fe(III) with alginate

Responsible Editor: VÃtor Pais Vilar

Electronic supplementary material The online version of this article (<https://doi.org/10.1007/s11356-018-04092-z>) contains supplementary material, which is available to authorized users.

✉ Vladimir Lavayen
vladimir.lavayen@ufrgs.br

✉ Carla Sirtori
carla.sirtori@ufrgs.br

¹ Instituto de Química, Universidade Federal do Rio Grande do Sul, Av. Bento Gonçalves, 9500, Porto Alegre, RS, Brazil

enables the synthesis of an environmentally friendly support for iron that is not harmful to health and offers the possibility of working with sunlight (Carra et al. 2014).

Previous studies have evaluated the efficiencies of simple Fenton-like solid catalysts produced using iron oxide minerals such as magnetite (Fe_3O_4) (Sun and Lemley 2011; Sun et al. 2013), hematite (Fe_2O_3) (Catalá et al. 2015; Arzate-Salgado et al. 2016), and pyrite (FeS_2) (Bae et al. 2013), among others, as potential materials for the elimination of emerging contaminants with ease of work at pH close to neutrality in the presence of UV radiation (Iervolino et al. 2015; Vaiano et al. 2015) showed a high percentage of mineralization in the first 40 min of treatment. The magnetic properties of these minerals enable the catalysts to be easily removed from the solution (Giannakis et al. 2016; Su 2017). However, the use of iron ions or mineral oxides immobilized in biodegradable material has received little attention for the degradation of pharmaceuticals in different matrices under mild operational working conditions.

On the other hand, simultaneously to the degradation of the pharmaceuticals which are generated, different intermediate species may be more stable or toxic than the parent compound (Kümmerer 2009). The monitoring of these species, known as transformation products (TPs), represents a serious challenge, in environmental matrices, because the TPs are present at very low levels ($< \text{ng L}^{-1}$). This necessitates the use of high-resolution mass spectrometric techniques, such as quadrupole time-of-flight tandem mass spectrometry (QTOF), for the detection and identification of unknown compounds, with the acquisition of full spectra with high mass accuracy and high sensitivity (Fatta-Kassinos et al. 2011). In addition to the low concentrations of TPs, their potential toxicity and low biodegradability are characteristics that indicate the importance of studies that can provide information concerning the degradation of these emerging pollutants.

The present work focuses on evaluating the degradation capacity of eight pharmaceutical contaminants from different homo/heterogeneous photo-Fenton processes using modified alginate spheres as a strategy to iron dosage in three different water matrices, which allows working at pH values close to neutrality. In addition, the identification of TPs through LC-QTOFMS using a purpose-built database allowed elucidating possible degradation pathways for some pharmaceuticals and made possible to evaluate the predicted biodegradability and the toxicological hazard of each TP.

Materials and methods

Chemicals

The reagents used for the chromatographic analyses, including LC-MS grade (Lichrosolv®) acetonitrile (ACN) and methanol (MeOH), as well as formic acid (98% purity), were

purchased from Merck (Darmstadt, Germany). The pharmaceuticals investigated in this work were purchased from different providers and were of analytical grade ($> 98.99\%$ purity). The catalysts were produced using sodium alginate (Dinâmica, São Paulo, Brazil), iron sulfate pentahydrate ($\text{Fe}_2(\text{SO}_4)_3 \cdot 5\text{H}_2\text{O}$; Synth, São Paulo, Brazil), and iron sulfate heptahydrate ($\text{FeSO}_4 \cdot 7\text{H}_2\text{O}$; Synth, São Paulo, Brazil). Photo-Fenton experiments were performed using alginate spheres containing Fe(II) and Fe(III) ions, reagent grade hydrogen peroxide (H_2O_2 , 35% w/v; Synth), and sulfuric acid (H_2SO_4 , 98%; Synth) for pH adjustment.

Immobilization of iron in alginate

The methodology for the immobilization of iron in alginate has been adapted from Souza et al. (2008). Alginate spheres were made from 2.0% (w/v) aqueous sodium alginate solution, which was prepared by mixing sodium alginate powder in ultrapure water at 60 °C. The sodium alginate solution was stirred for 24 h to facilitate the elimination of air bubbles formed during the mixing process, in order to decrease its viscosity and to reduce the drop size for the next step. Then, sodium alginate solution was added dropwise to 0.1 mol L^{-1} CaCl_2 solution, at 4 °C, to obtain resistant spheres of calcium alginate. These beads were placed in aqueous solution of FeSO_4 and $\text{Fe}_2(\text{SO}_4)_3$ (0.05 mol L^{-1}) each one for 15 days under refrigeration; in this step, the Fe(II) and Fe(III) were immobilized on the beads by an ion exchange process, and Fe(II)-alginate and Fe(III)-alginate beads were obtained, after which the spheres were washed repeatedly with distilled water to remove the excess iron in the surface.

In the case of the mining waste spheres, 10 g of mining waste was added to 100 mL of 2.0% (w/v) alginate solution, for its subsequent cross-linking with CaCl_2 solution; this material was denoted mining waste-alginate. Finally, materials consisting of mining waste and iron ions (Fe(II) or Fe(III)) supported on alginate were prepared. For this, spheres of the mining waste-alginate were placed in contact with Fe(II) or Fe(III) solutions following the methodology initially described. These two additional materials were denoted Fe(II)/mining waste-alginate, and Fe(III)/mining waste-alginate. Prior to use, all the spheres were dried for 24 h at 40 °C to eliminate water. Further information is provided in Fig. S.2.1 (Supporting Information).

The iron content in the mining waste powder used in this study was quantified by flame atomic absorption spectrometry, using a Perkin-Elmer AAnalyst 200 instrument fitted with a hollow cathode lamp (Lumina™, Perkin-Elmer). The results showed an iron content of 36.86% (w/w). The determination of immobilized iron in alginate for Fe(II)-alginate and Fe(III)-alginate was determined by UV-Vis spectrometry (Cary 50 UV-Vis spectrophotometer) with previous digestion of the sample in an acid solution $\text{HNO}_3:\text{HCl}$ (1:3) at 70 °C for 1 h,

subsequently; with an adequate dilution, its concentration was measured by colorimetric determination with 1,10-phenanthroline, according to the ISO (1998) procedure. It was determined that Fe(II)-alginate and Fe(III)-alginate contain 7.56 mg and 25.11 mg, respectively, of iron immobilized in 1 g of alginate spheres. In turn, Fe(II)/mining waste-alginate contain 1.76 mg of iron, and Fe(III)/mining waste-alginate contain 3.03 mg of iron immobilized in 1 g of the material.

Characterization of the different prepared alginate spheres

The alginate spheres were characterized using optical microscopy (Olympus BX41). X-ray diffraction (XRD) pattern was investigated by a Siemens D500 equipment operated at 30-kV voltage and 17-mA current using a monochromatic Cu K α radiation ($\lambda = 0.15406$ nm) on the measured range, with steps of 0.05° and counting time of 2 s per step. ATR-IR spectra were acquired using a Bruker Alpha FTIR spectrometer. The Alpha-p ATR accessory was equipped with a single-reflection diamond ATR hemisphere and a spring-loaded mechanical press for compacting solid samples at the ATR waveguide surface, under uniform and reproducible pressure (Müller et al. 2014). Each spectrum was recorded from 4000 to 500 cm⁻¹, with 24 co-added scans performed in ~1 min, with resolution of 4 cm⁻¹ for the samples and 24 cm⁻¹ for the background.

Solar homo/heterogeneous photo-Fenton process

Solar homo/heterogeneous photo-Fenton experiments were carried out using a solar batch photoreactor (1 L) equipped with a magnetic stirrer. In all the experiments, the pH was adjusted to pH 5.0 using H₂SO₄ (0.05 mol L⁻¹). This pH was selected because it was intermediate between pH 2.8–3.0 (which is the optimum pH for the Fenton process, but implies stronger conditions and higher reagent consumption) and neutral pH (which is close to the pH of hospital wastewater). For each degradation study, a quantity of 3 g of catalyst was used and 5 different types of catalysts (Fe(II)-alginate, Fe(III)-alginate, mining waste-alginate, Fe(II)/mining waste-alginate, and Fe(III)/mining waste-alginate) were used separately, followed by addition of hydrogen peroxide (35% w/v) at an initial concentration of 25 mg L⁻¹ at the beginning of the experiments. Solar UV radiation was measured by a solar energy meter (ICEL SP-2000), which provided data in terms of incident UV (W m⁻²). All these data were used to calculate t_{30W} (Nogueira et al. 2005).

Eight pharmaceuticals were selected for use in this study: nimesulide (NMD), furosemide (FRS), paracetamol (PCT), propranolol (PPN), dipyrone (DIP), fluoxetine (FXT), progesterone (PRG), and diazepam (DZP). The individual initial average concentrations were below 500 µg L⁻¹. Working

solutions were obtained by appropriate dilution of the stock solutions prepared using analytical standards of the compounds.

Experiments were carried out using three different water matrices: distilled water (DW), simulated wastewater (SW), and raw hospital wastewater (RHW). The SW composition was adapted from OECD (1999), in order to simulate the organic content of the real hospital wastewater employed in this work (composition for 1 L of SW: 160 mg L⁻¹ peptone, 110 mg L⁻¹ beef extract, 30 mg L⁻¹ urea, 2 mg L⁻¹ Mg₂SO₄·7H₂O, and 4 mg L⁻¹ CaCl₂·2H₂O). The characteristics of the RHW used were as follows: pH 8.98, 49.1 mg L⁻¹ chloride, conductivity of 722 µS cm⁻¹, BOD of 69 mg L⁻¹ O₂, 67.56 mg L⁻¹ DOC, COD of 217 mg L⁻¹ O₂, 9.45 mg L⁻¹ phosphate, 67 mg L⁻¹ total suspended solids, and 261 mg L⁻¹ total solids. The RHW employed in the degradation studies consisted of raw wastewater that was used as collected (without filtration). The pharmaceutical compounds were added to this water matrix before pH adjustment and before additions of the different iron-alginate spheres and H₂O₂.

Analytical determinations during the treatment processes

The total iron concentration was monitored by colorimetric determination with 1,10-phenanthroline, according to the ISSO (1998) procedure, using a Cary 50 UV-Vis spectrophotometer. Hydrogen peroxide was analyzed by a spectrophotometric method using ammonium metavanadate, based on formation of the red-orange peroxovanadium cation during the reaction of H₂O₂ with metavanadate (Nogueira et al. 2005).

Liquid chromatography-quadrupole time-of-flight mass spectrometry

Degradation of the pharmaceuticals and the TPs generated during the solar heterogeneous photo-Fenton process was monitored using a Shimadzu Nexera X2 UHPLC system connected to an Impact II QTOF mass spectrometer (BrukerDaltonics). The UHPLC system was equipped with a reversed phase Luna®Omega C18 analytical column (2.1 mm × 50 mm × 1.6 µm). The mobile phase was a mixture of MeOH acidified with 0.1% formic acid (eluent A) and H₂O acidified with 0.1% formic acid (eluent B), at a flow rate of 0.28 mL min⁻¹. The gradient elution was from 10% A (initial condition) to 90% A, in 10 min, with a final hold for 2 min. The QTOF mass spectrometer was operated in positive ionization mode, under the following conditions: capillary at 4000 V, nebulizer at 40 psig, drying gas at 9 L min⁻¹, and gas temperature of 200 °C. The QTOFMS system was operated in broadband collision-induced dissociation (bbCID) acquisition mode, which provided MS and MS/MS spectra at the

same time. All the MS information was recorded over the m/z range 50–1000, using a scan rate of 2 Hz. The bbCID mode allows operation with two different collision energies: a low collision energy of 10 eV and a high collision energy of 20 eV (to obtain MS/MS spectra). The pharmaceuticals were quantified using the TargetAnalysis and QuantAnalysis 2.2 software packages. The limits of detection (LOD) and quantification (LOQ) for determination of the pharmaceuticals during the treatment processes were calculated based on signal-to-noise ratios of three and ten, respectively (Table S.1.1, Supporting Information). The data from the TP analyses were processed using an automated method with a purpose-built database that was developed and adapted for this application (Cuervo Lumbaque et al. 2018). All data related to suspected TPs were evaluated using DataAnalysis 4.2 software. In most cases, possible elemental compositions for ions with a deviation of ± 5 ppm were assigned.

Predicted biodegradability and toxicological risk of the TPs

Toxtree software (v. 2.6.13) was used to evaluate the predicted biodegradability (START biodegradability) and the toxicological hazard (Cramer rules) of the TPs tentatively identified.

Results and discussion

Characterization of different alginate spheres

Observation using optical microscopy showed that the Fe(II)-alginate and Fe(III)-alginate samples consisted of beads with an average diameter of 2.5 mm (Figs. S.2.2 and S.2.3, Supporting Information). The spheres presented homogeneous structures, with small stretch marks caused by the drying process. The mining waste-alginate spheres could not be analyzed by optical microscopy, because their structure did not allow the light to pass through them.

The XRD analyses (Fig. S.2.4, Supporting Information) revealed the presence of (012), (104), (110), (113), (024), (116), (122), (208), (101), (220), and (128) planes related to the hematite phase (JCPDS card 33-0664). In addition, peaks corresponding to the SiO₂ phase were indexed at 2θ of 20.8° (100), 26.6° (101), 42.5° (200), 50.1° (112), 45.7° (201), 59.9° (211), 63.9° (113), 65.6° (300), 67.8° (300), and 77.7° (220) (JCPDS card 85-0335).

The diffractograms of the samples of alginate, Fe(II)-alginate, and Fe(III)-alginate, in the range 10–80°, showed the presence of the (311), (440), (422), (511), and (533) planes corresponding to the magnetite phase (JCPDS card 75-0033). The (311), (422), and (511) planes of the maghemite phase (JCPDS card 39-1346) are shown in Fig. S.2.5 (Supporting Information). However, it was not possible to index the low-

intensity plane present at 2θ of 69.6°. Overall, the mining waste sample presented hematite (α -Fe₂O₃), SiO₂, magnetite (Fe(III)₂Fe(II)O₄), and maghemite (γ -Fe₂O₃) as the main phases. Finally, the alginate phase showed three characteristic peaks at 2θ of 13.5°, 21.0°, and 39.6° (Cullity and Stock 2001; Sharma et al. 2012).

Particle size was determined using the Scherrer equation: $D_{hkl} = 0.94\lambda/\beta \cos \theta$, where λ is the wavelength of the X-ray source, β is the full width at half maximum (FWHM) of the main peak of each phase identified in the diffractogram, and θ is the Bragg diffraction angle of the measured plane. As a result, the average particle size values calculated from the hematite (D₁₀₄), maghemite (D₃₁₁), and magnetite (D₄₄₀) planes, and an average value from (311) and (111) planes of SiO₂ shows 53 nm, 43 nm, 27 nm and 47 nm, respectively. The lattice constants of the cubic iron oxide phases were also determined, with values of $a = 8.4176$ Å for the magnetite phase and $a = 8.4176$ Å for the maghemite phase. The lattice constant values shown on the JCPDS cards (referred to above) were $a = 8.3967$ Å and $a = 8.350$ Å, respectively.

The sample of alginate encapsulated with mining residue showed a decrease in the intensity of diffraction compared to the mining waste intensity pattern due to the presence of differences like the crystalline structure, which is related to the habit of the crystal sample. On the other hand, the samples encapsulated with the Fe(III) and Fe(II) salts initially appeared to be similar, although detailed analysis of the samples revealed small peaks in the range 35–40° in the diffractogram of the sample encapsulated with Fe(II), which were related to the (110) and (201) planes of the hematite phase. This finding could be interpreted as a result of the interaction between this particular ion and the polymer.

In high angle values, the diffraction patterns for the mining waste and encapsulated mining waste samples indicated that the behaviors of the indexed SiO₂ (119) and hematite (220) planes were opposite to those of the other planes present in the diffractograms shown in Fig. S.2.6 (Supporting Information). This could be explained by the existence of interactions of these planes with the alginate, specifically with the carboxylate group, as also indicated by the infrared results (see “Solar homo/heterogeneous photo-Fenton processes using SW and RHW”), with greater metal-polymer interaction leading to higher intensities for these planes. Finally, for the samples encapsulated with iron salts, the intensity of the plane (101) of SiO₂ shows lower values compared to the mining waste sample.

The main infrared modes of alginate, a linear polysaccharide, were found in the range 1800–600 cm⁻¹ (Fig. S.2.7 and Table S.2.1, Supporting Information), with strong bands at 1735, 1593, and 1406 cm⁻¹, corresponding to stretching modes of the C=O (–COOH) group, together with asymmetric and symmetric stretching modes of the carboxyl group. A band at 1317 cm⁻¹ was attributed to the bending mode of the

CH group, while a shoulder band at 1265 cm^{-1} was associated with the $\nu\text{C-O}$ ($-\text{COOH}$) mode. Finally, weak bands were present at 1123 cm^{-1} ($\nu\text{CO} + \nu\text{CC}$), 1085 cm^{-1} (νCO), and 946 cm^{-1} ($\nu\text{CO} + \nu\text{CCH} + \text{ring} + \delta\text{CH}$). All these corresponded to the alginate structure and were in agreement with literature reports (Petroni and McQuillan 2011; Xiao et al. 2014).

A band at 548 cm^{-1} was attributed to the stretching mode of hematite (Table S.2.1), while bands at 573 and 526 cm^{-1} corresponded to the maghemite phase. Petroni et al. (2011) reported that the ratio of the absorbance intensities of bands at 1593 cm^{-1} and 1038 cm^{-1} (I_{1593}/I_{1038}) could be used to indicate the degree of deprotonation of the alginate ion, with an I_{1593}/I_{1038} ratio of around 1.25 being indicative of a fully deprotonated sample. In the present work, an I_{1593}/I_{1038} value of 1.37 was obtained for the alginate sample, while the samples of iron-alginate with Fe(II) and Fe(III) presented values of 0.81 and 1.74, respectively. These values suggested that the alginate and Fe(III)-alginate samples were fully deprotonated, while the Fe(II)-alginate sample presented around 60% protonated alginic acid. Quadrado and Fajardo (2017) reported that iron binds to the M and G blocks of alginate according to a mechanism consisting of a combination of acid and ionotropic gelation, as a consequence of the union of iron ions with free carboxylate groups and the salts of alginic acid.

A detailed infrared analysis was performed of the surfaces of the Fe(II)/mining waste-alginate and Fe(III)/mining waste-alginate beads (Figs. S.2.8 and S.2.9, Table S.2.1, Supporting Information). Spectra were also acquired for these samples after leaving them in contact with solutions of Fe(II) and Fe(III) for 1 h. The resulting samples were denoted Fe(II)-alginate + 1 h and Fe(III)-alginate + 1 h. The vibrational modes observed are shown in Table S.2.1 (Supporting Information).

The Fe(II)/mining waste-alginate and Fe(II)-alginate 1-h samples showed a band at 1417 cm^{-1} , attributed to the stretching mode of carboxylate groups, which was not observed for the samples containing Fe(III). A band at 545 cm^{-1} (the T_{1u} phonon mode), associated with magnetite Fe-O, was observed for the Fe(II)/mining waste-alginate and Fe(II)-alginate + 1-h samples (Fig. S.2.9, Supporting Information).

In the range $600\text{--}500\text{ cm}^{-1}$, a band at 570 cm^{-1} , attributed to the maghemite phase vibrational mode (T_2 phonon mode, Fe + O), was observed for the Fe(III)-alginate + 1-h sample (Chamritski and Burns 2005). The same sample presented a band at 590 cm^{-1} , corresponding to stretching vibration of Si-OH. The Fe(II)-alginate sample showed the presence of carboxylate anions, indicative of a more basic environment, compared to the Fe(III) samples. The Fe(III)-alginate + 1-h sample showed a mode corresponding to silicon oxide/hydroxide, indicative of greater acidity of the surface environment,

compared to the samples with Fe(II). It was not possible to determine the I_{1593}/I_{1038} intensity ratios for these samples.

Solar homo/heterogeneous photo-Fenton processes

Preliminary adsorption and photolysis tests were performed, as shown in Fig. S.3.1 (Supporting Information). In the adsorption tests, the alginate spheres were placed in contact with solutions of the pharmaceuticals for 60 min, in the dark. The results indicated that PPN, NMD, FXT, and PRG were the compounds that adsorbed most strongly on the alginate. The chemisorption of pharmaceuticals has previously been reported as a possible mechanism in processes employing a catalytic surface, where part of the substrate is adsorbed onto the surface (Rahim Pouran et al. 2015; Titouhi and Belgaied 2016; Mirzaei et al. 2017). This behavior may be due to electrostatic interactions between the positively charged compounds and the negatively charged alginate surface. Adsorption may also occur when interactions (chemical bonding) are established between the compound and the alginate structure (Alvarino et al. 2018). The photolysis tests showed that FRS and DIP presented photosensitivity and were degraded under solar light (after 51 min of treatment), as reported previously by Isidori et al. (2006) and Gómez et al. (2008).

The consumption of H_2O_2 and the total amount of iron dissolved (by leaching of iron to the solution) were monitored during all the solar homo/heterogeneous photo-Fenton processes. For the Fe(II)-alginate system, the total iron concentration was 10.2 mg L^{-1} and 13.1 mg L^{-1} for Fe(III)-alginate system, with it evidencing an iron dosage to solution, so it could be considered that the iron used in the treatment systems is present in the sphere (heterogeneous) and in the solution (homogeneous) which makes the system have a synergy of solar homo/heterogeneous photo-Fenton process. The release of iron could be explained by the immersion of the Ca-alginate spheres in iron solutions for 15 days, with the ions diffusing into the structure of the Ca-alginate catalyst. Although some of the iron ions could be coordinated with carboxylic groups or with hydroxyl groups of the polysaccharide chains, most of the iron ions were trapped (non-coordinated) in the structures of the spheres and were not removed during washing and drying. When the catalyst was immersed in the solution, the non-coordinated iron was leached from the spheres to the solution. The concentrations of total iron dissolved at pH 5.0 could indicate that there are Fe(II) and Fe(III) ions forming aqua-complexes with water molecules $[\text{Fe}(\text{H}_2\text{O})_6]^{2+}$ and $[\text{Fe}(\text{H}_2\text{O})_6]^{3+}$, respectively (Rabajczyk and Namieśnik 2014) without evidence of precipitates. The H_2O_2 consumption was around 21.7 mg L^{-1} and 22.9 mg L^{-1} respectively for Fe(II) and Fe(III)-alginate system, which is indicative that the process is environmental friendly, since high concentrations of residual hydrogen peroxide represent toxicity to the aquatic organism. For more information on the behavior of hydrogen

peroxide consumption, see Fig. S.3.5 (Supporting Information).

Considering that Brazil is globally the second largest producer of iron, together with the fact that according to UNCTAD (United Nations Conference on Trade and Development), annual global iron mining production was around 1940 billion tons in 2015 (Heider 2017), iron (II and III), mining waste, and iron enhanced–mining waste were produced and tested. The first was prepared with the iron mining waste supported on alginate beads. Additional beads were prepared by separately placing these beads in contact with Fe(II) and Fe(III) solutions, generating two other materials: Fe(II)/mining waste-alginate and Fe(III)/mining waste-alginate.

The results (Fig. 1a) showed that most of the pharmaceuticals studied were degraded using Fe (II)-alginate and Fe (III)-alginate systems, with PCT, DZP, and PRG being the most persistent compounds. Use of the mining waste and the mining waste-alginate only resulted in significant degradation of DIP and FRS. These results were in agreement with other studies employing the photo-Fenton process (Gómez et al. 2008; Klameth et al. 2013; Assumpção et al. 2013), where DIP and FRS exhibited rapid degradation in the first minutes of treatment. The rapid degradation could also be due to the photosensitivity exhibited by both compounds. In the case of the mining waste without immobilization, previous studies have found that the presence of magnetite, hematite, and goethite in this material results in high efficiency of degradation by the Fenton process (Rad et al. 2015; Catalá et al. 2015). However, the processes were generally performed at acidic pH, with high concentrations of hydrogen peroxide, which influenced the performance of the system. The results obtained here using the Fe(II)/mining waste-alginate and Fe(III)/mining waste-alginate materials showed rapid degradation of DIP and FRS while the other pharmaceuticals evaluated (PCT, NMD, PPN, FXT, DZP, and PRG) were more persistent.

The H_2O_2 consumed and the total iron leached to the solution were determined during the solar heterogeneous photo-Fenton processes employing the Fe(II)/mining waste-alginate and Fe(III)/mining waste-alginate materials. At the end of the treatments, the Fe(II)/mining waste-alginate system presented a total iron concentration of 3.2 mg L^{-1} and H_2O_2 consumption of 19.6 mg L^{-1} , while the Fe(III)/mining waste-alginate system presented 4.1 mg L^{-1} of total iron and 22.9 mg L^{-1} H_2O_2 consumption after 116 min of treatment. Detailed information for each process is provided in the Supporting Information (Figs. S.3.2–S.3.4). Additionally, the high coefficient of molar absorptivity (ϵ) of the iron species generated in the different systems (7.749×10^3 to $8.352 \times 10^3 \text{ L mol}^{-1} \text{ cm}^{-1}$) represents an interesting form of iron storage and vehicle for its release, since the iron lixiviate throughout

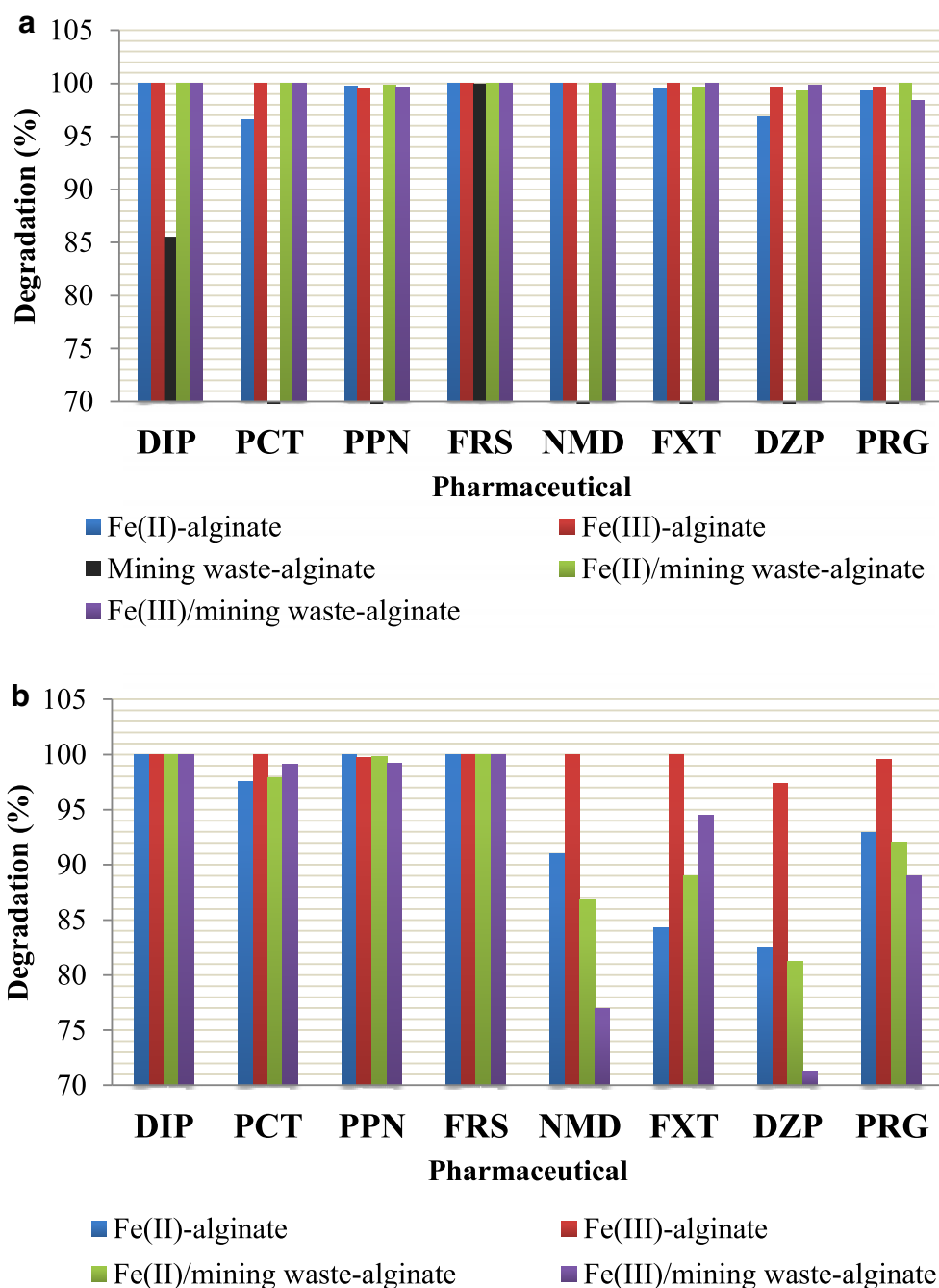
the process is very effective at absorbing light in visible wavelength range, which can have better performance to complete the cycle of reducing—oxidation of iron in photo-Fenton process.

The final concentrations of the pharmaceuticals in the systems that showed the best degradation performance are presented in Table 1. For all the systems evaluated, PPN could not be completely degraded. The other pharmaceuticals were degraded and reached concentrations lower than the LOD of the method at the end of the treatment (after 116 min).

Reuse of the Fe(II)-alginate, Fe(III)-alginate, Fe(II)/mining waste-alginate, and Fe(III)/mining waste-alginate spheres as catalysts in the solar heterogeneous photo-Fenton reaction was investigated for degradation of the pharmaceuticals in DW as the aqueous matrix, during three consecutive runs, each one with a time of 116 min. The results are shown in Figs. S.4.1–S.4.4 (Supporting Information). When the Fe(III)-alginate system was used, the degradation efficiency decreased slightly between the second and third cycle. The Fe(II)-alginate, Fe(II)/mining waste-alginate, and Fe(III)/mining waste-alginate systems showed substantial decreases of pharmaceutical degradation, with NMD, FXT, DZP, and PRG being the most persistent compounds in the reuse cycles, the catalytic efficiencies of these decrease with the increase of the number of reuse cycles since the mechanical resistance of the materials decreased, as reported by Li et al. (2010), who found that alginate can be depolymerized by HO^\cdot radicals under neutral and alkaline pH conditions ($\text{pH} \geq 5$) and during a longer reaction time. However, the Fe(III)-alginate spheres do not evidence a decrease in mechanical resistance which allows their prolonged recyclability, besides its extended photo-response efficient, being a great advantage reported in other studies of iron immobilization (Bansal et al. 2018). Quadrado and Fajardo (2017) reported high stability of Fe(III) in alginate, which was attributed to effective bonding between Fe(III) and the mannuronate and guluronate blocks of alginate. These results were supported by the findings of the infrared analyses, specifically concerning the differences in the vibrational modes associated with the carboxylate anion and silicon oxide. Accordingly, the Fe(III)-alginate system presented the best results in terms of pharmaceutical degradation and catalytic efficiency (Fig. 1b), so this material was selected for use in evaluation of degradation of the pharmaceuticals in more complex matrices (SW and RHW).

As mentioned previously, the immobilized Fe(III) material presented the best response in degradation of the eight pharmaceuticals, because the process involved synergistic effects of homogeneous and heterogeneous systems. Therefore, a more detailed investigation was made of the processes with Fe(III) supported on alginate, using Fe(III)-alginate (Fig. 2a) and Fe(III)/mining waste-alginate (Fig. 2c). The Fe(III)-

Fig. 1 Solar photo-Fenton process for degradation of pharmaceuticals. **a** Comparative of five materials tested. **b** Third use of four materials tested, (116 min of treatment time, 3 g of spheres of each catalyst, 25 mg L⁻¹ of H₂O₂ and pH 5.0)



alginate process was compared with a solar homogeneous photo-Fenton experiment with sequential additions of iron at the same concentrations found in the experiments employing Fe(III)-alginate (Fig. 2b). Degradation of the pharmaceuticals during the process was slower than Fe(III)-alginate, although the results were similar after 116 min of treatment, with the concentrations of most of the compounds decreasing to below the LOD of the method. This represents an advantage of the process using the Fe(III)-alginate spheres, since better results

were obtained in the first minutes of treatment, compared to the homogeneous process, avoiding successive additions and being able to reuse the same catalyst for more than three cycles, as observed in the reuse tests.

A similar study was carried out with Fe(III) and mining waste, in this case comparing two systems. The first was totally heterogeneous (Fig. 2d), with mining waste immobilized in alginate, in the presence of hydrogen peroxide. The second simulated the release of Fe(III) to the solution, using 3 g of

Table 1 Final concentration of pharmaceuticals for different systems studied after 116 min of treatment time

Compound/ system	Fe(II)- alginate ($\mu\text{g L}^{-1}$)	Fe(III)- alginate ($\mu\text{g L}^{-1}$)	Fe(II)/mining waste- alginate ($\mu\text{g L}^{-1}$)	Fe(III)/mining waste- alginate ($\mu\text{g L}^{-1}$)
DIP	< LOD	< LOD	< LOD	< LOD
PCT	18.07	< LOD	< LOD	< LOD
PPN	4.83	6.08	4.18	3.60
FRS	< LOD	< LOD	< LOQ	< LOD
NMD	< LOD	< LOD	< LOD	< LOD
FXT	< LOQ	< LOD	36.51	< LOD
DZP	9.75	< LOQ	0.60	0.13
PRG	6.65	4.81	< LOD	8.70

mining waste powder (Fig. 2e) and sequential additions of iron at the concentrations obtained using the Fe(III)/mining waste-alginate system. The results showed slower degradation of the pharmaceuticals, compared to use of the Fe (III)/mining waste-alginate, in accordance with low hydrogen peroxide consumption, hence demonstrating that the synergy among Fe(III), the mining waste, and the alginate contributed to degradation of the pharmaceuticals by HO[•] radicals.

These results demonstrated that the reason for the compounds' degradation is the release of iron into the solution. Therefore, it does not appear to be an adsorption process but a controlled release of iron from the spheres to the solution; this is related to studies that have shown that sequential additions of iron can improve the degradation process (Carra et al. 2013, 2014). Therefore, the findings showed that the Fe(III)-alginate and Fe(III)/mining waste-alginate materials were homo/heterogeneous systems that provided a strategy of iron dosage with better performance in degradation of pharmaceuticals, compared to similar systems.

The experimental results for the homo/heterogeneous and homogeneous systems were used to construct kinetic models. The systems using spheres of Fe(III)-alginate and Fe(III)/mining waste-alginate showed faster initial decomposition rates and higher degradation capacity in the first minutes of treatment, after which the efficiencies decreased. This behavior was investigated using the method described by Chan and Chu (2003), resulting in coefficients of determination (r^2) in the range from 0.96 to 1.00. The equation of the model and the results of the kinetic study are shown in Table S.3.1 (Supporting Information). The behaviors of the homogeneous systems employing Fe(III) and Fe(III) with mining waste could be described by pseudo-first-order models, with r^2 -values from 0.88 to 0.99.

Solar homo/heterogeneous photo-Fenton processes using SW and RHW

Solar homo/heterogeneous photo-Fenton processes were performed using the Fe(III)-alginate spheres with the SW and

RHW matrices. This catalyst was selected because it presented the best degradation rates for most of the pharmaceuticals evaluated and offered the possibility of being used more than twice. Figure 3 shows the degradation of the pharmaceuticals after 171 min of treatment.

Measurements of H₂O₂ consumption and the total iron concentration were made during the treatments using the SW and RHW matrices. The presence of additional organic matter in SW and RHW, compared to the DW matrix, necessitated additional doses of H₂O₂ after 61, 88, and 117 min of treatment (adding 25 mg L⁻¹ of H₂O₂ at each time). According to Fig. S.5.1, the release of iron in SW is easier than that in RHW; this is in agreement with the principle of counterion effect: the higher the conductivity, the higher the difficulty of transfer of ions into that solution; at the end of the processes, the total iron concentrations in the SW and RHW matrices were 14.6 and 12.7 mg L⁻¹, respectively; these results were below the maximum concentration limit for iron permitted by Brazilian legislation (15 mg L⁻¹). Once the iron ions are in the solution (homogenous phase), more H₂O₂ is consumed, and consequently the concentration of HO[•] radicals augment and the degradation effect as well.

The final concentrations of the pharmaceuticals were determined using calibration curves constructed with standards prepared in both of these water matrices. Table 2 presents the pharmaceutical concentrations for all the water matrices employed. The compounds PPN and PRG showed persistence in all the experiments, while NMD, FXT, and DZP were persistent in the RHW matrix. These results can be supported in studies made by Ioannou-Ttofa et al. (2019); according to the authors, the physicochemical characteristics of the wastewater matrix influence the degradation of pharmaceutical products independently of the pH value, which affects differently the oxidation of each pharmaceutical compound.

The low efficiencies of the treatment processes using the SW and RHW matrices could be explained by the presence of organic matter and various ionic species (Petroni and McQuillan 2011; Klammer et al. 2013), resulting in greater complexity of these matrices, with consequent effects on the

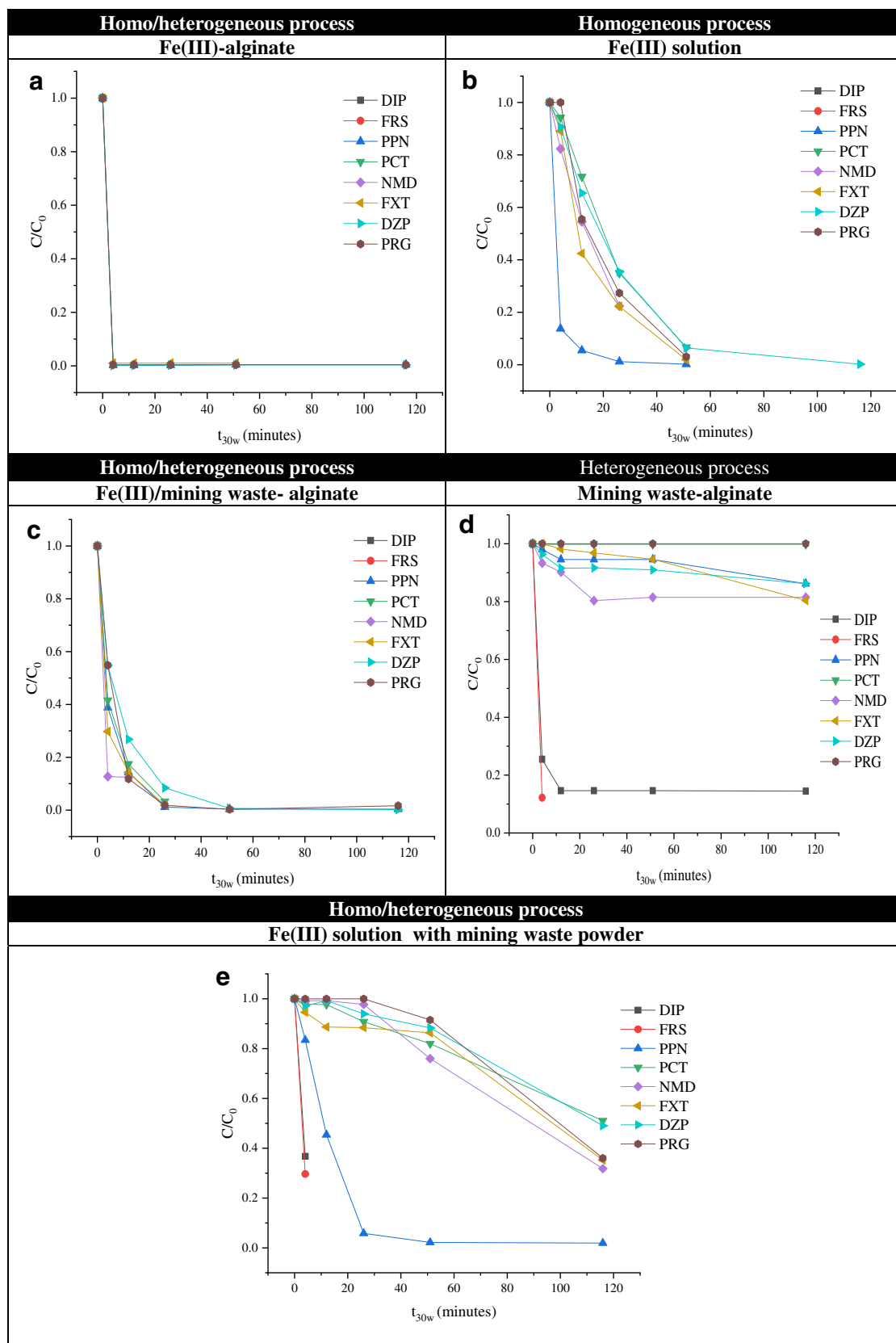


Fig. 2 Solar photo-Fenton process for degradation of pharmaceuticals. **a** Fe(III)-alginate. **b** Fe(III) solution. **c** Fe(III)/mining waste-alginate. **d** Mining waste-alginate. **e** Fe(III) with mining waste powder

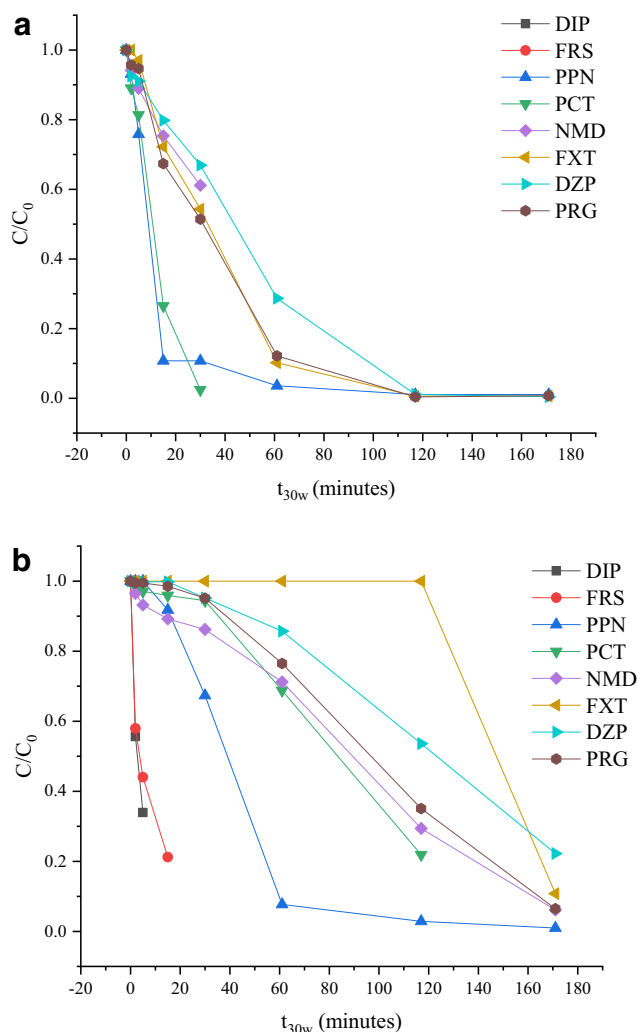


Fig. 3 Solar photo-Fenton process for degradation of pharmaceuticals. **a** SW. **b** RHW (3 g of Fe(III)-alginate spheres; 25 mg L⁻¹ of H₂O₂ (177 min of treatment time, with H₂O₂ additions at 0, 61, 88, and 117 min of treatment time and pH 5.0))

treatment process. Lanzafame et al. (2017) reported that the observed behavior was likely to be caused by the presence of different ions that are commonly found in wastewater. These

Table 2 Final concentrations of pharmaceuticals in SW and RHW using Fe(III)-alginate as catalyst

	DW ($\mu\text{g L}^{-1}$)	SW ($\mu\text{g L}^{-1}$)	RHW ($\mu\text{g L}^{-1}$)
DIP	< LOD	< LOD	< LOD
PCT	< LOD	< LOD	< LOQ
PPN	6.08	17.75	5.76
FRS	< LOD	< LOD	< LOQ
NMD	< LOD	< LOD	189.26
FXT	< LOD	47.75	276.01
DZP	< LOQ	< LOQ	138.76
PRG	4.81	10.71	104.93

species can act as scavengers of the hydroxyl radicals and lead to the formation of less reactive species, hence explaining the reduced degradation of the selected pharmaceuticals. However, it is important to highlight that the application of the solar photo-Fenton process at a pH close to neutral offers the advantage of avoiding excessive acidification of the effluents, which is important to reduce the operational cost of the process and the subsequent increase in the salinity of the treated effluent (Durán et al. 2018; Ioannou-Ttofa et al. 2019) with the possibility of reuse of the catalyst.

Transformation products

In order to detect the presence of possible TPs formed during the treatment processes, samples from each system were analyzed by UHPLC-QTOFMS operating in positive ionization mode. For this purpose, an adapted purpose-built database was employed and the results were used for qualitative identification of different TPs.

Table S.6.1 (Supporting Information) summarizes the information for the suspected TPs in all the processes and water matrices studied, including elemental compositions, theoretical and experimental masses of the ions and their respective errors (in ppm), and double bond equivalents (DBE), provided by the software. The low mass errors (below 5 ppm in most cases) enabled correct assignment of the elemental compositions.

According to the results presented in Table S.6.1, up to 19 TPs were identified: six for DIP (TP6 DIP, m/z 192.0648, C₁₀H₁₀NO₃; TP7 DIP, m/z 250.1186, C₁₂H₁₆N₃O₃; TP9 DIP, m/z 205.0971, C₁₁H₁₃N₂O₂; TP10 DIP, m/z 165.1018, C₉H₁₃N₂O; TP17 DIP, m/z 232.1078, C₁₂H₁₄N₃O₂; and TP18DIP, m/z 195.076, C₉H₁₁N₂O₃); eight for PPN (TP3 PPN, m/z 134.1176, C₆H₁₆NO₂; TP4 PPN, m/z 150.1127, C₆H₁₆NO₃; TP5/TP19 or TP20 PPN, m/z 282.1336, C₁₄H₂₀NO₅; TP6 PPN, m/z 292.1543, C₁₆H₂₂NO₄; TP7 PPN, m/z 266.1395, C₁₄H₂₀NO₄; TP26 PPN, m/z 308.1497, C₁₆H₂₂NO₅; TP27 PPN, m/z 308.1495, C₁₆H₂₂NO₅; TP28/TP29/TP30 or TP31 PPN, m/z 310.1649, C₁₆H₂₄NO₅); and one each for DZP (TP1 DZP, m/z 246.0676, C₁₄H₁₃ClNO), NMD (TP5 NMD, m/z 279.0798, C₁₃H₁₅N₂O₃S), FXT (TP1 FXT, m/z 326.1355, C₁₇H₁₉F₃NO₂), FRS (m/z 328.9995, C₁₂H₉ClN₂O₅S), and PRG (TP4 PRG, m/z 313.2157, C₂₁H₂₉O₂).

The DIP TPs were reported previously by Gómez et al. (2008) and Pérez-Estrada et al. (2007). The DIP TP structures identified were indicative of loss of the sulfonic group from DIP, with further oxidation yielding the corresponding quinone-imine intermediate TP17 DIP, while loss of the methylamine group and oxidation of C2 of the pyrazolinone group could lead to TP9 DIP. The identification of TP6 DIP was also consistent with the TP9 DIP structure, since it should originate from the loss of a methyl group and subsequent

formation of an isoxazole ring. The opening of the pyrazolinone ring by HO[•] radical attack on the double bond was indicated by the identification of TP7 DIP, which gave rise to the appearance of TP18 DIP by loss of methyl and secondary amide groups. In turn, TP10 DIP could be attributed to loss of the oxamoyl chain from TP7 DIP, or opening of the pyrazolinone ring and loss of the hydroxyl methyl aldehyde chain from TP9 DIP (further information is provided in Figs. S.6.1 and S.6.2 of the Supporting Information).

The TPs identified for PPN could be attributed to the generation of photocatalytic by-products, as reported by Santiago-Morales et al. (2013). Elucidation of TP5/TP19 or TP20 PPN was not possible, because the compounds showed the same mass and elemental composition and also shared the same fragments present for different retention times. No characteristic fragments were observed for these TPs, making it impossible to identify which of the two TPs was involved. Elucidation of TP28/TP29/TP30 or TP31 PPN was not possible, because the compounds had the same chromatographic profiles, with absence of characteristic fragments, as observed for TP5 PPN and its isomers. The addition of hydroxyl groups to the aromatic nuclei was probably the first step in the degradation pathway of PPN. TP6 PPN was a product of naphthol ring opening and oxidation of the PPN structure. The intermediates TP26 PPN, TP27 PPN, and TP28/TP29/TP30 or TP31 PPN were the consequence of attack of hydroxyl radicals during ring opening. TP7 could be formed by the loss of a carbonyl group from TP27 PPN. The oxidation of rings of TP28/29/30 or TP31 PPN, with loss of methyl alcohol, could lead to the corresponding TP5 PPN or its isomers. TP3 could be attributed to cleavage of the ether bond of PPN, as reported by Santiago-Morales et al. (2013). Finally, TP4 PPN could be attributed to oxidation of the aliphatic chains of any of the TPs mentioned above (for more information, see Figs. S.6.3 and S.6.4 of the Supporting Information).

Only one TP was observed for each of the compounds DZP, FRS, FXT, NMD, and PRG. TP1 DZP corresponded to opening of the benzodiazepinic ring of DZP. This TP was previously identified by Carpinteiro et al. (2017) in a study of the kinetics of the reaction of DZP during water chlorination. TP3 or TP4 FRS was a product of FRS reduction. TP1 FXT, resulting from hydroxylation of the FXT ring, was reported by Zhao et al. (2017) as an intermediate product generated after ozonation, especially at more alkaline pH, due to higher concentrations of hydroxyl radicals in the medium. TP5 NMD arose from reduction of the nitro group of NMD to an amino derivative, while TP4 PRG was produced by the reduction of PRG.

Finally, the tentatively identified TPs were evaluated using Toxtree software, which employs the chemical structure of a molecule for estimation of its biodegradability (START biodegradability) and toxicological hazard (Cramer rules) (Cramer et al. 1976). The results obtained for the TPs are

shown in Table S.6.2 (Supporting Information). Most of these substances showed significant toxicity or the presence of reactive functional groups, and were therefore classified as highly toxic, according to the Cramer rules. Evaluation of biodegradability showed that most of the TPs identified in this work could be classified as persistent substances. Previous work found that TP6 DIP, TP7 DIP, TP9 DIP, and TP10 DIP did not present significant acute toxicity towards *D. magna* (Gómez et al. 2008), while Pérez-Estrada et al. (2007) demonstrated that photo-Fenton treatment did not increase solution toxicity due to TP17 DIP and TP18 DIP. Santiago-Morales et al. (2013) showed the formation and accumulation of toxic transformation products in studies of PPN. Carpinteiro et al. (2017) found that TPs of DZP could exhibit higher toxicity (with lower concentrations causing acute and chronic toxicity), compared to the parent compound. However, it is important to note that the concentrations of the TPs were not determined in the present work. The presence of many different compounds at varying concentrations could influence the toxicity, increasing the complexity of the analysis and hindering prediction of the toxicities of the TPs generated during the treatment processes.

Conclusions

Characterization was made of different catalysts used in solar homo/heterogeneous photo-Fenton processes. The infrared and XRD analyses showed that several phases of iron oxide and silicon oxide were present in the samples studied. A difference in the chemical environment was detected in samples containing Fe(II) oxide, with infrared spectroscopy showing the presence of carboxylate anions. It was also possible to identify the magnetite, hematite, and goethite phases in the mining waste used.

The results obtained for removal of the pharmaceuticals and reuse of the catalysts showed that the alginate spheres containing Fe(III) provided the best performance as iron dosage for the degradation of pharmaceuticals in different matrices. The characterization techniques applied during the degradation and reuse experiments indicated that for the four main materials evaluated, the processes occurred according to a homo/heterogeneous solar photo-Fenton process. Additionally, the Fe(III)-alginate material presented slower pharmaceutical removal in the more complex matrices (SW and RHW), compared to its performance in the DW matrix.

Finally, identification of 19 TPs generated during the solar heterogeneous photo-Fenton process was achieved using a purpose-built database. The major TPs identified could be classified as highly toxic, according to Cramer's rules, with the presence of reactive functional groups. Biodegradability evaluation indicated that these compounds could be classified as persistent substances.

Acknowledgments The authors wish to thank Mrs. Eng. Tainá Flores da Rosa for the RHW. Carla Sirtori thanks the CNPq for her research grant (Processo: 303474/2015-7). V.L. thanks Professor Adriana Casagrande for the Infrared spectrometer facilities provided.

Funding information This study was financed in part by the Coordenação de Aperfeiçoamento de Pessoal de Nível Superior–Brasil (CAPES)–Finance Code 001 and received financial support from the CNPq (Processo: 403051/2016-9).

Publisher's Note Springer Nature remains neutral with regard to jurisdictional claims in published maps and institutional affiliations.

References

- Alalm MG, Tawfik A, Ookawara S (2015) Degradation of four pharmaceuticals by solar photo-Fenton process: kinetics and costs estimation. *J Environ Chem Eng* 3:46–51. <https://doi.org/10.1016/J.JECE.2014.12.009>
- Alvarino T, Suarez S, Lema J, Omil F (2018) Understanding the sorption and biotransformation of organic micropollutants in innovative biological wastewater treatment technologies. *Sci Total Environ* 615: 297–306
- Arzate-Salgado S, Morales-Pérez A, Solís-López M, Ramírez-Zamora R-M (2016) Evaluation of metallurgical slag as a Fenton-type photocatalyst for the degradation of an emerging pollutant: diclofenac. *Catal Today* 266:126–135. <https://doi.org/10.1016/J.CATTOD.2015.09.026>
- Assumpção M, Moraes A, De Souza R, Reis R, Rocha R, Gaubeur I, Calegari M, Hammer P, Lanza M, Santos M (2013) Degradation of dipyrone via advanced oxidation processes using a cerium nanostructured electrocatalyst material. *Appl Catal A Gen* 462–463: 256–261. <https://doi.org/10.1016/j.apcata.2013.04.008>
- Bae S, Kim D, Lee W (2013) Degradation of diclofenac by pyrite catalyzed Fenton oxidation. *Appl Catal B Environ* 134–135:93–102. <https://doi.org/10.1016/J.APCATB.2012.12.031>
- Bansal P, Verma A, Talwar S (2018) Detoxification of real pharmaceutical wastewater by integrating photocatalysis and photo-Fenton in fixed-mode. *Chem Eng J* 349:838–848. <https://doi.org/10.1016/j.cej.2018.05.140>
- Carpinteiro I, Rodil R, Quintana J, Cela R (2017) Reaction of diazepam and related benzodiazepines with chlorine. Kinetics, transformation products and in-silico toxicological assessment. *Water Res* 120: 280–289. <https://doi.org/10.1016/J.WATRES.2017.04.063>
- Carra I, Casas López J, Santos-Juanes L, Malato S, Sánchez Pérez J (2013) Iron dosage as a strategy to operate the photo-Fenton process at initial neutral pH. *Chem Eng J* 224:67–74. <https://doi.org/10.1016/j.cej.2012.09.065>
- Carra I, Malato S, Jiménez M, Maldonado M, Sánchez Pérez J (2014) Microcontaminant removal by solar photo-Fenton at natural pH run with sequential and continuous iron additions. *Chem Eng J* 235: 132–140. <https://doi.org/10.1016/j.cej.2013.09.029>
- Catalá M, Domínguez-Moruco N, Mígens A, Molina R, Martínez F, Valcárcel Y, Mastroianni N, López de Alda M, Barceló D, Segura Y (2015) Elimination of drugs of abuse and their toxicity from natural waters by photo-Fenton treatment. *Sci Total Environ* 520: 198–205. <https://doi.org/10.1016/J.SCITOTENV.2015.03.042>
- Chamritski I, Burns G (2005) Infrared and Raman-active phonons of magnetite, maghemite, and hematite: a computer simulation and spectroscopic study. *J Phys Chem B* 109:4965–4968. <https://doi.org/10.1021/jp048748h>
- Cramer G, Ford R, Hall R (1976) Estimation of toxic hazard—a decision tree approach. *Food Cosmet Toxicol* 16:255–276. [https://doi.org/10.1016/S0015-6264\(76\)80522-6](https://doi.org/10.1016/S0015-6264(76)80522-6)
- Cruz A, Couto L, Sans C, Esplugas S (2017) Study of the contribution of homogeneous catalysis on heterogeneous Fe(III)/alginate mediated photo-Fenton process. *Chem Eng J* 318:272–280. <https://doi.org/10.1016/j.cej.2016.09.014>
- Cuervo Lumbaque E, Cardoso RM, Dallegrave A, dos Santos L, Ibañez M, Hernández F, Sirtori C (2018) Pharmaceutical removal from different water matrixes by Fenton process at near-neutral pH: Doehlert design and transformation products identification by UHPLC-QTOF MS using a purpose-built database. *J Environ Chem Eng* 6:3951–3961. <https://doi.org/10.1016/J.JECE.2018.05.051>
- Cullity BD, Stock SR (2001) *Elements of X-ray diffraction*, 3rd edn. Pearson, Harlow
- Durán A, Monteagudo J, San Martín I (2018) Operation costs of the solar photo-catalytic degradation of pharmaceuticals in water: a mini-review. *Chemosphere* 211:482–488. <https://doi.org/10.1016/j.chemosphere.2018.07.170>
- Fatta-Kassinos D, Meric S, Nikolaou A (2011) Pharmaceutical residues in environmental waters and wastewater: current state of knowledge and future research. *Anal Bioanal Chem* 399:251–275. <https://doi.org/10.1007/s00216-010-4300-9>
- Giannakis S, Polo López MI, Spuhler D, Sánchez Pérez J, Fernández Ibañez P, Pulgarin C (2016) Solar disinfection is an augmentable, in situ-generated photo-Fenton reaction—Part 1: a review of the mechanisms and the fundamental aspects of the process. *Appl Catal B Environ* 199:199–223. <https://doi.org/10.1016/j.apcatb.2016.06.009>
- Gómez MJ, Sirtori C, Mezcua M, Fernández-Alba A, Agüera (2008) Photodegradation study of three dipyrone metabolites in various water systems: identification and toxicity of their photodegradation products. *Water Res* 42:2698–2706. <https://doi.org/10.1016/j.watres.2008.01.022>
- Heider M (2017) Production scenarios for iron ore in Brazil in 2030. Available from <https://inthemine.com.br/site/wp-content/uploads/2016/09/itm62-mercado.pdf> Accessed 16 June 2018 (in Portuguese)
- Iervolino G, Vaiano V, Sannino D, Rizzo L, Sarno G, Ciambelli P, Isupova L (2015) Influence of operating conditions in the photo-Fenton removal of tartrazine on structured catalysts. *Chem Eng Trans* 43:979–984. <https://doi.org/10.3303/CET1543164>
- Ioannou-Ttofa L, Raj S, Prakash H, Fatta-Kassinos D (2019) Solar photo-Fenton oxidation for the removal of ampicillin, total cultivable and resistant *E. coli* and ecotoxicity from secondary-treated wastewater effluents. *Chem Eng J* 355:91–102. <https://doi.org/10.1016/j.cej.2018.08.057>
- Isidori M, Nardelli A, Parrella A, Pascarella L, Previtera L (2006) A multispecies study to assess the toxic and genotoxic effect of pharmaceuticals: furosemide and its photoproduct. *Chemosphere* 63: 785–793. <https://doi.org/10.1016/J.CHEMOSPHERE.2005.07.078>
- ISO (1998) 6332: Water quality - determination of iron - spectrometric method using 1,10-phenanthroline
- Klamerth N, Malato S, Agüera A, Fernández-Alba A (2013) Photo-Fenton and modified photo-Fenton at neutral pH for the treatment of emerging contaminants in wastewater treatment plant effluents: a comparison. *Water Res* 47:833–840. <https://doi.org/10.1016/j.watres.2012.11.008>
- Kümmerer K (2009) The presence of pharmaceuticals in the environment due to human use – present knowledge and future challenges. *J Environ Manag* 90:2354–2366. <https://doi.org/10.1016/J.JENVMAN.2009.01.023>
- Lanzafame G, Sarakha M, Fabbri D, Vione D (2017) Degradation of methyl 2-aminobenzoate (methyl anthranilate) by H₂O₂/UV: effect of inorganic anions and derived radicals. *Molecules* 22:1–15. <https://doi.org/10.3390/molecules22040619>
- Li X, Xu A, Xie H, Yu W, Xie W, Ma X (2010) Preparation of low molecular weight alginate by hydrogen peroxide depolymerization

- for tissue engineering. *Carbohydr Polym* 79:660–664. <https://doi.org/10.1016/J.CARBPOL.2009.09.020>
- Liu Y, Wang J-S, Zhu P, Jin-Chao Z, Chuan-Jie Z, Guo Y (2016) Thermal degradation properties of biobased iron alginate film. *J Anal Appl Pyrolysis* 119:87–96. <https://doi.org/10.1016/J.JAAP.2016.03.014>
- Mirzaei A, Chen Z, Haghighat F, Yerushalmi L (2017) Removal of pharmaceuticals from water by homo/heterogeneous Fenton-type processes – a review. *Chemosphere* 174:665–688. <https://doi.org/10.1016/j.chemosphere.2017.02.019>
- Müller CM, Pejčić B, Esteban L, Piane C, Raven M, Mizaikoff B (2014) Infrared attenuated total reflectance spectroscopy: an innovative strategy for analyzing mineral components in energy relevant systems. *Sci Rep* 4:1–11. <https://doi.org/10.1038/srep06764>
- Nogueira R, Oliveira M, Paterlini W (2005) Simple and fast spectrophotometric determination of H₂O₂ in photo-Fenton reactions using metavanadate. *Talanta* 66:86–91. <https://doi.org/10.1016/j.talanta.2004.10.001>
- OECD (1999) Guideline for testing of chemicals, simulation test-aerobic sewage treatment 303A. Organization for Economic Co-operation and Development, Paris
- Pérez-Estrada L, Malato S, Agüera A, Fernández-Alba A (2007) Degradation of dipyrone and its main intermediates by solar AOPs. *Catal Today* 129:207–214. <https://doi.org/10.1016/j.cattod.2007.08.008>
- Petrone L, McQuillan A (2011) Alginate ion adsorption on a TiO₂ particle film and interactions of adsorbed alginate with calcium ions investigated by attenuated total reflection infrared (ATR-IR) spectroscopy. *Appl Spectrosc* 65:1162–1169
- Quadrado R, Fajardo A (2017) Fast decolorization of azo methyl orange via heterogeneous Fenton and Fenton-like reactions using alginate-Fe²⁺/Fe³⁺ films as catalysts. <https://doi.org/10.1016/j.carbpol.2017.08.083>
- Rabajczyk A, Namięśnik J (2014) Speciation of iron in the aquatic environment. *Water Environ Res* 86:741–758. <https://doi.org/10.2175/106143014X13975035525906>
- Rad L, Haririan I, Divsar F (2015) Comparison of adsorption and photo-Fenton processes for phenol and paracetamol removing from aqueous solutions: single and binary systems. *Spectrochim Acta A Mol Biomol Spectrosc* 136:423–428. <https://doi.org/10.1016/J.SAA.2014.09.052>
- Rahim Pouran S, Abdul Aziz A, Wan Daud W (2015) Review on the main advances in photo-Fenton oxidation system for recalcitrant wastewaters. *J Ind Eng Chem* 21:53–69. <https://doi.org/10.1016/j.jiec.2014.05.005>
- Rodríguez R, Espada J, Pariente M, Melero J, Martínez F, Molina R (2016) Comparative life cycle assessment (LCA) study of heterogeneous and homogenous Fenton processes for the treatment of pharmaceutical wastewater. *J Clean Prod* 124:21–29. <https://doi.org/10.1016/J.JCLEPRO.2016.02.064>
- Santiago-Morales J, Agüera A, Gómez M, Fernández-Alba A, Giménez J, Esplugas S, Rosal R (2013) Transformation products and reaction kinetics in simulated solar light photocatalytic degradation of propranolol using Ce-doped TiO₂. *Appl Catal B Environ* 129:13–29. <https://doi.org/10.1016/j.apcatb.2012.09.023>
- Sharma S, Sanpui P, Chattopadhyay A, Sankar Ghosh S (2012) Fabrication of antibacterial silver nanoparticle sodium alginate-chitosan composite films. *RSC Adv* 2:5837–5843
- Souza K, Peralta-Zamora P, Zawadzki S (2008) Immobilization of iron (II) in alginate matrix and its use in textile dye degradation by Fenton processes. *Quim Nova* 31:1145–1149. <https://doi.org/10.1590/S0100-40422008000500041>
- Su C (2017) Environmental implications and applications of engineered nanoscale magnetite and its hybrid nanocomposites: a review of recent literature. *J Hazard Mater* 322:48–84. <https://doi.org/10.1016/j.jhazmat.2016.06.060>
- Sun S, Lemley A (2011) p-Nitrophenol degradation by a heterogeneous Fenton-like reaction on nano-magnetite: process optimization, kinetics, and degradation pathways. *J Mol Catal A Chem* 349:71–79. <https://doi.org/10.1016/J.MOLCATA.2011.08.022>
- Sun S, Zeng X, Lemley A (2013) Nano-magnetite catalyzed heterogeneous Fenton-like degradation of emerging contaminants carbamazepine and ibuprofen in aqueous suspensions and montmorillonite clay slurries at neutral pH. *J Mol Catal A Chem* 371:94–103. <https://doi.org/10.1016/J.MOLCATA.2013.01.027>
- Titouhi H, Belgaied J (2016) Removal of ofloxacin antibiotic using heterogeneous Fenton process over modified alginate beads. *J Environ Sci* 45:84–93. <https://doi.org/10.1016/j.jes.2015.12.017>
- Vaiano V, Lervolino G, Sannino D, Rizzo L, Sarno G, Ciambelli P, Isupova L (2015) Food azo-dyes removal from water by heterogeneous photo-Fenton with LaFeO₃ supported on honeycomb corundum monoliths. *J Environ Eng* 141:2–8. [https://doi.org/10.1061/\(ASCE\)EE.1943-7870.0000986](https://doi.org/10.1061/(ASCE)EE.1943-7870.0000986)
- Xiao Q, Gu X, Suo T (2014) Drying process of sodium alginate films studied by two-dimensional correlation ATR-FTIR spectroscopy. *Food Chem* 164:179–184. <https://doi.org/10.1016/J.FOODCHEM.2014.05.044>
- Zhao Y, Yu G, Chen S, Zhang S, Wang B, Huang J, Deng S, Wang Y (2017) Ozonation of antidepressant fluoxetine and its metabolite product norfluoxetine: kinetics, intermediates and toxicity. *Chem Eng J* 316:951–963. <https://doi.org/10.1016/j.cej.2017.02.032>

SUPPORTING INFORMATION

Degradation of pharmaceuticals from different water matrixes by solar homo/heterogeneous solar photo-Fenton process over modified alginate spheres

Elisabeth Cuervo Lumbaque¹, Raquel Wielens Becker¹, Débora Salmoria Araújo¹, Alexandro Dallegrave¹, Tiago Fracari¹, Vladimir Lavayen^{1*}, Carla Sirtori^{1*}

^aInstituto de Química- Universidade Federal do Rio Grande do Sul, Av. Bento Gonçalves, 9500, Porto Alegre-RS, Brazil.

* All correspondence should be addressed to: carla.sirtori@ufrgs.br (C. Sirtori) and vladimir.lavayen@ufrgs.br (V. Lavayen)

S.1 Parameters for quantification method

Table S.1.1 Parameters for quantification method used to determine pharmaceuticals in different matrixes of study.

Pharmaceuticals	DW		SW		RHW	
	LOD ($\mu\text{g L}^{-1}$)	LOQ ($\mu\text{g L}^{-1}$)	LOD ($\mu\text{g L}^{-1}$)	LOQ ($\mu\text{g L}^{-1}$)	LOD ($\mu\text{g L}^{-1}$)	LOQ ($\mu\text{g L}^{-1}$)
Nimesulide (NMD)	0.24	0.82	0.42	1.39	1.03	3.45
Furosemide (FRS)	0.78	2.61	1.36	4.55	1.07	3.57
Paracetamol (PCT)	0.20	0.68	0.58	1.92	1.11	3.70
Propranolol (PPN)	0.01	0.03	0.39	1.32	1.76	5.88
Dipyron (DIP)	0.31	1.03	1.20	4.01	15.0	50.0
Fluoxetine (FXT)	0.31	1.04	5.17	17.24	5.36	17.86
Progesterone (PRG)	0.02	0.08	13.04	43.48	0.01	0.23
Diazepam (DZP)	0.01	0.03	0.01	0.02	0.01	0.02

S.2 Characterization of alginate spheres

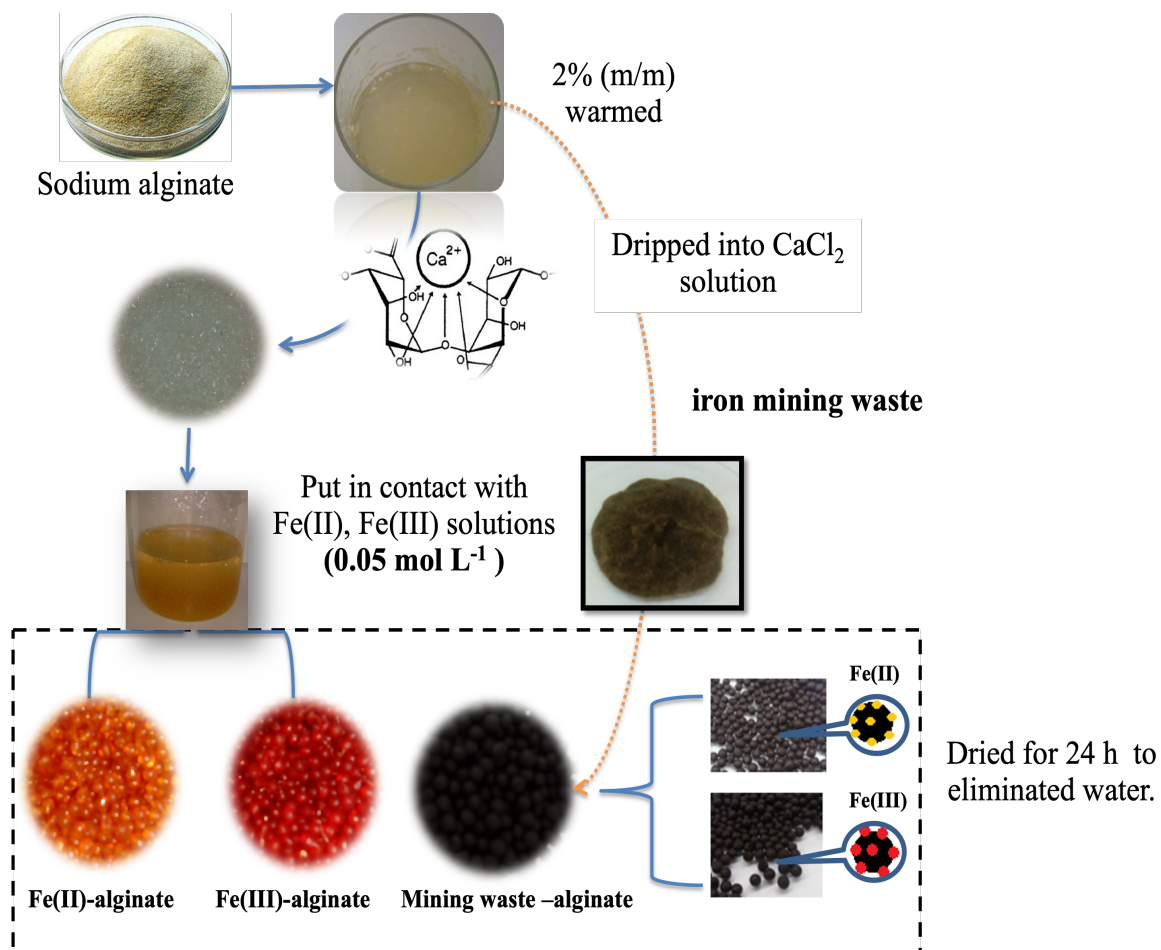


Fig S.2.1 Methodology for obtain the catalyst.

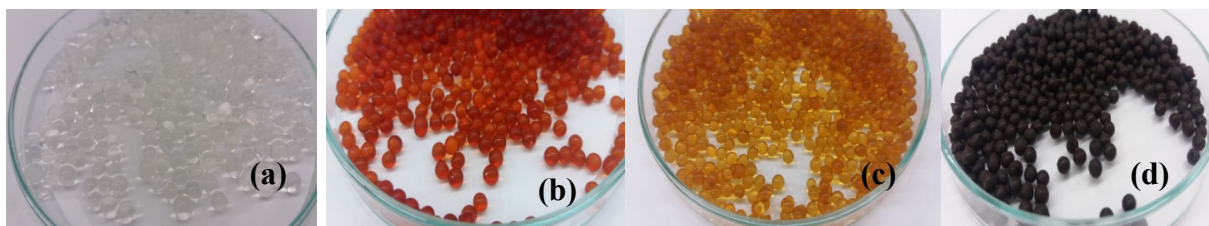


Fig S.2.2 Alginate spheres of (a) calcium alginate (reference), (b) Fe(III)-alginate, (c) Fe(II)-alginate and (d) mining waste-alginate.

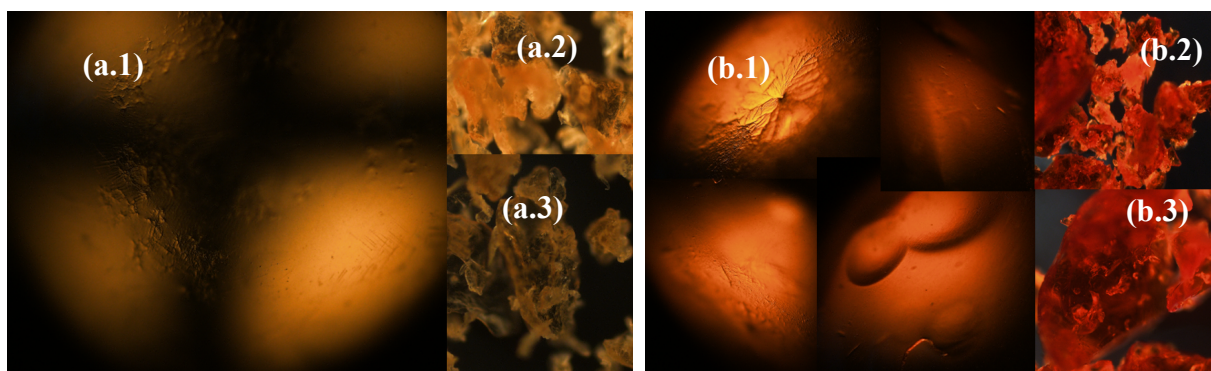


Fig S.2.3 Optical microscopy Fe (II)-alginate (a.1-a.3) and Fe (III)-alginate (b.1-b.3).

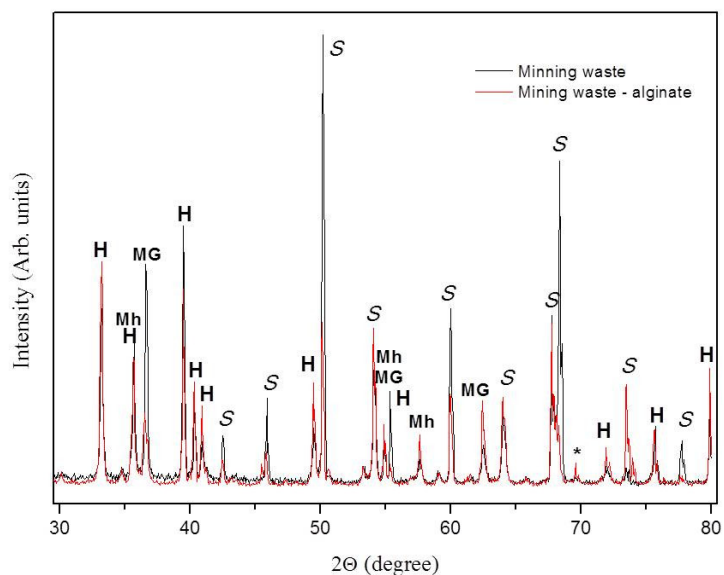


Fig S.2.4 Diffraction pattern of samples of mining waste and mining waste - alginate sample in the range of 30° - 80 °.The labels H, MG, Mh, S, and * correspond to hematite, magnetite, maghemite, SiO₂, and unidentified phase respectively.

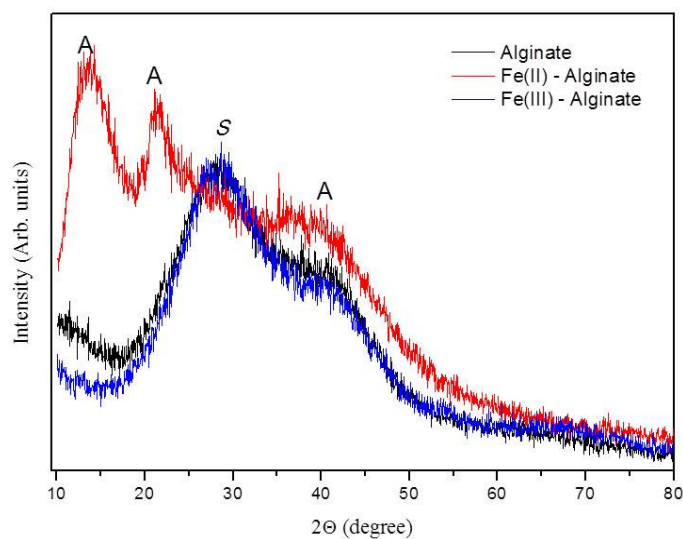


Fig S.2.5 The diffraction pattern of samples of alginate, Fe(II)-alginate and Fe(III)-alginate in the range of 10° - 80°.The label A, and S correspond to alginate and SiO₂ phase respectively.

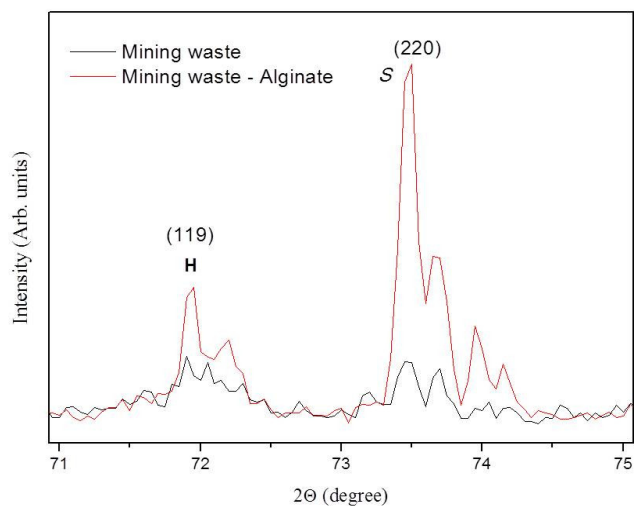


Fig S.2.6 The diffraction pattern of a waste residue sample and mining waste- alginate sample in the range of 71° - 75°. The label H, and S corresponds to hematite and SiO₂ phase respectively.

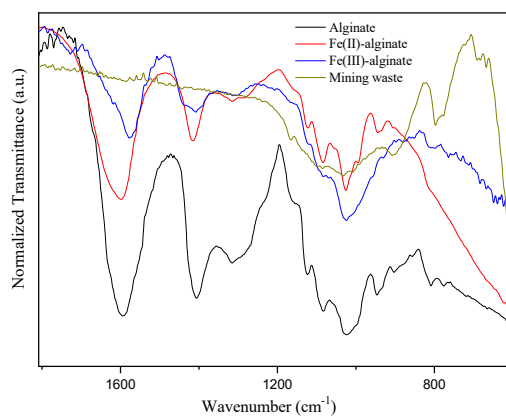


Fig S.2.7 Infrared spectra in the region from 1800 cm⁻¹ - 600 cm⁻¹ of different materials encapsulate in alginate samples.

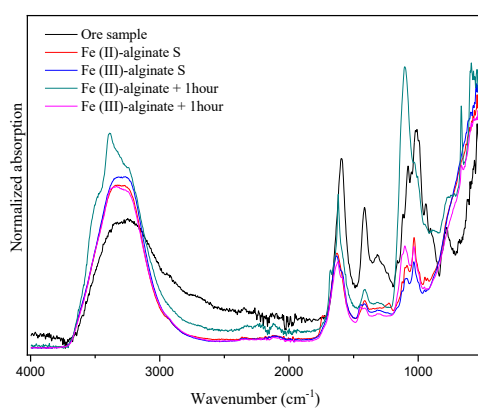


Fig S.2.8 Infrared spectra in the region from 1400 cm^{-1} - 500 cm^{-1} of mining waste sample, Fe(II)-alginate S, Fe(III)-alginate S, Fe(II)-alginate + 1-hour and Fe(III)-alginate + 1-hour samples.

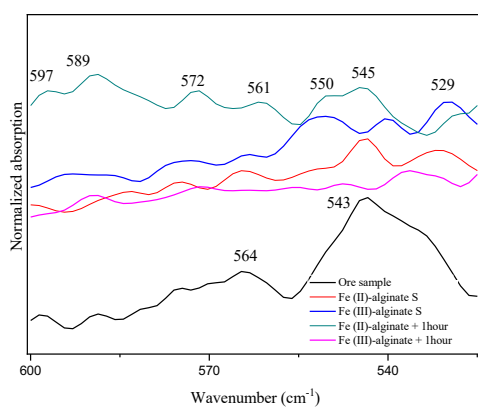


Fig S.2.9 Infrared spectra in the region from 600 cm^{-1} - 500 cm^{-1} of mining waste sample, Fe(II)-alginate S, Fe(III)-alginate S, Fe(II)-alginate + 1-hour and Fe(III)-alginate + 1-hour samples.

Table S.2.1. Infrared absorption band of alginate samples.

Alginate	Fe(II)-alginate	Fe(III)-alginate	Fe(II)-alginate/ Mining waste	Fe(III)-alginate/ Mining waste	Fe(II)-alginate after 1 hour	Fe(III)-alginate after 1 hour	Mining waste sample	Assignment ^a
3227 _(b,s)	3295 _(b,s)	3283 _(b,s)	3294 _(b,s)	3294 _(b,s)	3294 _(b,s)	3287 _(s) 3246 _(s,sh)	3294 _(b,s)	ν OH ν OH
2929 _(b,m) 1735 _(vw) 1672 _(sh,vw)	2934 _(sh,vw)	2934 _(m,vw) 1728 _(vw)			1681 _(w) 1619 _(m)			ν CH ν C=O (-COOH) δ OH (H ₂ O)
1593 _(s)	1599 _(m)	1621 _(vw) 1575 _(m)	1627 _(w)	1627 _(w)	1619 _(m)	1621 _(sh,w)		ν_{as} COO-
1406 _(s) 1317 _(sh,m) 1265 _(sh) 1226 _(sh)	1416 _(m) 1318 _(vw)	1407 _(w) 1304 _(vw)	1447 _(w) 1417 _(w)	1447 _(w)	1447 _(vw,sh) 1417 _(w)			ν_s COO- δ CH ν C-O (-COOH)
1163 _(sh) 1123 _(w)	1163 _(sh,w) 1122 _(w)	1168 _(sh,vw) 1123 _(sh,vw)	1126 _(vw)	1126 _(vw)	1126 _(vw) 1103 _(m)	1126 _(sh,vw) 1108 _(w)		ν CO + ν CC ν CO + ν COH + δ OH ν CO
1085 _(w) 1038 _(m)	1085 _(w) 1025 _(m) 991 _(sh,vw)	1082 _(sh,vw) 1024 _(m)	1086 _(vw) 1031 _(m)	1086 _(sh,vw) 1031 _(m)	1031 _(m,sh)	1031 _(m)	991 _(sh,vw)	ν CO + ν CCH + ring + δ CH
946 _(w) 904 _(vw) 809 _(vw)	943 _(vw) 817 _(sh,vw)	957 _(w) 928 _(vw) 812 _(vw)						
		573 _(vw) 548 _(vw)	545 _(vw)			666 _(vw) 594 _(vw) 572 _(vw)	903 _(b,vw) 594 _(b,vw) 571 _(vw) 542 _(vw)	ν Si-O-Si ν Si-OH ν Fe-O (maghemite) ν Fe-O ν Fe-O (maghemite)
	526 _(vw)			529 _(vw)	545 _(vw)			

^a Relative intensity: w, weak; b broad; s, strong; sh shoulder; mult., multiple; m, medium; d, double; vw, very weak; shp, sharp, ν stretching mode, δ bending mode.

S.3 Homo/heterogeneous photo-Fenton process

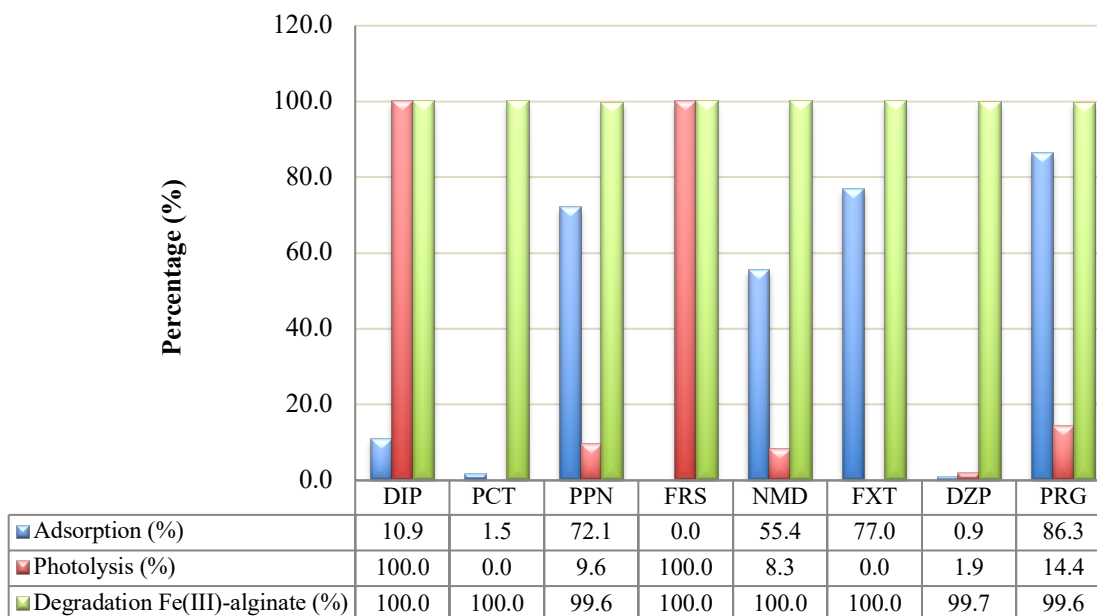


Fig S.3.1 Pharmaceutical photolysis and adsorption on calcium alginate.

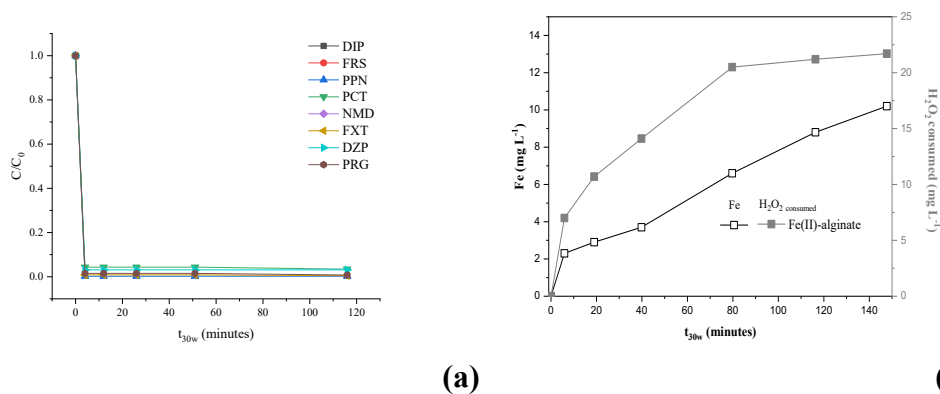
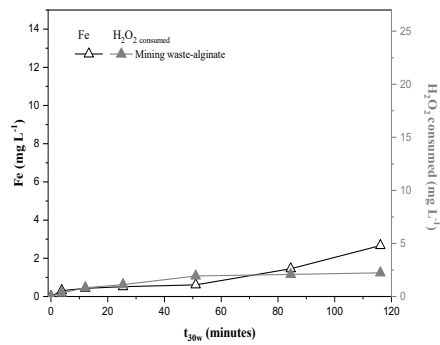
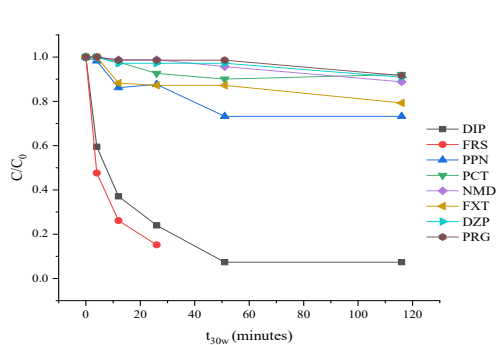


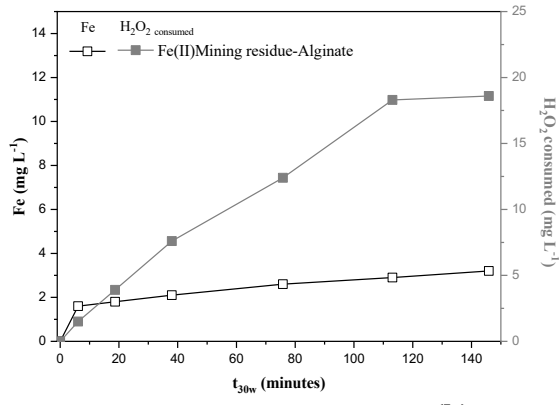
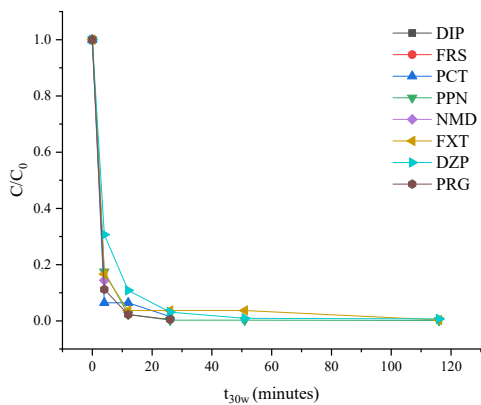
Fig S.3.2 Fe(II)-alginate process a) Pharmaceutical degradation b) Fe release and H₂O₂ consumed (25 mg L⁻¹ of H₂O₂ at pH 5.0).



(a)

(b)

Fig S.3.3 Mining waste powder process a) Pharmaceutical degradation b) Fe release and H₂O₂ consumed (25 mg L⁻¹ of H₂O₂ at pH 5.0).



(a)

(b)

Fig S.3.4 Fe(II)/mining waste-alginate process a) Pharmaceutical degradation b) Fe release and H₂O₂ consumed (25 mg L⁻¹ of H₂O₂ at pH 5.0).

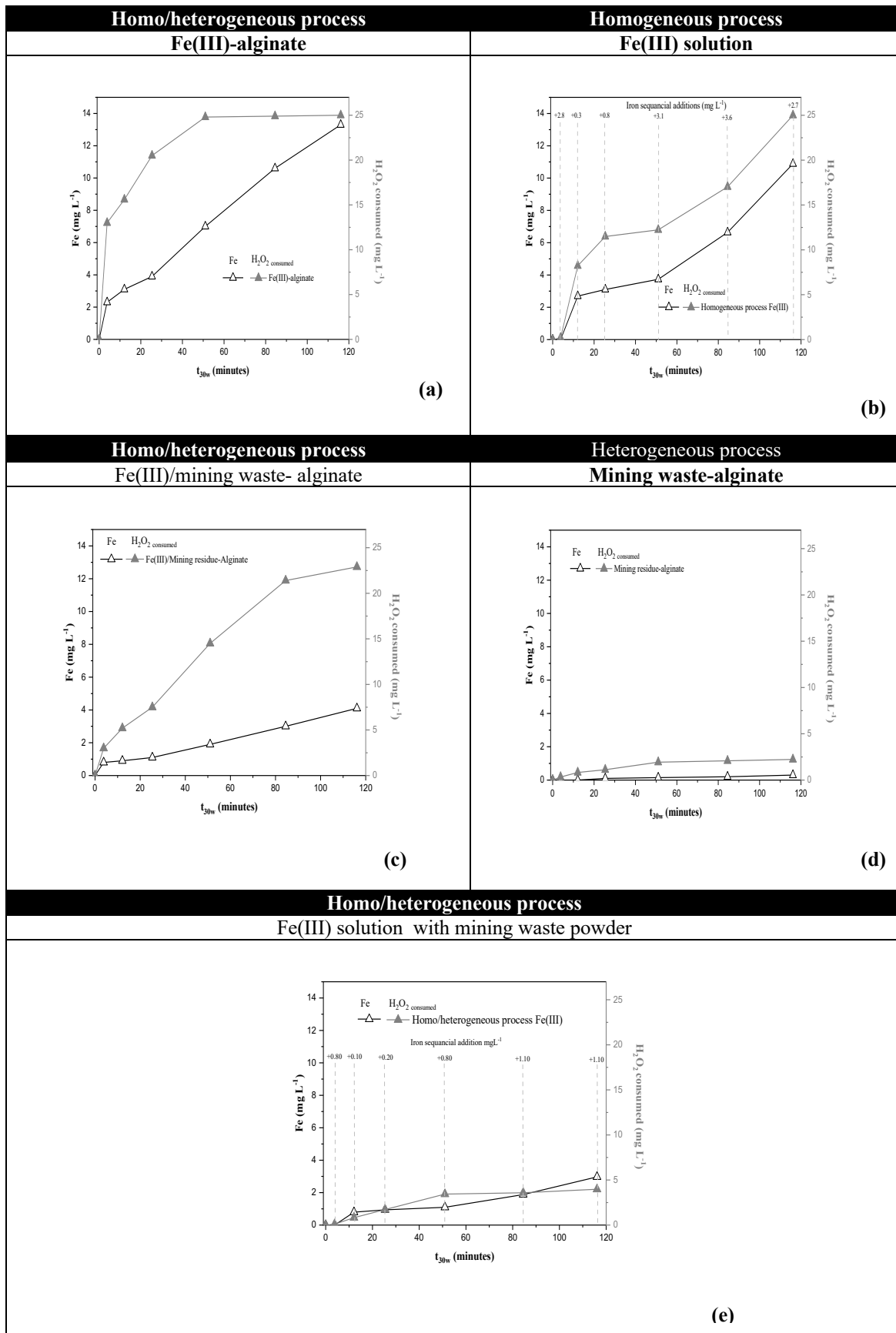


Fig S.3.5 Hydrogen peroxide consumed and iron release for (a) Fe(III)-alginate (b) Fe(III) solution (c) Fe(III)/mining waste-alginate (d) mining waste-alginate (e) Fe(III) with mining waste powder, (116 minutes of treatment time, 25 mg L⁻¹ of H₂O₂ and pH 5.0).

Table S.3.1 Kinetic model employed Fe(III) in DW matrix.

Pharm	Fe(III)-alginate		Fe(III) solution		Fe(III)/mining residue-alginate		Fe(III) solution with mining residue	
	Kinetic behavior	r ²	Kinetic behavior	r ²	Kinetic behavior	r ²	Kinetic behavior	r ²
DIP	I.D		I.D		I.D		I.D	
PCT	I.D		First order model	0.98027	First order model	0.98827	First order model	0.97608
FRS	I.D		I.D		I.D		I.D	
PPN	Chan & Chu model	1.00000	First order model	0.91265	Chan & Chu model	0.99951	Chan & Chu model	0.96954
NMD	I.D		First order model	0.99645	I.D		First order model	0.94303
FXT	Chan & Chu model	1.00000	First order model	0.98185	Chan & Chu model	0.99309	First order model	0.89384
DZP	Chan & Chu model	1.00000	First order model	0.99662	Chan & Chu model	0.99808	First order model	0.93032
PRG	Chan & Chu model	1.00000	First order model	0.98035	Chan & Chu model	0.99828	First order model	0.87501

I.D: Insufficient data number to perform the kinetics study.

Chan & Chu model

$$\frac{t}{1-(C/C_0)} = \rho + \sigma t \leftrightarrow \frac{d(C/C_0)}{dt} = \frac{-\rho}{(\rho + \sigma t)^2} \quad (1)$$

According to Chan & Chu model C is the concentration of the pharmaceutical remaining in the system after a reaction time t (min), C_0 is the initial concentration, and the parameters ρ (min) and σ (dimensionless) are two characteristic constants related to the reaction kinetics and the degradation capacity. Therefore, a higher value for $1/\rho$ indicates a faster initial degradation rate of the pharmaceutical. When t is high and approaching infinity, the reciprocal of constant σ is the theoretical maximum pharmaceutical removal fraction.

S.4 Test reuse of spheres Fe(II)-alginate, Fe(III)-alginate, Fe(II)/mining residue-alginate and Fe(III)/mining residue-alginate

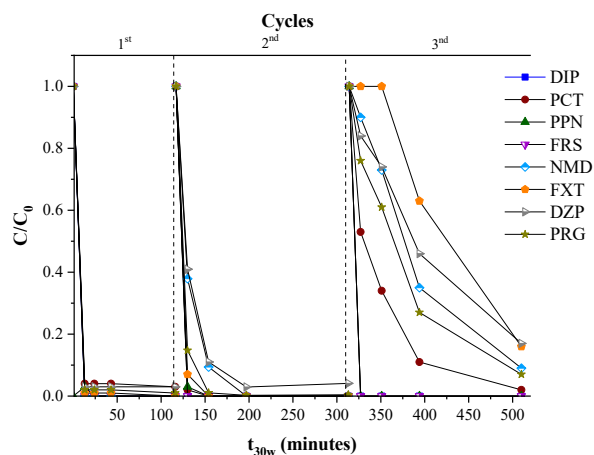


Fig S.4.1 Pharmaceutical degradation in solar photo-Fenton process after t_{30w} 116 min of treatment (3 g of Fe(II)-alginate spheres; 25 mg L⁻¹ of H₂O₂ and pH 5.0) in three cycles of use.

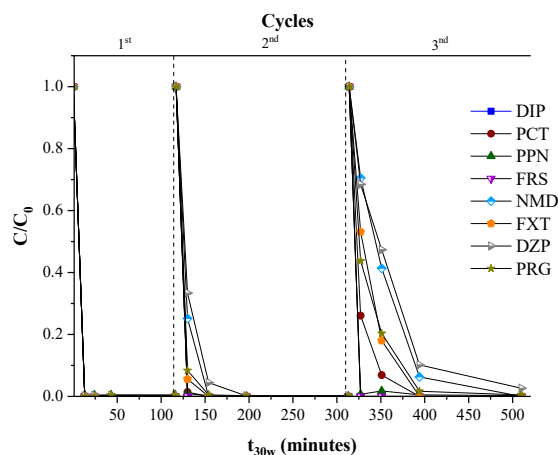


Fig S.4.2 Pharmaceutical degradation in solar photo-Fenton process after t_{30w} 116 min of treatment (3 g of Fe(III)-alginate spheres; 25 mg L⁻¹ of H₂O₂ and pH 5.0) in three cycles of use.

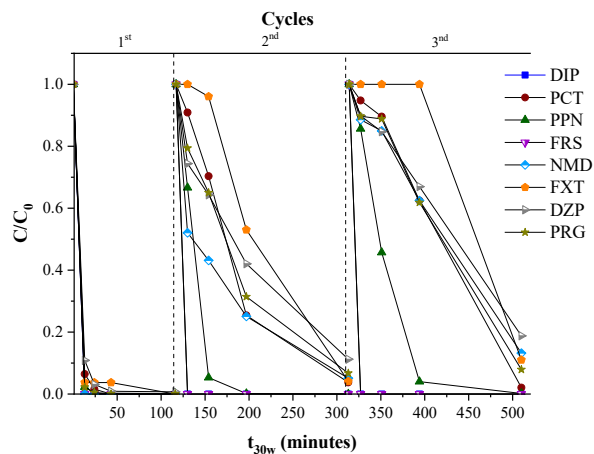


Fig S.4.3 Pharmaceutical degradation in solar photo-Fenton process after t_{30w} 116 min of treatment (3 g of Fe(II)/mining residue-alginate spheres; 25 mg L⁻¹ of H₂O₂ and pH 5.0) in three cycles of use.

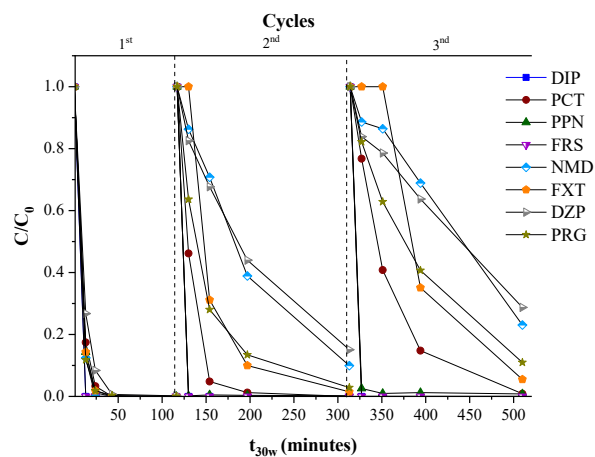


Fig S.4.4 Pharmaceutical degradation in solar photo-Fenton process after 116min of treatment time (3 g of Fe(III)/mining residue-alginate spheres; 25 mg L⁻¹ of H₂O₂ and pH 5.0) in three cycles of use.

S.5 Degradation of pharmaceuticals: SW and RHW matrixes.

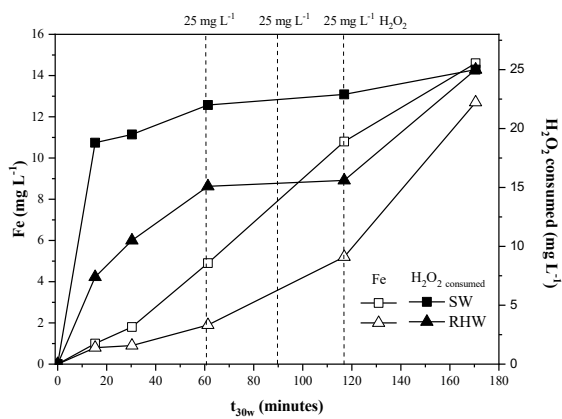


Fig S.5.1 Fe release and H₂O₂ consumed in treatment using Fe(III)-alginate spheres in RHW and SW.

S.6 Transformation products

Table S.6.1 TPs identified during the different heterogeneous Photo-Fenton process treatment.

	Ion Formula	Ion mass m/z		error [ppm]	RDB	PROCESS/MATRIX							
		Exper.	Calc.			FeII		FeIII		FeII/M	FeIII/M		
						DW	DW	SW	RHW	DW	DW		
TP6 DIP	C ₁₀ H ₁₀ NO ₃	192.0648	192.0655	3.8	6.5								
	C ₆ H ₈ N	94.0653	94.0651	-2.2	3.5		X	X					X
TP 7 DIP	C ₁₂ H ₁₆ N ₃ O ₃	250.1186	250.1186	0.2	6.5								
	C ₁₀ H ₁₄ N ₃ O ₂	208.1074	208.1081	3.3	5.5	X	X	X		X			X
	C ₉ H ₁₃ N ₂ O	165.1017	165.1022	3.5	4.5								
	C ₇ H ₁₁ N ₂	123.0914	123.0917	2	3.5								
TP9 DIP	C ₁₁ H ₁₃ N ₂ O ₂	205.0971	205.0972	0.3	6.5								
	C ₉ H ₈ NO	146.0598	146.06	1.9	6.5				X				X
	C ₇ H ₆ NO	120.0444	120.0444	0	5.5								
	C ₆ H ₈ N	94.0653	94.0651	-1.9	3.5								
	C ₃ H ₆ N	56.0495	56.0495	0.1	1.5								
TP 10 DIP	C ₉ H ₁₃ N ₂ O	165.1018	165.1022	2.7	4.5								
	C ₇ H ₁₁ N ₂	123.0914	123.0917	2	3.5	X	X		X	X			
TP 17DIP	C ₁₂ H ₁₄ N ₃ O ₂	232.1078	232.1081	0.9	7.5		X						
TP 18 DIP	C ₉ H ₁₁ N ₂ O ₃	195.076	195.0764	2.1	5.5		X						
TP1 DZP	C ₁₄ H ₁₃ ClNO	246.0676	246.068	1.8	8.5								
	C ₁₄ H ₁₁ ClN	228.0571	228.0575	1.5	9.5		X	X		X			X
TP5 NMD	C ₁₃ H ₁₅ N ₂ O ₃ S	279.0798	279.0798	-0.1	7.5		X						
TP1 FXT	C ₁₇ H ₁₉ F ₃ NO ₂	326.1355	326.1362	2.3	7.5		X	X					
TP3 or 4 FRS	C ₁₂ H ₁₀ ClN ₂ O ₅ S	328.9995	328.9993	-0.6	8.5	X	X			X			X
TP3 PPN	C ₆ H ₁₆ NO ₂	134.1176	134.1176	-0.4	-0.5								
	C ₆ H ₁₄ NO	116.1072	116.107	-1.7	0.5	X	X	X		X			X
	C ₃ H ₈ NO	74.06	74.06	0.7	0.5								
	C ₄ H ₁₀ N	72.0808	72.0808	0	0.5								
	C ₃ H ₆ N	56.0496	56.0495	-1.6	1.5								
TP4 PPN	C ₆ H ₁₆ NO ₃	150.1127	150.1125	-1.8	-0.5								
	C ₆ H ₁₄ NO ₂	132.102	132.1019	-0.7	0.5				X				X
	C ₆ H ₁₂ NO	114.091	114.0913	2.5	1.5								

	C ₃ H ₈ NO	74.0599	74.06	1.2	0.5						
TP 5 19 or 20 PPN	C ₁₄ H ₂₀ NO ₅	282.1336	282.1336	-0.1	5.5						
	C ₈ H ₅ O ₃	149.0233	149.0233	0.5	6.5	X	X			X	
	C ₆ H ₁₄ NO	116.1072	116.107	-2	0.5						
	C ₆ H ₁₂ N	98.0965	98.0964	-0.3	1.5						
	C ₃ H ₆ N	56.0497	56.0495	-3.5	1.5						
TP6 PPN	C ₁₆ H ₂₂ NO ₄	292.1543	292.1543	0.2	6.5	X	X			X	X
	C ₉ H ₇ O	131.0493	131.0491	-1.2	6.5						
TP7 PPN	C ₁₄ H ₂₀ NO ₄	266.1395	266.1387	-3.1	5.5						
	C ₁₄ H ₁₈ NO ₃	248.1294	248.1281	-5.3	6.5	X	X				
	C ₆ H ₁₂ N	98.097	98.0964	-5.5	1.5						
TP26 PPN	C ₁₆ H ₂₂ NO ₅	308.1497	308.1492	-1.6	6.5						
	C ₁₆ H ₂₀ NO ₄	290.1389	290.1387	-0.7	7.5						
	C ₁₀ H ₇ O ₃	175.0399	175.039	-5.1	7.5	X	X			X	X
	C ₁₁ H ₉ O	157.0658	157.0648	-6.2	7.5						
	C ₉ H ₇ O ₂	147.044	147.0441	0.5	6.5						
	C ₆ H ₁₄ NO	116.1072	116.107	-1.5	0.5						
	C ₆ H ₁₂ N	98.0966	98.0964	-2	1.5						
	C ₄ H ₁₀ N	72.0808	72.0808	-0.9	0.5						
	C ₃ H ₆ N	56.0495	56.0495	-0.6	1.5						
TP 27 PPN	C ₁₆ H ₂₂ NO ₅	308.1495	308.1492	-0.7	6.5						
	C ₁₆ H ₂₀ NO ₄	290.1387	290.1387	-0.1	7.5		X				X
	C ₁₀ H ₇ O ₃	175.0392	175.039	-1.6	7.5						
	C ₉ H ₇ O	131.0493	131.0491	-1	6.5						
	C ₆ H ₁₄ NO	116.1073	116.107	-2.8	0.5						
	C ₆ H ₁₂ N	98.0965	98.0964	-0.9	1.5						
	C ₄ H ₁₀ N	72.081	72.0808	-2.5	0.5						
TP 28 29 30 or 31 PPN	C ₁₆ H ₂₄ NO ₅	310.1649	310.1649	-0.1	5.5						
	C ₁₆ H ₂₂ NO ₄	292.1542	292.1543	0.6	6.5		X				
	C ₁₆ H ₂₀ NO ₃	274.1436	274.1438	0.7	7.5						
TP4 PRG	C ₂₁ H ₂₉ O ₂	313.2157	313.2162	1.7	7.5						
	C ₂₁ H ₂₇ O	295.2052	295.2056	1.6	8.5		X				X

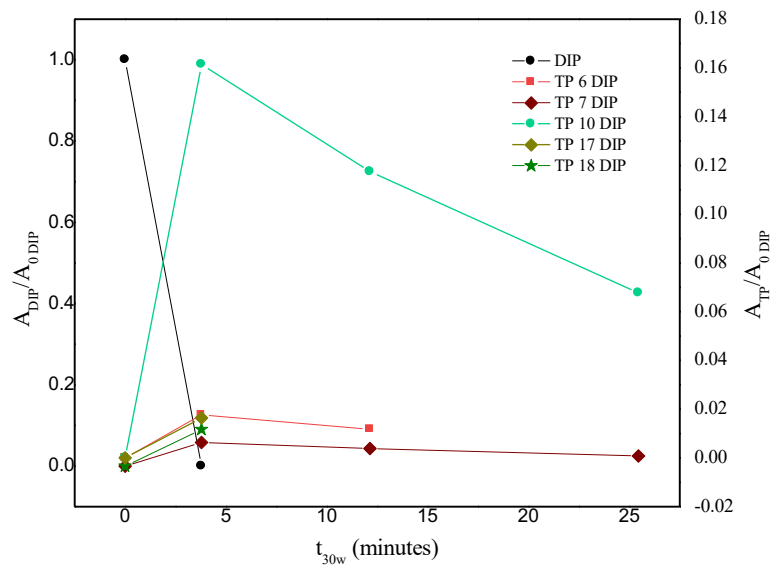


Fig S.6.1 Behavior of the main TPs DIP generated in DW.

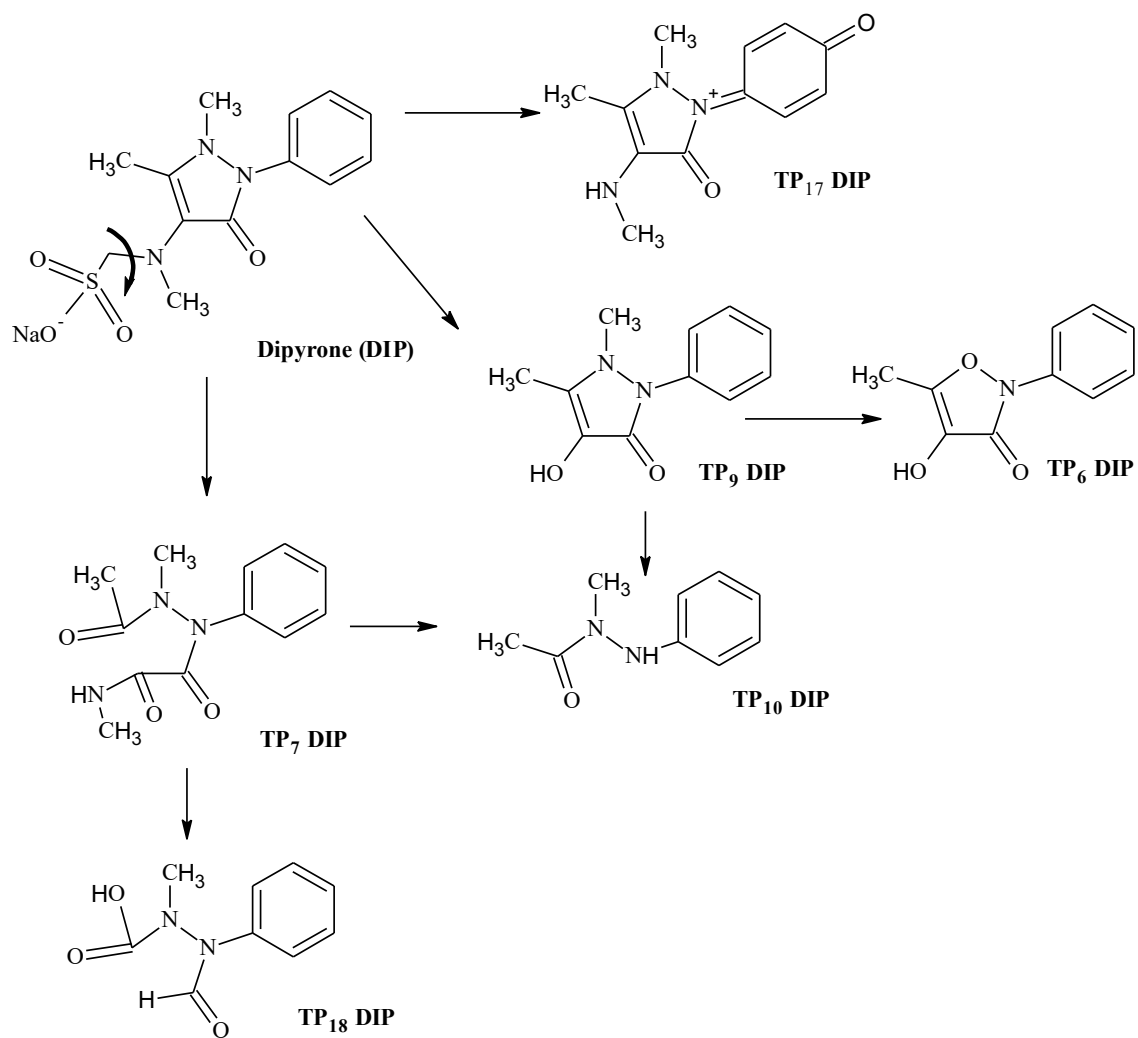


Fig S.6.2 Pathway degradation of TPs DIP.

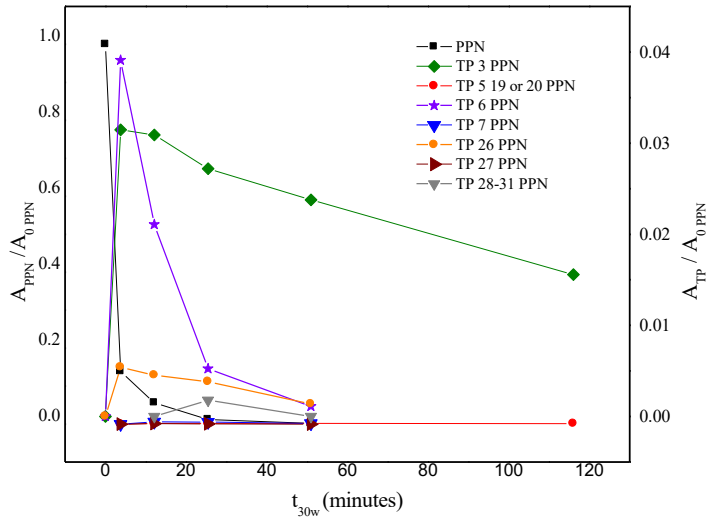


Fig S.6.3 Behavior of the main TPs PPN generated in DW.

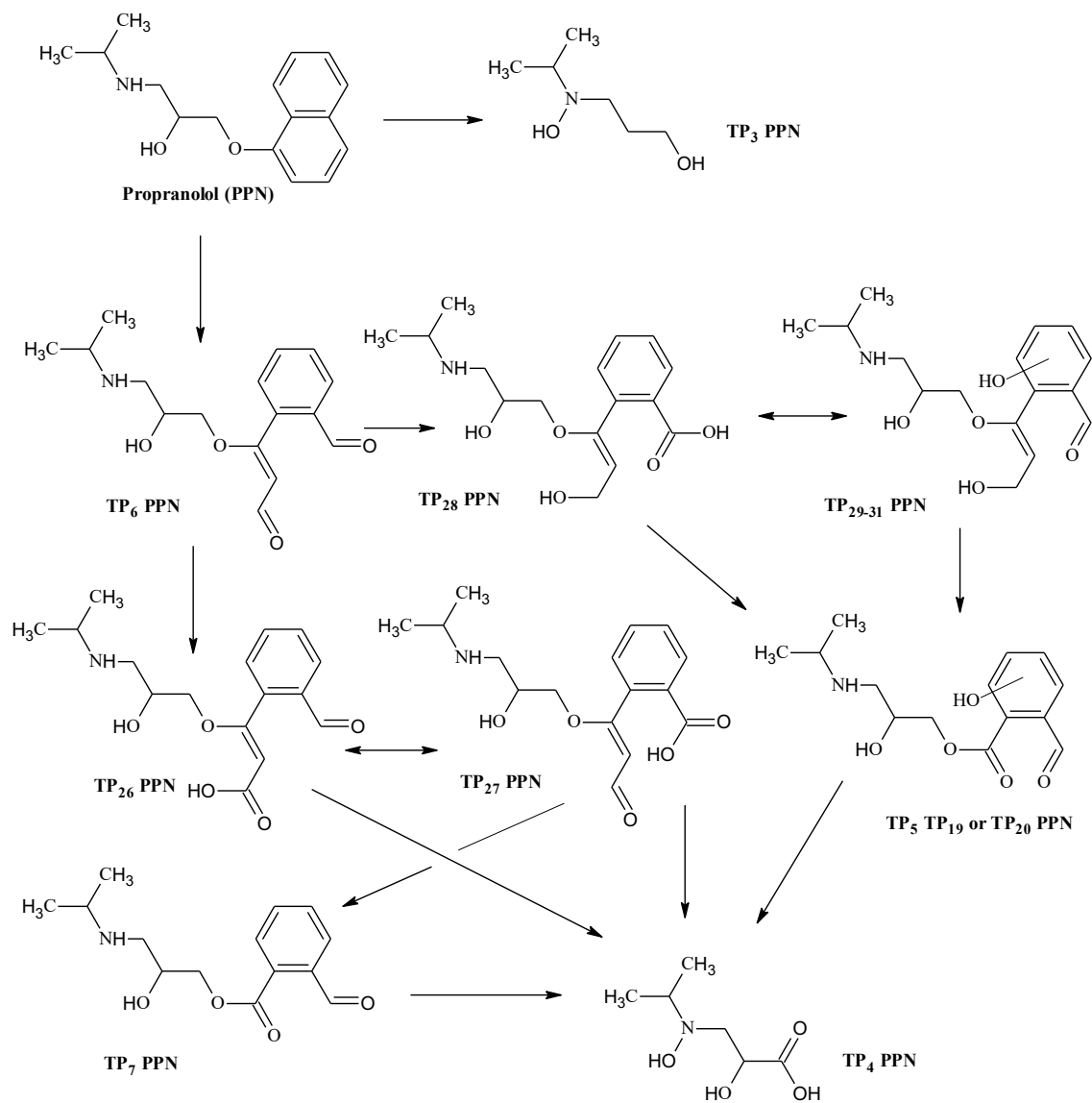
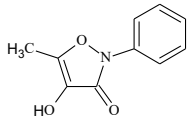
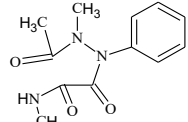
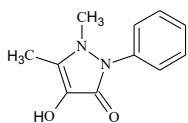
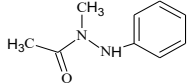
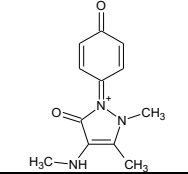
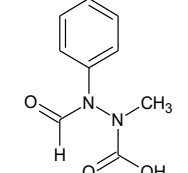
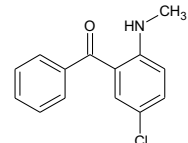
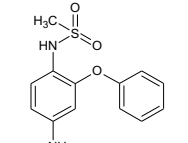
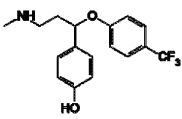
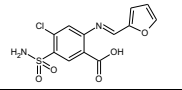
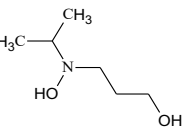
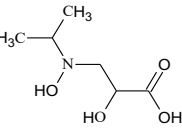
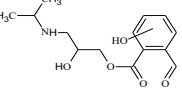
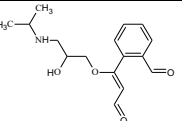
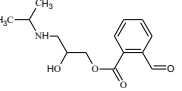
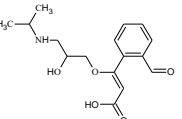
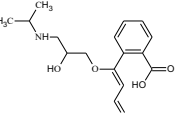
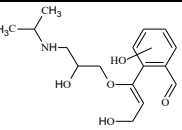
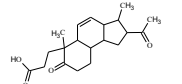


Fig S.6.2 Pathway degradation of TPs PPN.

Table S.6.2 Toxicological hazard, biodegradability and toxicity studies reported.

TP	Chemical structure proposed	Toxicological hazard	START biodegradability	Toxicity studies reported	
				Main results	Authors
TP6 DIP		High (Class III)	Persistent chemical (Class 2)	The TPs generated did not present significant acute toxicity to <i>D. magna</i>	<i>Daphnia magna</i> acute immobilization tests (Gómez <i>et al.</i> 2008)
TP7 DIP		High (Class III)	Persistent chemical (Class 2)		
TP9 DIP		High (Class III)	Persistent chemical (Class 2)		
TP10 DIP		High (Class III)	Persistent chemical (Class 2)		
TP 17 DIP		High (Class III)	Persistent chemical (Class 2)	The TPs generated did not present significant toxicity to <i>Vibrio fischeri</i> bacterium.	BioTox luminometric toxicity test kit with <i>Vibrio fischeri</i> bacterium (Pérez-Estrada <i>et al.</i> 2007)
TP 18 DIP		High (Class III)	Persistent chemical (Class 2)		
TP1 DZP		High (Class III)	Persistent chemical (Class 2)	The TP presented toxicity to <i>Daphnia magna</i>	<i>Daphnia magna</i> LC ₅₀ (Carpinteiro <i>et al.</i> 2017)
TP5 NMD		High (Class III)	Persistent chemical (Class 2)	Not reported	
TP1 FXT		High (Class III)	Persistent chemical (Class 2)	The toxicity decrease after the treatment but cannot be	Marine luminescent <i>Vibrio fischeri</i> bacterium

				fully removed.	(Zhao <i>et al.</i> 2017)	
TP3 or TP4 FRS		High (Class III)	Persistent chemical (Class 2)	Not reported		
TP3 PPN		Low (Class I)	Persistent chemical (Class 2)	TPs presented toxicity, which accumulated with the cycles of treatment.	Green algae <i>P. subcapitata</i> and bioluminescent marine <i>Vibrio fischeri</i> bacterium (Santiago-Morales <i>et al.</i> 2013)	
TP4 PPN		Low (Class I)	Persistent chemical (Class 2)			
TP 5 , 19 or 20 PPN		High (Class III)	Persistent chemical (Class 2)			
TP6 PPN		High (Class III)	Persistent chemical (Class 2)			
TP7 PPN		Low (Class I)	Easy biodegradable chemical (Class 1)			
TP 26 PPN		High (Class III)	Persistent chemical (Class 2)			
TP 27 PPN		High (Class III)	Persistent chemical (Class 2)			
TP 28 29 30 or 31		High (Class III)	Persistent chemical (Class 2)			
TP4 PRG		High (Class III)	Persistent chemical (Class 2)			Not reported

References Supporting Information

- Carpinteiro I, Rodil R, Quintana J, Cela R (2017) Reaction of diazepam and related benzodiazepines with chlorine. Kinetics, transformation products and in-silico toxicological assessment. *Water Res* 120:280–289. doi: 10.1016/J.WATRES.2017.04.063
- Gómez MJ, Sirtori C, Mezcuca M, Fernández Alba A, Agüera A (2008) Photodegradation study of three dipyrone metabolites in various water systems: Identification and toxicity of their photodegradation products. *Water Res* 42:2698–2706. doi: <http://dx.doi.org/10.1016/j.watres.2008.01.022>
- Pérez-Estrada L, Malato S, Agüera A, Fernández-Alba A (2007) Degradation of dipyrone and its main intermediates by solar AOPs. *Catal Today* 129:207–214. doi: <http://dx.doi.org/10.1016/j.cattod.2007.08.008>
- Santiago-Morales J, Agüera A, Gómez M del M, Fernández-Alba A, Giménez J, Esplugas S, Rosal R (2013) Transformation products and reaction kinetics in simulated solar light photocatalytic degradation of propranolol using Ce-doped TiO₂. *Appl Catal B Environ* 129:13–29. doi: <http://dx.doi.org/10.1016/j.apcatb.2012.09.023>
- Zhao Y, Yu G, Chen S, Zhang S, Wang B, Huang J, Deng S, Wang Y (2017) Ozonation of antidepressant fluoxetine and its metabolite product norfluoxetine: Kinetics, intermediates and toxicity. *Chem Eng J* 316:951–963. doi: <http://dx.doi.org/10.1016/j.cej.2017.02.032>

4.1.3 Solar photo-Fenton process: Fe³⁺:EDDS

Based on the photo-activity of the ferric species, the photo-Fenton process can be considered catalytic, and an enhanced form of the classic Fenton reaction inducing the formation of extra hydroxyl radicals for wastewater treatment⁵⁷. However, due to the insolubility of the ferric aquo or hydroxy species at neutral pH, the system is pH-dependent, and its full-scale application is subject to limitations. This drawback can be overcome by introducing ligands to iron and generate the subsequent ROS at neutral or weakly alkaline pH without initial acidification and/or subsequent neutralization.

Hence, this subsection presents a work focused on solar photo-Fenton like process in a homogeneous system with EDDS (chelating agent as biodegradable alternative). In this study (**Paper IV**)¹¹², the stability of the Fe³⁺:EDDS complex was evaluated in different proportions, pH values, presence of sunlight, and aqueous matrices. The optimization of experimental conditions was performed through Doehlert design and cyclic voltammetry.



Solar photo-Fenton-like process at neutral pH: Fe(III)-EDDS complex formation and optimization of experimental conditions for degradation of pharmaceuticals

Elisabeth Cuervo Lumbaqu^a, Débora Salmoria Araújo^a, Thágor Moreira Klein^a, Elaine R. Lopes Tiburtius^b, Jacqueline Argüello^{a,*}, Carla Sirtori^{a,*}

^a Instituto de Química- Universidade Federal do Rio Grande do Sul, Av. Bento Gonçalves, 9500, Porto Alegre, RS, Brazil

^b Universidade Estadual de Ponta Grossa, Av. General Carlos Cavalcanti, 4748, Ponta Grossa, PR, Brazil

ARTICLE INFO

Keywords:

Solar photo-Fenton
Fe(III)-EDDS complex
Neutral pH
Transformation products
Toxicity
Biodegradability

ABSTRACT

This paper demonstrates the effectiveness of Fe(III)-EDDS complex for degradation of pharmaceutical compounds in a solar photo-Fenton-like process at neutral pH in two different aqueous matrixes. Electrochemical experiments were performed to monitor the formation and stability of the complex, as a function of the amount of complexing agent and pH. Eight compounds, including diazepam, dipyrone, fluoxetine, furosemide, nimesulide, paracetamol, progesterone, and propranolol, were analyzed in distilled water and simulated wastewater, at initial concentrations of 500 $\mu\text{g L}^{-1}$. By applying Doehlert matrix design and the response surface methodology the optimal experimental conditions were found to be 0.28 mmol L^{-1} Fe(III)-EDDS and 5.00 mmol L^{-1} H_2O_2 , with a ratio of 1:2 for Fe(III)-EDDS. The most persistent transformation products (TPs) generated during the treatment process were investigated using liquid chromatography coupled with quadrupole time-of-flight mass spectrometry. 16 TPs were identified and classified as having high toxicity (according to the Cramer rules), low biodegradability (according to the START scheme), and possible carcinogenicity and/or mutagenicity. Most of the compounds were degraded in the first minutes of treatment, and most of the identified TPs had been successfully removed at the end of the process.

1. Introduction

The Fenton ($\text{Fe(II)/H}_2\text{O}_2$), Fenton-like ($\text{Fe(III)/H}_2\text{O}_2$) and photo-Fenton ($\text{UV/Fe(III)/H}_2\text{O}_2$) reactions are known as the most efficient advanced oxidation processes (AOPs) that have been used for the removal of different kinds of emerging pollutants from water and wastewater, including pharmaceutical compounds [1–4]. The traditional photo-Fenton-like process employs Fe(III) and H_2O_2 in acid condition (pH 2.8–3.0), leading to high degradation levels. At neutral pH, however, the process is limited due to the low solubility and poor stability of Fe(III), slowing the rate of HO^\cdot generation and decreasing the efficiency of this treatment process [5,6]. In order to improve the accessible pH range and efficiency of the photo-Fenton treatment, chelating agents such as aminopolycarboxylic acids (APCAs) have been used to maintain Fe(III) in solution [5,7]. Among the APCAs, ethylenediaminetetraacetic acid (EDTA) is widely used [8,9], but due to its low biodegradability [10] has been considered an emerging contaminant [6,11], representing a risk for aquatic organism [12].

As an alternative, ethylenediamine- $\text{N,N}'$ -disuccinic acid (EDDS), a structural isomer of EDTA but more environmentally friendly metal chelating, with high biodegradability and nontoxicity under environmental conditions, can be used for the solubilization of iron species [11,13–15] with high effectiveness in the pH range 3–9 [5,16]. The Fe(III)-EDDS complex offers higher photoabsorption compared to iron aquo complexes [7,16,17]. The photochemical activity is associated with the ligand-to-metal charge transfer (LMCT) transitions [18], with fast photochemical reactions occurring under solar UV radiation.

The HO^\cdot yield in the Fenton process strongly depends on the experimental conditions such as the pH value, iron/ H_2O_2 ratio and ligands present in the solution [19]. When the concentration of Fe(III):EDDS is high and the matrix contains high dissolved organic matter, these factors act as an HO^\cdot scavenger that inhibits the degradation of contaminants, similarly, large amounts of hydrogen peroxide have a negative effect [20]. In order to achieve high degradation rates is necessary to study the effects of concentration of Fe(III):EDDS and H_2O_2 involved in the processes. For this purpose, the use of

* Corresponding authors.

E-mail addresses: jacqueline.arguello@ufrgs.br (J. Argüello), carla.sirtori@ufrgs.br (C. Sirtori).

<https://doi.org/10.1016/j.cattod.2019.01.006>

Received 11 July 2018; Received in revised form 17 December 2018; Accepted 2 January 2019

Available online 04 January 2019

0920-5861/ © 2019 Elsevier B.V. All rights reserved.

experimental designs has been widely explored in recent years, determining the effects of each variable and their interactions, establishing an optimal experimental condition [21,22].

During the photo-Fenton process, several reactions occur in series and in parallel, including hydroxylation, decarboxylation, and dehydrogenation, among others [23,24], leading to a variety of reactive intermediates. The identification of these intermediates, known as transformation products (TPs), would be crucial to understanding the possible pathways involved in the degradation of these pharmaceuticals. Therefore, the goal of this paper is to define the optimal conditions to improve the removal of pharmaceuticals in a photo-Fenton-like process using Fe(III)-EDDS complex at neutral pH in two different aqueous matrixes. At the same time, using UHPLC-QTOF MS and database-built of transformation products (TPs) the main pathways are proposed.

2. Materials and methods

2.1. Electrochemical experiments

Electrochemical experiments were carried out using an Autolab PGSTAT302 N potentiostat with a conventional three-electrode cell setup. A saturated calomel electrode (SCE) was used as the reference electrode, together with a platinum wire as an auxiliary electrode and a glassy carbon electrode (GCE) as the working electrode. Prior to each measurement, the GCE was carefully polished to a mirror-like surface, using 0.5 μm alumina slurry, followed by thorough rinsing with deionized water. Cyclic voltammograms were recorded in 0.05 M KCl solution at a scan rate (v) of 50 mV s^{-1} . The electrolyte solutions were degassed by purging with high-purity argon (99.999%) before the measurements.

2.2. Chemicals and aqueous matrixes

All solutions were prepared and diluted using ultra-pure water (18.2 $\text{M}\Omega\cdot\text{cm}$ water repared Milli-Q system). The stock solution of the complex was prepared according to the methodology described by Soriano-Molina [25]. Briefly, $\text{Fe}_2(\text{SO}_4)_3\cdot 5\text{H}_2\text{O}$ (purity > 95%, purchased from Synth, São Paulo, Brazil) was dissolved in water, previously acidified to pH 3.0 with 1 mol L^{-1} HCl, to prepare a stock solution of 85 mmol L^{-1} . Next, EDDS (in different proportions) was added to the iron solution and the mixture was stirred for 5 min to ensure formation of the Fe(III)-EDDS complex followed by the adjustment to the required pH.

Standards of nimesulide (NMD), furosemide (FRS), paracetamol (PCT), propranolol (PPN), dipyrone (DIP), fluoxetine (FXT), diazepam (DZP), and progesterone (PRG) (analytical grade; purity > 90%) were used for degradation study. A mixed stock solution of pharmaceutical compounds was prepared at concentration of 14 g L^{-1} for each of these model compounds in ACN:MeOH (2:1) (v/v) and the initial pharmaceuticals concentration (each of them) for the degradation experiments (500 $\mu\text{g L}^{-1}$) was prepared by appropriate dilution of the stock solution.

The composition of the simulated wastewater (SW), adapted from the OECD [26], consisted of peptone 160 mg L^{-1} , beef extract 110 mg L^{-1} , urea 30 mg L^{-1} , $\text{Mg}_2\text{SO}_4\cdot 7\text{H}_2\text{O}$ 2 mg L^{-1} and $\text{CaCl}_2\cdot 2\text{H}_2\text{O}$ 4 mg L^{-1} .

2.3. Solar photo-Fenton-like process

Optimization of the conditions used for the solar photo-Fenton-like experiments was carried out using a Doehlert design with two variables (see Table 1) [19]. Batch experiments were performed using distilled water (DW) or simulated wastewater (SW) in a solar photoreactor (1 L) equipped with a magnetic stirrer. The Fe(III)-EDDS complex was added to the photoreactor containing the initial mixed pharmaceuticals solution, followed by the addition of hydrogen peroxide (35% w/v). In all experiments, after the complex addition, the pH was adjusted to 7.0

using sodium hydroxide (0.2 mol L^{-1}),

Solar UV radiation was measured using a solar energy meter (SP-2000, ICEL), which provided data in terms of incident radiation (W m^{-2}). These data were used to calculate the normalized irradiation time $t_{30\text{W}}$ [27].

2.4. Analytical determinations

The total iron concentration was monitored colorimetrically using 1,10-phenanthroline [28]. Hydrogen peroxide was determined by the ammonium metavanadate method [29], using a Cary 50 UV-vis spectrophotometer. Mineralization was evaluated by measuring the dissolved organic carbon (DOC) of the water samples. DOC measurements were performed by direct injection of filtered samples into a Shimadzu TOC-L CSH analyzer.

2.5. LC-QTOF MS instrumentation

Pharmaceuticals and their degradation products were monitored and quantified using an LC (Shimadzu Nexera X2) connected to a QTOF MS (Impact II, Bruker Daltonics). The identification of TPs was carried out through the implementation of a purpose-built-database with TPs reported in the literature, this database has more than 175 compounds [30], each TP is assigned a number with the acronym of the pharmaceutical from which it originated (for example, the first transformation product of dipyrone is coded as TP1 DIP). Further details are provided in the Supporting Information (Section S.1).

2.6. Predicted biodegradability and toxicological risk of the TPs

The Toxtree software was used to predict parameters such as biodegradability, toxicological risk, carcinogenicity and mutagenicity potentials of the identified TPs. It is a flexible and easy-to-use full-featured open source application that allows the estimation of toxic hazards by applying a decision tree approach for the toxicological hazard Cramer rules [31,32]. It also evaluates biodegradation and persistence, based on a compilation of structural alerts for environmental persistence and biodegradability potentials, according to the Canadian EPA [33], in turn estimated carcinogenicity and mutagenicity using the European Commission report. [34].

3. Results and discussion

3.1. Characterization of the Fe(III)-EDDS complex

Electrochemical experiments were performed to evaluate the Fe(III):EDDS complex formation. Fig. 1(a) shows cyclic voltammograms registered in 0.05 M KCl solution containing the metal and the ligand at different molar ratios. The measurements were carried out at pH 3.0 in order to maintain the iron ions in solution. In the first scan, the sharp peak depicted at -0.153 V corresponds to the reduction of Fe(III) to Fe(II). After the first addition of EDDS, the current substantially decreased while a new reduction peak appeared at -0.262 V due to formation of the iron complex. This peak continued to increase until it reached the 1:1 metal-ligand ratio, from which it remained constant. This result indicates that Fe(III) ions formed a stable complex with EDDS at a stoichiometry of 1:1, which is in agreement with previous reports [7]. The peak due to the oxidation of Fe(II), however, continue to grow and become constant only from a ratio of 1:2.5, pointing out that an excess of EDDS become necessary to stabilize the Fe(II) signal. Gomes Júnior et al. [16] already reported that increased availability of the organic ligand promotes the stability of the metal complex, offering a favorable condition for the photo-Fenton reaction.

Since the pH of the medium plays a crucial role in the iron cycle and the Fe(III):EDDS speciation, the influence of the pH on the stability of the complex was evaluated in the pH range 3.0-9.0. According to the

Table 1
Doehlert designs for pharmaceuticals degradation in DW and SW matrixes.

VARIABLE 1					
Codified value	-1	-0.5	0	0.5	1
[H ₂ O ₂] (mmol L ⁻¹)	0.01	2.51	5.00	7.50	10.00
VARIABLE 2					
Codified value	-0.866		0	0.866	
[Fe(III)-EDDS] (mmol L ⁻¹)	0.05		0.28	0.50	
QUADRATIC MODEL					
Experiment number	[H ₂ O ₂]	[Fe(III)-EDDS]	Response (% decrease Σ area) ^a		
			DW	SW	
1	10.00	0.28	97.95	74.63	
2	7.50	0.50	92.94	80.53	
3	0.01	0.28	65.32	41.53	
4	2.51	0.05	50.56	44.19	
5	7.50	0.05	90.77	43.58	
6	2.51	0.50	96.08	65.59	
7	5.00	0.28	97.92	79.32	
8	5.00	0.28	97.67	79.44	
9	5.00	0.28	98.70	70.78	

^aSolar photo-Fenton treatment time (t_{30w}): 15.8 min.

The box in Table 1 represents the optimum conditions of the solar photo-Fenton process or the central point in Doehlert design performed as is described in second paragraph of section 3.2.

literature [6,11,35], four different complexes can be found depending on the pH, FeL⁻ (pH 2.0–7.5), FeOHL²⁻ (pH 7.5–9.75), Fe(OH)₂L³⁻ (pH 9.75–10.75) and Fe(OH)₄⁻ (pH > 10.75). On the other hand, L⁻⁴ is not the predominant specie at pH < 9 considering the protonation constant of EDDS KHL³⁻/L⁴⁻ = 10. Fig. 1 (b) shows the voltammograms obtain in 0.05 mol L⁻¹ KCl and a mixture of the Fe(III) and EDDS salts in a molar ratio of 1:2. The current and potential remained almost unchanged up to pH 6. However, a slight decreased in the current intensity and small shifting of the potential were observed at higher pH values. Since these variations did not significantly affect the stability of the complex, Fe(III)-EDDS (at 1:2) could be employed at neutral pH or even under alkaline conditions.

The stability of the complex was also evaluated under exposure to solar light at pH 5.0, 7.0, and 9.0. A treatment performed at neutral pH would help to reduce operating costs in industrial-scale applications. Furthermore, most hospital wastewater has pH from neutral to alkaline [36]. The cyclic voltammograms recorded at different times are shown in Figs. S.2.1, S.2.2, and S.2.3 (Supporting Information). The peaks corresponding to the Fe(III)-EDDS redox remain unaffected in the first 10 min of exposure, and almost disappeared after 180 min, which could be interpreted as being due to degradation of the complex under the effect of sunlight. Given these results, 120 min was established as the maximum time that the complex remained stable under incident sunlight. Fig. 1(c) shows a comparative graph of the behaviors of the complex at the three pH values, under sunlight, at the beginning and at the end of the experiment (120 min).

The stability of the complex in the SW matrix (Fig. S.2.4, Supporting Information), that have a high organic loading similar to that of a real hospital effluent, was also evaluated. Lower signal intensity was obtained under this condition, due to adsorption of some species on the carbon electrode surface with a consequent decrease in the electron transfer. Nevertheless, the results confirmed the stability of the Fe(III)-EDDS complex and its suitability for use in solar photo-Fenton-like processes.

3.2. Optimization of experimental conditions: Doehlert design

A multivariate experimental design was applied for the assays using DW and SW, in order to optimize the most important variables for the homogeneous photo-Fenton process in different matrixes. The variables evaluated were the Fe(III)-EDDS concentration (using a ratio of 1:2) and the H₂O₂ concentration. The pH was set at 7.0, since this value is close to the pH of real hospital wastewaters [36]. Nine experiments were required and the percentage decrease of the summed peak areas of the pharmaceuticals ((1- $\Sigma(C_i/C_0)$)*100), after 15.8 min of treatment using the solar photo-Fenton-like process, was used as the analytical response (Table 1).

The optimum conditions of the solar photo-Fenton processes using the DW and SW matrixes were found for the central point according to Doehlert design with 5.00 mmol L⁻¹ of H₂O₂ and 0.28 mmol L⁻¹ of Fe (III)-EDDS (1:2) (experiments 7, 8, and 9 of Table 1). This condition was selected because the response was very close to those for the experiments with the most significant responses (experiment 1 using DW and experiment 2 using SW), but required lower concentrations of H₂O₂ and the complex, hence making the process more environmentally friendly and economically viable.

The quality of fit of the mathematical model to the experimental data was assessed by analysis of variance (ANOVA), using electronic spreadsheets, with evaluation of the significance of the regression [37]. All the results obtained from the Doehlert design are presented in the Supporting Information, with the concentrations of H₂O₂ and Fe(III)-EDDS being the principal factors that influenced the solar photo-Fenton process [38,39].

3.3. Degradation of pharmaceutical compounds

The solar photo-Fenton-like process was carried out for t_{30w} of 110.4 min, using the DW and SW matrixes under the optimized conditions. The results showed that some of the compounds were eliminated in the first minutes of treatment. DIP presented the highest degradation rates in both DW and SW, while PPN, FXT, DZP, and PRG were more persistent in both matrixes evaluated (Fig. 2a and b).

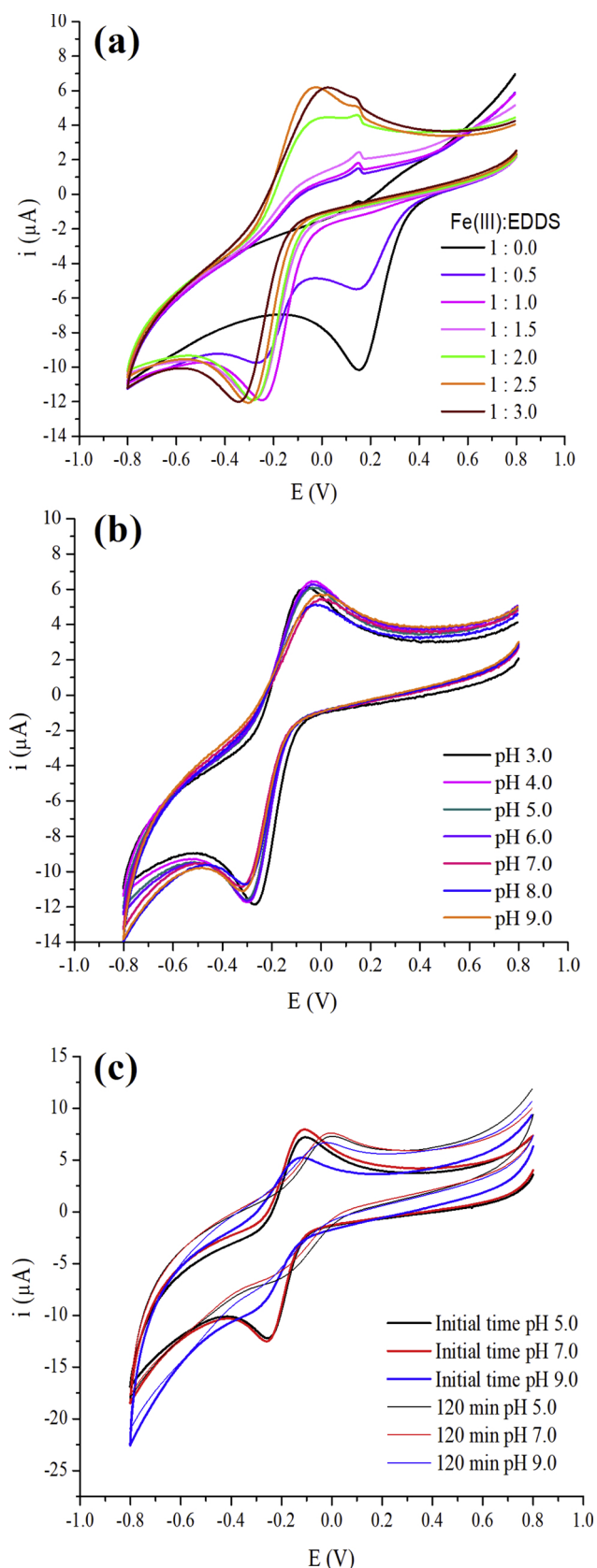


Fig. 1. Cyclic voltammograms recorded in 0.05 mol L⁻¹ KCl containing 0.5 mmol L⁻¹ Fe(III), $v = 50 \text{ mVs}^{-1}$. (a) different Fe(III)-EDDS complex relationships at pH = 3.0 (b) Fe(III)-EDDS (1:2) at different pHs (3.0–9.0) (c) Fe(III)-EDDS (1:2) before and after solar-light irradiation at pH 5.0, 7.0 and 9.0.

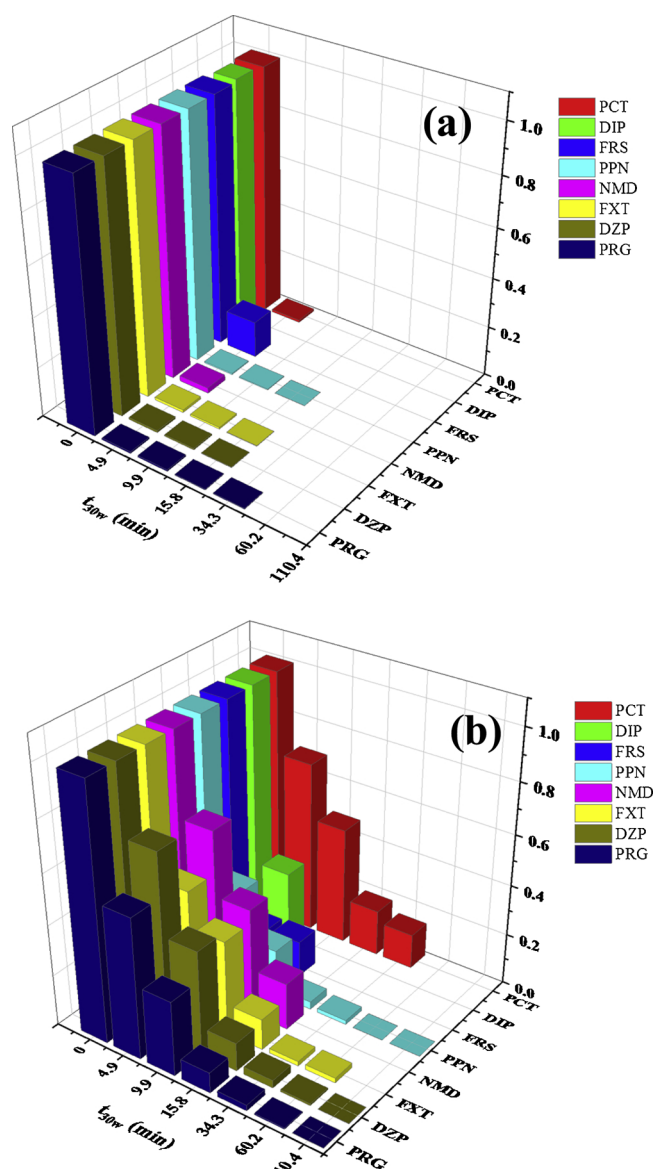
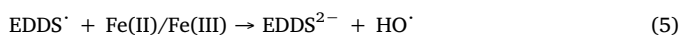
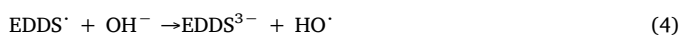
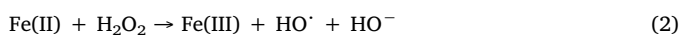
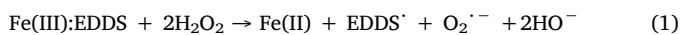


Fig. 2. Pharmaceutical degradation employed solar photo-Fenton-like process at neutral pH in DW matrix (a) and SW matrix (b).

For DW, the compounds showed concentrations $< \text{LOD}$ at the final treatment time, PCT ($< 0.20 \mu\text{g L}^{-1}$), DIP ($< 0.31 \mu\text{g L}^{-1}$), FRS ($< 0.78 \mu\text{g L}^{-1}$), PPN ($< 0.01 \mu\text{g L}^{-1}$), NMD ($< 0.24 \mu\text{g L}^{-1}$), FLX ($< 0.31 \mu\text{g L}^{-1}$), DZP ($< 0.01 \mu\text{g L}^{-1}$) and PRG ($< 0.02 \mu\text{g L}^{-1}$). Blank experiments were carried out in DW matrix to determine the impact of the direct photolysis and the concentration of H_2O_2 used on the degradation of pharmaceuticals in the absence of Fe(III)-EDDS complex (see Figs. S.4.1–S.4.3), the results indicated a total degradation of DIP and FRS by direct photolysis and with photolysis + H_2O_2 , the use of H_2O_2 in the absence of sunlight confirmed that light and H_2O_2 has a greater effect on the degradation of pharmaceutical compounds. However, when comparing 60 min of blank experiments and a solar photo-Fenton-like process, it was evidenced that the presence of the Fe(III)-EDDS complex improves the degradation rates, this shows the real impact and the positive effect of the Fe(III)-EDDS complex in the degradation of pharmaceuticals at neutral pH.

When the process was performed using the SW matrix, the most pharmaceuticals presented values lower than LOD, DIP ($< 1.20 \mu\text{g L}^{-1}$) and FRS ($< 1.36 \mu\text{g L}^{-1}$) were easily degraded, this behavior is reported in other works using photo-Fenton [27–30], NMD ($< 0.42 \mu\text{g L}^{-1}$)

L⁻¹), PCT (< 0.58 µg L⁻¹) and FXT (< 5.17 µg L⁻¹) were more persistent through time, while PPN (< 1.32 µg L⁻¹), DZP (< 0.02 µg L⁻¹), and PRG (< 43.48 µg L⁻¹) presented concentrations < LOQ, these three are the pharmaceuticals that showed the greatest resistance to oxidation using the photo-Fenton like process. The results presented in this paper present a rapid degradation of pharmaceutical compounds, which is a result of the synergy effect of the EDDS radicals, H₂O₂, HO[•] and O₂^{•-} [40] (Eqs. (1)–(5)). These radicals have different standard reduction potentials such as HO[•] (+2.8 V), perhydroxyl radical HO₂[•] (+1.7 V) and superoxide radical O₂^{•-} (-2.4 V) [41], which makes the HO[•] has greatest contribution in the oxidation process [42–44],



The final concentrations of dissolved Fe(III)-EDDS were 0.17 mmol L⁻¹ for DW and 0.19 mmol L⁻¹ for SW. The final H₂O₂ concentration was 0.66 mmol L⁻¹ for DW, and 0.15 of H₂O₂ was found for SW, the UV-vis spectra of Fe(III)-EDDS and H₂O₂ behavior during the solar photo Fenton-like process in DW can see in Fig. 3a and 3b, for more information about UV-vis spectra in SW see Fig. S.4.4 of Supporting Information. About 28.41% of the DOC mineralization was achieved in DW (DOC₀ 67.5 mg L⁻¹) after t_{30w} 110.4 min. The DOC DW profile are characterized by an initial fast reaction rate, mainly associated to the fast reduction of Fe(III) to Fe(II), enhanced by the photodecarboxylation of Fe(III):EDDS complex under UV-vis light, followed by a very slow reaction rate after t_{30w} 15.8 min, which is correlated to the low consumption of H₂O₂. However, only 12.72% of mineralization was attained in SW matrix (DOC₀ 170.75 mg L⁻¹) in the final time of photo-Fenton-like treatment (Fig. 3c). These results are similar to the work carried out by Trovó et al [45], where the authors analyzed the degradation of caffeine in different water matrixes through the photo-Fenton process, the results showed lower mineralization rates verified for a high load organic.

The performance of Fenton-like process can be affected by the presence of constituents of SW matrix, such as organic matter, dissolved and suspended solids, alkalinity, as well presence of ions. Suspended solids and color can hinder photochemical reactions by light scattering and absorption and may impair the performance. Carbonate, bicarbonate, and chloride ion, are known to act as radical scavengers, these compounds compete with pharmaceuticals for hydroxyl radicals; therefore their presence increases oxidant demands and lowers the treatment efficiency. Also Cl⁻, Ca²⁺ and Mg²⁺ SO₄²⁻ can compete with Fe(III) for the complexing agents [46,47]. The recalcitrance of some pharmaceuticals such as FLX, PPN, DZP and PRG can be explained due those compounds also contain aromatic moieties contain electron-withdrawing group as trihalides, halides, ketones or amide that leads to this low reactivity with the radicals generated [48], these groups make aromatic substitution reactions slower and more complex.

The results for the solar photo-Fenton process in DW showed a faster initial decay rate and higher degradation capacity in the first minutes of treatment, after which the efficiency decreased. This behavior was investigated using the method described by Chan and Chu [49], who derived a mathematical model (Eq. (6)) to simulate the reaction kinetics:

$$\frac{t}{1 - (C/C_0)} = \rho + \sigma t \Leftrightarrow \frac{d(C/C_0)}{dt} = \frac{-\rho}{(\rho + \sigma t)^2} \quad ((6))$$

where *C* is the concentration of the pharmaceutical remaining in the system after a reaction time *t* (min), *C*₀ is the initial concentration, and the parameters ρ (min) and σ (dimensionless) are two characteristic

constants related to the reaction kinetics and the degradation capacity. Therefore, a higher value for 1/ ρ indicates a faster initial degradation rate of the pharmaceutical. When *t* is high and approaching infinity, the reciprocal of constant σ is the theoretical maximum pharmaceutical removal fraction. In the present case, this was equivalent to the maximum oxidation capacity of the solar photo-Fenton process at the end of the reaction.

For the solar photo-Fenton-like processes performed with the DW and SW matrixes, the coefficients (*r*²) in the range from 0.91 to 1.00 were obtained, indicating that the degradation kinetics of the pharmaceuticals were well described by the model (with the exception of NMD), showing pseudo-first order kinetic behavior (Table 2). These results were in agreement with the findings of Frontistis et al. [50].

3.4. Transformation products

With support of the purpose-built-database for the identification of pharmaceuticals TPs, a total of sixteen TPs were identified in the SW matrix and four in the DW matrix (Table S.5.1, Supporting Information). For DIP, identification was made of six TPs (TP6, *m/z* 192.0655; TP7, *m/z* 250.1185; TP8, *m/z* 136.0757; TP9, *m/z* 205.0971; TP10, *m/z* 165.1022; and TP16, *m/z* 94.0652) and one metabolite (TP2 AAA, *m/z* 262.1183, C₁₃H₁₆N₃O₃). There were three proposed TPs for DZP (TP2, *m/z* 304.0735; TP5, *m/z* 271.0627; and TP6, *m/z* 301.0733), one for FXT (TP5 FXT, *m/z* 260.0893), one for PRG (TP1 PRG, *m/z* 335.2206), and four for PPN (TP1, *m/z* 118.0864; TP3, *m/z* 134.1178; TP25, *m/z* 294.1707; and TP 28, *m/z* 310.1663).

The DIP TP structures identified were indicative of loss of the sulfonic group from DIP, followed by loss of the methylamine group and oxidation of C2 of the pyrazolinone group, resulting in TP9 DIP. The identification of TP6 DIP was also consistent with the TP9 structure, since it should originate from the loss of a methyl group and subsequent formation of an isoxazole ring. The opening of the pyrazolinone ring was indicated by the identification of TP7 DIP. In turn, TP10 DIP could be attributed to loss of the oxamoyl chain from TP7 DIP, or opening of the pyrazolinone ring and loss of the hydroxyl methyl aldehyde chain from TP9 DIP. The formation of TP8 DIP suggested the loss of a methyl group from TP10 DIP, or pyrazolinone ring opening, loss of a molecule of H₂O, and subsequent loss of an ethyl group from TP6 DIP. Finally, aniline (TP16 DIP) could originate from the loss of an amino carbonyl chain from TP7 DIP, TP10 DIP, or TP8 DIP (see Figs. S.5.1 and S.5.2, Supporting Information). The TPs identified were previously reported by Gómez et al. and Pérez Estrada et al. [51,52].

Three DZP TPs were identified: TP2 DZP, TP5 DZP, and TP6 DZP. In the case of TP5 DZP, a 6-member ring was formed, resulting in a quinazolinone moiety. TP6 DZP and TP2 DZP could be produced by opening and oxidation of the benzodiazepinic ring, while TP6 DZP could originate from DZP or TP2 DZP, with addition of an alcoholic group in the N-methyl group (Figs. S.5.3 and S.5.4, Supporting Information). These TPs of the DZP were also reported by Carpinteiro et al and Kosjek et al [53,54].

Santiago-Morales et al. [55] studied the TPs of PPN formed during photocatalytic degradation under simulated solar light. Five PPN TPs were identified in the present study: TP1 PPN, TP3 PPN, TP25 PPN, TP28 PPN, and other three isomers (TP29 PPN, TP30 PPN, and TP31 PPN) that could not be fully elucidated. Unfortunately, it was not possible to observe specific fragments of the suspected TPs (TP29 PPN, TP30 PPN, and TP31 PPN), preventing specific identification of these compounds. The addition of hydroxyl groups to the aromatic nucleus is probably the first step in the PPN degradation pathway (Figs. S.5.5 and S.5.6, Supporting Information). TP25 PPN, TP28 PPN, TP29 PPN, TP30 PPN, and TP31 PPN were the consequence of ring-opening attack of hydroxyl radicals on the naphthol moiety. TP3 PPN could be attributed to cleavage of the ether bond of PPN, with its reduction producing TP1 PPN.

Other TPs identified were TP5 FXT, TP1 PRG, and TP2 AAA (see

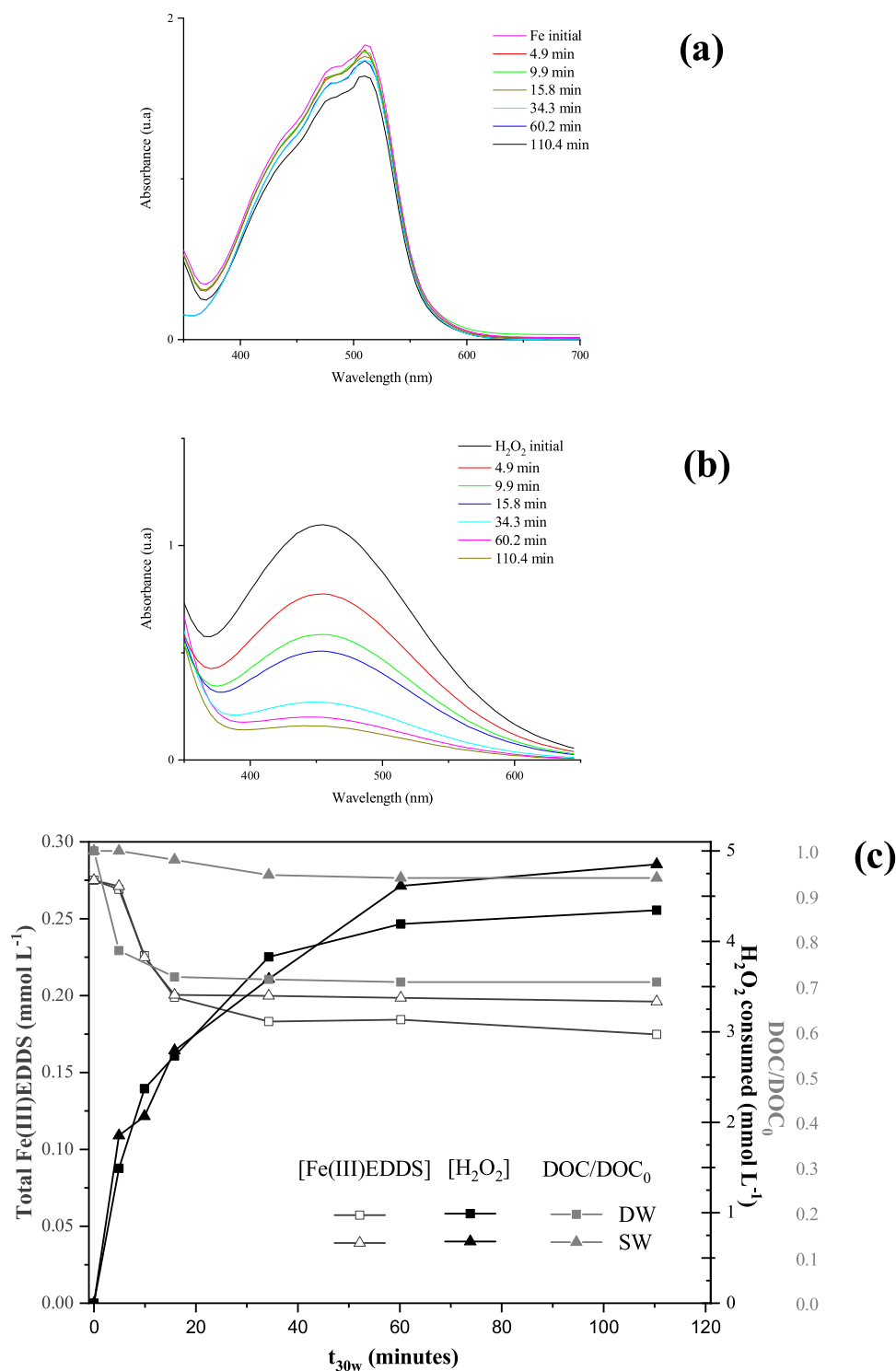


Fig. 3. UV–vis spectrum of total iron in DW (a); UV–vis spectrum of H₂O₂ in DW (b); Total iron in solution, H₂O₂ consumed and DOC in DW and SW matrices employed solar photo-Fenton process (c).

Table S.5.2, Supporting Information). These TPs have previously been identified as intermediate products generated after ozonation of FXT, PRG, and acetamino antipyrine (AAA) [56–58].

Finally, the TPs tentatively identified were evaluated using Toxtree software, the results obtained are shown in Table S.5.2 (Supporting Information). According to the Cramer rules, ten of the TPs could present high toxicity (Class III). These substances showed chemical structures that precluded any strong initial impression of safety, and that could even be suggestive of significant toxicity. TP7 DIP was

classified as Class II, with a structure that was less innocuous, compared to the TPs in Class I, but without structural features suggestive of toxicity (such as those of the TPs in Class III). TP8 DIP, TP10 DIP, TP16 DIP, TP1 PPN, TP25 PPN, and TP28 PPN, classified in Class I, were innocuous substances with simple chemical structures and known metabolic pathways. The most readily biodegradable TPs were TP1 PPN, TP3 PPN, and TP1 PRG.

Most of the TPs identified presented predicted structures with alerts for potential genotoxicity and carcinogenicity, based on a list of

Table 2
Kinetic modeling of pharmaceuticals degradation by solar photo-Fenton-like process.

Pharmaceuticals	DW			SW		
	$\rho^{-1}(\text{min}^{-1})$	σ^{-1}	r^2	$\rho^{-1}(\text{min}^{-1})$	σ^{-1}	r^2
PCT	b	b	b	0.1858	0.9803	0.9133
DIP	b	b	b	b	b	b
FRS	b	b	b	62.5	0.8584	1.0000
PPN	100	1.0000	1.0000	0.7309	1.0152	0.9993
NMD	b	b	b	c	c	0.9820
FXT	45.4545	0.9980	1.0000	0.3014	1.0416	0.9893
DZP	66.6666	0.9980	1.0000	0.1864	1.0263	0.9866
PRG	67.1141	0.9971	1.0000	0.3519	1.0309	0.9972

^b Insufficient data for calculate.

^c pseudo-firts order.

structural alerts (SA) according to electrophilicity theory. The SAs for carcinogenicity are defined as molecular functional groups or sub-structures that are linked to carcinogenic activity of the chemicals, with attack leading to alteration of DNA being the main step in the mechanism of action of many carcinogens (such as the so-called genotoxic carcinogens).

However, the TPs identified in this work were degraded by the solar photo-Fenton-like process with Fe(III)-EDDS at neutral pH. The only TPs that persisted after 110.4 min of treatment were TP1 PPN and TP3 PPN, indicating that the treatment process can be incorporated into a later biological treatment for total degradation of the pharmaceuticals and their TPs. In turn, this study allowed to know some of the TPs that can be generated when working with real hospitals wastewaters, which due to the complexity of the matrix can generate even more toxic and persistent compounds.

4. Conclusions

Electrochemical experiments were performed to evaluate formation and stability of the Fe(III)-EDDS complex, this allowed to identify a broad stability of the complex with variables such as pH and the sunlight incidence. The use of the Doehlert quadratic model with RSM enabled determination of the optimal experimental conditions for degradation of eight pharmaceutical compounds present in distilled water and simulated wastewater matrixes. For both matrixes, the treatment process provided effective degradation of all the compounds, in most cases achieving concentrations < LOD, with total consumption of H₂O₂, FLX, PPN, DZP and PRG presented more recalcitrance, the effect of the matrix was evidenced in the degradation behavior of pharmaceuticals between DW and SW. In both cases showed a faster initial decay rate and higher degradation capacity in the first minutes of treatment, after which the efficiency decreased. Sixteen TPs were identified by LC-QTOF MS, the most of these were hydroxylation products of pharmaceuticals initially present. Using Toxtree software, these TPs were mostly classified as high toxicity persistent chemicals with potential carcinogenicity and mutagenicity. The identification of TPs is very useful because by implementing this process in a real hospital wastewater matrix with greater organic load and complexity, the process could not be completely efficient and it is very important to know the structures and the behavior of the intermediate products.

Acknowledgments

This study was financed in part by the Coordenação de Aperfeiçoamento de Pessoal de Nível Superior - Brasil (CAPES) - Finance Code 001. The authors wish to thank CNPq (Processo: 403051/2016-9). Carla Sirtori thanks the CNPq for her Research grant (Processo: 303474/2015-7). Jacqueline Argüello gratefully acknowledges the financial support from INCTBio (Processo CNPq/INCT 465389/2014-7).

Appendix A. Supplementary data

Supplementary data associated with this article can be found, in the online version, at <https://doi.org/10.1016/j.cattod.2019.01.006>.

References

- [1] J.I. Martínez-Costa, J. Rivera-Utrilla, R. Leyva-Ramos, M. Sánchez-Polo, I. Velo-Gala, A.J. Mota, Individual and simultaneous degradation of the antibiotics sulfamethoxazole and trimethoprim in aqueous solutions by Fenton, Fenton-like and photo-Fenton processes using solar and UV radiations, *J. Photochem. Photobiol. A: Chem.* 360 (2018) 95–108, <https://doi.org/10.1016/j.jphotochem.2018.04.014>.
- [2] S. Foteinis, J.M. Monteagudo, A. Durán, E. Chatzisyseon, Environmental sustainability of the solar photo-Fenton process for wastewater treatment and pharmaceuticals mineralization at semi-industrial scale, *Sci. Total Environ.* 612 (2018) 605–612, <https://doi.org/10.1016/j.scitotenv.2017.08.277>.
- [3] S. Arzate, J.L. García Sánchez, P. Soriano-Molina, J.L. Casas López, M.C. Campos-Mañas, A. Agüera, J.A. Sánchez Pérez, Effect of residence time on micropollutant removal in WWTP secondary effluents by continuous solar photo-Fenton process in raceway pond reactors, *Chem. Eng. J.* 316 (2017) 1114–1121, <https://doi.org/10.1016/j.cej.2017.01.089>.
- [4] D. Kanakaraju, B.D. Glass, M. Oelgemöller, Advanced oxidation process-mediated removal of pharmaceuticals from water: a review, *J. Environ. Manage.* 219 (2018) 189–207, <https://doi.org/10.1016/j.jenvman.2018.04.103>.
- [5] W. Huang, M. Brigante, F. Wu, K. Hanna, G. Mailhot, Development of a new homogenous photo-Fenton process using Fe(III)-EDDS complexes, *J. Photochem. Photobiol. A: Chem.* 239 (2012) 17–23, <https://doi.org/10.1016/j.jphotochem.2012.04.018>.
- [6] W. Huang, M. Brigante, F. Wu, C. Mousty, K. Hanna, G. Mailhot, Assessment of the Fe(III)-EDDS complex in fenton-like processes: from the radical formation to the degradation of bisphenol A, *Environ. Sci. Technol.* 47 (2013) 1952–1959, <https://doi.org/10.1021/es304502y>.
- [7] J. Li, G. Mailhot, F. Wu, N. Deng, Photochemical efficiency of Fe(III)-EDDS complex: OH radical production and 17 β -estradiol degradation, *J. Photochem. Photobiol. A: Chem.* 212 (2010) 1–7, <https://doi.org/10.1016/j.jphotochem.2010.03.001>.
- [8] T. Zhou, K. Feng, W. Xiang, Y. Lv, X. Wu, J. Mao, C. He, Rapid decomposition of diclofenac in a magnetic field enhanced zero-valent iron/EDTA Fenton-like system, *Chemosphere* 193 (2018) 968–977, <https://doi.org/10.1016/j.chemosphere.2017.11.090>.
- [9] A.V. Vorontsov, Advancing Fenton and photo-Fenton water treatment through the catalyst design, *J. Hazard. Mater.* (2018) 1–10, <https://doi.org/10.1016/j.jhazmat.2018.04.033>.
- [10] Z. Yuan, J.M. VanBriesen, The formation of intermediates in EDTA and NTA biodegradation, *Environ. Eng. Sci.* 23 (2006) 533–544, <https://doi.org/10.1089/ees.2006.23.533>.
- [11] M. Orama, H. Hyvonen, H. Saarinen, R. Aksela, Complexation of [S,S] and mixed stereoisomers of N,N-ethylenediaminedisuccinic acid (EDDS) with Fe(III), Cu(II), Zn (II) and Mn(II) ions in aqueous solution, *J. Chem. Soc.* (2002) 4644–4648, <https://doi.org/10.1039/B207777A>.
- [12] C.K. Schmidt, M. Fleig, F. Sacher, H.-J. Brauch, Occurrence of aminopolycarboxylates in the aquatic environment of Germany, *Environ. Pollut.* 131 (2004) 107–124, <https://doi.org/10.1016/j.envpol.2004.01.013>.
- [13] M. Kowalczyk, Z. Hubicki, D. Kołodzyńska, Removal of heavy metal ions in the presence of the biodegradable complexing agent of EDDS from waters, *Chem. Eng. J.* 221 (2013) 512–521, <https://doi.org/10.1016/j.cej.2013.02.010>.
- [14] A. Rastogi, S.R. Al-Abed, D.D. Dionysiou, Effect of inorganic, synthetic and naturally occurring chelating agents on Fe(II) mediated advanced oxidation of chlorophenols, *Water Res.* 43 (2009) 684–694, <https://doi.org/10.1016/j.watres.2008.10.045>.
- [15] N. Klammerth, S. Malato, A. Agüera, A. Fernández-Alba, G. Mailhot, Treatment of municipal wastewater treatment plant effluents with modified photo-Fenton As a tertiary treatment for the degradation of Micro pollutants and disinfection, *Environ.*

- Sci. Technol. 46 (2012) 2885–2892, <https://doi.org/10.1021/es204112d>.
- [16] P. Soriano-Molina, J.L. García Sánchez, O.M. Alfano, L.O. Conte, S. Malato, J.A. Sánchez Pérez, Mechanistic modeling of solar photo-Fenton process with Fe³⁺-EDDS at neutral pH, Appl. Catal. B Environ. 233 (2018) 234–242, <https://doi.org/10.1016/j.apcatb.2018.04.005>.
- [17] Y. Zhang, N. Klammerth, P. Chelme-Ayala, M. Gamal El-Din, Comparison of nitrotri-acetic acid and [S,S]-Ethylenediamine-N,N'-disuccinic acid in UV-Fenton for the treatment of oil sands process-affected water at natural pH, Environ. Sci. Technol. 50 (2016) 10535–10544, <https://doi.org/10.1021/acs.est.6b03050>.
- [18] S. Papoutsakis, F.F. Brites-gaNóbre, C. Pulgarin, S. Malato, Benefits and limitations of using Fe(III)-EDDS for the treatment of highly contaminated water at near-neutral pH, J. Photochem. Photobiol. A: Chem. 303–304 (2015) 1–7, <https://doi.org/10.1016/j.jphotochem.2015.01.013>.
- [19] A. Fischbacher, C. von Sonntag, T.C. Schmidt, Hydroxyl radical yields in the Fenton process under various pH, ligand concentrations and hydrogen peroxide/Fe(II) ratios, Chemosphere. 182 (2017) 738–744, <https://doi.org/10.1016/J.CHEMOSPHERE.2017.05.039>.
- [20] A. Babuponnusami, K. Muthukumar, A review on Fenton and improvements to the Fenton process for wastewater treatment, J. Environ. Chem. Eng. 2 (2014) 557–572, <https://doi.org/10.1016/j.jece.2013.10.011>.
- [21] H. Ebrahimi, R. Leardi, M. Jalali-Heravi, Experimental design in analytical chemistry-part I: theory, J. AOAC Int. 97 (2014) 3–11.
- [22] H. Ebrahimi, R. Leardi, M. Jalali-Heravi, Experimental design in analytical chemistry-part II: applications, J. AOAC Int. 97 (2014) 12–18.
- [23] O. Gomes Júnior, V.M. Silva, A.E.H. Machado, C. Sirtori, C.R. Lemos, A.M. Freitas, A.G. Trovó, Correlation between pH and molar iron/ligand ratio during ciprofloxacin degradation by photo-Fenton process: identification of the main transformation products, J. Environ. Manage. 213 (2018) 20–26, <https://doi.org/10.1016/J.JENVMAN.2018.02.041>.
- [24] A. Gupta, A. Garg, Degradation of ciprofloxacin using Fenton's oxidation: effect of operating parameters, identification of oxidized by-products and toxicity assessment, Chemosphere. 193 (2018) 1181–1188, <https://doi.org/10.1016/J.CHEMOSPHERE.2017.11.046>.
- [25] P. Soriano-Molina, J.L. García Sánchez, S. Malato, L.A. Pérez-Estrada, J.A. Sánchez Pérez, Effect of volumetric rate of photon absorption on the kinetics of micro-pollutant removal by solar photo-Fenton with Fe³⁺-EDDS at neutral pH, Chem. Eng. J. 331 (2018) 84–92, <https://doi.org/10.1016/J.CEJ.2017.08.096>.
- [26] OECD, Guidelines for Testing of Chemicals, Simulation Test-Aerobic Sewage Treatment 303^a, (1999).
- [27] S. Malato, P. Fernández-Ibáñez, M.I. Maldonado, J. Blanco, W. Gernjak, Decontamination and disinfection of water by solar photocatalysis: recent overview and trends, Catal. Today 147 (2009) 1–59, <https://doi.org/10.1016/J.CATTOD.2009.06.018>.
- [28] I.S.O. 6332, Water Quality - Determination of Iron - Spectrometric Method Using 1,10-phenanthroline, (1988).
- [29] R. Nogueira, M. Oliveira, W. Paterlini, Simple and fast spectrophotometric determination of H₂O₂ in photo-Fenton reactions using metavanadate, Talanta. 66 (2005) 86–91, <https://doi.org/10.1016/j.talanta.2004.10.001>.
- [30] E. Cuervo Lumbaque, R.M. Cardoso, A. Dallegrave, L.O. dos Santos, M. Ibáñez, F. Hernández, C. Sirtori, Pharmaceutical removal from different water matrices by Fenton process at near-neutral pH: doehlert design and transformation products identification by UHPLC-QTOF MS using a purpose-built database, J. Environ. Chem. Eng. 6 (2018) 3951–3961, <https://doi.org/10.1016/J.JECE.2018.05.051>.
- [31] G.M. Cramer, R.A. Ford, R.L. Hall, Estimation of toxic hazard—a decision tree approach, Food Cosmet. Toxicol. 16 (1976) 255–276, [https://doi.org/10.1016/S0015-6264\(76\)80522-6](https://doi.org/10.1016/S0015-6264(76)80522-6).
- [32] H.J.M. Verhaar, C.J. van Leeuwen, J.L.M. Hermens, Classifying environmental pollutants, Chemosphere. 25 (1992) 471–491, [https://doi.org/10.1016/0045-6535\(92\)90280-5](https://doi.org/10.1016/0045-6535(92)90280-5).
- [33] EPA, Guidance Manual for the Categorization of Organic and Inorganic Substances on Canada's Domestic Substances List, Existing Substances, Canada, (2003).
- [34] R. Benigni, C. Bossa, N. Jeliakova, T. Netzeva, A. Worth, The Benigni/Bossa Rulebase for Mutagenicity and carcinogenicity-a Module of Toxtree, (2008).
- [35] Y. Wu, M. Brigante, W. Dong, P. de Sainte-Claire, G. Mailhot, Toward a better understanding of Fe(III)-EDDS photochemistry: theoretical stability calculation and experimental investigation of 4-tert-Butylphenol degradation, J. Phys. Chem. A 118 (2014) 396–403, <https://doi.org/10.1021/jp409043e>.
- [36] P. García-Muñoz, G. Pliego, J.A. Zazo, M. Muñoz, Z.M. de Pedro, A. Bahamonde, J.A. Casas, Treatment of hospital wastewater through the CWPO-Photoassisted process catalyzed by ilmenite, J. Environ. Chem. Eng. 5 (2017) 4337–4343, <https://doi.org/10.1016/J.JECE.2017.08.023>.
- [37] R.F. Teófilo, M.M.C. Ferreira, Quimiometria II: planilhas eletrônicas para cálculos de planejamentos experimentais, um tutorial, Quim. Nova 29 (2006) 338–350, <https://doi.org/10.1590/S0100-40422006000200026>.
- [38] V.A.B. Paiva, C.E.S. Paniagua, I.A. Ricardo, B.R. Gonçalves, S.P. Martins, D. Daniel, A.E.H. Machado, A.G. Trovó, Simultaneous degradation of pharmaceuticals by classic and modified photo-Fenton process, J. Environ. Chem. Eng. 6 (2018) 1086–1092, <https://doi.org/10.1016/J.JECE.2018.01.013>.
- [39] N. Klammerth, S. Malato, A. Agüera, A. Fernández-Alba, Photo-Fenton and modified photo-Fenton at neutral pH for the treatment of emerging contaminants in wastewater treatment plant effluents: a comparison, Water Res. 47 (2013) 833–840, <https://doi.org/10.1016/j.watres.2012.11.008>.
- [40] S. Miralles-Cuevas, I. Oller, A. Ruíz-Delgado, A. Cabrera-Reina, L. Cornejo-Ponce, S. Malato, EDDS as complexing agent for enhancing solar advanced oxidation processes in natural water: effect of iron species and different oxidants, J. Hazard. Mater. (2018) 1–8, <https://doi.org/10.1016/J.JHAZMAT.2018.03.018>.
- [41] S.G. Huling, B.E. Pivetz, In-situ Chemical Oxidation (No. EPA/600/R-06/072), Washington, DC, (2006).
- [42] S. Giannakis, M. López, D. Spuhler, J.A.S. Pérez, P.F. Ibáñez, C. Pulgarin, Solar disinfection is an augmentable, in situ-generated photo-Fenton reaction-Part 2: a review of the applications for drinking water and wastewater disinfection, Appl. Catal. B Environ. (2016), <https://doi.org/10.1016/j.apcatb.2016.06.007>.
- [43] A. Mirzaei, Z. Chen, F. Haghghat, L. Yerushalmi, Removal of pharmaceuticals from water by homo/heterogenous Fenton-type processes – a review, Chemosphere. 174 (2017) 665–688, <https://doi.org/10.1016/j.chemosphere.2017.02.019>.
- [44] G. Boczkaj, A. Fernandes, Wastewater treatment by means of advanced oxidation processes at basic pH conditions: a review, Chem. Eng. J. 320 (2017) 608–633, <https://doi.org/10.1016/j.cej.2017.03.084>.
- [45] A.G. Trovó, T.F.S. Silva, O. Gomes, A.E.H. Machado, W.B. Neto, P.S. Muller, D. Daniel, Degradation of caffeine by photo-Fenton process: optimization of treatment conditions using experimental design, Chemosphere. 90 (2013) 170–175, <https://doi.org/10.1016/J.CHEMOSPHERE.2012.06.022>.
- [46] S. Miralles-Cuevas, I. Oller, J.A.S. Pérez, S. Malato, Removal of pharmaceuticals from MWTP effluent by nanofiltration and solar photo-Fenton using two different iron complexes at neutral pH, Water Res. 64 (2014) 23–31, <https://doi.org/10.1016/j.watres.2014.06.032>.
- [47] A.Y.-C. Lin, X.-H. Wang, C.-F. Lin, Impact of wastewaters and hospital effluents on the occurrence of controlled substances in surface waters, Chemosphere. 81 (2010) 562–570, <https://doi.org/10.1016/J.CHEMOSPHERE.2010.08.051>.
- [48] R. Broséus, S. Vincent, K. Abouffadl, A. Daneshvar, S. Sauvé, B. Barbeau, M. Prévost, Ozone oxidation of pharmaceuticals, endocrine disruptors and pesticides during drinking water treatment, Water Res. 43 (2009) 4707–4717, <https://doi.org/10.1016/J.WATRES.2009.07.031>.
- [49] K.H. Chan, W. Chu, Modeling the reaction kinetics of Fenton's process on the removal of atrazine, Chemosphere. 51 (2003) 305–311.
- [50] Z. Frontistis, N.P. Xekoukoulotakis, E. Hapeshi, D. Venieri, D. Fatta-Kassinos, D. Mantzavinos, Fast degradation of estrogen hormones in environmental matrices by photo-Fenton oxidation under simulated solar radiation, Chem. Eng. J. 178 (2011) 175–182, <https://doi.org/10.1016/J.CEJ.2011.10.041>.
- [51] M.J. Gómez, C. Sirtori, M. Mezcuca, A.R. Fernández-Alba, A. Agüera, Photodegradation study of three dipyrone metabolites in various water systems: identification and toxicity of their photodegradation products, Water Res. 42 (2008) 2698–2706, <https://doi.org/10.1016/j.watres.2008.01.022>.
- [52] L.A. Pérez-Estrada, S. Malato, A. Agüera, A.R. Fernández-Alba, Degradation of dipyrone and its main intermediates by solar AOPs, Catal. Today 129 (2007) 207–214, <https://doi.org/10.1016/j.cattod.2007.08.008>.
- [53] I. Carpinteiro, R. Rodil, J.B. Quintana, R. Cela, Reaction of diazepam and related benzodiazepines with chlorine. Kinetics, transformation products and in-silico toxicological assessment, Water Res. 120 (2017) 280–289, <https://doi.org/10.1016/J.WATRES.2017.04.063>.
- [54] T. Kosjek, S. Perko, M. Zupanc, M. Zanoski, T. Landeka, D. Zigon, B. Kompare, E. Heath, Environmental occurrence, fate and transformation of benzodiazepines in water treatment, Water Res. 46 (2012) 355–368.
- [55] J. Santiago-Morales, A. Agüera, Mdel M. Gómez, A.R. Fernández-Alba, J. Giménez, S. Esplugas, R. Rosal, Transformation products and reaction kinetics in simulated solar light photocatalytic degradation of propranolol using Ce-doped TiO₂, Appl. Catal. B Environ. 129 (2013) 13–29, <https://doi.org/10.1016/j.apcatb.2012.09.023>.
- [56] Y. Zhao, G. Yu, S. Chen, S. Zhang, B. Wang, J. Huang, S. Deng, Y. Wang, Ozonation of antidepressant fluoxetine and its metabolite product norfluoxetine: kinetics, intermediates and toxicity, Chem. Eng. J. 316 (2017) 951–963, <https://doi.org/10.1016/j.cej.2017.02.032>.
- [57] E. Barron, M. Deborde, S. Rabouan, P. Mazellier, B. Legube, Kinetic and mechanistic investigations of progesterone reaction with ozone, Water Res. 40 (2006) 2181–2189, <https://doi.org/10.1016/j.watres.2006.03.034>.
- [58] M. Favier, R. Dewil, K. Van Eyck, A. Van Schepdael, D. Cabooter, High-resolution MS and MSn investigation of ozone oxidation products from phenazone-type pharmaceuticals and metabolites, Chemosphere 136 (2015) 32–41, <https://doi.org/10.1016/J.CHEMOSPHERE.2015.04.010>.

SUPPORTING INFORMATION

Solar photo-Fenton-like process at neutral pH: Fe(III)-EDDS complex formation and optimization of experimental conditions for degradation of pharmaceuticals

*Elisabeth Cuervo Lumbaque^a, Débora Salmoria Araujo^a, Thágor Moreira Klein^a,
Elaine R. Lopes Tiburtius^b, Jacqueline Argüello^{a*}, Carla Sirtori^{a*}*

^aInstituto de Química- Universidade Federal do Rio Grande do Sul, Av. Bento Gonçalves, 9500, Porto Alegre-RS, Brazil.

^bUniversidade Estadual de Ponta Grossa, Av. General Carlos Cavalcanti, 4748, Ponta Grossa- PR, Brazil.

* To whom all correspondence should be addressed

e-mails: jacqueline.arguello@ufrgs.br (Prof. Jacqueline Argüello) and
carla.sirtori@ufrgs.br (Prof. Carla Sirtori)

S.1 LC-QTOF MS analysis

The LC was equipped with a reverse-phase Luna[®]Omega C18 analytical column (2.1 mm × 50 mm × 1.6 μm). When ionization in positive mode was selected, the mobile phase was a mixture of MeOH acidified with 0.1% formic acid (A) and H₂O acidified with 0.1% formic acid (B) at a flow rate of 0.28 mL/min. In this case, the gradient progressed from 10% A (initial conditions) to 90% A in 10 min, and then maintained for 2 min. The QTOF mass spectrometer was operated in positive ionization mode under the following conditions: capillary 4000 V, nebulizer 40 psi, drying gas 9 L/min, gas temperature 200 °C. In all analyses, the injection volume was 10 μL. The samples injected were previously filtered through a 0.22 μm PVDF filter. The QTOF MS system was operated in broadband collision-induced dissociation (bbCID) acquisition mode that provided MS and MS/MS spectra at the same time. All MS information was recorded over the *m/z* range of 50–1000 with a scan rate of 2 Hz. The bbCID mode allowed for work with two different collision energies: one with a Low Collision Energy (LE) of 10 eV, and a second that applies a High Collision Energy (HE) of 70 eV to obtain MS/MS spectra. Target Analysis and Data Analysis 4.2 software's were employed for analyzes and, in most cases, for ions with a deviation of ±5 ppm of error were assigned possible elemental compositions and double-bond equivalent (RDB).

Limit of detection (LOD) and limit of quantification (LOQ) for each pharmaceutical studied, in both water matrixes, were determined for the quantification method developed in this work (see Table S.2.1).

Table S.1.1. Parameters for quantification method used to determine pharmaceuticals in different matrixes studied.

Pharmaceuticals	DW		SW	
	LOD ($\mu\text{g L}^{-1}$)	LOQ ($\mu\text{g L}^{-1}$)	LOD ($\mu\text{g L}^{-1}$)	LOQ ($\mu\text{g L}^{-1}$)
Nimesulide (NMD)	0.24	0.82	0.42	1.39
Furosemide (FRS)	0.78	2.61	1.36	4.55
Paracetamol (PCT)	0.20	0.68	0.58	1.92
Propranolol (PPN)	0.01	0.03	0.39	1.32
Dipyron (DIP)	0.31	1.03	1.20	4.01
Fluoxetine (FXT)	0.31	1.04	5.17	17.24
Progesterone (PRG)	0.02	0.08	13.04	43.48
Diazepam (DZP)	0.01	0.03	0.01	0.02

S.2 Characterization Fe(III)-EDDS complex

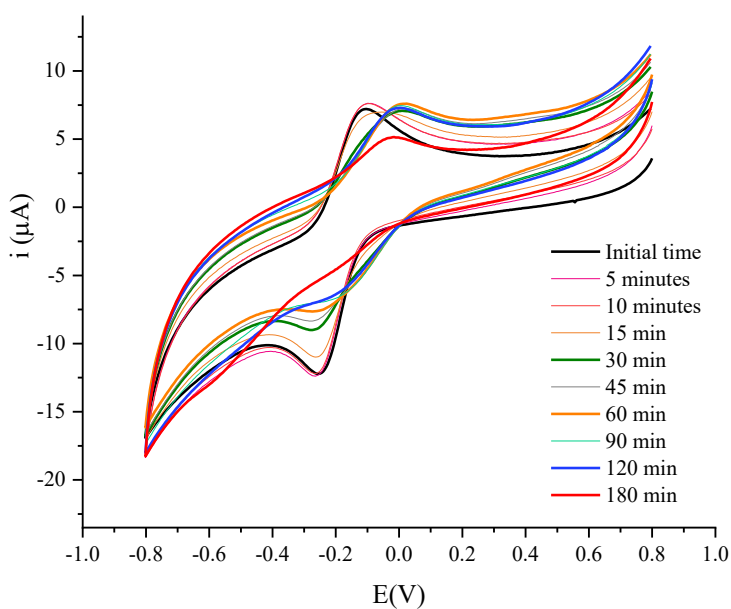


Figure S.2.1 Cyclic voltammograms of Fe(III)-EDDS (1:2) at pH 5.0 under solar-light irradiation ($\text{KCl } 0.05 \text{ mol L}^{-1}$, $\text{Fe(III) } 0.5 \text{ mmol L}^{-1}$ and $v = 50 \text{ mVs}^{-1}$).

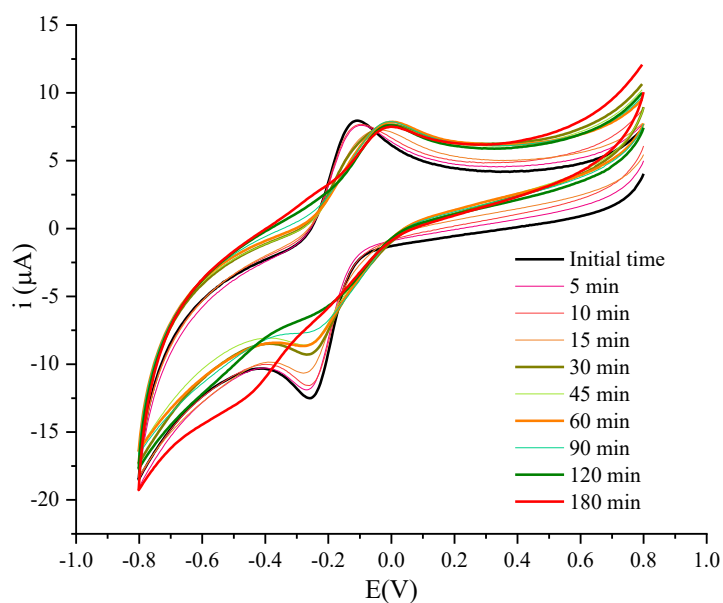


Figure S.2.2 Cyclic voltammograms of Fe(III)-EDDS (1:2) at pH 7.0 under solar-light irradiation (KCl 0.05 mol L⁻¹, Fe(III) 0.5 mmol L⁻¹ and $v= 50\text{mVs}^{-1}$).

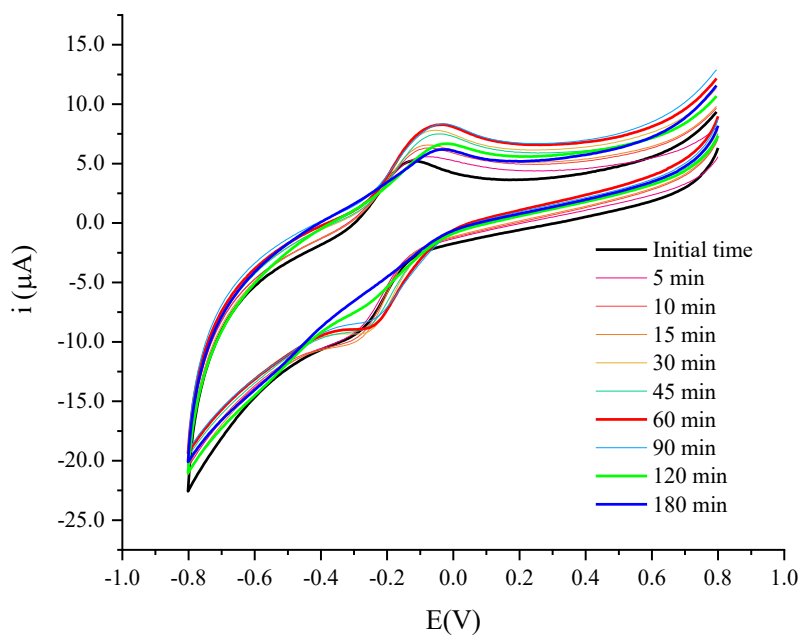


Figure S.2.3 Cyclic voltammograms of Fe(III)-EDDS (1:2) at pH 9.0 under solar-light irradiation (KCl 0.05 mol L⁻¹, Fe(III) 0.5 mmol L⁻¹ and $v= 50\text{mVs}^{-1}$).

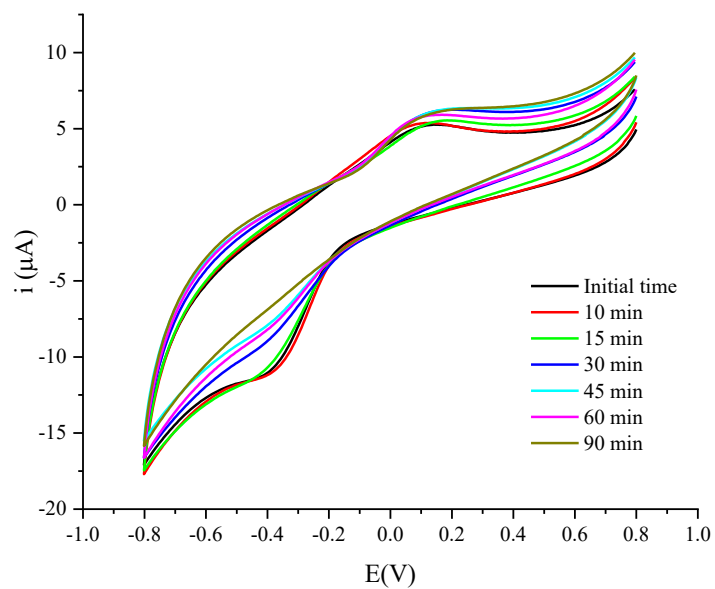


Figure S.2.4 Cyclic voltammograms of Fe(III)-EDDS (1:2) in SW matrix at pH 7.0 under solar-light irradiation (KCl 0.05 mol L^{-1} , Fe(III) 0.5 mmol L^{-1} and $v= 50\text{mVs}^{-1}$).

S.3 Optimization of experimental conditions: Doehlert Design

Table S.3.1 Selected ANOVA parameters for DW and SW matrixes.

ANOVA parameters		
Matrixes	DW	SW
Parameter number (p)	6	
Experiments number (n)	9	
Level number (m)	7	
Significance (α)	0.051	

Table S.3.2 Analysis of variance for quadratic model in photo-Fenton process for DW and SW matrixes.

Analysis of Variance - Quadratic Model										
VS Matrixes	QS		DF		QM		F test.		P	
	DW	SW	DW	SW	DW	SW	DW	SW	DW	SW
Regression	2413.2	2112.7	5		482.64	422.54	374.83 ^b	11.734 ^b	2E-04	0.035
Residuals	3.8629	108.03	3		1.2876	36.011				
Lack off it	3.2856	58.719	1		3.2856	58.719	11.383	2.3814	0.078	0.263
Pure error	0.5773	49.314	2		0.2886	24.657				
Total	2417	2112.7	8							
<i>% variance explained</i>							99.84	95.14		
<i>% maximum variance explainable</i>							99.98	97.78		

^b Significant values

VS: variance source, QS: quadratic sums, DF: degrees of freedom, QA: quadratic mean, F test: calculated value of measured test F, p: statistical parameter p.

Table S.3.3 Coefficients for DW and SW matrixes.

Coefficients		
	DW	SW
x₀	98.10	76.51
x₁	17.06	13.42
x₂	13.77	16.84
x₁²	-16.46	-18.43
x₂²	-15.19	-17.91
x₁x₂	-25.03	8.98

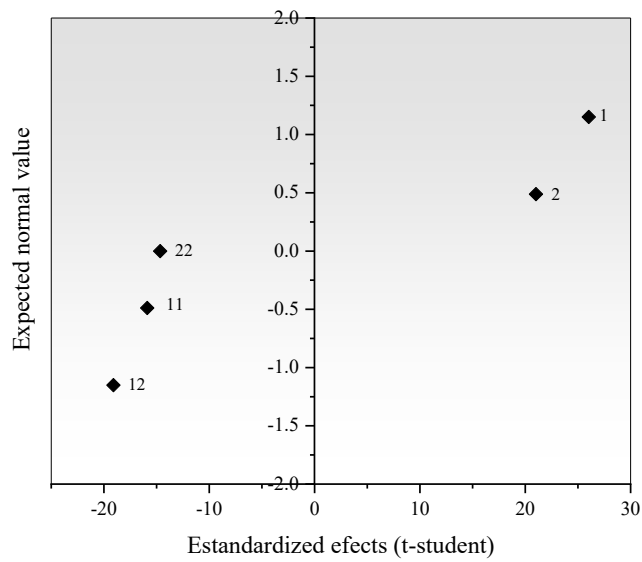


Figure S.3.1 Normal probability graph of Doehlert design in DW matrix optimization.

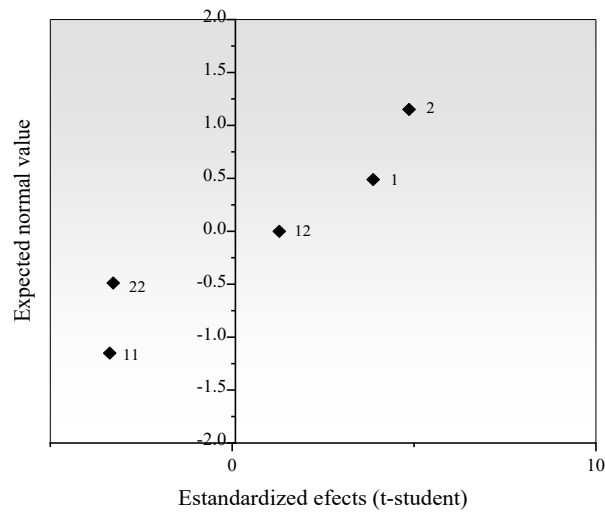
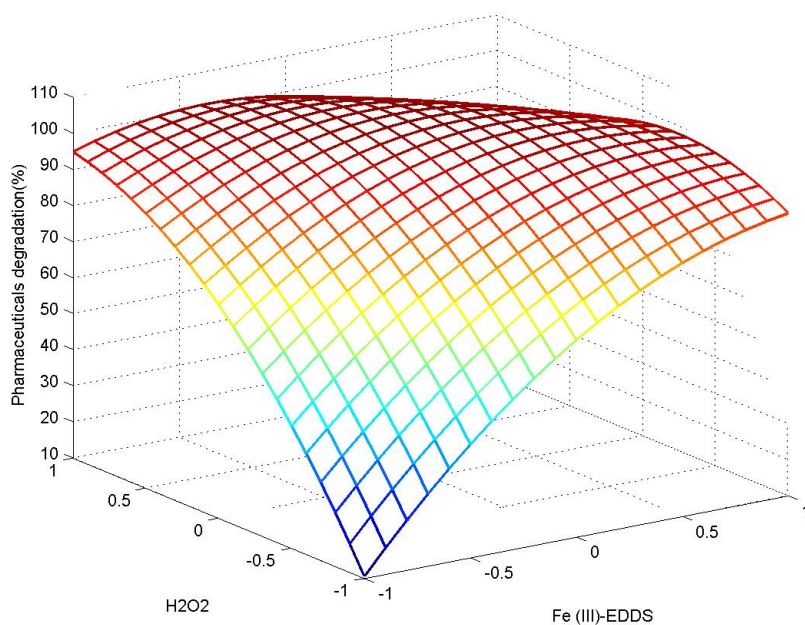


Figure S.3.2 Normal probability graph of Doehlert design in SW matrix optimization.



$$Y = 98.1 + 17.06*(x_1) + 13.77*(x_2) - 25.03*(x_1*x_2) - 16.46*(x_1^2) - 15.19*(x_2^2) \quad \text{(Equation I)}$$

Figure S.3.3. Response surface for Doehlert design in DW matrix.

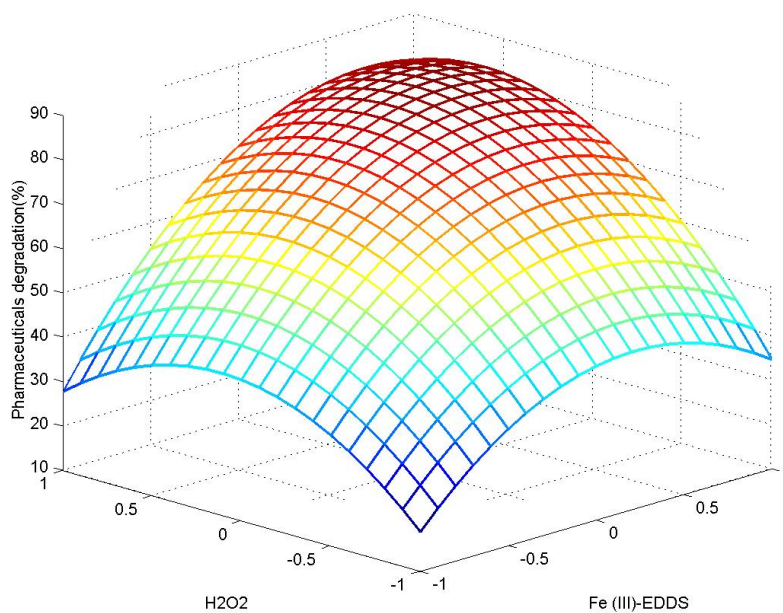


Figure S.3.4. Response surface for Doehlert design in SW matrix.

$$Y = 76.51 + 13.42*(x_1) + 16.84*(x_2) + 8.978*(x_1*x_2) - 18.43*(x_1^2) - 17.91*(x_2^2) \quad \text{(Equation 2)}$$

S.4 Degradation of pharmaceutical compounds: blank experiments

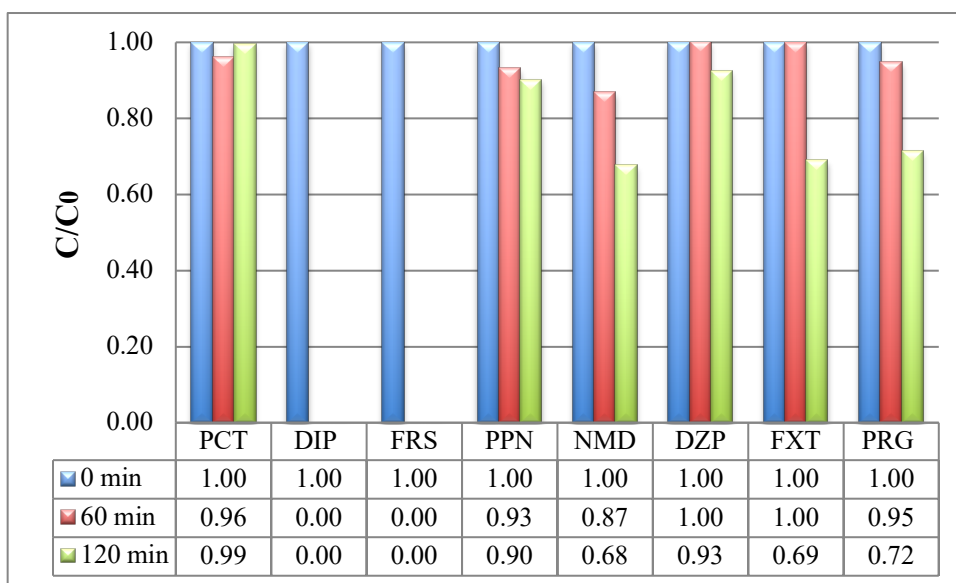


Figure S.4.1 Degradation of pharmaceutical compounds with direct photolysis at neutral pH.

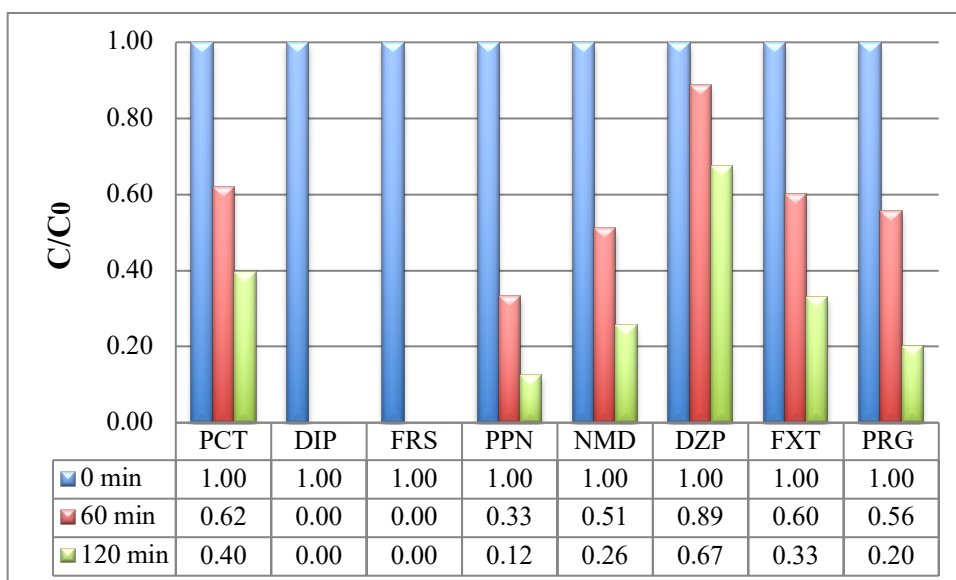


Figure S.4.2 Degradation of pharmaceutical compounds with direct photolysis with H_2O_2 (5 mmol L^{-1}) at neutral pH.

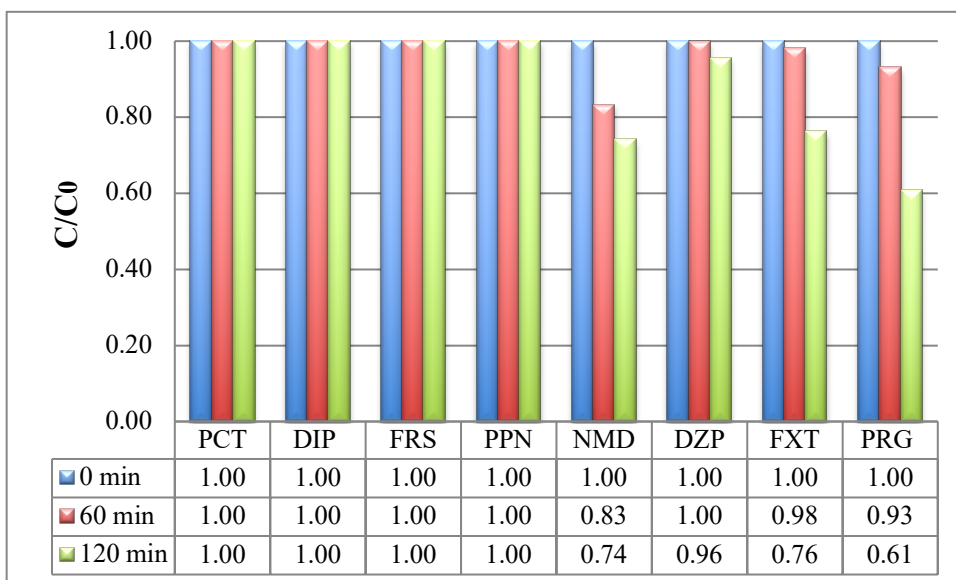


Figure S.4.3 Degradation of pharmaceutical compounds with H_2O_2 (5 mmol L^{-1}) in dark (without sunlight) at neutral pH.

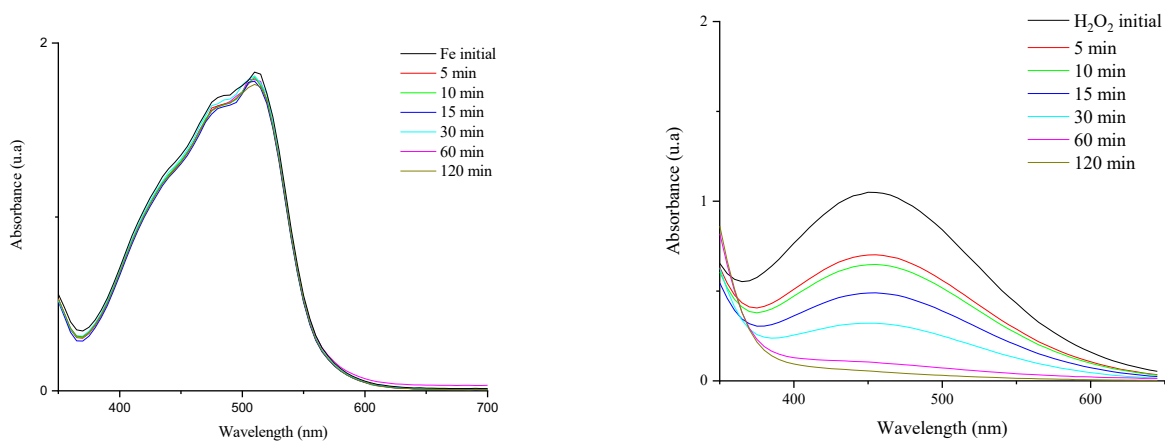


Figure S.4.4 UV-vis spectrum of total iron in SW (a); UV-vis spectrum of H_2O_2 in SW (b).

S.5 Transformation products

Table S.5.1. TPs identified through solar photo-Fenton process at pH 7.0 in DW and SW matrixes.

Compound	Ion Formula [M+H]	Ion mass (m/z)		Error [ppm]	RDB	Presence in matrix	
		Experimental	Calculated			DW	SW
TP2 AAA	C₁₃H₁₆N₃O₃	262.1183	262.1186	1.1	7.5		X
	C ₁₀ H ₁₁ N ₂ O ₂	191.0812	191.0815	1.7	6.5		
TP6 DIP	C₁₀H₁₀NO₃	192.0655	192.0655	0.1	6.5		X
	C ₁₀ H ₁₅ N ₂ O ₂	195.1123	195.1128	2.4	4.5		
	C ₈ H ₁₀ NO	136.0756	136.0757	0.9	4.5		
	C ₈ H ₇ O	119.0492	119.0491	-0.2	5.5		
	C ₆ H ₈ N	94.0652	94.0651	-0.4	3.5		
TP 7 DIP	C₁₂H₁₆N₃O₃	250.1185	250.1186	0.6	6.5		X
	C ₁₀ H ₁₄ N ₃ O ₂	208.1077	208.1081	1.7	5.5		
	C ₉ H ₁₃ N ₂ O	165.1022	165.1022	-0.0	4.5		
	C ₇ H ₁₁ N ₂	123.0914	123.0917	2.2	3.5		
TP8 DIP	C₈H₁₀NO	136.0757	136.0757	-0.3	4.5		X
	C ₈ H ₇ O	119.0492	119.0491	-0.2	5.5		
	C ₆ H ₈ N	94.0652	94.0651	-0.4	3.5		
TP 9 DIP	C₁₁H₁₃N₂O₂	205.0971	205.0972	0.2	6.5	X	X
	C ₃ H ₆ N	56.0493	56.0495	2.3	1.5		
TP 10 DIP	C₉H₁₃N₂O	165.1022	165.1022	0.3	4.5	X	X
	C ₇ H ₁₁ N ₂	123.0914	123.0917	2.2	3.5		
TP 16 DIP	C₆H₈N	94.0652	94.0651	-0.8	3.5		X
	C ₇ H ₇	91.0542	91.0542	0.2	4.5		
TP2 DZP	C₁₆H₁₅ClNO₃	304.0735	304.0735	-0.1	9.5		X
	C ₁₅ H ₁₄ ClN ₂ O	273.0779	273.0789	3.7	9.5		
TP5 DZP	C₁₅H₁₂ClN₂O	271.0627	271.0633	1.9	10.5		X
	C ₅ H ₁₂ NO	102.0912	102.0913	1.1	0.5		
TP6 DZP	C₁₆H₁₄ClN₂O₂	301.0733	301.0738	1.7	10.5		X
	C ₁₄ H ₁₁ ClNO	244.0516	244.0524	3.2	9.5		
TP5 FXT	C₁₂H₁₃F₃NO₂	260.0893	260.0893	-0.1	5.5		X
	C ₁₀ H ₉	129.0696	129.0699	2.0	6.5		
TP1 PRG	C₂₀H₃₁O₄	335.2206	335.2217	3.2	5.5	X	X
	C ₂₀ H ₂₉ O ₃	317.2114	317.2111	-0.8	6.5		
	C ₂₀ H ₂₇ O ₂	299.2002	299.2006	1.2	7.5		
TP1 PPN	C₅H₁₂NO₂	118.0864	118.0863	-1.0	0.5	X	X
	C ₂ H ₆ NO ₂	76.0391	76.0393	2.7	0.5		
	C ₄ H ₁₀ N	72.0808	72.0808	0.2	0.5		
TP3 PPN	C₆H₁₆NO₂	134.1178	134.1176	-2.0	-0.5		X
	C ₂ H ₄ NO ₂	74.0236	74.0237	0.3	1.5		
	C ₄ H ₁₀ N	72.0808	72.0808	-0.5	0.5		
	C ₃ H ₆ N	56.0494	56.0495	0.9	1.5		

TP 25 PPN	$C_{16}H_{24}NO_4$	294.1707	294.1700	-2.5	5.5	X
	C_3H_8NO	74.0601	74.0600	-1.0	0.5	
TP 28 PPN	$C_{16}H_{24}NO_5$	310.1648	310.1649	0.2	5.5	X
	$C_{16}H_{22}NO_4$	292.1547	292.1543	-1.4	6.5	
	$C_{16}H_{20}NO_3$	274.1411	274.1438	9.6	7.5	
TP 29 PPN	$C_{16}H_{24}NO_5$	310.1663	310.1649	-4.5	5.5	X
	$C_{16}H_{22}NO_4$	292.1548	292.1543	-1.6	6.5	
	$C_5H_{10}NO_2$	116.0706	116.0706	-0.2	1.5	
	$C_4H_{10}N$	72.0806	72.0808	2.2	0.5	
TP 30 PPN	$C_{16}H_{24}NO_5$	310.1645	310.1649	1.2	5.5	X
	$C_{16}H_{22}NO_4$	292.1547	292.1543	-1.2	6.5	
TP 31 PPN	$C_{16}H_{24}NO_5$	310.1646	310.1649	0.8	5.5	X
	$C_{16}H_{22}NO_4$	292.1549	292.1543	-2.0	6.5	
	$C_{16}H_{20}NO_3$	274.1434	274.1438	1.4	7.5	

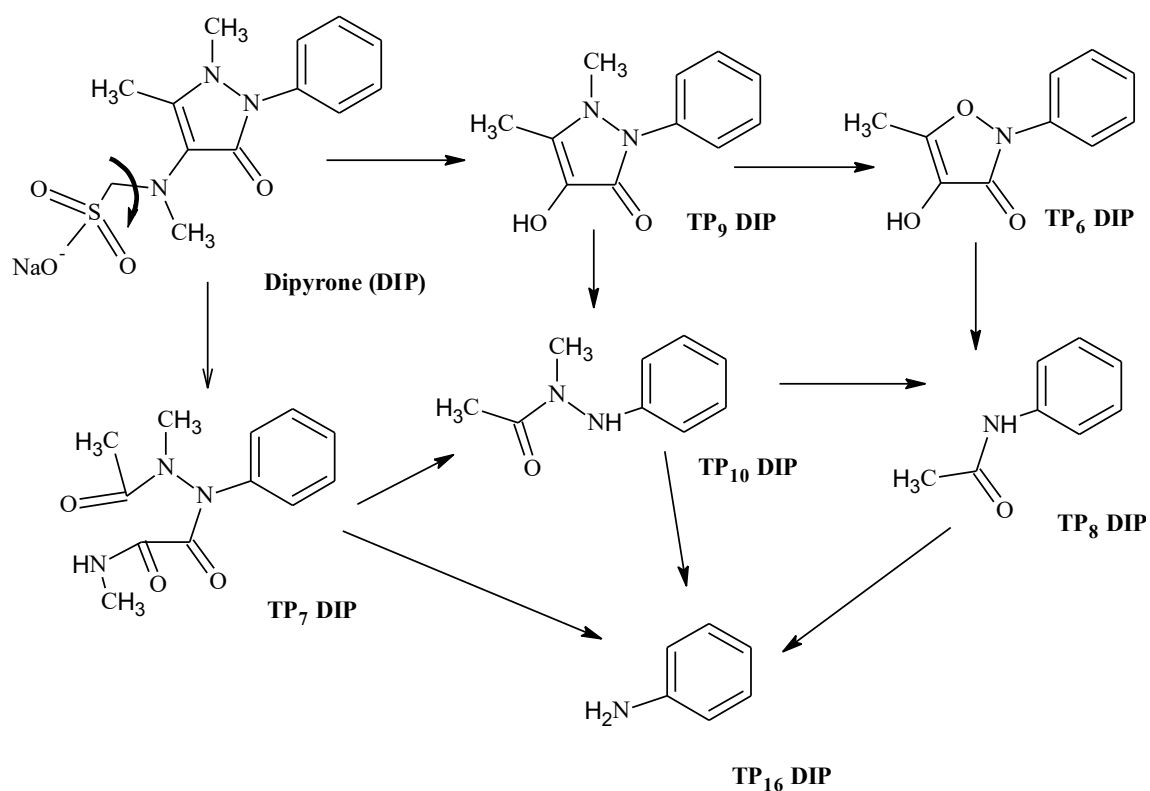


Figure S.5.1 Degradation pathway of dipyrone in Solar photo-Fenton like process at neutral pH (SW matrix).

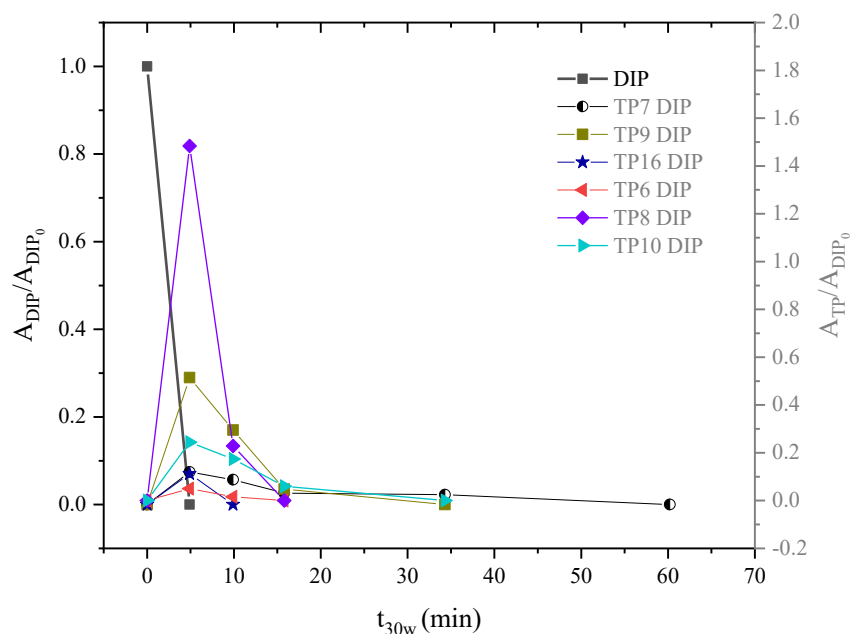


Figure S.5.2 DIP and its TPs in Solar photo-Fenton like process at pH 7.0.

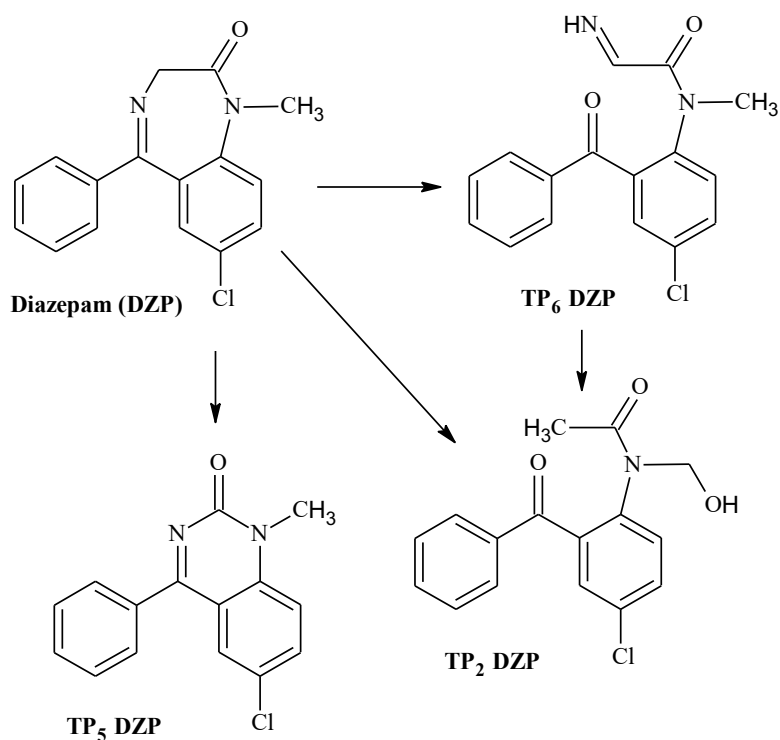


Figure S.5.3 Degradation pathway of diazepam in Solar photo-Fenton like process at neutral pH (SW matrix).

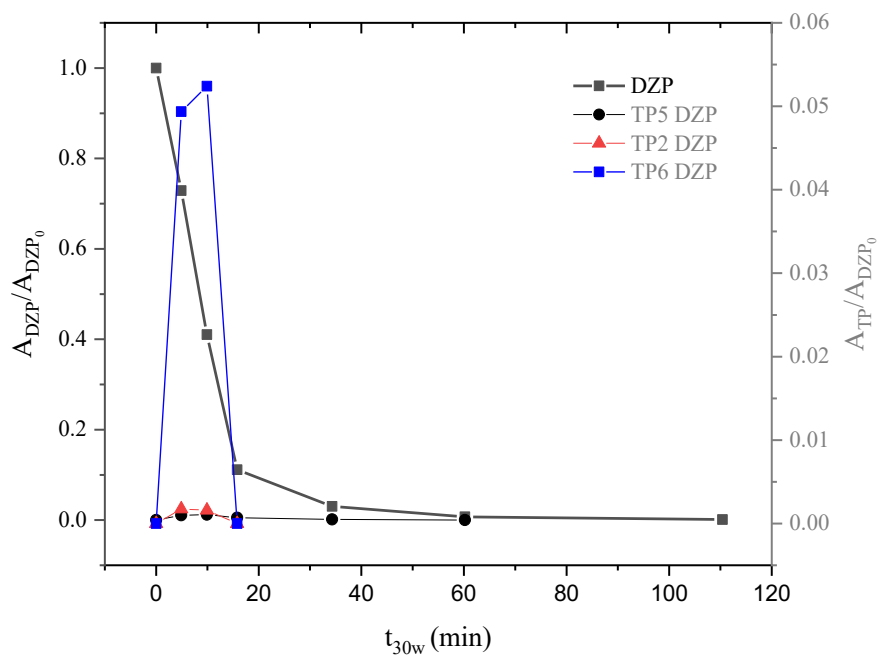


Figure S.5.4 DZP and its TPs in Solar photo-Fenton like process at pH 7.0.

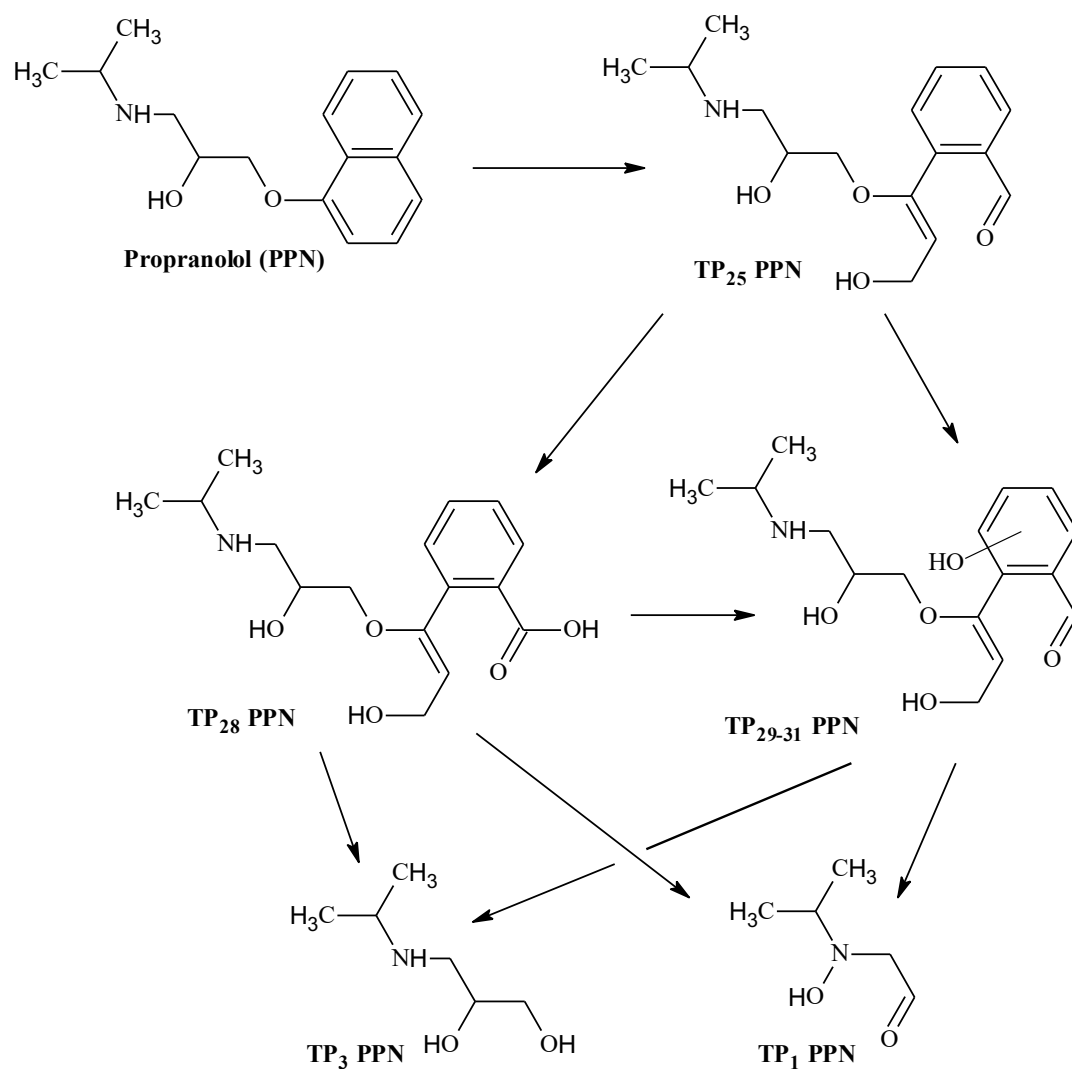


Figure S.5.5 Degradation partway of propranolol in Solar photo-Fenton like process at neutral pH (SW matrix).

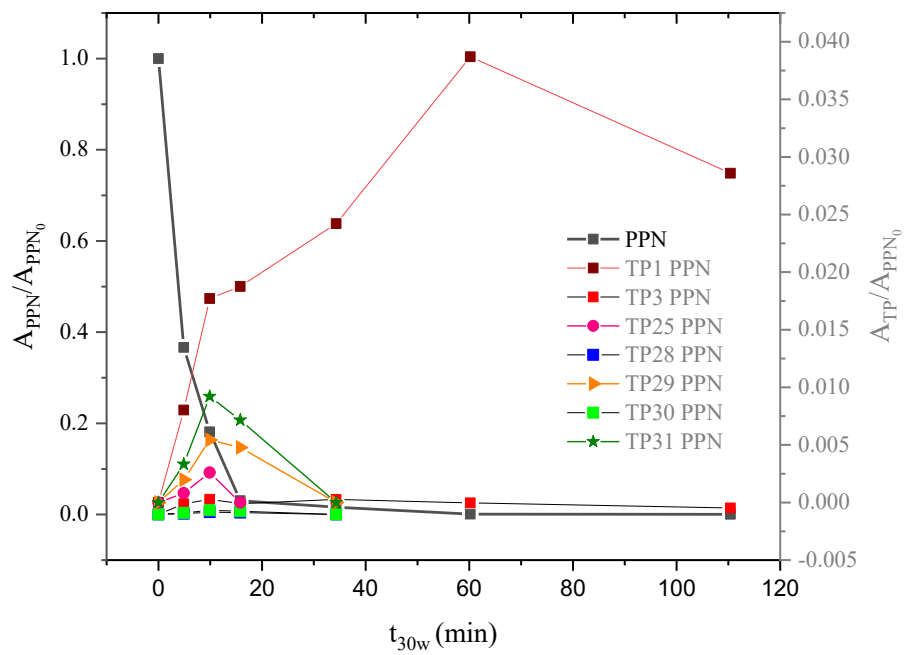
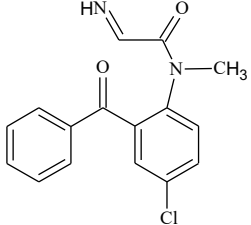
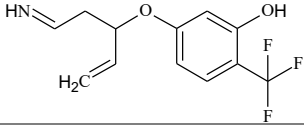
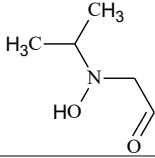
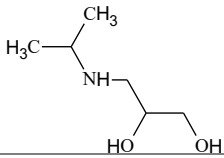
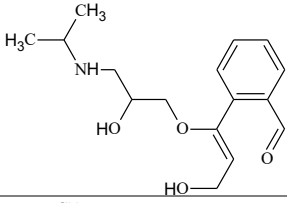
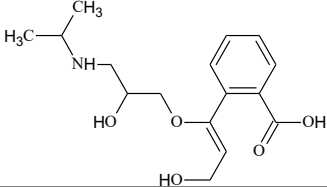
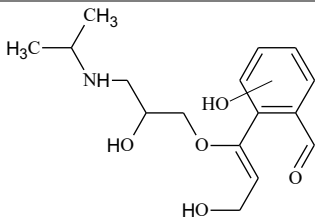
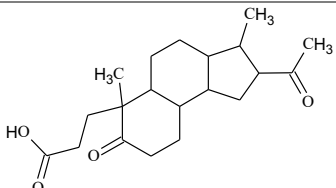


Figure S.5.6 PPN and its TPs in Solar photo-Fenton like process at pH 7.0.

Table S.5.2. Toxicological Hazard, biodegradability and carcinogenicity of TPs generated through the solar photo-Fenton like process.

Name	Structure	Cramer rule	START biodegradability	Mutagenic and carcinogenicity
TP2 AAA		High (Class III)	Persistent chemical (Class 2)	Structural alert for genotoxic carcinogenic
TP6 DIP		High (Class III)	Persistent chemical (Class 2)	Structural alert for genotoxic carcinogenic
TP7 DIP		Intermediate (Class II)	Persistent chemical (Class 2)	Structural alert for genotoxic carcinogenic
TP8 DIP		Low (Class I)	Persistent chemical (Class 2)	Structural alert for genotoxic carcinogenic
TP9 DIP		High (Class III)	Persistent chemical (Class 2)	Structural alert for genotoxic carcinogenic
TP10 DIP		Low (Class I)	Persistent chemical (Class 2)	Structural alert for genotoxic carcinogenic
TP16 DIP		Low (Class I)	Persistent chemical (Class 2)	Structural alert for genotoxic carcinogenic
TP2 DZP		High (Class III)	Persistent chemical (Class 2)	Structural alert for genotoxic carcinogenic
TP5 DZP		High (Class III)	Persistent chemical (Class 2)	Structural alert for genotoxic carcinogenic

TP6 DZP		High (Class III)	Persistent chemical (Class 2)	Structural alert for genotoxic carcinogenic
TP5 FXT		High (Class III)	Persistent chemical (Class 2)	Structural alert for genotoxic carcinogenic
TP1 PPN		Low (Class I)	Easy biodegradable chemical (Class 1)	Structural alert for genotoxic carcinogenic
TP 3 PPN		High (Class III)	Easy biodegradable chemical (Class 1)	Structural alert for genotoxic carcinogenic
TP25 PPN		Low (Class I)	Persistent chemical (Class 2)	Structural alert for genotoxic carcinogenic
TP28 PPN		Low (Class I)	Persistent chemical (Class 2)	Structural alert for genotoxic carcinogenic
TP 29-31 PPN		High (Class III)	Persistent chemical (Class 2)	Structural alert for genotoxic carcinogenic
TP1 PRG		High (Class III)	Easy biodegradable chemical (Class 1)	Negative

4.1.4 Homemade *raceway pond* reactor: pharmaceutical degradation, TPs identification and degradation pathways assessment

The first outdoor engineering scale reactor developed was a parabolic solar collector through which contaminated water could flow. Since then, different outdoor engineering-scale reactors have been developed¹¹³. The treatment of pharmaceuticals in wastewater by photocatalytic oxidation using solar irradiation like solar photo-Fenton has been successfully described at lab scale in current literature. However, one of the most important drawbacks for large-scale application is their cost, especially the investment in the photo-reactor and reagents¹¹⁴.

The current study (**Manuscript V**) focuses on the fabrication and use of a low-cost *raceway pond* reactor. The *raceway pond* type reactors consist of two open channels through which the wastewater is recirculating and in contact with solar radiation⁵⁹. The cost-effective *raceway pond* reactor was created with low-cost materials and is similar to the widely recognized version of this type of reactor.

The objective of this study was to use *raceway ponds* to scale-up the solar photo-Fenton process using EDDS. The research explored Fe³⁺:EDDS (1:2) and (1:1) proportions, as well as initial pharmaceutical concentrations of 50 µg L⁻¹ and the environmental fate of generated TPs with the use of (Q)SAR software programmes.

Removal of pharmaceuticals in hospital wastewater by solar photo-Fenton with Fe³⁺-EDDS using a homemade raceway pond reactor: transformation products and *in silico* toxicity assessment

Elisabeth Cuervo Lumbaque^a, Renata M. Cardoso^a, Adriano de Araújo Gomes^a, Sixto Malato^b, José A. Sánchez Pérez^c, Carla Sirtori^{a}.*

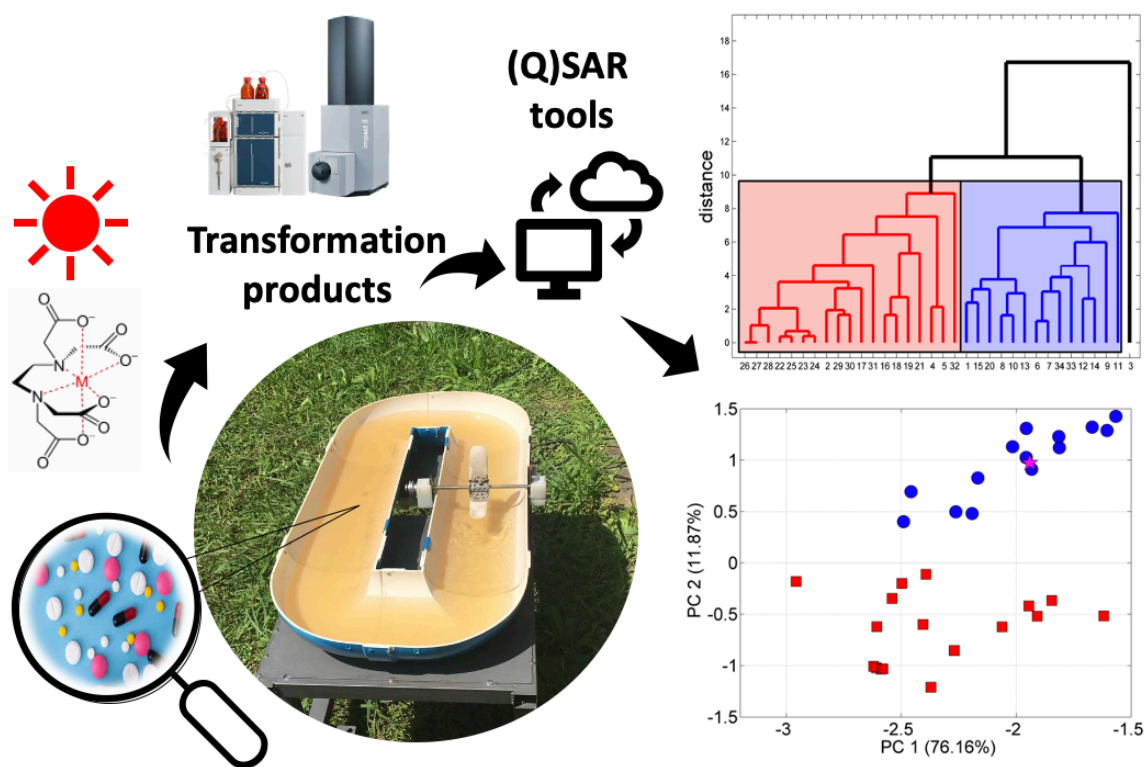
^a Instituto de Química- Universidade Federal do Rio Grande do Sul, Av. Bento Gonçalves, 9500, Porto Alegre-RS, Brazil.

^b Plataforma Solar de Almería-CIEMAT. Ctra. Senés km 4, 04200 Tabernas (Almería), Spain.

^c Chemical Engineering Department, University of Almería, Ctra. de Sacramento s/n, E-04120 Almería, Spain.

* To whom all correspondence should be addressed

e-mail: carla.sirtori@ufrgs.br (Prof. Carla Sirtori)



Highlights

- Solar photo-Fenton process was operated in homemade RPR to remove pharmaceuticals
- 77% pharmaceutical removal with Fe^{3+} -EDDS (1:2) after 30 min in hospital wastewater
- Fe^{3+} -EDDS ratio affect solar photo-Fenton process performance in hospital wastewater
- The (Q)SAR endpoints of the transformation products were analyzed with PCA

Abstract

This study investigated the removal of six representative emerging pharmaceuticals (PHCs), including dipyrone (DIP), diazepam (DZP), fluoxetine (FXT), paracetamol (PCT), propranolol (PPN), and progesterone (PRG) at 50 and 500 $\mu\text{g L}^{-1}$ in hospital wastewater (RHWW) treated with solar photo-Fenton with Fe^{3+} -EDDS. The effect of the molar ratio (1: 1 and 1: 2), their relationship with the degradation of pharmaceuticals and formation of their TPs during the treatments were studied. Additionally, (Q)SAR *in silico* toxicity predictions for all TPs identified were evaluated. Experiments were carried out under sunlight and a total volume of 10 L of RHWW. The reactant concentrations were i) to $\text{PHCs}_{(\text{mix})}$ (500 $\mu\text{g L}^{-1}$), Fe^{3+} -EDDS (1:1; 15.35 mg L^{-1} of iron) and H_2O_2 (230 mg L^{-1}); ii) to $\text{PHCs}_{(\text{mix})}$ (50 $\mu\text{g L}^{-1}$), Fe^{3+} -EDDS (1:2; 5 mg L^{-1} of iron) and H_2O_2 (50 mg L^{-1}), with all experiments at pH 7. The H_2O_2 was carefully dosed during the first 30 min of solar photo-Fenton treatment to avoid its continued excess and inefficient use. The main results obtained indicate the degradation of pharmaceuticals is highly favored in Fe^{3+} :EDDS (1:2) providing total consumption of H_2O_2 , increased iron stability, degradation percentages above 77% in most PHCs and total degradation of some TPs formed throughout the process at $t_{30\text{W}} = 57$ min. Twenty-one TPs were identified using LC-QTOF MS associated with a purpose-built database for both molar ratio (1:1 and 1:2) of Fe^{3+} -EDDS. To perform the (Q)SAR predictions of the PHCs and TPs identified, the toxicity, biodegradability, mutagenicity, and bioaccumulation were calculated on the basis of *in silico* tools. Principal component analysis (PCA) was also performed to compare the toxicity of the TPs, allowing the consideration of two principal components which characterized 88% of the predicted results. Most of the TPs did not show mutagenicity or bioaccumulation characteristics.

Keywords: Pharmaceuticals, hospital effluent, transformation products, (Q)SAR, homemade raceway pond, PCA.

Introduction

The treatment of PHCs in wastewater by photocatalytic oxidation using solar irradiation such as solar photo-Fenton has been successfully described at lab scale in current literature. Despite this, one of the most important drawbacks for large-scale application is the cost, especially the investment in the photo-reactor and reagents [1]. There is, therefore, a growing interest in performing these processes at natural pH. To improve the accessible pH range and efficiency of the solar photo-Fenton treatment, chelating agents such as aminopolycarboxylic acids (APCAs) have been used to maintain iron in solution [2]. In this context, the ethylenediamine-N,N'-disuccinic acid (EDDS), is an alternative to environmentally friendly metal chelating, with high biodegradability, nontoxicity under environmental conditions, keeping the iron species in solution at a wide range of pH, which is advantageous for the photo-Fenton process [3].

The solar photo-Fenton reaction through Fe^{3+} -EDDS may be briefly summarized in the following stages: i) Fe^{3+} -EDDS is oxidized and reduced cyclically; ii) Fe^{2+} -EDDS reacts with hydrogen peroxide in a very fast reaction ($k=1.9 \times 10^3 \text{ mM}^{-1} \text{ min}^{-1}$) yielding hydroxyl radicals (HO^\bullet) [4]; iii) Fe^{3+} -EDDS can absorb light in the UV-Vis range, undergoing a metal charge transfer excitation regenerating Fe^{2+} -EDDS; iv) re-catalyzes the decomposition of H_2O_2 producing additional HO^\bullet and; v) also yielding $[\text{Fe}^{3+}\text{-EDDS}]^*$, EDDS^\bullet and $\text{Fe}(\text{OH})_3$ [4,5]. In turn, EDDS^\bullet can react with O_2 to generate the superoxide radical $\text{O}_2^{\bullet-}$ ($\text{HO}_2^\bullet/\text{O}_2^{\bullet-}$, pka 4.33) [6,7].

Moreover, Fe^{3+} -EDDS enhance the ligand-to-metal charge transfer (LMCT) transitions because it usually has higher molar absorption coefficients in the near-UV and visible regions, from 200 nm to 400 nm with a molar absorption coefficient of $6530 \text{ L mol}^{-1} \text{ cm}^{-1}$ at 239 nm [3], this guarantees the conversion of Fe^{2+} which is essential for the homogeneous photo-Fenton process.

Current study focuses on the use of low-cost reactors, such as raceway pond reactors (RPR). These RPR consist of two open channels through which water. RPR is provided with a motor to vary the flow conditions and the depth of the liquid can be changed according to the availability of UV radiation [8]. Due to its simplicity, it is easy to make an adapted model with low-cost materials.

In addition, another important subject to be studied is the identification of TPs, which are formed from multiple and simultaneous reactions during the solar photo-Fenton process performed in RPR. The identification of these TPs is key to understanding how the degradation of these pharmaceuticals takes place and could give a view of the advantages

or disadvantages of the solar photo-Fenton process performed in RPR in the final (often short) treatment time.

Therefore, the aim of this study is to investigate the ability of the Fe^{3+} -EDDS assisted solar-photo Fenton process at pH 7 to remove a pharmaceutical and, particularly, their toxic/bioaccumulated/mutagenic TPs from hospital wastewater (RHWW) by using a homemade-RPR. Firstly, assays were conducted to evaluate the degradation of the PHCs in RHWW using Fe^{3+} -EDDS in 1:1 and 1:2 molar ratio. Secondly, suspected TPs were identified through LC-QTOF MS analysis with a purpose-built database. Finally, the toxicity of each TP identified was predicted and evaluated by quantitative structure-activity relationship ((Q)SAR) models and PCA.

2. Material and Methods

2.1 Reagents

Iron source $\text{Fe}_2(\text{SO}_4)_3 \cdot 5\text{H}_2\text{O}$ (purity > 95%) and hydrogen peroxide (35% w/v) were purchased from Synth (São Paulo, Brazil), (S,S)-ethylenedi-amine-N,N-dissuccinic acid trisodium salt solution (35%) was provided by Sigma–Aldrichand, sulfuric acid (H_2SO_4 , 98%) used for pH adjustment was purchased from Synth (São Paulo, Brazil). Acetonitrile and Methanol for the LC mobile phase was LC-MS grade.

2.2 Solutions

Standards of paracetamol (PCT), propranolol (PPN), dipyrone (DIP), fluoxetine (FXT), diazepam (DZP), and progesterone (PRG) (analytical grade; purity >90%) were used for degradation study. A mixed stock solution was prepared at a concentration of 14 g L^{-1} of each of target compounds in acetonitrile:methanol (2:1 v/v). Dilutions of the stock solution were prepared at the initial concentrations of $500 \text{ } \mu\text{g L}^{-1}$ and $50 \text{ } \mu\text{g L}^{-1}$ in RHWW. The RHWW matrix in the degradation studies was used as collected (without filtration). Pharmaceuticals were spiked into the different aqueous matrices, prior to pH adjustment. The stock solution of the complex Fe^{3+} -EDDS was prepared according to the methodology described by Soriano-Molina et al. [9].

2.3 Hospital wastewater characterization

The RHWW used to carry out all the experiments were supplied by a local hospital from Porto Alegre city (Brazil). The characterization of RHWW was pH 8, chloride 50.7 mg L^{-1} , conductivity $838 \text{ } \mu\text{S cm}^{-1}$, biochemical oxygen demand (BOD) $96 \text{ mg L}^{-1} \text{ O}_2$,

chemical oxygen demand (COD) 246 mg L⁻¹ O₂, total organic carbon (TOC) 123.7 mg L⁻¹, inorganic carbon (IC) 57.68 mg L⁻¹, phosphate 18.5 mg L⁻¹, total suspended solids 81 mg L⁻¹, and total solids 313 mg L⁻¹.

2.4 Experimental set-up and procedure

The RPR used was built with PVC materials available in hardware stores. The RPR contains a paddle linked to an engine to obtain a well-mixed and homogeneous flow. The engine, adapted from a fan, is connected to a variable frequency drive to control the paddle's speed. The photoreactor was filled with 10 L, resulting in a liquid depth of 4 cm. A scheme of the reactor is shown in Figure S.1 (supplementary material). The reactor was covered to protect the system from light while the mixing and recirculation time of 5 min was allowed for homogenization, following the addition of the PHCs mixture, and Fe³⁺-EDDS. After the addition of H₂O₂, the reactor was uncovered and the treatment started. The concentration of reactants used for the degradation of the PHCs mixture (500 µg L⁻¹) were determined by optimization studies shown in previous works with synthetic matrices [10]. The experiments were performed at *Universidade Federal do Rio Grande do Sul*, Brazil (latitude 30° 4' 21.0864" S, longitude 51° 7' 11.838" W) using natural sunlight irradiation on sunny days around noon. Solar UV radiation was measured using a solar energy meter (SP-2000, ICEL), which provided data in terms of incident radiation (W m⁻²). These data were used to calculate the normalized irradiation time t_{30W} [11].

2.5 Analytical methods

The total iron concentration and H₂O₂ was monitored using the adapted method of 1,10-phenanthroline [12] and NH₄VO₃ [13], respectively. Both methods were performed in a Cary 50 UV-Vis spectrophotometer. Mineralization was monitored by measuring the TOC by Analytik Jena AG multi N/C 2100 S.

The pharmaceuticals and their TPs were quantified and identified, respectively, using a liquid chromatograph (Nexera X2, Shimadzu) connected to a QTOF mass spectrometer (Impact II, Bruker Daltonics). Further details are provided in Text S.1 (supplementary material). Identification of the TPs was carried out by constructing a purpose-built database with TPs reported in current literature, including over 180 compounds. This database was updated from a previous study [14]. Each TP was assigned with a number and the acronym of the pharmaceutical from which it originated.

2.6 Toxicity assessment with *in silico* (Q)SAR tools

To evaluate the ecotoxicity of the TPs identified by the LC-QTOF MS, four (Q)SAR software were used: i) Ecological Structure Activity Relationships (ECOSAR, 2.0, Washington DC, USA); ii) Toxicity Estimation Software Tool (T.E.S.T, version 4.2.1 Washington DC, USA); iii) EPI Suite™ and, iv) TOXTREE v. 13.0.

These tools are methods freely available to users and utilize the SMILES form of chemical structure for predictions, which estimate endpoints toxicity based on the difference of the physiochemical characteristics of chemicals and their biological activities. ECOSAR and T.E.S.T were used to indicate acute and chronic toxicity of *fish*, *D. magna*, *green algae*, *F. minnow* and oral rat endpoints. Moreover, the prediction of mutagenicity and bioaccumulation factor endpoints (T.E.S.T) were related with bioconcentration, biodegradability (EPISuite™) and oral toxicity (Cramer rules-TOXTREE). The consensus method was used based on the average of toxicity prediction in T.E.S.T.

Finally, the principal component analysis (PCA) was used to improve the identification of correlations between endpoints from (Q)SAR software of TPs identified. The results were reported in the form of a bivariate scatter plot, where the data are plotted in two axes representing the first two PCs. All chemometric calculations were carried out in MatLab Environmental 2012 through `pca_toolbox`, a freeware package available at <https://michem.unimib.it/>. In all cases the data set was previous autoscaling.

3. Results and Discussion

3.1 Removal of pharmaceuticals and Fe³⁺-EDDS molar ratio effect

The use of Fe³⁺-EDDS at near-neutral pH was considered with different Fe³⁺-EDDS ratios (1:1 and 1:2) in the RHW matrix. Considering the concentrations of each model PHC spiked in RHW (500 µg L⁻¹), the molar ratio of PHC_{S(mix)}:H₂O₂ was calculated at 1:500, suggesting that scavenging of HO• by larger H₂O₂ dose could limit PHCs and TPs removal. For this reason, the degradation studies were carried out using six consecutive doses of the H₂O₂ in the first 30 min of the process (t_{30w} of 0, 2.5, 5, 10, 15, and 30 min). The time evolution of PHCs concentration in different complex ratios is shown in Figure 1. As seen in Figure 1(a) and 1(c), the initial degradation of pharmaceuticals is very fast in both processes. The effect of the Fe³⁺-EDDS molar ratio at pH 7.0, keeping the 1:1 ratio achieved degradation profit of DIP (> LOD; 0.35 µg L⁻¹), DZP (68 %), FXT (47 %),

PCT (63 %), PPN (99 %) and PRG (71 %). Fe³⁺-EDDS (1:2) achieved pharmaceutical abatement of more than 77% for 57 minutes of treatment time (DIP approx. 100%, DZP 88 %, FXT 77 %, PCT 82 %, PPN 99.7 % and PRG 99%), exhibiting a much faster decay than Fe³⁺-EDDS (1:1).

The total dissolved Fe and H₂O₂ during the solar photo-Fenton processes are shown in Fig. 1((c) and (d)). The results showed that Fe³⁺-EDDS complex was decomposed during the solar photo-Fenton process. The decomposition of EDDS by H₂O₂ releases iron into the solution, which forms insoluble hydroxides at pH 7.0 [9], the iron precipitates more quickly in the ratio 1: 1 than 1: 2. This can be attributed to iron being released into the solution by complex break up due to solar irradiation and decomposition of EDDS, a small quantity of iron could have reacted in the photo-Fenton cycle, or the complex could be regenerated if there is still EDDS available in the solution, which resulted in degradation of PHCs.

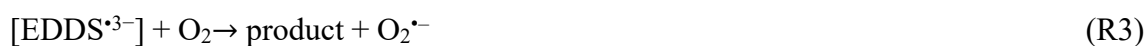
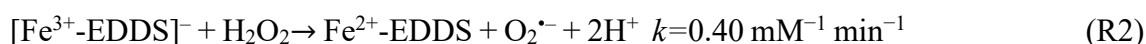
The positive effect of EDDS can be attributed to two main reasons: i) the complex formed between Fe³⁺ and EDDS enhances the dissolution and stability of iron, which leads to the higher activity of iron in the complex matrix like RHHW; ii) the Fe³⁺-EDDS complex is photochemically efficient leading to a higher quantum yield for the formation of HO[•] (Φ HO[•] 0.034 pH 7.0) at 365 nm [2].

Alternatively the negative effect of high temperatures (around 40°C) lead to a faster depletion of EDDS [7], causing fast iron precipitation and loss of degradation efficiency. In the experiments performed, the maximum temperature recorded was 28°C, hence, the temperature was not considered a determining factor in the precipitation of iron.

The consumption of H₂O₂ boosted with the increase of Fe³⁺-EDDS ratio, 84.4% of H₂O₂ was consumed under Fe³⁺-EDDS (1:1) and total consumption was presented under the Fe³⁺-EDDS (1:2). Moreover, it was remarkable that the EDDS contributed to the TOC content in the RHHW. The molar ratio of EDDS:PHCs was >46:1 under the Fe³⁺-EDDS (1:2) conditions, hence scavenging of HO[•] by EDDS could be a limiting factor for the degradation of PHCs. Mineralization at the final time was around 8% for Fe³⁺-EDDS (1:1) and 11% for Fe³⁺-EDDS (1:2) system.

The solar photo-Fenton process with Fe³⁺-EDDS is related mainly to the synergistic effect of the EDDS³⁻, H₂O₂, and radical oxygen species-ROS (HO[•] and O₂^{•-}), which are represented by reactions 1-5[4,15]. Besides, EDDS²⁻/EDDS³⁻ species can be found under the conditions of this study (pH =7). At higher pH than 4.8 (pK_a of the couple HO₂[•]/O₂^{•-})

$O_2^{\bullet -}$ becomes the dominant reactive oxygen species, which suggests the formation of H_2O_2 and the recovery of Fe^{2+} .



Iron complexes can react with molecular oxygen and its reduced species, leading to the production of very reactive high-valent iron-oxo species [3]. Hence, it is possible that several ROS coexist in the solar photo-Fenton system with Fe^{3+} -EDDS and the predominance of these ROS depend on the environmental conditions.

Conversely, in the absence of enough EDDS, the presence of $Fe(OH)_3$ could probably contribute to PPN, FXT, and PRG disappearance, as ferric iron precipitates upon incidence of a photon, it can have possible heterogeneous reactions which enable the oxidation of PHCs adsorbed on the surface [16]. In relation to this, FXT (log P 3.82), PPN (log 3.48), and PRG (log P 3.87) have a higher log P than the other PHCs, in which sorption to iron-sludge is likely to play an important role in the removal from wastewater. The experiments previously reported have been conducted at concentrations well above those commonly found at the RHHW. Hence, it is convenient to explore the behavior of those compounds at lower concentrations, that is, in conditions closer to the real ones for RHHW. For this purpose, a solar experiment was performed, using as an initial concentration, $50 \mu\text{g L}^{-1}$ of each pharmaceutical in the RHHW. These experiments were carried out with mild concentrations of reagents: 5 mg L^{-1} Fe^{3+} -EDDS (1:1) and 50 mg L^{-1} H_2O_2 at pH 7.0. Figure 2a shows PHCs degradation under these conditions. As previously stated, DIP and PPN were the PHCs with the highest removal rates and therefore $50 \mu\text{g L}^{-1}$ did not substantially change their degradation rate DIP ($> \text{LOD}$; $0.35 \mu\text{g L}^{-1}$), DZP (37%), FXT (37%), PCT (15%), PPN (73%) and, PRG (42%). The decrease in the reactant concentrations represented at least 1.3-fold less % of degradation for FXT, DZP, and PRG with PCT being the most affected PHCs with 4-fold less removal.

The low degradation percentages could be mainly due to the concentration of H_2O_2 since total consumption of H_2O_2 was observed with the continued presence of dissolved iron in RHHW at 57 min of treatment (Figure 2b). The molar ratio of $Fe^{3+}:H_2O_2$ for $500 \mu\text{g L}^{-1}$

¹of PHCs was calculated at 1:25 and 50 $\mu\text{g L}^{-1}$ of PHCs was calculated at 1:16, suggesting that proportions over 25 are necessary when the experiments are worked with EDDS.

The degradation of each PCH in the mixture with 500 $\mu\text{g L}^{-1}$ and 50 $\mu\text{g L}^{-1}$ fitted the model by Chan and Chu [17] kinetics with determination coefficients above 0.99, except for FXT in 50 $\mu\text{g L}^{-1}$, which only fit the first order.

On another hand, it is well known that inorganic species (chloride, sulfate, phosphates etc.) are often detrimental to the photo-Fenton reaction rate, due to complexation of Fe^{3+} , which decreases the concentration and activity of iron species, or the scavenger effect of hydroxyl radicals and the formation of less reactive radicals [5,18,19]. Nevertheless, it has also been observed that these ions significantly reduce the photo-Fenton reaction rate only if they occur at concentrations higher than 500 mg L^{-1} , these concentrations are far from the concentration found in RHW (section 2.3), therefore this effect is not considered predominant to the detriment of the efficiency of the process.

The degradation of PHCs could be affected by the presence of $\text{HCO}_3^-/\text{CO}_3^{2-}$ ions and organic matter due to: i) HCO_3^- (99.92% at $\text{pH} = 7$; $\text{pK}_{a1} = 3.50$ and $\text{pK}_{a2} = 10.32$) being one of the major scavenger agents of HO^\bullet ($k_{\text{HO}^\bullet/\text{HCO}_3^-} = 8.5 \times 10^6 \text{ M}^{-1}\text{s}^{-1}$) [20], the IC in the RHW (IC= 57.68 mg L^{-1} , for $\text{pH} 8$) could act as hydroxyl radical scavengers leading $\text{CO}_3^{\bullet-}$ and destabilizing effects on the soluble iron [21]; and ii) a high concentration of organic matter competing with the PHCs and acting as HO^\bullet radicals scavenger ($k_{\text{HO}^\bullet/\text{C}} = 3.8 \pm 1.9 \times 10^8 \text{ L (mol C)}^{-1} \text{ s}^{-1}$) [22].

3.2 Identification of suspected TPs using LC-QTOF MS and a purpose built-database

Table S.2.1 summarizes the TPs generated by solar photo-Fenton process using the Fe^{3+} -EDDS ratios (1:1) and (1:2). Twenty-one TPs were identified with a purpose-built TPs database [14]. For all TPs identified, adequate concordance agreement between the experimental accurate mass measurements and the proposed formula (< 5.0 ppm error) was determined. TPs chemical structures were proposed based on scientific studies published in current literature and consider, the timings, the knowledge of the precursor molecule and the oxidative processes that took place.

For DIP (Figure 3a), the opening of the pyrazolinone ring was confirmed by the detection of TP14 DIP [23], TP31 DIP and TP32 DIP [24]. These TPs were yielded by addition of HO^\bullet radicals to the double bond of the pyrazolinone ring followed by $\text{C}=\text{C}$ bonds breaking due to the high electron density and low steric hindrance on the double-bond, which makes it more reactive [25]. In turn, the formation of hydroxylated derivatives, the consequence of the addition of HO^\bullet yielded the corresponding quinone-imine

intermediate TP17 DIP [26]. Additionally, TPs from two of the most common DIP metabolites (AAA and FAA) were observed. TP2 AAA and TP2 FAA are products of oxirane formation induced by a loss of water and further decarbonization [25].

For PPN (Figure 3b) the ring-opening attack of hydroxyl radicals on the naphthol moiety may occur in different positions of the ring, despite this, confirmatory fragments, that can clearly indicate where this attack occurred, were not identified for $C_{14}H_{20}NO_5$, (m/z 282.1336) and for $C_{16}H_{24}NO_5$ (m/z 310.1652). Due to the non-identification of the confirmatory fragments and according to the TPs database, the value of m/z 282.1336 could be assigned to TP5, 18 or 19 PPN, at the same time that m/z 310.1652 could be TP8, 29, 30 or 31 PPN. In turn, the confirmatory fragment C_8H_7 (m/z 103.0389) from $C_{16}H_{22}NO_4$ (m/z 292.1537) was identified, it suggests the presence of TP6 PPN, which was reported in solar runs and photocatalytic oxidation [27]. The attack on the secondary amine group lead to the formation of di-hydroxyl propoxyl naphthalene (TP32 PPN). The oxidative ring opening reaction of naphthol, and further decarboxylation forms p-hydroxy di-ketone (TP37 PPN), the TP32 and TP37 were identified in studies on oxidative degradation of PPN by electro-Fenton process using sub-stoichiometric titanium oxide (Ti_4O_7) anode [28].

For FXT (Figure 3c) the main TPs formed by hydroxylation of HO^\bullet on the aromatic ring led TP16 FXT [29] followed by defluorination with an attack of HO^\bullet in the C8 position of the ring that is adjacent to the e $-CF_3$ substituent yield TP9 FXT [30] and the hydroxylation of aliphatic chain led TP11 FXT [31].

Additionally, DZP TPs (Figure 3d) shows that TP1 DZP is produced by opening of the benzodiazepinic ring from DZP. This structure has been reported as a photo-transformation product as well as oxidation product [32]. DZP can also lead to the formation of hydroxylated products like TP9 DZP [33] and carbon addition reactions in N–C double bond (TP 20 DZP).

PCTTPs identification (Figure 3e) indicated that the degradation of PCT involves the attack of HO^\bullet radicals onto the aromatic ring to give ortho-, meta- or para- hydroxylations with respect to the HO- group (TP4 PCT). Some studies [34] showed that hydroxylation at the meta-position is of minor relevance. Subsequently, TP4 PCT has been reported in different studies [35,36]. Moreover, TP34 PCT, which is formed by the attack of hydroxyl radicals and aromatic ring opening can also be identified in our study. The cleavage of the bond between nitrogen and carbon from the carbonyl group yielded hydroquinone (not detected in this study), from which the opening of the aromatic moiety led to the

formation of TP26 PCT [35]. The TPs from PCT are in accordance with the HO[•] attack mechanism proposed by other authors [37].

In turn, with regard to PRG (Figure 3f) only one TP was identified. The formation of TP17 PRG is facilitated by the addition of one oxygen atom at the C17 position and subsequent dehydrogenation in the ring A and B take a place. This finding is in accordance with other studies [38].

Summing up the TPs analysis, it is remarkable that: i) oxidation of DIP usually occurs on pyrazol-3-ones by electron transfer, breakdown of N=N bond and on side-chain substituents, such as primary amino groups, or the nitrogen atom of the lactam group; ii) the diazepine ring of DZP bears an electrophilic imine carbon C-11, which is the main site of the reaction; iii) FXT have two main reactivity sites, N which favor the H abstraction atom and the C sites 14 and 15 (in trifluoromethyl-phenoxy moiety) by addition of the ROS to a double bond site [39]; iv) in PCT, the phenol moiety is the target of the ROS; v) the reactive sites of PPN are the N-C sites 2 and addition of the ROS to a double bond site in the naphthol moiety and; vi) the characteristic reaction of degradation of PRG is the loss of one H and hydroxylation in its carbonyl moiety.

The time profile (formation and degradation) of the main PHCs TPs during both experimental conditions evaluated (Fe³⁺-EDDS (1:1) and Fe³⁺-EDDS (1:2)) were performed in our study (Figures 4 and 5). As can be seen, most TPs formed had maximum signal intensity in the first 15 min from the beginning of the solar experiment. The TPs were partially degraded and tended to accumulate in Fe³⁺-EDDS (1:1). Furthermore, some TPs generated in the Fe³⁺-EDDS (1:2) system were totally degraded within 30 min of treatment.

3.3 Ecotoxicity assessment using (Q)SAR tools

Ecotoxicity assessment of PHCs and their identified TPs were predicted by (Q)SAR models (details of these models were described in the section 2.7) with the use of SMILES (Table S.3.1, supplementary material).

Exploratory analysis of the *in silico* data were carried out by means of an/the unsupervised pattern recognition approach. First, using clustering analysis (CA) based on euclidean distance and complete linkage. As can be seen in Figure 6a, the dendrogram shows two groups of samples and the codes assigned for the clustering analysis are in table S.3.5 (supplementary material).

The red cluster contains all the TP of PPN, TP of PCT and DIP 14, 31 and 32, with these structures representing the loss of aromaticity, opening of the aromatic ring and loss of carbon chain.

The blue cluster contains the parent compounds with the exception of PCT, and all identified TPs that are originated by FXT, DZP and PRG. This indicates that the red cluster contains the structures with more aromaticity, with the presence of electron withdrawing groups and more persistent structures in the solar photo-Fenton process with Fe^{3+} -EDDS. TP17 DIP has values in the endpoints that are considerably different from the other TPs and PHCs, therefore, according to the analysis, it is not classified into either of the two groups.

Endpoint values according to (Q)SAR were evaluated by using PCA (Figure 6b). This analysis allowed the visualization of relationships between TPs as well as between the models. The two-dimensional plane defined by the first two main components represent 88% of the variance explained, however the groups of samples identified in CA are discriminated against by PC2. The horizontal lines in the Figure 6c correspond to the significant limits of loading on PCA calculated based on t test. The variables identified as significant were Bioaccumulation factor (V4), nonlinear biodegradation probability model (V8), MITI nonlinear biodegradation model (V12), ready biodegradability (V14) and oral toxicity according to Cramer's rules (V23).

The endpoint V8 and V12 are estimations made with the Biodegradation Probability Program (BIOWIN) of the EPI Suite™ software of the US-EPA[40], the estimates V8 (BIOWIN model 2 – table S.3.4) and V12 (BIOWIN model 6 – table S.3.4) are based upon fragment constants that were developed using multiple non-linear regression analyses. The BIOWIN model 6 was developed by the Japanese Ministry of International Trade and Industry (MITI) [41]. The criteria for the prediction of ready biodegradability (V14) was performed according to model 3 BIOWIN and model 5 BIOWIN [42].

Note that compounds of red cluster (class1 in Table S.3.5), are characterized by high values of the nonlinear biodegradation probability model, MITI nonlinear biodegradation model and ready biodegradability. In the opposite direction, these samples have lower values of bioaccumulation factor and oral toxicity.

In addition, the pair wise correlation between the variables considered to be significant were inspected as in Figure 6d. High positive correlation was observed between bioaccumulation factor and ready biodegradability. In addition, the greatest inverse

correlation was observed for bioaccumulation factor and MITI nonlinear biodegradability model.

On the other hand, acute and ChV toxicity levels were determined according to the Globally Harmonized System of Classification and Labelling of Chemicals[43], which is given by $LC_{50}/EC_{50}/ChV \leq 1$ (very toxic), $1 > LC_{50}/EC_{50}/ChV \leq 10$ (toxic), $10 > LC_{50}/EC_{50}/ChV \leq 100$ (harmful) and $LC_{50}/EC_{50}/ChV > 100$ (unharmful). Most TPs have an acute and chronic toxicity (Table S.3.2; supplementary material), according to acute toxicity values TP 26 PCT is very toxic to *Green algae* and FXT is very toxic to *Daphnia* and *Green algae*. Chronic toxicity values of TP2AAA, TP2FAA and all DZP's TPstended to be very toxic for *Fish*; TP2 AAA, TP1 DZP and most of PPN's TPs inclined to be very toxic for *Daphnia*; and TP11 FXT and TP16 FXT were very toxic for three test organisms.

The relative toxicity ratio was calculated by the relation between PHCs and TPs formed (LC_{50} ratios (TP/PHC)), table S.3.2 summarizes the results obtained from the ECOSAR and illustrates the potential higher toxicity of some TPs compared to their parent compounds; 7 TPs (TP31 DIP, TP32 DIP, TP2 AAA, TP2 FAA, TP1 DZP, TP20 DZP and TP26 PCT) showed acute toxicity by at least two-fold higher than the parent compound for *fish*, *Daphnia* and *green algae* and most of these TPs were formed by Fe^{3+} -EDDS (1:1), these TPs remained at the final reaction time. On average, the order of susceptibility among the three endpoints by ECOSAR was: *Fish* > *Daphnids* > *Green algae* and the order of susceptibility by T.E.S.T was *Fish* \approx *Daphnids* and no harmful to Oral rat LD_{50} (Table S.3.3; supplementary material).

In this study, the prediction of mutagenicity was performed in the AMES test by T.E.S.T software, the (Q)SAR analysis for mutagenicity resulted in 4 TPs (TP32 DIP, TP2AAA, TP4 PCT and TP32 PPN) with positive mutagenicity prediction, these TPs were formed by both systems Fe^{3+} -EDDS (1:1) and Fe^{3+} -EDDS (1:2) and TP4 PCT with positive mutagenicity prediction were formed and completely degraded in less than 15 minutes of reaction with Fe^{3+} -EDDS (1:2).

The log P values of PHCs and their TPs ranged from -4.33 to 6.61 (Table S.3.4; supplementary material). According to EPA, chemicals should be classified as moderate-high hydrophobic (i.e., $\log P > 4$) or low hydrophobic (i.e., $\log P < 4$), therefore, the substances with a $\log P > 4$ have a high potential for bioaccumulation and/or the high potential to cross biological membranes[44]. According to the values of Log P, the bioconcentration factor (BCF) and bioaccumulation factor (BAF) predictions (Table

S.3.3 and S.3.4; supplementary material), the structures that represent a high potential for accumulation in biological membranes are TP1 DZP, TP11 FXT and PHCs like FXT and PRG.

Conclusions

In this study the effect of Fe^{3+} -EDDS molar ratio in the solar photo-Fenton process is evaluated using a homemade RPR. It has been found that Fe^{3+} -EDDS (1:2) has significant positive degradation results on both PHCs and their TPs at neutral pH. The removal of over 77% of the PHCs was demonstrated. This is mainly due to the presence of EDDS, which can stabilize iron in RHW, preventing its precipitation and with a total consumption of H_2O_2 . Moreover, experiments were performed at $50 \mu\text{g L}^{-1}$ with mild concentration of reactants, values demonstrated a decrease in degradation by at least 1.3-fold lower than high concentrations. Therefore, constituents of RHW affect the action of ROS species at neutral pH with low molar ratio Fe^{3+} -EDDS and $\text{Fe}^{3+}:\text{H}_2\text{O}_2$. Another point evaluated in the present study was in relation to the behavior of TPs during diverse experimental conditions tested. It was evident that Fe^{3+} -EDDS (1: 2) has positive degradation results and much higher than Fe^{3+} -EDDS (1: 1) in relation to the degradation of the identified TPs. Twenty-one TPs identified present characteristics such as hydroxylation of the aromatic ring, cleavage of N-O, N = N, C-F, and C-O bonds as well as hydrogen abstraction. (Q)SARs assessments have shown i) PCA allows a consideration of two principal components (PC1 and PC2) which characterized 88% of the predicted dates; ii) according to the cluster analysis, it is possible to classify two groups characterized by the non-linear model of biodegradability, high bioaccumulation factor and oral toxicity; iii) TPs from DIP, DZP and PCT tend to be more toxic than the parent compound for most endpoints; iv) TP31 DIP and TP32 PPN have prediction as highly mutagenic and v) TP1 DZP and TP11 FXT have the highest bioaccumulation factor. In this context, the treatment process must be conducted, to at least, the point where the most toxic/mutagenic/bioaccumulated TPs can be degraded.

Acknowledgements

Brazilian authors thank CNPq (Process: 403051/2016-9). Elisabeth Cuervo Lumbaque thanks CNPq for her PhD. research grant (Process number 158197/2019-4).

References

- [1] S. Miralles-Cuevas, I. Oller, A. Ruíz-Delgado, A. Cabrera-Reina, L. Cornejo-Ponce, S. Malato, EDDS as complexing agent for enhancing solar advanced oxidation processes in natural water: Effect of iron species and different oxidants, *J. Hazard. Mater.* (2018) 1–8. doi:10.1016/J.JHAZMAT.2018.03.018.
- [2] J. Li, G. Mailhot, F. Wu, N. Deng, Photochemical efficiency of Fe(III)-EDDS complex: OH radical production and 17 β -estradiol degradation, *J. Photochem. Photobiol. A Chem.* 212 (2010) 1–7. doi:10.1016/J.JPHOTOCHEM.2010.03.001.
- [3] Y. Zhang, N. Klammerth, S.A. Messele, P. Chelme-Ayala, M. Gamal El-Din, Kinetics study on the degradation of a model naphthenic acid by ethylenediamine-N,N'-disuccinic acid-modified Fenton process, *J. Hazard. Mater.* 318 (2016) 371–378. doi:https://doi.org/10.1016/j.jhazmat.2016.06.063.
- [4] P. Soriano-Molina, J.L. García Sánchez, O.M. Alfano, L.O. Conte, S. Malato, J.A. Sánchez Pérez, Mechanistic modeling of solar photo-Fenton process with Fe³⁺-EDDS at neutral pH, *Appl. Catal. B Environ.* 233 (2018) 234–242. doi:10.1016/J.APCATB.2018.04.005.
- [5] W.S. Hamd, J. Dutta, Chapter 11 - Heterogeneous photo-Fenton reaction and its enhancement upon addition of chelating agents, in: B. Bonelli, F.S. Freyria, I. Rossetti, R.B.T.-N. for the D. and R. of W.P. Sethi (Eds.), *Micro Nano Technol.*, Elsevier, 2020: pp. 303–330. doi:https://doi.org/10.1016/B978-0-12-818489-9.00011-6.
- [6] Z. Ye, E. Brillas, F. Centellas, P.L. Cabot, I. Sirés, Expanding the application of photoelectro-Fenton treatment to urban wastewater using the Fe(III)-EDDS complex, *Water Res.* 169 (2020) 115219. doi:https://doi.org/10.1016/j.watres.2019.115219.
- [7] S. Papoutsakis, F.F. Brites-gaNóbre, C. Pulgarin, S. Malato, Benefits and limitations of using Fe(III)-EDDS for the treatment of highly contaminated water at near-neutral pH, *J. Photochem. Photobiol. A Chem.* 303–304 (2015) 1–7. doi:10.1016/j.jphotochem.2015.01.013.
- [8] P. Soriano-Molina, P. Plaza-Bolaños, A. Lorenzo, A. Agüera, J.L.G. Sánchez, S. Malato, J.A.S. Pérez, Assessment of solar raceway pond reactors for removal of contaminants of emerging concern by photo-Fenton at circumneutral pH from very different municipal wastewater effluents, *Chem. Eng. J.* 366 (2019) 141–149.
- [9] P. Soriano-Molina, J.L. García Sánchez, S. Malato, L.A. Pérez-Estrada, J.A.

- Sánchez Pérez, Effect of volumetric rate of photon absorption on the kinetics of micropollutant removal by solar photo-Fenton with Fe³⁺-EDDS at neutral pH, *Chem. Eng. J.* 331 (2018) 84–92. doi:10.1016/J.CEJ.2017.08.096.
- [10] E. Cuervo Lumbaqué, D. Salmoria Araújo, T. Moreira Klein, E.R. Lopes Tiburtius, J. Argüello, C. Sirtori, Solar photo-Fenton-like process at neutral pH: Fe(III)-EDDS complex formation and optimization of experimental conditions for degradation of pharmaceuticals, *Catal. Today.* (2019). doi:10.1016/J.CATTOD.2019.01.006.
- [11] S. Malato, P. Fernández-Ibáñez, M.I. Maldonado, J. Blanco, W. Gernjak, Decontamination and disinfection of water by solar photocatalysis: Recent overview and trends, *Catal. Today.* 147 (2009) 1–59. doi:10.1016/J.CATTOD.2009.06.018.
- [12] ISO 6332, Water quality - Determination of iron - Spectrometric method using 1,10-phenanthroline, 1988.
- [13] R.F.P. Nogueira, M.C. Oliveira, W.C. Paterlini, Simple and fast spectrophotometric determination of H₂O₂ in photo-Fenton reactions using metavanadate, *Talanta.* 66 (2005) 86–91. doi:10.1016/J.TALANTA.2004.10.001.
- [14] E. Cuervo Lumbaqué, R.M. Cardoso, A. Dallegrave, L.O. dos Santos, M. Ibáñez, F. Hernández, C. Sirtori, Pharmaceutical removal from different water matrixes by Fenton process at near-neutral pH: Doehlert design and transformation products identification by UHPLC-QTOF MS using a purpose-built database, *J. Environ. Chem. Eng.* 6 (2018) 3951–3961. doi:10.1016/J.JECE.2018.05.051.
- [15] Y. Wu, M. Passananti, M. Brigante, W. Dong, G. Mailhot, Fe (III)–EDDS complex in Fenton and photo-Fenton processes: from the radical formation to the degradation of a target compound, *Environ. Sci. Pollut. Res.* 21 (2014) 12154–12162.
- [16] S. Miralles-Cuevas, I. Oller, J.A.S. Pérez, S. Malato, Removal of pharmaceuticals from MWTP effluent by nanofiltration and solar photo-Fenton using two different iron complexes at neutral pH, *Water Res.* 64 (2014) 23–31. doi:10.1016/j.watres.2014.06.032.
- [17] K.H. Chan, W. Chu, Modeling the reaction kinetics of Fenton's process on the removal of atrazine, *Chemosphere.* 51 (2003) 305–311.
- [18] J.J. Pignatello, E. Oliveros, A. MacKay, Advanced Oxidation Processes for Organic Contaminant Destruction Based on the Fenton Reaction and Related

- Chemistry, *Crit. Rev. Environ. Sci. Technol.* 36 (2006) 1–84. doi:10.1080/10643380500326564.
- [19] N. Klammerth, S. Malato, M.I. Maldonado, A. Agüera, A. Fernández-Alba, Modified photo-Fenton for degradation of emerging contaminants in municipal wastewater effluents, *Catal. Today*. 161 (2011) 241–246. doi:10.1016/J.CATTOD.2010.10.074.
- [20] S. Waclawek, H. V Lutz, K. Grübel, V.V.T. Padil, M. Černík, D.D. Dionysiou, Chemistry of persulfates in water and wastewater treatment: a review, *Chem. Eng. J.* 330 (2017) 44–62.
- [21] S. Miralles-Cuevas, F. Audino, I. Oller, R. Sánchez-Moreno, J.A. Sánchez Pérez, S. Malato, Pharmaceuticals removal from natural water by nanofiltration combined with advanced tertiary treatments (solar photo-Fenton, photo-Fenton-like Fe(III)-EDDS complex and ozonation), *Sep. Purif. Technol.* 122 (2014) 515–522. doi:10.1016/j.seppur.2013.12.006.
- [22] T. Arakaki, C. Anastasio, Y. Kuroki, H. Nakajima, K. Okada, Y. Kotani, D. Handa, S. Azechi, T. Kimura, A. Tsuchioka, A general scavenging rate constant for reaction of hydroxyl radical with organic carbon in atmospheric waters, *Environ. Sci. Technol.* 47 (2013) 8196–8203.
- [23] M.J. Gómez, C. Sirtori, M. Mezcua, A.R. Fernández-Alba, A. Agüera, Photodegradation study of three dipyrone metabolites in various water systems: Identification and toxicity of their photodegradation products, *Water Res.* 42 (2008) 2698–2706. doi:http://dx.doi.org/10.1016/j.watres.2008.01.022.
- [24] A.S. Giri, A.K. Golder, Fenton, photo-fenton, H₂O₂ Photolysis, and TiO₂ Photocatalysis for Dipyrone Oxidation: Drug Removal, Mineralization, Biodegradability, and Degradation Mechanism, *Ind. Eng. Chem. Res.* 53 (2014) 1351–1358. doi:10.1021/ie402279q.
- [25] M. Favier, R. Dewil, K. Van Eyck, A. Van Schepdael, D. Cabooter, High-resolution MS and MSn investigation of ozone oxidation products from phenazone-type pharmaceuticals and metabolites, *Chemosphere*. 136 (2015) 32–41. doi:10.1016/J.CHEMOSPHERE.2015.04.010.
- [26] L.A. Pérez-Estrada, S. Malato, A. Agüera, A.R. Fernández-Alba, Degradation of dipyrone and its main intermediates by solar AOPs, *Catal. Today*. 129 (2007) 207–214. doi:http://dx.doi.org/10.1016/j.cattod.2007.08.008.
- [27] J. Santiago-Morales, A. Agüera, M. del M. Gómez, A.R. Fernández-Alba, J.

- Giménez, S. Esplugas, R. Rosal, Transformation products and reaction kinetics in simulated solar light photocatalytic degradation of propranolol using Ce-doped TiO₂, *Appl. Catal. B Environ.* 129 (2013) 13–29. doi:http://dx.doi.org/10.1016/j.apcatb.2012.09.023.
- [28] S.O. Ganiyu, N. Oturan, S. Raffy, G. Esposito, E.D. van Hullebusch, M. Cretin, M.A. Oturan, Use of Sub-stoichiometric Titanium Oxide as a Ceramic Electrode in Anodic Oxidation and Electro-Fenton Degradation of the Beta-blocker Propranolol: Degradation Kinetics and Mineralization Pathway, *Electrochim. Acta.* 242 (2017) 344–354. doi:10.1016/J.ELECTACTA.2017.05.047.
- [29] L. Szabó, V. Mile, D.J. Kiss, K. Kovács, T. Földes, T. Németh, T. Tóth, R. Homlok, G.T. Balogh, E. Takács, L. Wojnárovits, Applicability evaluation of advanced processes for elimination of neurophysiological activity of antidepressant fluoxetine, *Chemosphere.* 193 (2018) 489–497. doi:10.1016/J.CHEMOSPHERE.2017.11.047.
- [30] Y. Zhao, G. Yu, S. Chen, S. Zhang, B. Wang, J. Huang, S. Deng, Y. Wang, Ozonation of antidepressant fluoxetine and its metabolite product norfluoxetine: Kinetics, intermediates and toxicity, *Chem. Eng. J.* 316 (2017) 951–963. doi:10.1016/J.CEJ.2017.02.032.
- [31] H. Shao, M. Wu, F. Deng, G. Xu, N. Liu, X. Li, L. Tang, Electron beam irradiation induced degradation of antidepressant drug fluoxetine in water matrices, *Chemosphere.* 190 (2018) 184–190.
- [32] I. Carpinteiro, R. Rodil, J.B. Quintana, R. Cela, Reaction of diazepam and related benzodiazepines with chlorine. Kinetics, transformation products and in-silico toxicological assessment, *Water Res.* 120 (2017) 280–289. doi:10.1016/J.WATRES.2017.04.063.
- [33] B. Yang, C. Xu, R.S. Kookana, M. Williams, J. Du, G. Ying, F. Gu, Aqueous chlorination of benzodiazepines diazepam and oxazepam: Kinetics, transformation products and reaction pathways, *Chem. Eng. J.* 354 (2018) 1100–1109. doi:10.1016/J.CEJ.2018.08.082.
- [34] E. Moctezuma, E. Leyva, C.A. Aguilar, R.A. Luna, C. Montalvo, Photocatalytic degradation of paracetamol: Intermediates and total reaction mechanism, *J. Hazard. Mater.* 243 (2012) 130–138. doi:10.1016/J.JHAZMAT.2012.10.010.
- [35] J. Li, Q. Ye, J. Gan, Degradation and transformation products of acetaminophen in soil, *Water Res.* 49 (2014) 44–52.

- doi:<https://doi.org/10.1016/j.watres.2013.11.008>.
- [36] L. Yang, L.E. Yu, M.B. Ray, Degradation of paracetamol in aqueous solutions by TiO₂ photocatalysis, *Water Res.* 42 (2008) 3480–3488. doi:[10.1016/J.WATRES.2008.04.023](https://doi.org/10.1016/J.WATRES.2008.04.023).
- [37] H.N. Phong Vo, G.K. Le, T.M. Hong Nguyen, X.-T. Bui, K.H. Nguyen, E.R. Rene, T.D.H. Vo, N.-D. Thanh Cao, R. Mohan, Acetaminophen micropollutant: Historical and current occurrences, toxicity, removal strategies and transformation pathways in different environments, *Chemosphere.* 236 (2019) 124391. doi:<https://doi.org/10.1016/j.chemosphere.2019.124391>.
- [38] X. Yang, H. Lin, X. Dai, Z. Zhang, B. Gong, Z. Hu, X. Jiang, Y. Li, Sorption, transport, and transformation of natural and synthetic progestins in soil-water systems, *J. Hazard. Mater.* 384 (2020) 121482. doi:<https://doi.org/10.1016/j.jhazmat.2019.121482>.
- [39] C. Muraro, M. Dalla Tiezza, C. Pavan, G. Ribaud, G. Zagotto, L. Orian, Major Depressive Disorder and Oxidative Stress: In Silico Investigation of Fluoxetine Activity against ROS, *Appl. Sci.* 9 (2019) 3631.
- [40] US EPA, EPI Suite™-Estimation Program Interface, (2019). <https://www.epa.gov/tsca-screening-tools/epi-suitetm-estimation-program-interface> (accessed November 3, 2019).
- [41] J. Tunkel, P.H. Howard, R.S. Boethling, W. Stiteler, H. Loonen, Predicting ready biodegradability in the Japanese Ministry of International Trade and Industry test, *Environ. Toxicol. Chem. An Int. J.* 19 (2000) 2478–2485.
- [42] M. Zachary, G.M. Greenway, Comparative PBT screening using (Q)SAR tools within REACH legislation, *SAR QSAR Environ. Res.* 20 (2009) 145–157. doi:[10.1080/10629360902724143](https://doi.org/10.1080/10629360902724143).
- [43] United Nations. Economic Commission for Europe. Secretariat., Globally harmonized system of classification and labelling of chemicals (GHS)., United Nations, 2011.
- [44] USEPA, Development of National Bioaccumulation Factors: Supplemental Information for EPA’s 2015 Human Health Criteria Update, Washington, DC, 2016.

Figures

Figure 1. Effect of molar ratio on the PHCs degradation in solar photo-Fenton ($500 \mu\text{g L}^{-1}$): **a)** $\text{Fe}^{3+}:\text{EDDS}$ (1:1); **c)** $\text{Fe}^{3+}:\text{EDDS}$ (1:2); **b-d)** Consumption profile of $[\text{Fe}^{3+}]_0=15.35 \text{ mg L}^{-1}$ (\bullet), $[\text{H}_2\text{O}_2]_0=230 \text{ mg L}^{-1}$ (\square), PCT (\blacksquare), DIP (\bullet), PPN (\blacktriangle), FXT (\blacktriangledown), DZP (\blacktriangleleft) and PRG (\blacktriangleright).

Figure 2. Degradation of PHCs through solar photo-Fenton ($50 \mu\text{g L}^{-1}$) in $\text{Fe}^{3+}:\text{EDDS}$ (1:1). PCT (\blacksquare), DIP (\bullet), PPN (\blacktriangle), FXT (\blacktriangledown), DZP (\blacktriangleleft) and PRG (\blacktriangleright); **b)** $[\text{Fe}^{3+}]_0=5 \text{ mg L}^{-1}$ (\bullet) and $[\text{H}_2\text{O}_2]_0=50 \text{ mg L}^{-1}$ (\square).

Figure 3. The proposed degradation pathways of selected PHCs **(a)** DIP, **(b)** PPN, **(c)** FXT, **(d)** DZP, **(e)** PCT and **(f)** PRG.

Figure 4. Time profile of TPs in $\text{Fe}^{3+}:\text{EDDS}$ (1:1)

Figure 5. Time profile of TPs in $\text{Fe}^{3+}:\text{EDDS}$ (1:2)

Figure 6. (Q)SAR analysis: **a)** dendrogram by clustering analysis and **b)** PCA plot.

Figure 1

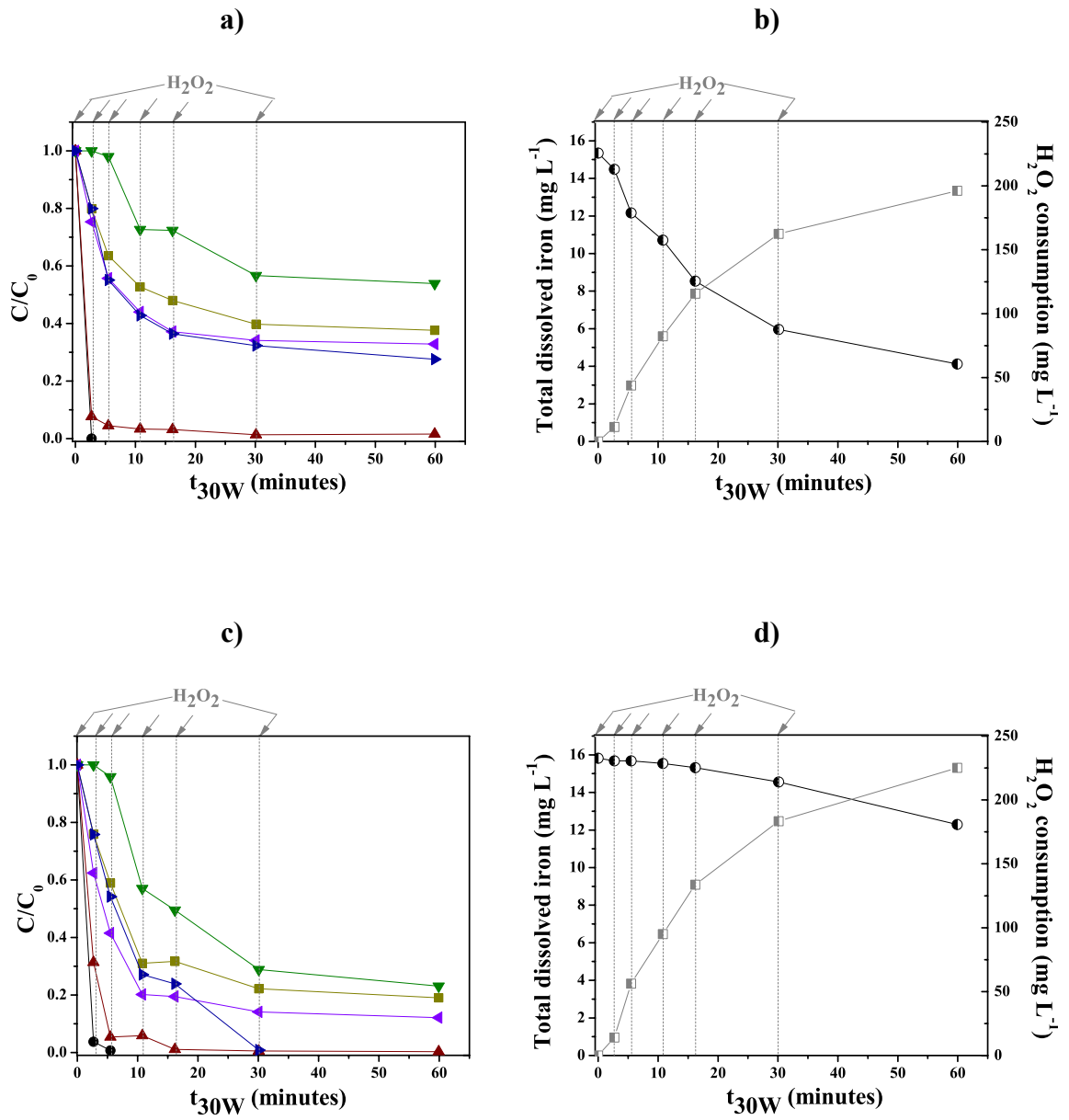


Figure 2

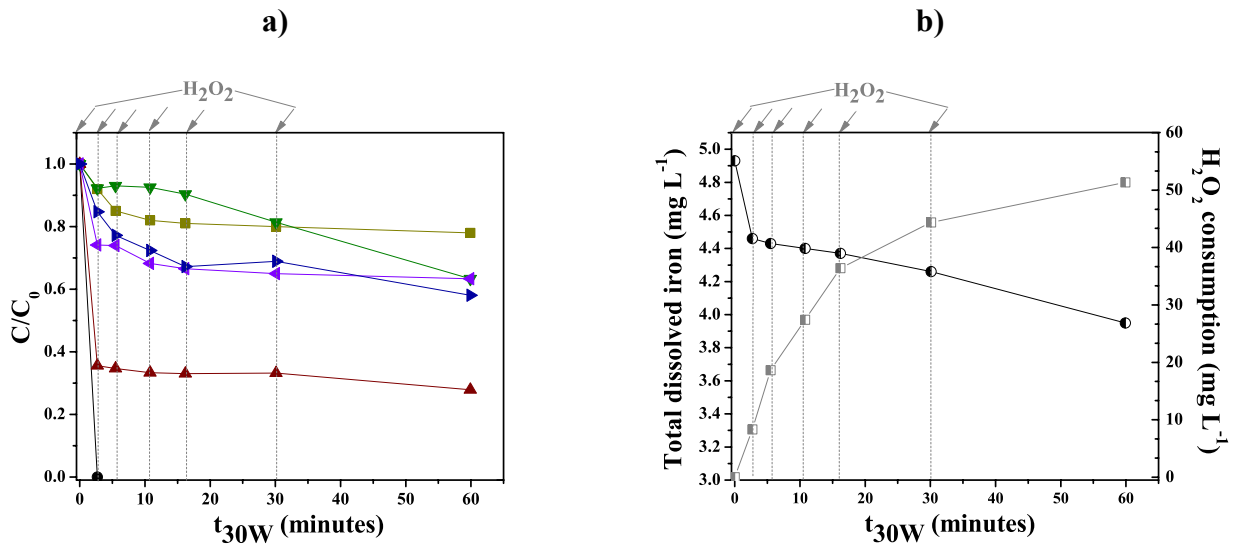
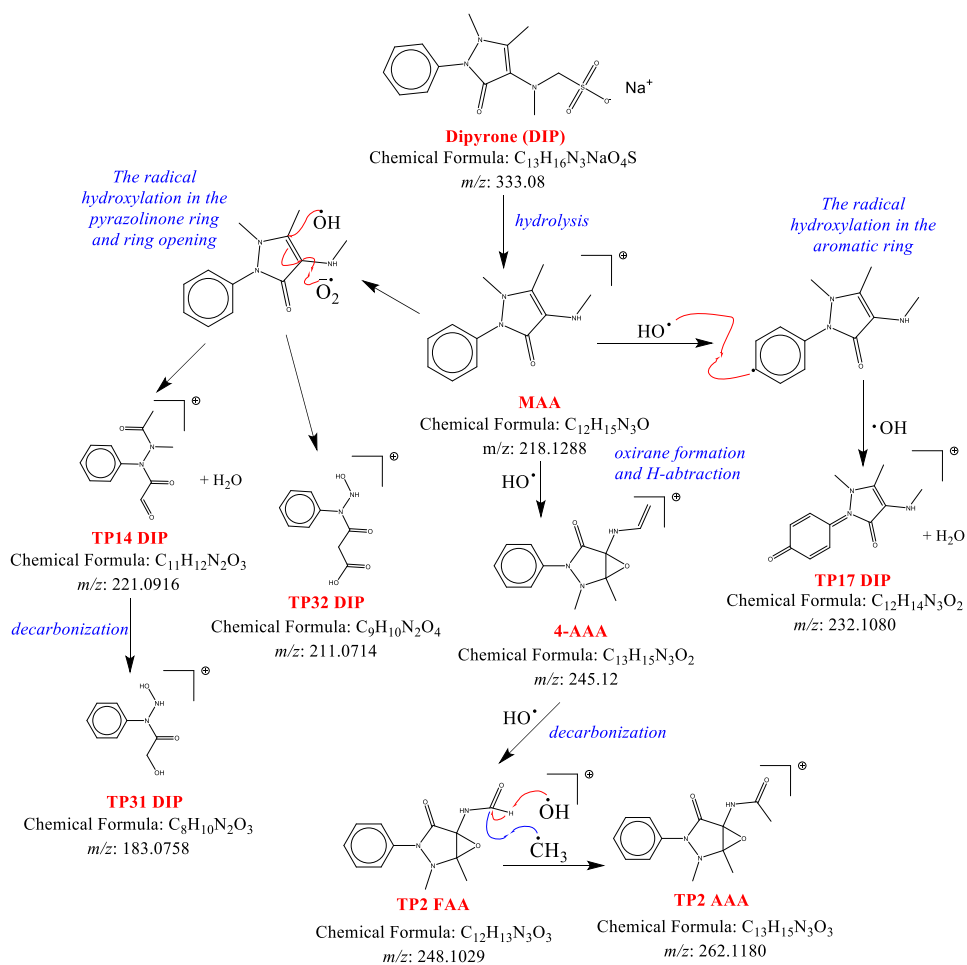
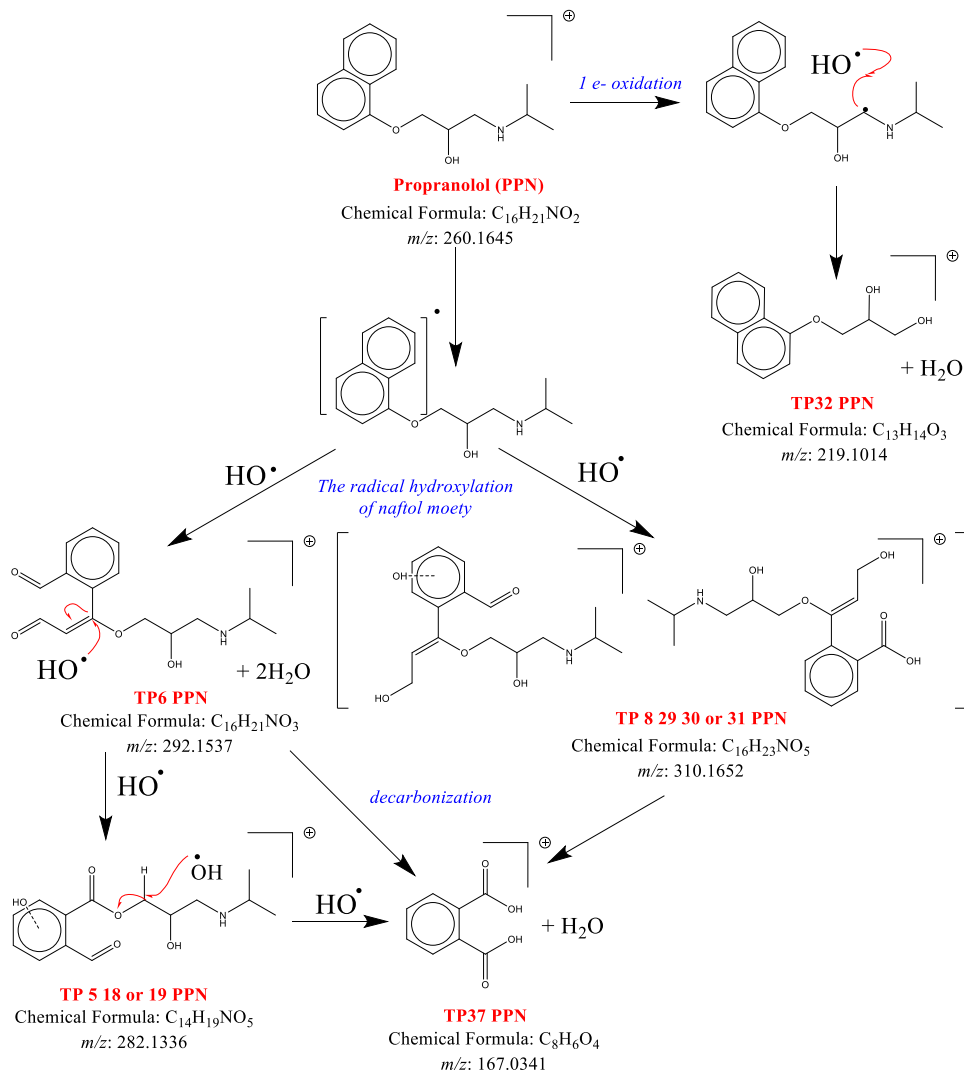


Figure 3

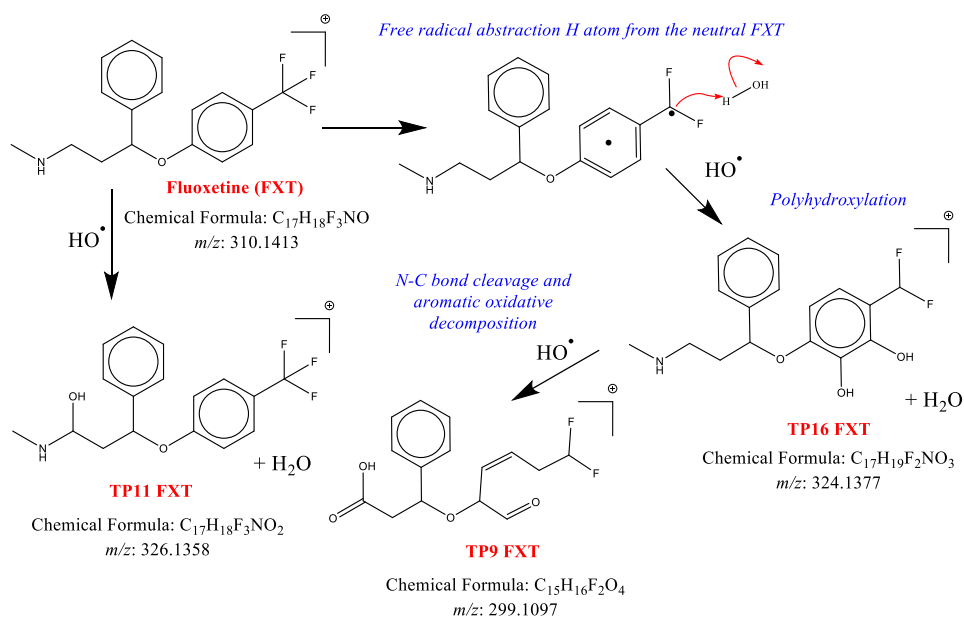
DIP-a)



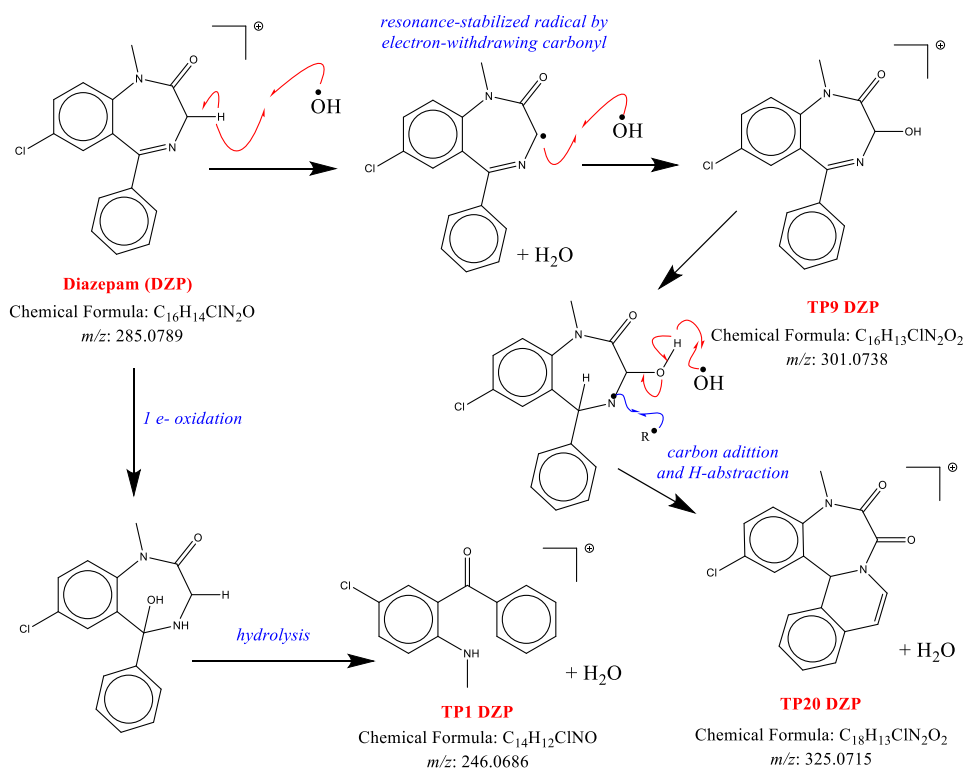
PPN- b)



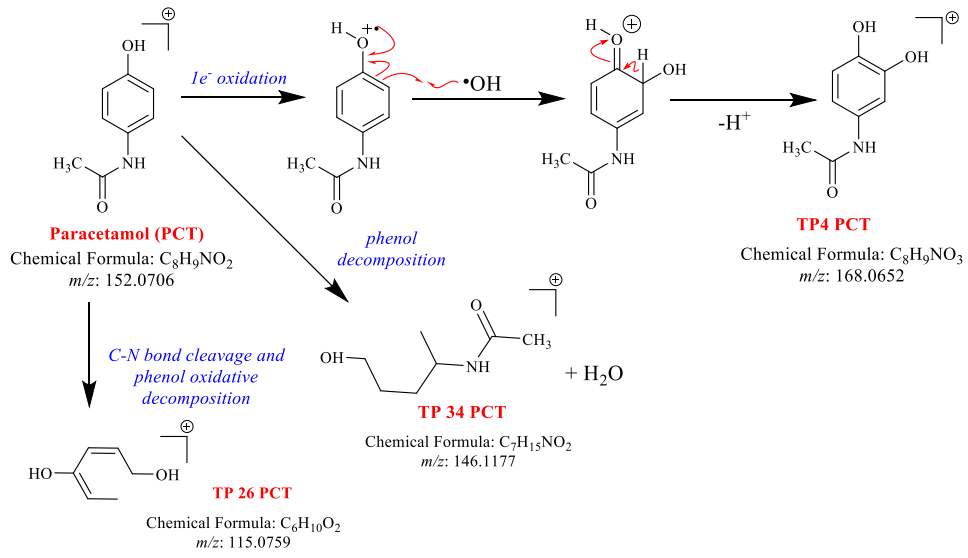
FXT-c)



DZP- d)



PCT-e)



PRG-f)

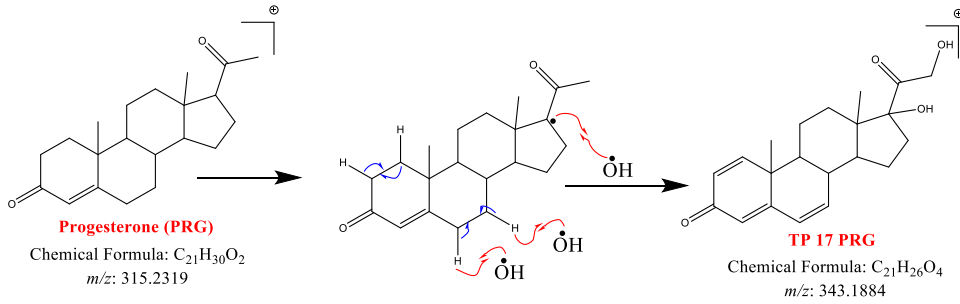


Figure 4

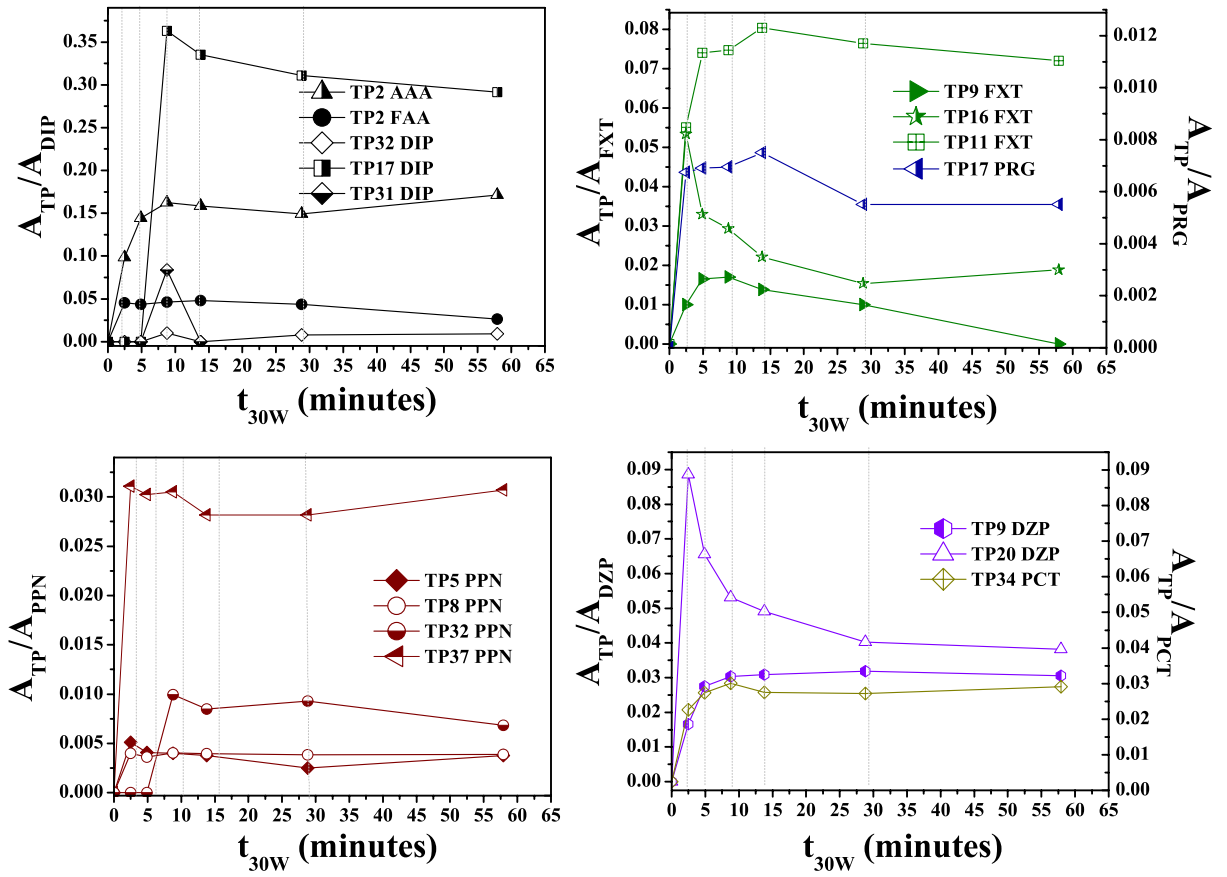


Figure 5

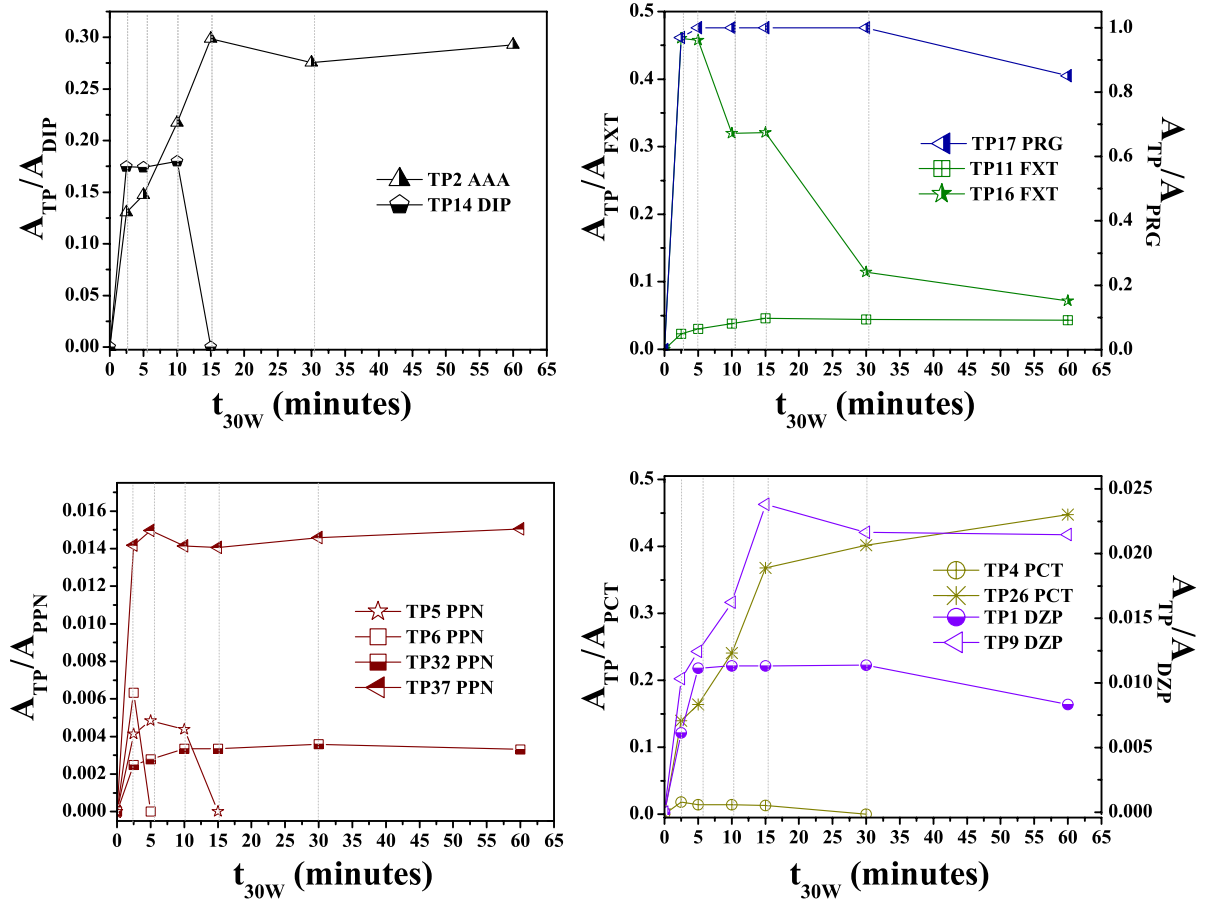
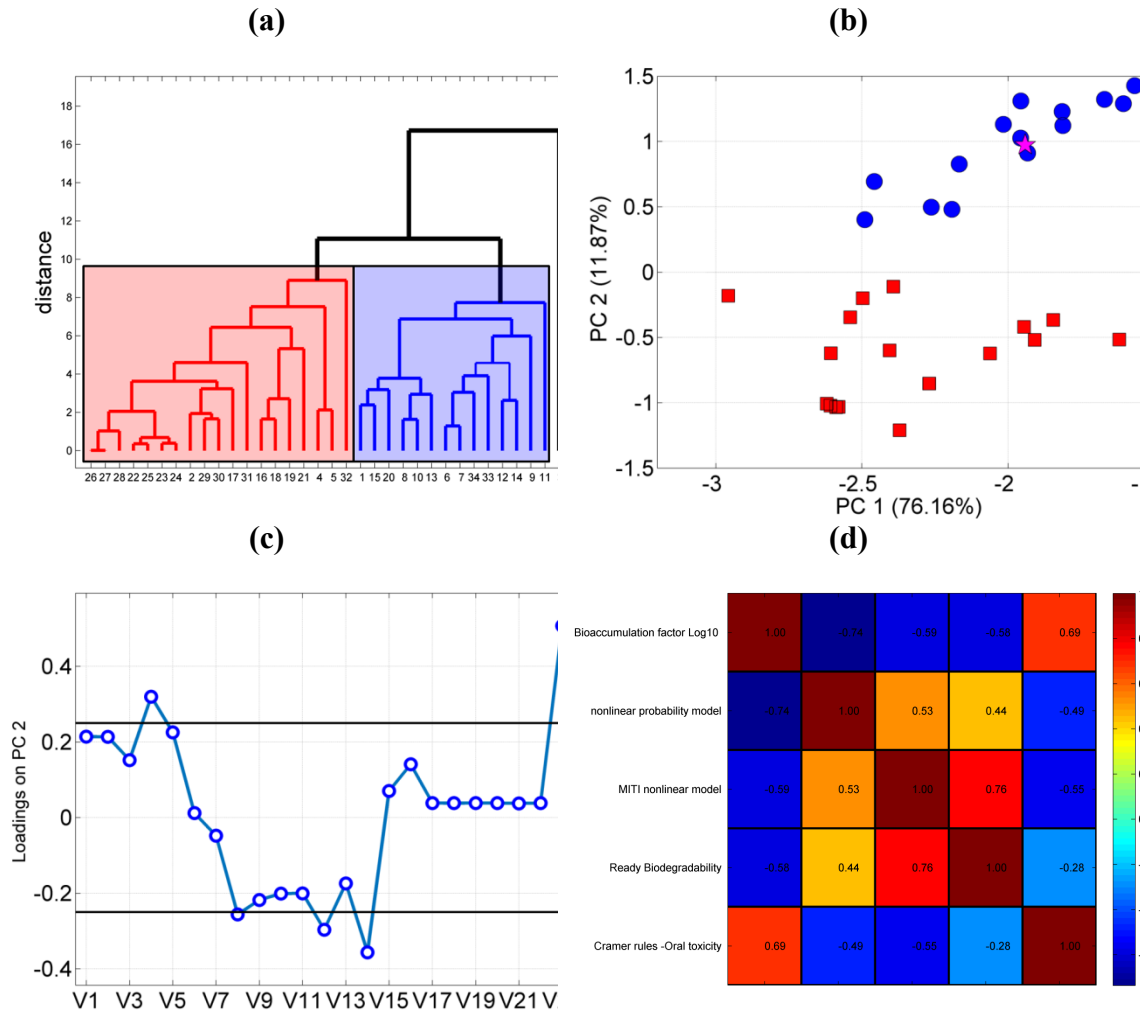


Figure 6



Removal of pharmaceuticals in hospital wastewater by solar photo-Fenton with Fe³⁺-EDDS using a raceway pond reactor homemade: transformation products and *in silico* toxicity assessment

Elisabeth Cuervo Lumbaque^a, Renata M. Cardoso^a, Adriano de Araújo Gomes^a, Sixto Malato^b, José A. Sánchez Pérez^c, Carla Sirtori^{a*}

^a Instituto de Química- Universidade Federal do Rio Grande do Sul, Av. Bento Gonçalves, 9500, Porto Alegre-RS, Brazil.

^b Plataforma Solar de Almería-CIEMAT. Ctra. Senés km 4, 04200 Tabernas (Almería), Spain.

^c Chemical Engineering Department, University of Almería, Ctra. de Sacramento s/n, E-04120 Almería, Spain.

* To whom all correspondence should be addressed

e-mail: carla.sirtori@ufrgs.br (Prof. Carla Sirtori)

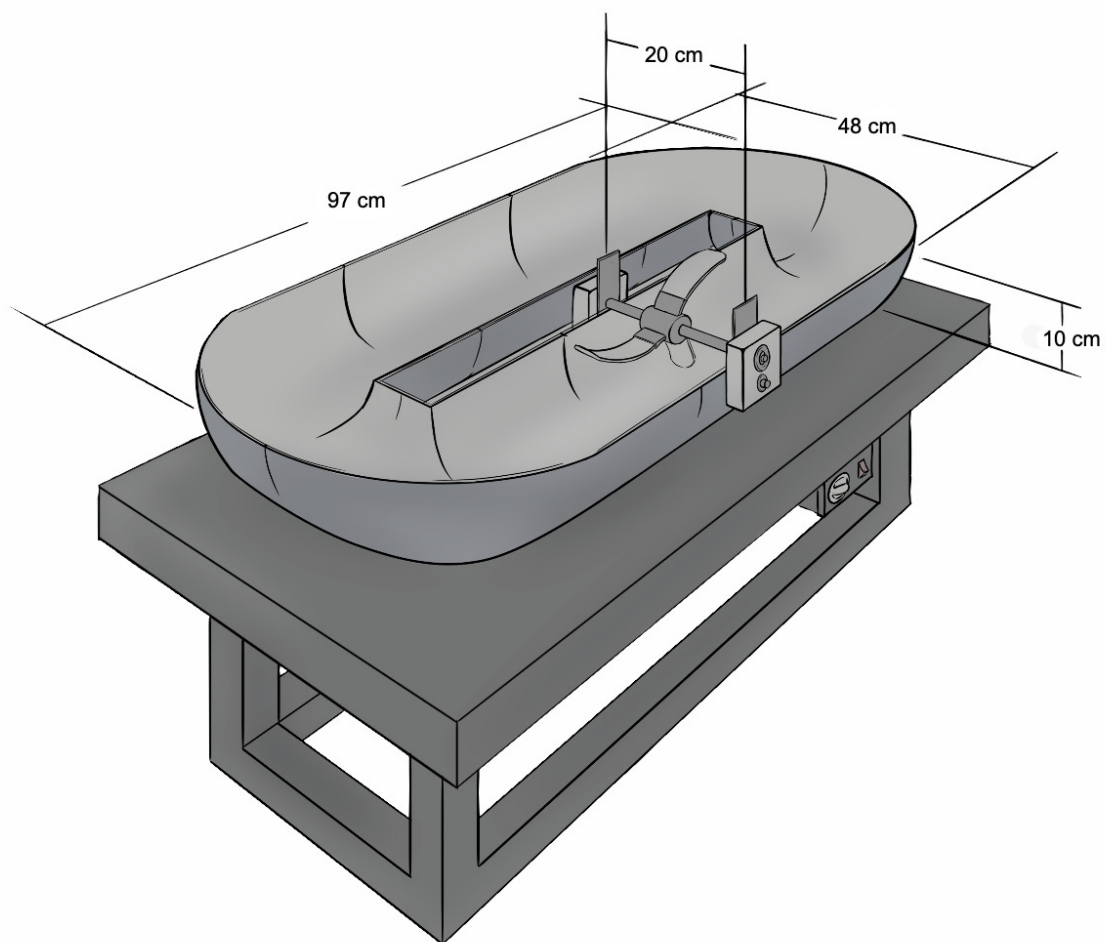


Figure S.1. Homemade raceway pound reactor.

S.1 LC-QTOF MS instrumentation

The LC was equipped with a reverse-phase Hypersil Gold C18 analytical column (2.1 mm × 150 mm × 3 μm). When ionization in positive mode was selected, the mobile phase was a mixture of MeOH acidified with 0.1% formic acid (A) and H₂O acidified with 0.1% formic acid (B) at a flow rate of 0.5 mL/min. In this case, the gradient progressed from 10% A (initial conditions) to 90% A in 10 min, and then maintained for 2 min. The QTOF mass spectrometer was operated in positive ionization mode under the following conditions: capillary 4000 V, nebulizer 40 psi, drying gas 9 L/min, gas temperature 200 °C. In all analyses, the injection volume was 5 μL. The samples injected were previously filtered through a 0.22 μm PVDF filter. The QTOF MS system was operated in broadband collision-induced dissociation (bbCID) acquisition mode that provided MS and MS/MS spectra at the same time. All MS information was recorded over the *m/z* range of 50–1000 with a scan rate of 2 Hz. The bbCID mode allowed for work with two different collision energies: one with a Low Collision Energy (LE) of 10 eV, and a second that applies a High Collision Energy (HE) of 70 eV to obtain MS/MS spectra. TargetAnalysis and DataAnalysis 4.2 software's were employed for analyzes and, in most cases, for ions with a deviation of ±5 ppm of error were assigned possible elemental compositions and double-bond equivalent (RDB).

Limit of detection (LOD) and limit of quantification (LOQ) for each pharmaceutical studied, in RHWW, were determined for the quantification method developed in this study(see Table S.1.1).

Table S.1.1. Parameters for quantification method used to determine pharmaceuticals in different matrixes studied.

Matrix	RHWW			
Pharmaceuticals	LOD ($\mu\text{g L}^{-1}$)	LOQ ($\mu\text{g L}^{-1}$)	Linear range	R²
Paracetamol (PCT)	0.1	0.33	0.25-1000 $\mu\text{g L}^{-1}$	0.9975
Propranolol (PPN)	0.07	0.23	0.25-1000 $\mu\text{g L}^{-1}$	0.9992
Dipyron (DIP)	0.35	1.17	1-1000 $\mu\text{g L}^{-1}$	0.9977
Fluoxetine (FXT)	6.25	20.83	25-750 $\mu\text{g L}^{-1}$	0.9831
Progesterone (PRG)	0.16	0.53	0.5-1000 $\mu\text{g L}^{-1}$	0.9934
Diazepam (DZP)	0.02	0.06	0.1-1000 $\mu\text{g L}^{-1}$	0.9994

S2. Transformation products

Table S.2.1. Accurate mass measurements of TPs identified by LC-QTOFMS using bbCID in positive ionization mode.

Compound	Rt	Ion Mass (<i>m/z</i>)		Error (ppm)	DBE*	Fe ³⁺ :EDDS (1:1)	Fe ³⁺ :EDDS (1:2)
		Ion Formula [M-H] ⁺	Experimental				
TP14 DIP	2.0	C₁₁H₁₃N₂O₃	221.0916	221.0921	2.0	6.5	X
		C ₁₀ H ₁₁ N ₂ O	175.0863	175.0866	1.5	6.5	
		C ₁₀ H ₈ NO	158.0598	158.0600	1.7	7.5	
TP 17 DIP	4.3	C₁₂H₁₄N₃O₂	232.1080	232.1081	0.1	7.5	X
		C ₁₂ H ₁₂ N ₃ O	214.0974	214.0975	0.3	8.5	
		C ₁₁ H ₁₄ N ₃ O	204.1130	204.1131	0.8	6.5	
		C ₈ H ₁₀ NO	136.0760	136.0757	-2.4	4.5	
		C ₃ H ₆ N	56.0495	56.0495	-0.9	1.5	
TP 31 DIP	1.1	C₈H₁₁N₂O₃	183.0758	183.0764	3.3	4.5	X
		C ₈ H ₅ O ₂	133.0278	133.0284	4.7	6.5	
TP 32 DIP	1.0	C₉H₁₁N₂O₄	211.0714	211.0713	-0.4	5.5	X
		C ₈ H ₁₁ N ₂ O ₃	183.0761	183.0764	1.9	4.5	
		C ₇ H ₁₁ N ₂ O ₂	155.0814	155.0815	0.8	3.5	
		C ₅ H ₉ N ₂ O	113.0709	113.0709	0.2	2.5	
TP2 AAA	3.9	C₁₃H₁₆N₃O₃	262.1180	262.1186	2.2	7.5	X
		C ₁₃ H ₁₄ N ₃ O ₂	244.1081	244.1081	-0.3	8.5	
		C ₁₁ H ₁₄ N ₃ O ₂	220.1076	220.1081	2.0	6.5	
		C ₁₁ H ₁₂ N ₃ O	202.0976	202.0975	-0.6	7.5	
TP2 FAA	3.7	C₁₂H₁₄N₃O₃	248.1029	248.1030	0.4	7.5	X
		C ₆ H ₆ NO	108.0441	108.0444	2.5	4.5	
TP1 DZP	6.8	C₁₄H₁₃ClNO	246.0686	246.0680	-2.4	8.5	X
		C ₁₄ H ₁₁ ClN	228.0575	228.0575	-0.3	9.5	
TP9 DZP	6.6	C₁₆H₁₄ClN₂O₂	301.0738	301.0738	0.1	10.5	X
		C ₁₅ H ₁₄ ClN ₂ O	273.0789	273.0789	0.1	9.5	
TP20 DZP	6.9	C₁₈H₁₄ClN₂O₂	325.0715	325.0738	7.3	12.5	X
		C ₁₆ H ₁₆ ClN ₂ O ₂	303.0889	303.0895	1.9	9.5	
		C ₁₆ H ₁₃ ClNO ₂	286.0620	286.0629	3.3	10.5	
		C ₁₄ H ₁₁ ClN	228.0571	228.0575	1.5	9.5	
		C ₇ H ₅ O	105.0334	105.0335	1.0	5.5	
TP 9 FXT	6.2	C₁₅H₁₇F₂O₄	299.1097	299.1089	-2.6	6.5	X
		C ₄ H ₇ O ₂	87.0441	87.0441	-0.6	1.5	
TP 11 FXT	7.4	C₁₇H₁₉F₃NO₂	326.1358	326.1362	1.3	7.5	X
		C ₁₀ H ₁₁ O ₂	163.0754	163.0754	-0.2	5.5	
TP16 FXT	4.4	C₁₇H₂₀F₂NO₃	324.1377	324.1406	8.9	7.5	X
		C ₇ H ₆ N	104.0496	104.0495	-1.2	5.5	
TP 26 PCT	5.5	C₆H₁₁O₂	115.0759	115.0754	-4.8	1.5	X
		C ₄ H ₇ O	71.0492	71.0491	-0.6	1.5	
TP4 PCT	1.6	C₈H₁₀NO₃	168.0652	168.0655	1.9	4.5	X
		C ₈ H ₁₀ NO	136.0753	136.0757	2.6	4.5	
TP34 PCT	0.8	C₇H₁₆NO₂	146.1177	146.1176	-1.0	0.5	X
		C ₇ H ₈ NO ₂	138.0550	138.0550	-0.5	4.5	
		C ₆ H ₁₆ NO ₂	134.1181	134.1176	-4.1	-0.5	
TP6 PPN	4.6	C₁₆H₂₂NO₄	292.1537	292.1543	2.1	6.5	X
		C ₈ H ₇	103.0389	103.0390	0.7	1.5	
TP5,18,19	4.0	C₁₄H₂₀NO₅	282.1336	282.1336	0.0	5.5	X

PPN							
		C ₆ H ₁₄ NO	116.1067	116.1070	2.2	0.5	
TP8, 29-31	1.3	C₁₆H₂₄NO₅	310.1652	310.1649	-1.0	5.5	X
		C ₆ H ₈ NO	110.0601	110.0600	-0.7	3.5	
		C ₆ H ₆ NO	108.0444	108.0444	-0.5	4.5	
		C ₆ H ₆ N	92.0496	92.0495	-1.2	4.5	
TP32 PPN	10.2	C₁₃H₁₅O₃	219.1014	219.1016	0.9	6.5	X
		C ₈ H ₅ O ₃	149.0232	149.0233	1.1	6.5	
TP37 PPN	11.3	C₈H₇O₄	167.0341	167.0339	-1.5	5.5	X
		C ₈ H ₅ O ₃	149.0236	149.0233	-1.6	6.5	
TP17 PRG	10.5	C₂₁H₂₇O₄	343.1884	343.1904	5.9	8.5	X
		C ₉ H ₇ O ₃	163.0393	163.0390	-2.0	6.5	
		C ₆ H ₁₃ O ₃	133.0860	133.0859	-0.7	0.5	

*double bond equivalents (DBE)

S3 (Q)SAR tools

Table S.3.1 SMILES of PHCs and TPs identified in the solar photo-Fenton process

	SMILES
DIP	<chem>O=C1N(C2=CC=CC=C2)N(C)C(C)=C1NC</chem>
TP14 DIP	<chem>CN(N(C(=O)C=O)c1ccccc1)C(C)=O</chem>
TP 17 DIP	<chem>CNC=1C(=O)\[N+](=C2/C=CC(=O)C=C2)N(C)C=1C</chem>
TP 31 DIP	<chem>ONN(C(=O)CO)c1ccccc1</chem>
TP 32 DIP	<chem>ONN(C(=O)CC(=O)O)c1ccccc1</chem>
TP2 AAA	<chem>O=C(C)NC12OC2(C)N(C)N(C1=O)c1ccccc1</chem>
TP2 FAA	<chem>O=CNC12OC2(C)N(C)N(C1=O)c1ccccc1</chem>
DZP	<chem>ClC1=CC=C2C(C(C3=CC=CC=C3)=NCC(N2C)=O)=C1</chem>
TP1 DZP	<chem>CNc1ccc(Cl)cc1C(=O)c1ccccc1</chem>
TP9 DZP	<chem>Clc1ccc2c(c1)C(=NC(O)C(=O)N2C)c1ccccc1</chem>
TP20 DZP	<chem>Clc1cc2CC=CN3c2c(c1)C(=NC(O)C3=O)c1ccccc1</chem>
FXT	<chem>FC(F)(F)C1=CC=C(OC(CCNC)C2=CC=CC=C2)C=C1</chem>
TP 9 FXT	<chem>Oc1ccc(cc1O)C(CC)OC(/C=C\C(F)F)C=O</chem> <chem>Oc1cc(cc(O)c1)C(CC)OC(/C=C\C(F)F)C=O</chem>
TP 11 FXT	<chem>FC(F)(F)c1ccc(OC(CC(O)NC)c2ccccc2)cc1</chem>
TP16 FXT	<chem>Oc1c(O)c(ccc1OC(CCNC)c1ccccc1)C(F)F</chem> <chem>Oc1c(cccc1O)C(CCNC)Oc1ccc(cc1)C(F)F</chem> <chem>Oc1cc(O)ccc1C(Oc1ccc(cc1)C(F)F)CCNC</chem> <chem>Oc1ccc(O)cc1C(Oc1ccc(cc1)C(F)F)CCNC</chem>
PCT	<chem>CC(NC1=CC=C(O)C=C1)=O</chem>
TP 26 PCT	<chem>OC1=CC(O)CCC1</chem> <chem>OC1C=CC(O)CC1</chem> <chem>OC1C=CCCC1O</chem>
TP 4PCT	<chem>Oc1cc(O)ccc1NC(C)=O</chem> <chem>Oc1ccc(NC(C)=O)cc1O</chem>
TP34 PCT	<chem>OC(=O)Nc1ccccc1</chem>
PPN	<chem>OC(CNC(C)C)COC1=CC=CC2=CC=CC=C21</chem>
TP6 PPN	<chem>O=Cc1ccccc1C(=C\C=O)/OCCCNC(C)C</chem>
TP 5,18,19 PPN	<chem>Oc1ccccc(C=O)c1C(=O)OCC(O)CNC(C)C</chem> <chem>O=Cc1ccc(O)cc1C(=O)OCC(O)CNC(C)C</chem> <chem>Oc1cc(C=O)c(cc1)C(=O)OCC(O)CNC(C)C</chem> <chem>O=Cc1c(cccc1O)C(=O)OCC(O)CNC(C)C</chem>
TP 8, 29-31 PPN	<chem>O=Cc1ccccc1C(=C\CO)\OCC(O)CNC(C)C</chem> <chem>O=Cc1ccccc1C(=C\CO)\OCC(O)CNC(C)C</chem> <chem>O=Cc1ccccc1C(=C\CO)\OCC(O)CNC(C)C</chem> <chem>O=Cc1ccccc1C(=C\CO)\OCC(O)CNC(C)C</chem> <chem>OC(=O)c1ccccc1C(=C\CO)\OCC(O)CNC(C)C</chem>
TP 32 PPN	<chem>OCC(O)COc1ccc2ccccc21</chem>
TP37 PPN	<chem>OC(=O)c1ccccc1C(=O)O</chem>
PRG	<chem>O=C1C=C2CCC3C(CCC4C(C)=O)C4(C)CCC3C2(C)CC1</chem>
TP17 PRG	<chem>OCC(=O)C1(O)CC[C@H]2[C@@H]3C=CC4=CC(=O)C=C[C@]4(C)[C@H]3CC[C@]21C</chem>

Table S.3.2 ECOSAR -toxicity endpoints

Compound	Organic module	Acute toxicity (mg L ⁻¹)			Chronic toxicity (ChV) (mg L ⁻¹)			LC ₅₀ ratios (TP/PHC)		EC ₅₀ ratios (TP/PHC)
		Fish 96h-LC ₅₀	Daphnid 48h-LC ₅₀	Green algae 96h-EC ₅₀	Fish 96h-LC ₅₀	Daphnid 48h-LC ₅₀	Green algae 96h-EC ₅₀	Fish 96h	Daphnid 48h	Green algae 96h
DIP	Aliphatic amines	474	46.9	56.0	48.8	3.21	16.3	1	1	1
TP14 DIP	Aldehydes (mono)	735	950	372	640	5.31	82.2	1.55	20.26	6.64
TP 17 DIP	Aliphatic amines	1.81E+7	7.98E+5	4.69E+6	2.17E+7	2.5E+4	7.62E+5	38185.65	17014.93	83750.00
TP 31 DIP	Hydrazines	10.3	8.53	3.0	36	5.15	288	0.02	0.18	0.05
TP 32 DIP	Hydrazines	141	109	38.2	52.5	71.5	3.61	0.30	2.32	0.68
TP2 AAA	Epoxide	4.35	6.49	5.05	0.0060	0.619	5.45	0.01	0.14	0.09
TP2 FAA	Epoxide	7.24	12.6	10.9	0.0081	1.21	10.1	0.02	0.27	0.19
DZP	Amides	22.6	19.8	3.55	0.402	4.24	3.08	1	1	1
TP1 DZP	Neutral organics	1.99	1.39	2.42	0.248	0.24	1	0.09	0.07	0.68
TP9 DZP	Amides	64.2	61.1	8.23	0.895	10.7	5.61	2.84	3.09	2.32
TP20 DZP	Amides	19.3	16.5	3.21	0.368	3.75	3.0	0.85	0.83	0.90
FXT	Aliphatic amines	1.08	0.175	0.79	0.25	0.19	0.33	1	1	1
TP 9 FXT	Aliphatic amines	29.2	73.2	52.3	1.62	7.27	38	27.04	418.29	66.20
	Aliphatic amines	29.3	73.3	52.4	1.63	7.28	39	27.13	418.86	66.33
TP 11 FXT	Aliphatic amines	11.7	1.58	1.01	0.458	0.147	0.37	10.83	9.03	1.28
TP16 FXT	Aliphatic amines	17.9	2.34	1.60	0.776	0.211	0.57	16.57	13.37	2.03
	Aliphatic amines	12.1	1.64	1.05	0.481	0.152	0.38	11.20	9.37	1.33
	Aliphatic amines	12.1	1.64	1.05	0.481	0.152	0.38	11.20	9.37	1.33
	Aliphatic amines	12.1	1.64	1.05	0.481	0.152	0.38	11.20	9.37	1.33
PCT	Phenols	320	63.3	26.3	26.5	5.12	37	1	1	1
TP 26 PCT	Vinyl/Allyl/Alcohols	4.40	13	0.429	3.02	1.11	3.20	0.01	0.21	0.02
	Vinyl/Allyl/Alcohols	6.82	21.8	0.798	8.08	2.49	6.28	0.02	0.34	0.03
	Vinyl/Allyl/Alcohols	6.82	21.8	0.798	8.08	2.49	6.28	0.02	0.34	0.03
TP 4PCT	Amides	1.31E+3	1.7E+3	81.5	7.63	142	22.9	4.09	26.86	3.10
	Amides	2.48E+3	3.38E+3	135	12.3	248	32.4	7.75	53.40	5.13
TP34 PCT	Neutral organics	3.17e+3	1.55E+3	624	260	99.9	117	9.91	24.49	23.73
PPN	Aliphatic amines	20.2	2.58	1.85	0.95	0.23	0.65	1	1	1
TP6 PPN	Aliphatic amines	81.8	9.43	8.31	5.28	0.75	2.69	4.05	3.66	4.49
TP 5,18,19 PPN	Aldehydes (mono)	24.7	23.2	13.2	4.12	0.245	4.92	1.22	8.99	7.14

TP 8, 29-31 PPN	Aldehydes (mono)	48	48	25	10.9	0.45	8.63	2.38	18.60	13.51
	Aldehydes (mono)	48	48	25	10.9	0.45	8.63	2.38	18.60	13.51
	Aldehydes (mono)	20.5	18.9	10.9	3.14	0.206	4.21	1.01	7.33	5.89
	Aldehydes (mono)	82.9	86.4	43.5	23.5	0.743	13.7	4.10	33.49	23.51
	Aldehydes (mono)	82.9	86.4	43.5	23.5	0.743	13.7	4.10	33.49	23.51
	Aldehydes (mono)	82.10	86.5	43.6	23.6	1.743	13.8	4.06	33.53	23.57
	Aldehydes (mono)	82.11	86.6	43.7	23.7	2.743	13.9	4.06	33.57	23.62
TP 32 PPN	Aliphatic amines	6.43E+03	638	756	654	243.9	220	318.32	247.29	408.65
	Neutral organics	167	94.9	71.7	16.4	9.34	18.9	8.27	36.78	38.76
TP37 PPN	Neutral organics	9.32E+3	4.86E+1	2.54E+3	824	373	549	461.39	18.84	1372.97
PRG	Vinyl/Allyl/Alcohols	17.1	6.78	5.57	2.53	1.48	3.63	1	1	1
TP17 PRG	Vinyl/Allyl/Alcohols	97.8	51.9	35.4	21.5	9.26	15.5	5.72	7.65	6.36

*Globally Harmonized System of Classification and Labelling of Chemicals, which is given by $LC_{50}/EC_{50}/ChV \leq 1$ (very toxic), $1 > LC_{50}/EC_{50}/ChV \leq 10$ (toxic), $10 > LC_{50}/EC_{50}/ChV \leq 100$ (harmful) and $LC_{50}/EC_{50}/ChV > 100$ (no harmful).

**More toxic in relation with the parent compound: very toxic and toxic

Table S.3.3. T.E.S.T – toxicity, bioaccumulation and mutagenicity endpoints

T.E.S.T SOFTWARE						
	Fathead minnow LC ₅₀ (96 hr) -Log10(mol/L)	Daphnia magna LC ₅₀ (48 hr) -Log10(mol/L)	Oral rat LD ₅₀ - Log10(mol/kg)	Bioaccumulation factor Log10 (BAF)	Predicted Developmental Toxicity	Predicted Mutagenicity
DIP	4.20	4.13	2.25	0.63	0.71	0.45
TP14 DIP	3	3.33	2.23	-0.01	0.87	0.29
TP 17 DIP	4.03	3.78	2.33	0.06	1.01	0.41
TP 31 DIP			2.07	-0.04	0.60	0.42
TP 32 DIP			1.91	0.03	0.67	0.82
TP2 AAA	5.47	4.89	2.31	1.40	0.98	0.53
TP2 FAA	4.75	4.76	2.62	1.00	1.02	0.46
DZP	5.77	4.87	1.66	1.43	0.83	-0.01
TP1 DZP	4.96	5.28	1.96	1.87	0.68	0.44
TP9 DZP	6.17	4.55	2.19	1.16	0.95	0.03
TP20 DZP	6.32	4.89	2.31	1.57	0.91	0.17
FXT	5.88	5.44	2.49	2.39	0.80	0.13
TP 9 FXT	5.37	5.13	2.02		0.89	-0.06
	5.37	5.15	2.17		0.82	-0.02
TP 11 FXT	6	4.86	2.29	2.00	0.93	0.13
TP16 FXT	5.92	4.91	2.63	1.36	0.81	0.24
	6.41	5.35	2.73	1.28	0.88	0.21
	5.85	5.33	2.48	1.36	0.93	0.30
	6.41	5.09	2.68	1.53	0.82	0.20
PCT	3.27	3.60	1.92	0.50	0.52	0.43
TP 26 PCT	2.28	2.77	1.71	0.50	0.58	0.23
	2.49	3.08	2.09	0.94	0.65	0.14
	2.54	3.00	1.80	0.60	0.74	0.49
TP4 PCT	3.35	3.95	1.77	0.34	0.29	0.57
	3.17	3.94	1.91	0.03	0.33	0.58
TP34 PCT	3.27	3.49	2.10	0.20	0.54	0.21
PPN	4.13	4.33	2.16	1.59	0.79	0.21
TP6 PPN	4.87	3.86			0.68	0.44

TP 5, 18, 19 PPN	4.32	3.92	2.07		0.76	0.21
	4.65	3.79	2.03		0.71	0.19
	4.67	3.89	2.03		0.71	0.11
	4.57	3.83	2.00		0.80	0.19
TP 8, 29-31 PPN	3.98	3.40	1.95		0.70	0.11
	3.98	3.40	1.95		0.70	0.11
	3.98	3.40	1.95		0.70	0.11
	3.98	3.40	1.95		0.70	0.11
	3.74	3.02	2.36	0.47	0.74	0.09
TP 32 PPN	4.06	3.53	2.36	1.00	0.99	0.80
TP37 PPN	3.64	3.40	1.49	-0.17	0.53	0.35
PRG	5.31	4.44	2.47	2.06	0.96	-0.05
TP17 PRG	5.09	4.23	3.23	1.43	0.94	0.29

*Classification adapted from Globally Harmonized System of Classification and Labelling of Chemicals for: very toxic, toxic, harmful and no harmful.

**High bioaccumulation factor

***Mutagenicity: very mutagenic and mutagenic

Table S.3.4. EPI Suite™ and TOXTREE endpoint

	BIOWIN- EPI Suite™							EPI Suite™			TOXTREE
	Model 1	Model 2	Model 3	Model 4	Model 5	Model 6	Model 7	Ready Biodegradability	Log P	BCF	Cramer rules
DIP	0.9260	0.9444	2.7655	3.5824	0.1414	0.0332	0.5157	NO	0.39	0.06	3
TP14 DIP	1.0554	0.9999	2.7568	3.7215	0.5103	0.3896	0.5405	YES	-1.64	-0.49	3
TP 17 DIP	0.6433	0.3193	2.6612	3.4890	0.1526	0.0498	-0.5263	NO	-4.33	-0.49	3
TP 31 DIP	0.9476	0.9657	2.9786	3.7192	0.0488	0.0	0.7359	NO	-0.99	-0.48	1
TP 32 DIP	0.8483	0.9217	3.1213	3.9349	-0.014	0.0	0.7899	NO	-1.17	-0.48	1
TP2 AAA	0.2462	0.0437	2.1567	3.3645	0.2405	0.0583	-1.1552	NO	3.43	1.82	3
TP2 FAA	0.2529	0.0528	2.1877	3.3847	0.2818	0.0835	-1.0756	NO	2.98	1.43	3
DZP	0.7678	0.8085	2.3311	3.4819	0.0837	0.0217	-0.8789	NO	2.82	1.76	3
TP1 DZP	0.3493	0.0449	2.3142	3.2022	0.0135	0.0148	-0.8607	NO	4.23	2.502	3
TP9 DZP	0.9189	0.9114	2.4557	3.5883	0.1900	0.0257	-0.5867	NO	2.19	1.16	3
TP20 DZP	0.9622	0.9287	2.3278	3.4851	0.0665	0.0106	-0.6805	NO	2.86	1.53	3
FXT	0.4937	0.1305	1.9910	3.2523	0.2360	0.0001	0.5562	NO	3.82	2.68	3
TP 9 FXT	0.7735	0.9868	2.6619	3.6808	0.4200	0.0001	0.1033	NO	2.21	0.64	3
	0.7735	0.9868	2.6619	3.6808	0.4200	0.0001	0.1033	NO	2.21	0.64	3
TP 11 FXT	0.6448	0.2679	2.1156	3.3587	0.2494	0.0	0.4971	NO	6.61	2.02	3
TP16 FXT	1.2391	0.9955	2.5857	3.5859	0.2792	0.0	0.9416	NO	2.82	0.81	3
	1.2391	0.9955	2.5857	3.5859	0.2792	0.0	0.9416	NO	3.08	1.41	3
	1.1110	0.9732	2.5637	3.5810	0.2792	0.0	0.7234	NO	3.08	1.41	3
	1.1110	0.9732	2.5637	3.5810	0.2792	0.0	0.7234	NO	3.08	1.41	3
PCT	1.0015	0.9886	2.8673	3.8748	0.4866	0.5090	-0.1124	NO	0.43	-0.007	1
TP 26 PCT	1.0107	0.9740	3.2669	3.9420	0.7727	0.8638	0.7075	YES	0.94	0.18	3
	1.0107	0.9740	3.2669	3.9420	0.7716	0.8190	0.7934	YES	0.29	0.006	2
	1.0107	0.9740	3.2669	3.9420	0.7716	0.8190	0.7934	YES	0.29	0.006	2
TP4 PCT	1.1097	0.9942	2.8883	3.8914	0.4950	0.4856	0.0638	NO	0.14	-0.036	1
	1.1097	0.9942	2.8883	3.8914	0.4950	0.4856	0.0638	NO	-0.21	-0.042	1
TP34 PCT	0.8103	0.9459	2.9181	3.6548	0.3452	0.3031	0.5771	NO	0.39	0.018	1
PPN	1.1097	0.9942	2.8883	3.8914	0.4950	0.4856	0.0638	NO	3.48	2.39	3
TP6 PPN	0.9922	1	2.6511	3.8773	0.8880	0.8036	0.2990	NO	1.71	0.79	1
TP 5, 18, 19 PPN	1.5008	1	2.9808	4.0799	0.9120	0.8654	0.7961	YES	1.67	0.35	1
	1.5008	1	2.9808	4.0799	0.9120	0.8654	0.7961	YES	1.06	0.007	1
	1.5008	1	2.9808	4.0799	0.9120	0.8654	0.7961	YES	1.06	0.007	1

	1.5008	1	2.9808	4.0799	0.9120	0.8654	0.7961	YES	1.84	0.49	1
TP 8, 29-31 PPN	1.0164	0.9974	2.9089	3.9136	0.6946	0.5134	0.27621	YES	0.60	0.11	1
	1.0164	0.9974	2.9089	3.9136	0.6946	0.5134	0.2761	YES	0.60	0.11	1
	1.0164	0.9974	2.9089	3.9136	0.6946	0.5134	0.2761	YES	0.60	0.11	2
	1.0164	0.9974	2.9089	3.9136	0.6946	0.5134	0.2761	YES	0.60	0.11	3
	0.9011	0.7220	2.9391	3.7016	0.6126	0.3303	0.4191	YES	0.53	0.048	3
TP 32 PPN	1.0930	0.9878	2.9787	3.8689	0.6860	0.7606	0.4977	YES	2.04	1.01	3
TP37 PPN	1022	0.9959	3.0078	3.6235	1.0047	0.9569	0.9855	YES	0.73	0.12	1
PRG	0.2436	0.0030	2.0350	3.0427	0.3623	0.0674	-1.7307	NO	3.87	2.65	3
TP17 PRG	0.2051	0.0011	1.9211	2.9784	0.4903	0.0892	-1.6801	NO	2.72	1.552	3

*High bioaccumulation factor

Table S.3.5 Codes assigned to pharmaceuticals and TPs for clustering analysis

	Compound or TP	Code
1	DIP	2
2	TP14 DIP	1
3	TP 17 DIP	3
4	TP 31 DIP	1
5	TP 32 DIP	1
6	TP2 AAA	2
7	TP2 FAA	2
8	DZP	2
9	TP1 DZP	2
10	TP9 DZP	2
11	TP20 DZP	2
12	FXT	2
13	TP 9 FXT	2
14	TP 11 FXT	2
15	TP16 FXT	2
16	PCT	1
17	TP 26 PCT	1
18	TP 4PCT	1
19	TP34 PCT	1
20	PPN	2
21	TP6 PPN	1
22	TP 5,18 or 19 PPN (a)	1
23	TP 5,18 or 19 PPN (b)	1
24	TP 5,18 or 19 PPN (c)	1
25	TP 5,18 or 19 PPN (d)	1
26	TP 8, 29 30 or 31 PPN (a)	1
27	TP 8, 29 30 or 32 PPN (b)	1
28	TP 8, 29 30 or 33 PPN (c)	1
29	TP 8, 29 30 or 34 PPN (d)	1
30	TP 8, 29 30 or 35 PPN (e)	1
31	TP 32 PPN	1
32	TP37 PPN	1
33	PRG	2
34	TP17 PRG	2

*TP with the mention (a)-(e) represent different positions of the hydroxyl radical in the structure of TP.

4.1.5 PhotoMetrix PRO®

The analytical control of Fenton processes must be careful and carried out throughout the degradation treatment. In this context, when Fenton or solar photo-Fenton processes are performed, the determinations of iron species and H_2O_2 play a vital role in keeping the process "active".

Currently, advances in new technologies for image acquisition and processing have attracted the attention of the scientific and educational community, mainly due to the proof of the effectiveness of their results in comparison to traditional colorimetric equipment. Analyses previously restricted to laboratory equipment, such as spectrophotometers and colorimeters, can now be investigated, *in loco*, using a fast, easy, low cost and less waste generation methodology. The processing of these images occurs through the variation of the RGB color components of each pixel that forms them.

In this context, a smartphone application called PhotoMetrix PRO® (developed by two research groups from UFRGS and UNISC – both universities in Brazil) captures and analyzes digital images through mathematical models¹¹⁵. Image capture can be done through the device's camera, and instantly perform calibration curves and capture samples of unknown concentration. In this thesis, the use of smartphones to obtain the images allowed the development of a much more practical, simple and accessible method when compared to the standard method referenced. The app provides the user with a degree of reliability in measurement and opening up perspective applications in fieldwork and solar experiments in the future.

The objective of **Paper VI**¹¹⁶ was to develop an alternative method of spectrophotometry to determine H_2O_2 and Fe in different matrices treated by AOPs, through the acquisition of digital images by smartphone with PhotoMetrix PRO®.



Total dissolved iron and hydrogen peroxide determination using the PhotoMetrixPRO application: A portable colorimetric analysis tool for controlling important conditions in the solar photo-Fenton process

Elisabeth C. Lumbaqu^a, Bruna A. da Silva^a, Fernanda C. Böck^a, Gilson A. Helfer^b,
Marco F. Ferrão^{a,c,**}, Carla Sirtori^{a,*}

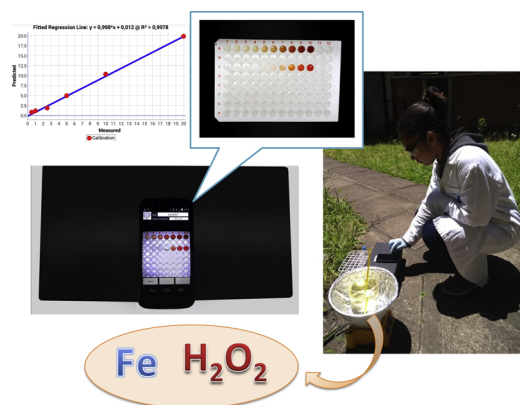
^a Instituto de Química, Universidade Federal do Rio Grande do Sul, Av. Bento Gonçalves, 9500, Porto Alegre, RS, Brazil

^b Departamento de Computação, Universidade de Santa Cruz do Sul, Avenida Independência, 2293, Santa Cruz do Sul, RS, Brazil

^c Instituto Nacional de Ciência e Tecnologia-Bioanalítica (INCT-Bioanalítica), Cidade Universitária, Zeferino Vaz s/n, Campinas, SP, Brazil



GRAPHICAL ABSTRACT



ARTICLE INFO

Keywords:

Total dissolved iron
Hydrogen peroxide
Solar photo-Fenton process
PhotoMetrixPRO
Portable devices

ABSTRACT

The use of the solar photo-Fenton process for water treatment requires monitoring of the main conditions, especially the total dissolved iron concentration and the consumption of hydrogen peroxide. In this study, a new methodology using the PhotoMetrixPRO application was validated for rapid monitoring of total dissolved iron and hydrogen peroxide concentrations, and was tested in the solar photo-Fenton process. A comparison was made between the results obtained using a reference spectrophotometric method and the PhotoMetrixPRO application employing a portable device. Both methods were validated in terms of linearity, sensitivity, precision, robustness, and matrix effects. The degree of dispersion between the series of measurements obtained using UV-vis and portable device tool was low and was in compliance with the established Brazilian and ICH validation criteria. Additionally, PhotoMetrixPRO enabled the use of a smaller sample volume. The total volume generated of each sample is 1 mL, reducing 6 and 10 times the wastes produced in different validated methods.

* Corresponding author.

** Corresponding author at: Instituto de Química, Universidade Federal do Rio Grande do Sul, Av. Bento Gonçalves, 9500, Porto Alegre, RS, Brazil.
E-mail addresses: marco.ferrao@ufrgs.br (M.F. Ferrão), carla.sirtori@ufrgs.br (C. Sirtori).

<https://doi.org/10.1016/j.jhazmat.2019.06.017>

Received 30 January 2019; Received in revised form 4 June 2019; Accepted 5 June 2019

Available online 06 June 2019

0304-3894/ © 2019 Elsevier B.V. All rights reserved.

These results evidencing that the miniaturization can provide positive advantages in terms of simplicity, cost effectiveness, and less environmental impact. PhotoMetrixPRO offers significant advantages including rapid analysis, smaller sample volumes, and greater portability and accessibility.

1. Introduction

Fenton and photo-Fenton processes are based on oxidation reactions involving species such as the hydroxyl (HO^\cdot), hydroperoxyl (HO_2^\cdot), and superoxide anion ($\text{O}_2^{\cdot-}$) radicals, which are generated by the decomposition of hydrogen peroxide catalyzed by iron ions [1,2]. These radicals are capable of oxidizing a wide range of substances and are employed in advanced oxidation processes (AOPs) for the degradation of pollutants. The solar photo-Fenton process is combination of Fenton reagents (H_2O_2 and Fe^{2+} (Eq. (1)) and UV-vis solar light radiation ($\lambda < 600\text{ nm}$) that produces an additional HO^\cdot and HO_2^\cdot radicals by photo-reduction of Fe^{3+} to Fe^{2+} and hydrogen peroxide reaction (Eqs. (2)–(4) [3]. In turn, it increases the degradation rate of organic pollutants. This process reduces the formation of sludge waste that is produced in the original Fenton process since this treatment accumulates Fe^{3+} ions in the system and the reaction does not proceed generating sludge [4]. The ferrous ions generated react again with H_2O_2 generating an additional HO^\cdot and ferric ion, continuing in this way with the cycle [5]. Currently, solar photo-Fenton process is considered one of the most appropriate and sustainable treatment compared to other AOPs systems allowing to work with a renewable source of energy, pHs closer to neutrality and good yields of emergent contaminants degradation. This is shown in the increase in solar treatment studies in recent years [6–8].



However, at high concentrations, both Fe and H_2O_2 can have adverse biological impacts [9]. Therefore, the total Fe concentration and the consumption of H_2O_2 are important parameters that must be quantified and controlled during these treatment processes.

Brazilian environmental legislation [10] sets a maximum permissible limit of 15 mg L^{-1} for total dissolved iron in effluent discharged into receiving water bodies, since high concentrations of iron ions in natural waters can cause acidification and loss of buffering capacity. This condition results in the extinction of organisms capable of photosynthesis, together with the production of hydrogen sulfide and carbon dioxide under anaerobic conditions [11,12], leading to the perturbation of ecosystems. According to European regulations [13], H_2O_2 is considered toxic or moderately toxic to aquatic organisms, with LC_{50} values for fish ranging from 16.4 to 37.4 mg L^{-1} , a 48-h EC_{50} for invertebrates of 2.34 mg L^{-1} , and an EC_{50} for the marine diatom *Skeletonema costatum* of 2.39 mg L^{-1} . H_2O_2 can also cause biological damage including DNA oxidation, causing mutagenesis and death in bacteria.

At present, monitoring of total dissolved Fe and H_2O_2 in AOPs is traditionally performed using spectrophotometric methods, in order to control their concentrations during the course of the treatment [14–16].

As an alternative, the use of new image acquisition and processing technologies, employing portable equipment, can provide a simpler solution that offers savings of both in time and cost. For this purpose, the application called PhotoMetrixPRO is a powerful tool for the monitoring of process conditions. This application uses multivariate analysis techniques including linear regression and partial least squares regression (PLS), which are applied to exploratory data obtained from the decomposition of digital images acquired with the cameras of electronic devices such as Android and Windows smartphones [17]. The

application is free and users can easily install it.

PhotoMetrixPRO is based on color theory, where an image can be defined as the human perception for the combination of two or more wavelengths of the electromagnetic spectrum, in the region of visible light, reflecting on a surface. The combinations are represented by color spaces such as RGB (Red, Green, Blue) and are defined as three-dimensional arrangements of these primary colors [18].

The use of multivariate image analysis (MIA) to provide chemical analytical signals involves the joint application of multivariate data analysis tools and digital image processing [19]. It enables the extraction of useful information to describe, segment, and classify images, with the prediction of properties based on the intensities of the RGB channels [20].

The multivariate calibration procedure uses mathematical models to establish a relationship between properties that can be monitored and some other property of interest. The PLS method is a model based on latent variables (factors), where the objective is to try to achieve the maximum possible congruence between each spectral factor and the corresponding concentration factor, hence obtaining the best linear relationship between the projections (scores) of the predicted and measured concentration data.

There are many published studies concerning evaluation of the Fenton and photo-Fenton processes. In all cases, it was necessary to monitor the experimental conditions in order to control the total dissolved iron concentration and the consumption of hydrogen peroxide during the treatments. The purpose of this work was to develop and validate a simple, fast, inexpensive, and reproducible technique using PhotoMetrixPRO for the determination of total dissolved and speciation of iron for two different methods and for hydrogen peroxide during solar photo-Fenton treatment process.

2. Experimental

2.1. Reagents and water matrices

Modified ISO 6332 method for total dissolved iron determination: Iron sulfate heptahydrate ($\text{FeSO}_4 \cdot 7\text{H}_2\text{O}$) (stock solution of 50 mg L^{-1}) was purchased from Reagen (Rio de Janeiro, Brazil); for complex formation were employed 1,10-phenantroline (2.5 g L^{-1}) (Merck), an acetic buffer of pH 3.6 contained 177 mL of glacial acetic (Quimex, Brazil) and 62.5 g of ammonium acetate (Reagen, Brazil) in a 250 mL of solution, and ascorbic acid (Merck).

Hydroquinone method for total dissolved iron and speciation determination: Ammonium ferrous sulfate ($(\text{Fe}(\text{NH}_4)_2\text{SO}_4) \cdot 6\text{H}_2\text{O}$) (stock solution of 40 mg L^{-1}) (Reagen, Brazil); for complex formation were employed hydroquinone (10 g L^{-1}), 1,10-phenantroline (2.5 g L^{-1}) and sodium citrate (25 g L^{-1}) (purchased from Neon, Brazil).

Hydrogen peroxide determination: H_2O_2 (35% w/v) (purchased from Synth, Brazil). The concentration of the purchased H_2O_2 solution was determined by titration with KMnO_4 (Synth) (0.02 mol L^{-1}). All the reagents were analytical grade and the solutions were prepared with distilled water. For adjusted of pH in solar photo Fenton experiment was employed a solution of H_2SO_4 (98% purity) (0.5 mol L^{-1}) purchased from Synth.

The experiments were carried out using two different water matrices: distilled water (DW) and simulated wastewater (SW). The SW composition was adapted from the OECD recommendation [21], using 160 mg L^{-1} of peptone was from Kasvi (Paraná, Brazil), 110 mg L^{-1} of beef extract (Kasvi), 30 mg L^{-1} of urea (Kasvi), 2 mg L^{-1} of $\text{MgSO}_4 \cdot 7\text{H}_2\text{O}$ (Synth), and 4 mg L^{-1} of $\text{CaCl}_2 \cdot 2\text{H}_2\text{O}$ (purchased from

Dinâmica, Brazil), in a total volume of 1 L.

2.2. Analytical determinations

The presence of Fe^{2+} is extremely important in the performance of oxidation process. For this reason, the determination of the amount of iron is essential to ensure the correct performing of solar photo-Fenton process. One of the methodologies for the determination of total dissolved iron was adapted from ISO 6332 [22], this adapted method employed the complexation of iron with 1,10-phenantroline in the presence of acid buffer and ascorbic acid, which results in the formation of orange-red complex. This modification was made with the objective of decrease the environmental impact of the waste generated when changing hydroxylammonium chloride to ascorbic acid. The formation of this complex occurs in a pH range of 2–9. Although sufficiently broad to ensure quantitative formation of the complex, it is necessary to maintain the pH between 3 and 3.5. The absorption measure at 510 nm of the complex is proportional to the concentration of the ferrous ion. Due to the presence of H_2O_2 in the solar photo-Fenton treatment the ferrous ion oxidizes to ferric ion, so most of the samples measure total iron by reducing all Fe^{3+} in solution to Fe^{2+} through the addition of ascorbic acid. In this way it is possible to verify if the amount of catalyst added at the beginning of the process remains constant during the process or is decreasing due to its precipitation.

Another possibility to determine the total dissolved iron is using hydroquinone method [23]; with this is possible to identify the speciation of iron throughout the solar photo-Fenton process. Hydroquinone reduces all iron species present in solution to Fe^{2+} (total dissolved iron) and without hydroquinone Fe^{3+} complex with 1,10-phenantroline determined spectrophotometrically in the same wavelength. With the difference between dissolved total iron and Fe^{3+} it is possible to determine the behavior and concentration of Fe^{2+} during the process. This complex is stable indefinitely at pH values of 3 or higher adjusted with sodium citrate. Measuring the analyte solutions absorbance at 505 nm is a sensitive method for determining iron concentration.

The ammonium metavanadate method used for the determination of hydrogen peroxide was adapted from Nogueira et al. [24], where the reaction of H_2O_2 with ammonium metavanadate in acidic medium produces the formation of a red-orange color peroxovanadium cation.

In order to compare the traditional colorimetric methods with the PhotoMetrixPRO application, absorption measurements were performed with a Cary 50 spectrophotometer, using a quartz cuvette with optical path length of 1 cm and wavelengths(λ)of 510 nm for total dissolved iron (modify ISO 6332 method) and 505 nm for speciation of iron. Moreover, H_2O_2 determination was in 450 nm (Fig. S2 shows the spectra of all methods studied, Supporting information).

The multivariate analysis method using PhotoMetrixPRO and PLS regression employed two cell phones for the quantification: a Motorola Moto G operating with Android 5.0.2 and equipped with a 5 MP camera, and a Samsung Galaxy J5 operating with Android 5.1.1 and equipped with a 13MP camera, with ROI of 32×32 pixels. The flash option of the cell phones was used for capture of the images, with the devices supported in a black box so as to maintain constant illumination and a distance of 10 cm between the lens and the sample, hence minimizing possible sources of error [17] (Fig. S1, Supporting information). Further information about the PhotoMetrixPRO system is available at <https://www.youtube.com/watch?v=Su9x4uqNEHo> [25].

2.3. Analytical method validation

The validation parameters are quantitative indicators of the scope and optimal performance of the techniques, the principal parameters described in the specialized literature as: analytical curve fit and determination of its linearity range, sensitivity of the method, represented by limits of detection (LOD) and quantification (LOQ), precision and

robustness. The developed methods were then validated in accordance with recommendations from the ICH guidelines [26] and the Brazilian INMETRO standard [27].

A digital validation spreadsheet was used for the validation of both methods. This public domain tool was developed by Ribeiro et al. [28] as an alternative to commercial software packages for method validation. The analytical figures of merit studied were as follows: linearity (calibration curve fit), limit of detection (LOD), limit of quantification (LOQ), precision (repeatability, intermediate precision, and reproducibility), and robustness (using miniaturization of the volume for determination of Fe and H_2O_2 using PhotoMetrixPRO). Additionally, evaluation was made of matrix effects using distilled water and simulated wastewater. Statistical analyses were performed in Excel, using analysis of variance (ANOVA) with a significance level of $\alpha = 0.05$ (assuming one-tailed tests).

2.3.1. Linearity and sensitivity

In testing for linearity, determined aliquots were pipetted from stock solution to prepare solutions of concentrations ranging from 0.5 to 6.0 mg L^{-1} (modified ISO 6332 method), $0.1\text{--}4.0 \text{ mg L}^{-1}$ (hydroquinone method) and $2.48\text{--}88.0 \text{ mg L}^{-1}$ (H_2O_2 determination), due to the wide range of concentrations in the determination of H_2O_2 , the analytical curve was divided into a low concentration range ($2.48\text{--}17.72 \text{ mg L}^{-1}$) and a high concentration range ($17.72\text{--}88.0 \text{ mg L}^{-1}$), in all cases using distilled water. The absorbances and concentrations of these solutions were recorded in replicates, using distilled water as the blank. The linearity test was in accordance with the proposed in the spreadsheet developed by Ribeiro et al. [28], which is done by comparing the residuals of the linear adjustment and quadratic adjustment using an F-test of significance, the residuals of the values were also plotted against concentration to further prove linearity. For all methods, the absence of outliers for each level of concentration was checked using the graphical residual analysis and homoscedasticity (equality of variances). The LOD and LOQ values were calculated according to the simplified analytical curve method [27], using $3s/b$ and $10s/b$, respectively, where s is the standard deviation of ten measurements of the blank and b is the slope of the curve.

2.3.2. Precision

The precision of the methods were determined by using different levels of Fe and H_2O_2 concentration, LQC (low quantified concentration), MQC (medium quantified concentration) and HQC (high quantified concentration), prepared from independent stock solution and analyzed ($N = 7$). Inter-day and Intra-day variation was taken to determine repeatability (RP) and intermediate precision (IP) of UV-vis and PhotoMetrixPRO, the IP was carry out on two different days. The variation instrument (different cell phones) was employed to determine the reproducibility (RPR) in PhotoMetrixPRO with the same concentration levels taken in intermediate precision study. The relative standard deviation (RSD%) of the predicted concentrations from the regression equation was taken as precision.

2.3.3. Robustness

Evaluation of the robustness of the proposed methods (Fe and H_2O_2 determinations) using PhotoMetrixPRO was performed with miniaturization of the scale, reducing the final analysis volumes from 4 mL to 1 mL in case of modified ISO 6332 method and from 10 mL to 1 mL for hydroquinone method and H_2O_2 determination. The results were analyzed using one-way ANOVA, Snedecor F-test of variance homogeneity and the Student's t-test for comparison of the means for the same three concentration levels employed in the precision evaluation (LQC, MQC and HQC).

2.3.4. Matrix effects

The effects of the DW and SW matrices on the precision of quantification of the analytes were evaluated using the same three

concentration levels employed in the precision tests. Statistical analysis of the results employed the *F*-test and the Student's *t*-test.

2.4. Solar photo-Fenton experiments

Evaluation of the applicability of the methods using PhotoMetrixPRO for the determination of total dissolved iron, speciation of iron and H_2O_2 was performed using solar photo-Fenton degradation assays with different pharmaceutical compounds. In all the experiments, eight compounds were used (dipyron, diazepam, fursemide, fluoxetine, nimesulide, paracetamol, progesterone, and propranolol), each at a concentration of $500 \mu\text{g L}^{-1}$. It was carried out two different types of solar photo-Fenton process; the initial experiment was at pH 5.0 (adjusted with $0.01 \text{ mol L}^{-1} \text{H}_2\text{SO}_4$), iron concentration of 5 mg L^{-1} , and H_2O_2 concentration of 50 mg L^{-1} (added in a single dose at the start of the reaction). Another experiment was performed at pH 3.0 with zero valent iron (ZVI) and H_2O_2 concentration of 37.5 mg L^{-1} . Solar UV radiation was measured with a solar energy meter (ICEL SP-2000), which provided data in terms of incident UV (W m^{-2}), enabling calculation of $t_{30\text{W}}$ [29].

3. Results and discussion

3.1. Determination of total dissolved iron

3.1.1. Linearity and sensitivity

Construction of the calibration curves for the modified ISO 6332 method (Fig. 1a.1, and b.1) and hydroquinone method (Fig. 2 a.1 and b.1) in UV-vis spectroscopy employed electronic spreadsheets. In the case of the PhotoMetrixPRO method, the application automatically provided the calibration graphs and the equations of the curves (Figs. 1

and 2b.1 and b.2). The graphs obtain in UV-vis were plot of concentration against absorbance, while the graphs for the PhotoMetrixPRO were plots of the real measurements against the values predicted by the application. All the curves presented R^2 higher than 0.99. For both methods, the results showed linearity and homoscedasticity, without outliers, for each level of concentration (Table S3.1, Fig. S3.2.1, Supporting information).

The graphical analysis of residuals (Fig. S3.2, Supporting information) showed an absence of random behavior, confirming that the linear model could satisfactorily explain the behavior of the data. The LOD and LOQ values calculated for the PhotoMetrixPRO for both methods are approximately 5 times higher than the LOD and LOQ for UV-vis, however, it is important to note that these limits represent the detection and quantification of low concentrations, which gives importance to the use of this application as a potential tool to be used in the monitoring of low concentrations of iron in processes *in loco* that involve this specie in solution.

3.1.2. Precision

The precision study was performed by obtaining seven values for LQC, MQC and HQC of total dissolved iron (0.75 , 2.00 and 5.00 mg L^{-1}) for modified ISO 6332 method and (0.75 , 2.00 and 3.00 mg L^{-1}) for hydroquinone method. The Brazilian INMETRO standard states that the RP value (RSD%) for an analytical technique should not exceed 11% for concentrations above 1 mg L^{-1} , 7.3% for concentrations above 10 mg L^{-1} , and 5.3% for concentrations above 100 mg L^{-1} . For RPR, the results should not exceed 16% for concentrations above 1 mg L^{-1} , 11% for concentrations above 10 mg L^{-1} , and 8% for concentrations above 100 mg L^{-1} . Table 1 shows the RSD values for both methods in UV-vis and PhotoMetrixPRO, at the different concentration levels complied with the INMETRO standards.

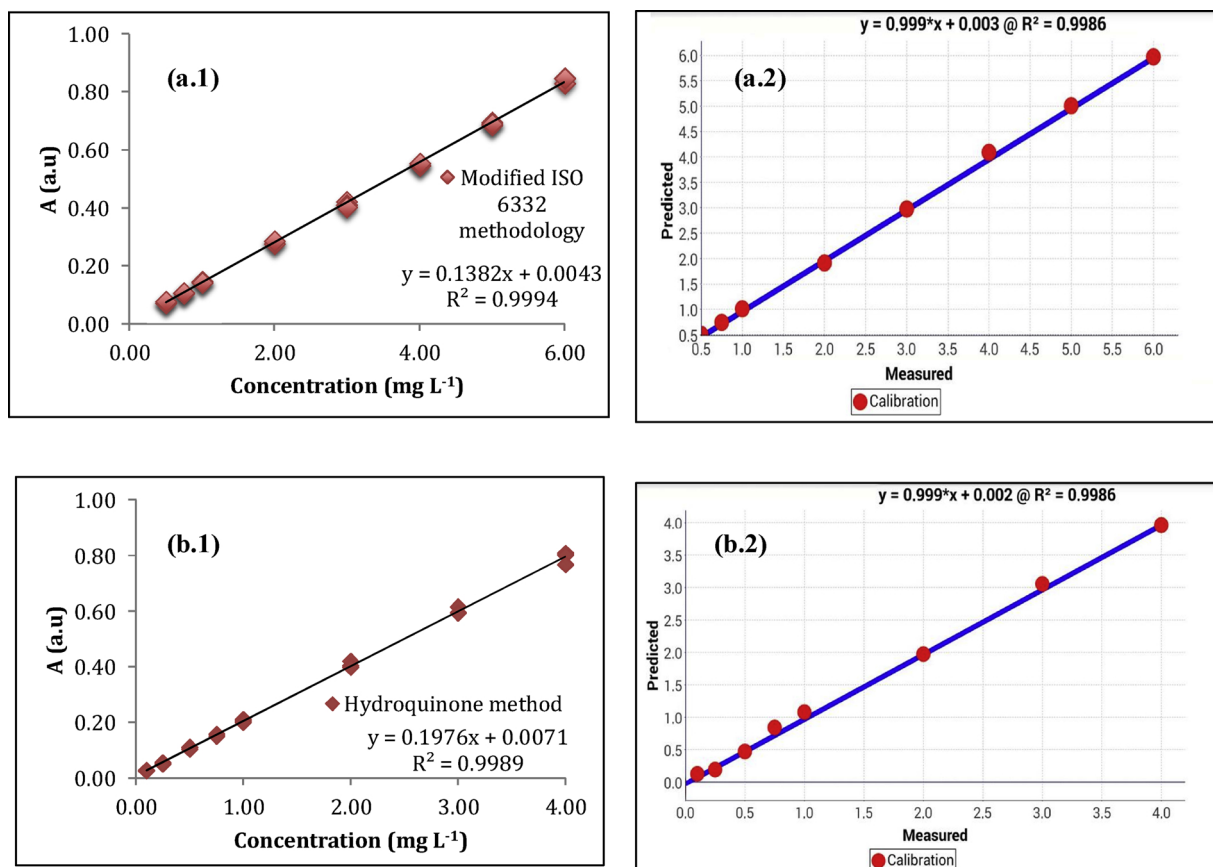


Fig. 1. Calibration curves for total dissolved iron with modify ISO 6332 methodUV-vis spectroscopy (a.1) and PhotoMetrixPRO(a.2); total dissolved iron with hydroquinone methodUV-vis spectroscopy (b.1) and PhotoMetrixPRO(b.2).

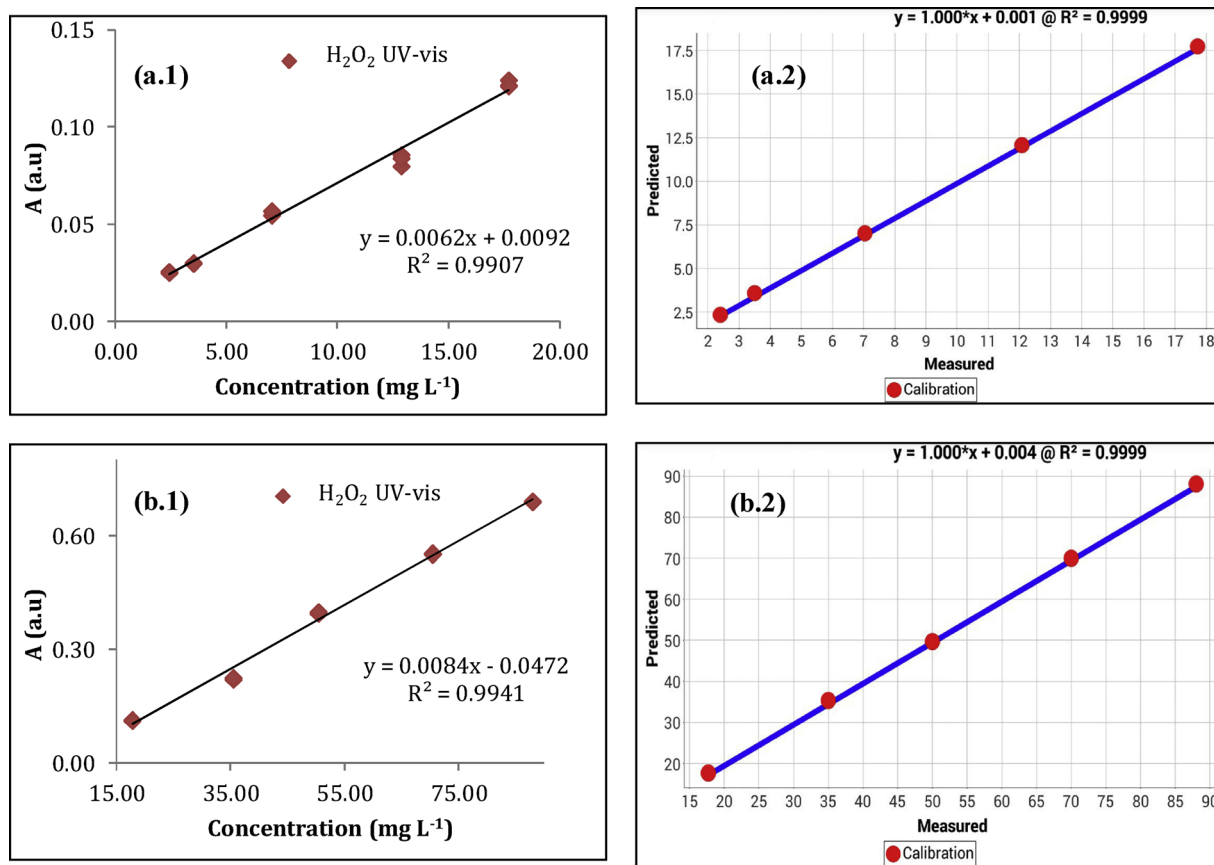


Fig. 2. Calibration curves for H_2O_2 low range UV-vis spectroscopy (a.1) and PhotoMetrixPRO (a.2); H_2O_2 high range UV-vis spectroscopy (b.1) and PhotoMetrixPRO (b.2).

The RSD values showed discreet variability between the two different methods, the values of RP and I.P study were not more than 4.0% in all the cases; these values were within the acceptable range indicating that these methods have excellent repeatability and intermediate precision. The precision of both methods does not show dependence on the analyte concentration.

For evaluation of the PhotoMetrixPRO method, the three parameters considered were repeatability, intermediate precision, and reproducibility. The RSD% values for all of these parameters were within the ranges considered acceptable by INMETRO. The degree of dispersion between the series of measurements obtained using the portable tool was low and was in compliance with the established Brazilian and ICH validation criteria. Therefore, the PhotoMetrixPRO could be considered sufficiently precise for determination of total dissolved iron.

3.1.3. Robustness

Based on the fundamentals of green analytical chemistry concerning clean and ecological methods [30,31], miniaturization was an additional aspect studied in application of the PhotoMetrixPRO method. This technique enabled the use of a smaller sample volume, compared to the amount required for UV-vis analysis, with PhotoMetrixPRO only requiring 340 μL of sample, while 3 mL were required for the UV-vis spectrophotometry analysis. For the modified ISO 6332 method 6 mL of sample are generated, while the hydroquinone method generates 10 mL. With the miniaturization, the total volume of the sample generated is 1 mL, with this the volume reduction is 6 and 10 times, respectively.

The results for the two techniques were not significantly different ($\alpha < 0.05$), with values of F lower than F_{critical} , evidencing that the miniaturization had no effect on precision, at the different concentration levels employed. Similarly, the values of t were lower than t_{critical} ,

showing that the volume decrease did not affect the results (Table S4.1, Supporting information). Miniaturization can provide positive advantages in terms of simplicity, cost effectiveness, and environmental impact, with reductions of the volumes of reagents required and the quantities of waste generated.

3.1.4. Matrix effects

The evaluation of matrix effects was performed using three different concentrations (LQC, MQC and HQC) for each matrix. The matrix effects has greater predominance in the values analyzed for UV-vis spectrophotometry compared to PhotoMetrixPRO, the concentrations in LQC, MQC and HQC showed statistically significant differences between both methods analyzed (considering $\alpha < 0.05$) with values of F higher than F_{critical} , indicating that the matrix had an effect on the precision. Similarly, the values of t were higher than t_{critical} (Table S.4.2.1, Supporting information).

In the case of the UV-vis technique, the appearance of matrix effects depends on whether the other components significantly compete with the analyte molecules present in the light path, which usually results in an increase of the absorbance value. The matrix can also affect the tonality of the complex formed, hence influencing quantification using both the UV-vis method and the PhotoMetrixPRO technique. Since the majority of the data showed statistically significant differences, it was necessary to consider the matrix effects in the total dissolved iron determinations for both methods.

3.2. Hydrogen peroxide determination

3.2.1. Linearity and sensitivity

A wide range of H_2O_2 concentrations have been reported for use in Fenton and photo-Fenton treatments [26,23,24]. Therefore, the

Table 1

Statistical data of the regression equations and validation parameters for total dissolved and speciation of iron methods.

		Total dissolved iron							
		Total dissolved iron (Modified ISO 6332 method)				Methodology of iron speciation (Hydroquinone method)			
Regression analysis									
Method		UV-vis		PhotoMetrixPRO		UV-vis		PhotoMetrixPRO	
Range		0.5–6.0 mg L ⁻¹				0.1–4.0 mg L ⁻¹			
Slope (SE ^a)		0.00045		0.0073		0.0038			
Intercept (SE ^a)		0.001837		0.020		0.00043			
Regression coefficient (r ²)		0.999		0.9999		0.998		0.9999	
LOD (mg L ⁻¹)		0.03		0.15		0.006		0.029	
LOQ (mg L ⁻¹)		0.11		0.50		0.021		0.097	
Validation parameters									
Predicted concentrations (mg L ⁻¹)									
		UV-vis		PhotoMetrixPRO		UV-vis		PhotoMetrixPRO	
		Mn ± SD	% RSD	Mn ± SD	% RSD	Mn ± SD	% RSD	Mn ± SD	% RSD
RP	LQC	0.75 ± 0.01	1.63	0.75 ± 0.01	1.00	0.76 ± 0.01	1.76	0.75 ± 0.00	0.61
	MQC	2.04 ± 0.0	0.07	2.05 ± 0.08	3.89	2.0 ± 0.04	1.92	2.0 ± 0.03	1.46
	HQC	5.00 ± 0.01	0.11	5.04 ± 0.08	1.55	2.99 ± 0.02	0.66	2.94 ± 0.04	1.50
I.P	LQC	0.76 ± 0.01	0.95	0.80 ± 0.02	2.59	0.74 ± 0.01	1.56	0.75 ± 0.02	2.55
	MQC	2.03 ± 0.04	2.19	2.11 ± 0.08	3.61	2.0 ± 0.01	0.53	1.96 ± 0.13	6.43
	HQC	5.00 ± 0.06	1.11	5.09 ± 0.03	0.52	3.06 ± 0.02	0.52	3.09 ± 0.11	3.69
RPR	LQC	na		0.75 ± 0.00	0.16	na		0.75 ± 0.00	0.16
	MQC	na		2.04 ± 0.05	2.57	na		2.02 ± 0.01	0.69
	HQC	na		5.06 ± 0.05	1.04	na		3.03 ± 0.00	0.15
RBS	LQC	na		0.75 ± 0.00	0.16	na		0.75 ± 0.03	4.44
	MQC	na		2.08 ± 0.01	0.58	na		2.06 ± 0.05	2.62
	HQC	na		5.01 ± 0.00	0.04	na		3.0 ± 0.01	0.47
M.E	LQC	1.09 ± 0.04	3.25	0.75 ± 0.07	9.10	1.04 ± 0.01	1.43	0.89 ± 0.03	3.20
	MQC	2.36 ± 0.15	6.37	2.14 ± 0.09	4.00	2.16 ± 0.01	0.61	2.15 ± 0.09	4.00
	HQC	5.31 ± 0.17	3.24	5.09 ± 0.02	0.38	3.32 ± 0.02	0.57	3.06 ± 0.18	5.99

n.a: Analysis not applicable.

^a Standard error of mean.

H₂O₂ data were separated into low and high concentration calibration curves, with ranges of 2.43–17.72 mg L⁻¹ (Fig. 2a.1 and a.2) and 17.72–88.00 mg L⁻¹ (Fig. 2b.1 and b.2), respectively. The high range covered the initial concentrations most frequently adopted in photo-Fenton processes. At concentrations above 88 mg L⁻¹, high concentrations of residual hydrogen peroxide remain in treated water, which can cause potential harm in aquatic ecosystems. Construction of the calibration curves for the UV–vis and PhotoMetrixPRO followed the same procedure mentioned in the section 3.1.1 for total dissolved iron.

All the curves presented R² higher than 0.99 for both ranges, the results for linearity showed homoscedasticity without outliers (Table S3.1 and Fig. S3.2.2, Supporting information). The graphical analysis of residuals (Fig. S3.2.2, Supporting information) showed an absence of random behavior, confirming that the linear model could satisfactorily explain the behavior of the data. The LOD and LOQ values calculated for the PhotoMetrixPRO method were close to those found for the UV–vis method (Table 2), indicating that the application offers excellent potential for use with the same ranges H₂O₂ concentrations monitored using UV–vis spectroscopy. These findings confirmed that PhotoMetrixPRO could provide sufficiently high sensitivity to detect and quantify the species evaluated.

3.2.2. Precision

Table 2 shows the RSD values for each range, at the different concentration levels (LQC, MQC and HQC) for low range calibration (2.43, 7.04 and 17.72 mg L⁻¹) and high range calibration (17.72, 50.40 and

88 mg L⁻¹), as result all the values complied with the INMETRO standards.

The RSD values showed variability between UV–vis and PhotoMetrixPRO. The precision of a method is generally dependent on the analyte concentration. In the present case, the highest RSD% values for RP and I.P were found at the low level for H₂O₂.

For evaluation of the PhotoMetrixPRO the RSD% values for all of these parameters were within the ranges considered acceptable by INMETRO. The degree of dispersion between the series of measurements obtained using the portable tool was low and was in compliance with the established Brazilian and ICH validation criteria. Therefore, the PhotoMetrixPRO could be considered sufficiently precise for determination of H₂O₂.

3.2.3. Robustness

For the traditional determination of H₂O₂ 10 mL are generated, with the miniaturization, the total volume of the sample is 1 mL, with which the volume reduction is 10 times. The results for the two techniques (traditional and miniaturization) were not significantly different ($\alpha < 0.05$), with values of F lower than F_{critical}, evidencing that the miniaturization had no effect on precision, at the different concentration levels employed. Similarly, the values of t were lower than t_{critical}, showing that the volume decrease did not affect the results (Table S4.1, Supporting information). This results support the positive advantages of miniaturization in terms of reduction of cost, volumes of reagents required, quantities of waste generated and environmental impact for the

Table 2
Statistical data of the regression equations and validation parameters for hydrogen peroxide method.

		Hydrogen peroxide							
		Low range calibration				High range calibration			
<i>Regression analysis</i>									
Range		2.48–17.72mg L ⁻¹				17.72–88.00mg L ⁻¹			
Slope (SE ^a)		0.00013				4.71x10 ⁻⁰⁵			
Intercept (SE ^a)		0.00065				0.0006			
Method		UV-vis		PhotoMetrixPRO		UV-vis		PhotoMetrixPRO	
Regression coefficient (r ²)		0.991		0.9999		0.9941		0.9999	
LOD (mg L ⁻¹)		0.65		0.72		0.65		0.72	
LOQ (mg L ⁻¹)		2.18		2.40		2.18		2.40	
<i>Validation parameters</i>									
Predicted concentrations (mg L ⁻¹)									
		Mn ± SD		% RSD		Mn ± SD		% RSD	
		Mn ± SD		% RSD		Mn ± SD		% RSD	
RP	LQC	2.55 ± 0.01	0.48	2.49 ± 0.16	6.53	17.60 ± 0.28	1.60	17.22 ± 0.68	3.95
	MQC	7.05 ± 0.06	0.84	7.05 ± 0.24	3.42	50.96 ± 0.29	0.56	50.39 ± 0.69	1.36
	HQC	17.25 ± 0.04	0.21	17.22 ± 0.71	4.10	88.12 ± 2.31	2.62	88.04 ± 0.38	0.44
I.P	LQC	2.65 ± 0.15	5.80	2.38 ± 0.13	5.37	17.97 ± 0.90	5.00	17.96 ± 0.23	1.27
	MQC	7.61 ± 0.27	3.51	7.15 ± 0.23	3.21	50.78 ± 0.76	1.59	48.38 ± 1.12	2.31
	HQC	17.60 ± 0.28	1.60	18.24 ± 0.80	4.40	88.71 ± 0.40	0.46	87.29 ± 1.32	1.51
RPR	LQC	na		2.53 ± 0.20	7.81	na		15.87 ± 0.64	4.02
	MQC	na		7.08 ± 0.42	5.93	na		52.37 ± 0.81	1.55
	HQC	na		17.16 ± 0.70	4.06	na		86.05 ± 1.69	1.97
RBS	LQC	na		2.38 ± 0.14	5.95	na		17.05 ± 0.51	2.99
	MQC	na		7.22 ± 0.31	4.23	na		50.58 ± 0.53	1.06
	HQC	na		17.05 ± 0.51	2.99	na		87.73 ± 1.33	1.51
M.E	LQC	2.45 ± 0.03	1.29	2.08 ± 0.08	4.01	17.38 ± 0.37	2.11	17.09 ± 0.83	4.87
	MQC	7.56 ± 0.08	1.01	7.80 ± 0.11	1.42	50.99 ± 0.89	1.75	50.84 ± 0.76	1.49
	HQC	17.38 ± 0.37	2.11	17.09 ± 0.83	4.87	87.47 ± 0.95	1.09	88.89 ± 0.73	0.82

n.a: Analysis not applicable.

^a Standard error of mean.

Table 3

Monitoring of total dissolved iron and H₂O₂ during photo-Fenton process (Fe_{initial}: 5 mg L⁻¹, H₂O_{2initial}:50 mg L⁻¹, pH: 5.0, matrix: DW with 500 µg L⁻¹ of each pharmaceutical, reaction time (t_{30w}): 50 min).

t _{30w} (min) ^a	Total dissolved iron (mg L ⁻¹) Modified ISO 6332 method		RSD %	Hydrogen peroxide (mg L ⁻¹)		RSD %
	UV-vis	PhotoMetrixPRO		UV-vis	PhotoMetrixPRO	
	0	4.94		5.07	1.12	
5	4.86	5.05	2.71	49.61	49.37	0.34
10	4.68	4.48	3.09	48.35	49.16	1.17
15	4.42	4.35	1.13	43.21	45.18	3.15
20	4.39	4.35	0.65	43.05	43.45	0.65
30	4.12	4.04	1.39	35.77	35.14	1.26
40	2.58	2.59	0.27	33.58	35.19	3.31
50	1.68	1.57	4.79	29.00	30.04	2.49

^a Normalized value of time related to radiation.

determination of total dissolved iron using different methods such as the determination of H₂O₂ simultaneously.

3.2.4. Matrix effects

The evaluation of matrix effects for H₂O₂ determination shows in most cases, a statistically significant difference (considering $\alpha < 0.05$), with values of F higher than F_{critical}, indicating that the matrix had an effect on the precision. Similarly, the values of t were higher than t_{critical}, reflecting an effect of the matrix (Table S.4.2.2, Supporting information). Since the majority of the data showed statistically significant differences, it was necessary to consider the matrix effects in the H₂O₂ determination.

3.3. Solar photo-Fenton experiments

The concentrations of iron and H₂O₂ were determined in eight samples collected during a solar photo-Fenton process performed for 50 min of solar treatment (t_{30w}), comparing the values obtained using the PhotoMetrixPRO and UV-vis spectroscopy techniques, in this case was used the modified ISO 6332 method for determination of total dissolved iron. The RSD values were in the ranges 0.27–4.79% for iron and 0.34–3.31% for H₂O₂ (Table 3). The results indicated that the PhotoMetrixPRO technique could be successfully used for *in loco* monitoring of photo-Fenton process, with a high degree of precision. The RSD values closer to 5% were associated with the quantification of iron at low levels of the calibration curve, at which there was poorer

Table 4

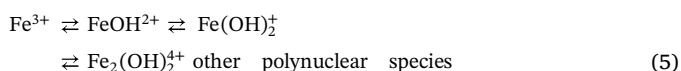
Monitoring of speciation of iron and H₂O₂ during solar photo-advanced Fenton process (Fe⁰_{initial}: 2 g; 37.5 mg L⁻¹, pH: 3.0, matrix: DW with 500 µg L⁻¹ of each pharmaceutical, reaction time (t_{30w}): 60 min).

t _{30w} (min) ^a	Hydroquinone method						Hydrogen peroxide (mg L ⁻¹)		
	Total dissolved iron (Fe ²⁺ /Fe ³⁺)(mg L ⁻¹)			Fe ²⁺ (mg L ⁻¹)			UV-vis	PhotoMetrix PRO	RSD %
	UV-vis	PhotoMetrix PRO	RSD %	UV-vis	PhotoMetrix PRO	RSD %			
0	0.45	0.47	1.82	0.40	0.43	4.00	37.5	39.00	1.96
5	0.55	0.53	1.85	0.53	0.50	2.58	29.2	27.33	3.31
10	0.64	0.65	0.78	0.60	0.59	0.84	23.5	21.20	5.15
15	0.70	0.73	2.10	0.64	0.65	0.78	17.5	15.14	7.23
30	0.98	0.94	2.26	0.94	0.96	0.88	11.6	9.80	8.41
60	1.05	1.01	1.78	0.99	1.08	3.90	4.99	4.01	10.89

^a Normalized value of time related to radiation.

discriminatory image analysis capacity, as reported previously by Lazarini et al. [34].

The experiments were carried out at pH 5 based in other studies conducted in the same pH [7,32,33], showed that there is iron in solution at neutral pH, this approach is a new perspective in the advanced oxidation processes that decreases the cost of operation and is more environmental friendly [29,35–38]. In solution the Fe³⁺ exists as the hexaquoion [Fe(H₂O)₆]³⁺ as pH increases, the ion undergoes extensive hydrolysis (Eq. (5)), the ferric oxyhydroxides can precipitate, it depends of different factors such as counter ion, ionic strength and total iron concentration [2]. The iron concentration and the aqueous matrix favored the stability of iron in solution.



Besides, in order to demonstrate the efficiency in the determination of total dissolved iron and Fe²⁺ in low concentrations and their behavior throughout the a type of solar photo-Fenton process (solar photo-advanced Fenton), iron speciation was performed using the hydroquinone method comparing the responses obtained by UV-vis and PhotoMetrixPRO (Table 4). Solar photo-advanced Fenton uses ZVI as a source of iron in the presence of sunlight and H₂O₂ [39,40], ZVI is a source of iron, during the solar process the iron ions are leached to the solution, so this concentration increases with time. It is possible to quantify the total dissolved iron and Fe²⁺ in solution with UV-vis and PhotoMetrixPRO obtaining RSD values in the ranges 0.78–4.00% for iron, the values show that, in its great majority, the total dissolved iron corresponds to the Fe²⁺ species. RSD values for H₂O₂, were calculated in a range of 1.96 – 10.89%, the higher values of RSD is due low concentration of H₂O₂, in some cases the total iron dissolved can act as an interfering agent [24], which could influence in the precision of mobile tool.

It is very important to highlight that the advantages of the PhotoMetrixPRO method include the reduced amount of sample required and the shorter analysis time. For the analysis of eight samples using the reference method, the user would take about 60 min to perform the analyses and calculate the concentrations (using the calibration curve), with a sample volume of 3 mL per analysis. Using the PhotoMetrixPRO application, the same number of samples could be analyzed in around 15 min, with the concentrations being provided directly by the application, without requiring any additional calculations. Furthermore, this method requires a volume of only 340 µL per sample, enabling miniaturization of the process and a consequent reduction of the volume of wastewater generated. The results demonstrated that the PhotoMetrixPRO application can provide greater flexibility for use under different conditions, with the advantages of being faster, simpler, cheaper, and more environmentally friendly than the traditional method. It enables the *in loco* monitoring of total dissolved

iron and H₂O₂ used in Fenton and photo-Fenton processes for the degradation of contaminants present in water and wastewater matrices.

4. Conclusions

This validation study compared the use of UV-vis spectrophotometry and the PhotoMetrixPRO technique for the determination and monitoring of total dissolved iron and H₂O₂ in distilled water and simulated wastewater matrices during photo-Fenton treatment. Analytical parameters including precision, sensitivity, reproducibility, robustness, and matrix effects were determined for both analytical methodologies. Statistical analysis showed that the values obtained were satisfactory. PhotoMetrixPRO was successfully validated as a sensitive and precise method for the quantification of total dissolved iron and H₂O₂, in compliance with the INMETRO and ICH norms. The results demonstrated the simplicity, cost-effectiveness, flexibility, and speed of the analyses performed with the new method. In photo-Fenton experiments, the data obtained using PhotoMetrixPRO were very similar to the results using UV-vis spectroscopy. The findings confirmed the potential of the PhotoMetrixPRO application as an alternative simpler, faster, and cheaper technique for the monitoring of solar photo-Fenton processes, offering advantages including a short analysis time, portability, and the requirement for only a small volume of sample.

Acknowledgments

This study was financed in part by the Coordenação de Aperfeiçoamento de Pessoal de Nível Superior - Brasil (CAPES) - Finance Code 001. The authors wish to thank CNPq (Processo:403051/2016-9). Carla Sirtori thanks the CNPq for her Research grant (Processo: 303474/2015-7).

Appendix A. Supplementary data

Supplementary material related to this article can be found, in the online version, at doi:<https://doi.org/10.1016/j.jhazmat.2019.06.017>.

References

- [1] A. Babuponnusami, K. Muthukumar, A review on Fenton and improvements to the Fenton process for wastewater treatment, *J. Environ. Chem. Eng.* 2 (2014) 557–572, <https://doi.org/10.1016/j.jece.2013.10.011>.
- [2] J.J. Pignatello, E. Oliveros, A. MacKay, Advanced oxidation processes for organic contaminant destruction based on the Fenton reaction and related chemistry, *Crit. Rev. Environ. Sci. Technol.* 36 (2006) 1–84, <https://doi.org/10.1080/10643380500326564>.
- [3] S. Rahim Pouran, A.R. Abdul Aziz, W.M.A. Wan Daud, Review on the main advances in photo-Fenton oxidation system for recalcitrant wastewaters, *J. Ind. Eng. Chem.* 21 (2015) 53–69, <https://doi.org/10.1016/j.jiec.2014.05.005>.
- [4] J.M. Poyatos, M.M. Muñio, M.C. Almcija, J.C. Torres, E. Hontoria, F. Osorio,

- Advanced oxidation processes for wastewater treatment: state of the art, *Water Air Soil Pollut.* 205 (2009) 187, <https://doi.org/10.1007/s11270-009-0065-1>.
- [5] A.R. Ameta, K. Chohadia, A. Jain, P.B. Punjabi, Fenton and photo-Fenton processes, *Adv. Oxid. Process. Waste Water Treat.* (2018) 49–87, <https://doi.org/10.1016/B978-0-12-810499-6.00003-6>.
- [6] M. Tobajas, C. Belver, J.J. Rodriguez, Degradation of emerging pollutants in water under solar irradiation using novel TiO₂-ZnO/clay nanoarchitectures, *Chem. Eng. J.* 309 (2017) 596–606, <https://doi.org/10.1016/j.cej.2016.10.002>.
- [7] L. Clarizia, D. Russo, I. Di Somma, R. Marotta, R. Andreozzi, Homogeneous photo-Fenton processes at near neutral pH: a review, *Appl. Catal. B Environ.* 209 (2017) 358–371, <https://doi.org/10.1016/j.apcatb.2017.03.011>.
- [8] S. Foteinis, J.M. Monteagudo, A. Durán, E. Chatzisympson, Environmental sustainability of the solar photo-Fenton process for wastewater treatment and pharmaceuticals mineralization at semi-industrial scale, *Sci. Total Environ.* 612 (2018) 605–612, <https://doi.org/10.1016/j.scitotenv.2017.08.277>.
- [9] C.C. Winterbourn, Toxicity of iron and hydrogen peroxide: the Fenton reaction, *Toxicol. Lett.* 82–83 (1995) 969–974, [https://doi.org/10.1016/0378-4274\(95\)03532-X](https://doi.org/10.1016/0378-4274(95)03532-X).
- [10] Brazil, National Council for the Environment—CONAMA. Resolution n° 430, (2011) (Accessed 12 December 2018) (in Portuguese), <http://www2.mma.gov.br/port/conama/legiabre.cfm?codlegi=646>.
- [11] A. Rabajczyk, J. Namieśnik, Speciation of iron in the aquatic environment, *Water Environ. Res.* 86 (2014) 741–758, <https://doi.org/10.2175/106143014X13975035525906>.
- [12] R. Krachler, F. Jirsa, S. Ayromlou, Factors Influencing the Dissolved Iron Input by River Water to the Open Ocean, (2018) (Accessed 12 December 2018), www.biogeosciences.net/bg/2/311/SRef-ID:1726-4189/bg/2005-2-311EuropeanGeosciencesUnion.
- [13] European Union, Regulation (EU) No 528/2012 Concerning the Making Available on the Market and Use of Biocidal Products, Finland, (2015).
- [14] S. Giannakis, S. Liu, A. Carratalà, S. Rtimi, M. Talebi Amiri, M. Bensimon, C. Pulgarin, Iron oxide-mediated semiconductor photocatalysis vs. heterogeneous photo-Fenton treatment of viruses in wastewater. Impact of the oxide particle size, *J. Hazard. Mater.* 339 (2017) 223–231, <https://doi.org/10.1016/j.jhazmat.2017.06.037>.
- [15] N. Klammer, S. Malato, M.I. Maldonado, A. Agüera, A. Fernández-Alba, Modified photo-Fenton for degradation of emerging contaminants in municipal wastewater effluents, *Catal. Today* 161 (2011) 241–246, <https://doi.org/10.1016/J.CATTOD.2010.10.074>.
- [16] C. Sirtori, Agüera Ana, Carra Irene, A. Sánchez Pérez José, Identification and monitoring of thiabendazole transformation products in water during Fenton degradation by LC-QTOF-MS, *Anal. Bioanal. Chem.* 406 (2014) 5323–5337, <https://doi.org/10.1007/s00216-014-7942-1>.
- [17] G.A. Helfer, V.S. Magnus, F.C. Böck, A. Teichmann, M.F. Ferrão, A.B. da Costa, PhotoMetrix: an application for univariate calibration and principal components analysis using colorimetry on mobile devices, *J. Braz. Chem. Soc.* 28 (2016) 328–335, <https://doi.org/10.5935/0103-5053.20160182>.
- [18] D. Damasceno, T.G. Toledo, M.S. Godinho, C.P. Da Silva, S.B. De Oliveira, A.E. De Oliveira, Análise multivariada de imagens na química: Um experimento para determinação do pH de águas potáveis, *Quim. Nova.* 38 (2015) 836–841, <https://doi.org/10.5935/0100-4042.20150082>.
- [19] J.M. Prats-Montalbán, A. de Juan, A. Ferrer, Multivariate image analysis: a review with applications, *Chemometr. Intell. Lab. Syst.* 107 (2011) 1–23, <https://doi.org/10.1016/J.CHEMOLAB.2011.03.002>.
- [20] M.C.A. Marcelo, K.C. Mariotti, R.S. Ortiz, M.F. Ferrão, M.J. Anzanello, Scott test evaluation by multivariate image analysis in cocaine samples, *Microchem. J.* 127 (2016) 87–93, <https://doi.org/10.1016/J.MICROC.2016.02.012>.
- [21] OECD, Guidelines for Testing of Chemicals, Simulation Test-Aerobic Sewage Treatment 303^a, (1999).
- [22] ISO, 6332: Water Quality - Determination of Iron - Spectrometric Method Using 1,10-phenanthroline, (1998).
- [23] R.C. Atkins, Colorimetric determination of iron in vitamin supplement tablets. A general chemistry experiment, *J. Chem. Educ.* 52 (1975) 550, <https://doi.org/10.1021/ed052p550>.
- [24] R. Nogueira, M. Oliveira, W. Paterlini, Simple and fast spectrophotometric determination of H₂O₂ in photo-Fenton reactions using metavanadate, *Talanta* 66 (2005) 86–91, <https://doi.org/10.1016/j.talanta.2004.10.001>.
- [25] G. Helfer, PhotoMetrix - Multivariate Analysis, (2015) (Accessed 8 December 2018), <https://www.youtube.com/watch?v=Su9x4uqNEHo>.
- [26] International Conference on Harmonisation (ICH), Guidance for Industry Q2(R1): Text on Validation of Analytical Procedures, November (2005).
- [27] INMETRO, Orientação sobre validação de métodos analíticos, (2018).
- [28] F.A. de L. Ribeiro, M.M.C. Ferreira, S.C. Morano, L.R. da Silva, R.P. Schneider, Validation spreadsheet: a new tool for estimating the analytical figures of merit for the validation of univariate methods, *Quim. Nova* 31 (2008) 164–171.
- [29] I. Carra, S. Malato, M. Jiménez, M.I. Maldonado, J.A. Sánchez Pérez, Microcontaminant removal by solar photo-Fenton at natural pH run with sequential and continuous iron additions, *Chem. Eng. J.* 235 (2014) 132–140, <https://doi.org/10.1016/j.cej.2013.09.029>.
- [30] S. Armenta, S. Garrigues, M. de la Guardia, Green analytical chemistry, *TRAC Trends Anal. Chem.* 27 (2008) 497–511, <https://doi.org/10.1016/J.TRAC.2008.05.003>.
- [31] A. Gałuszka, Z. Migaszewski, J. Namieśnik, The 12 principles of green analytical chemistry and the SIGNIFICANCE mnemonic of green analytical practices, *TRAC Trends Anal. Chem.* 50 (2013) 78–84, <https://doi.org/10.1016/J.TRAC.2013.04.010>.
- [32] E. Cuervo Lumbaque, R.M. Cardoso, A. Dallegrave, L.O. dos Santos, M. Ibáñez, F. Hernández, C. Sirtori, Pharmaceutical removal from different water matrices by Fenton process at near-neutral pH: doehler design and transformation products identification by UHPLC-QTOF MS using a purpose-built database, *J. Environ. Chem. Eng.* 6 (2018) 3951–3961, <https://doi.org/10.1016/J.JECE.2018.05.051>.
- [33] A. Mirzaei, Z. Chen, F. Haghight, L. Yerushalmi, Removal of pharmaceuticals from water by homo/heterogeneous Fenton-type processes – a review, *Chemosphere* 174 (2017) 665–688, <https://doi.org/10.1016/j.chemosphere.2017.02.019>.
- [34] A.L. Lazzarini, R.A. Levine, R.J. Ploutz-Snyder, S.O. Sanderson, Advances in digital quantification technique enhance discrimination between mild and advanced liver fibrosis in chronic hepatitis C, *Liver Int.* 25 (2005) 1142–1149, <https://doi.org/10.1111/j.1478-3231.2005.01155.x>.
- [35] E. Cuervo Lumbaque, D. Salmoria Araújo, T. Moreira Klein, E.R. Lopes Tiburtius, J. Argüello, C. Sirtori, Solar photo-Fenton-like process at neutral pH: Fe(III)-EDDS complex formation and optimization of experimental conditions for degradation of pharmaceuticals, *Catal. Today.* 328 (2019) 259–266, <https://doi.org/10.1016/J.CATTOD.2019.01.006>.
- [36] O. Gomes Júnior, V.M. Silva, A.E.H. Machado, C. Sirtori, C.R. Lemos, A.M. Freitas, A.G. Trovó, Correlation between pH and molar iron/ligand ratio during ciprofloxacin degradation by photo-Fenton process: identification of the main transformation products, *J. Environ. Manage.* 213 (2018) 20–26, <https://doi.org/10.1016/J.JENVMAN.2018.02.041>.
- [37] I. Carra, J.L. Casas López, L. Santos-Juanes, S. Malato, J.A. Sánchez Pérez, Iron dosage as a strategy to operate the photo-Fenton process at initial neutral pH, *Chem. Eng. J.* 224 (2013) 67–74, <https://doi.org/10.1016/j.cej.2012.09.065>.
- [38] S. Miralles-Cuevas, I. Oller, A. Ruíz-Delgado, A. Cabrera-Reina, L. Cornejo-Ponce, S. Malato, EDDS as complexing agent for enhancing solar advanced oxidation processes in natural water: Effect of iron species and different oxidants, *J. Hazard. Mater.* (2018) 1–8, <https://doi.org/10.1016/J.JHAZMAT.2018.03.018>.
- [39] P. Xie, L. Zhang, J. Chen, J. Ding, Y. Wan, S. Wang, Z. Wang, A. Zhou, J. Ma, Enhanced degradation of organic contaminants by zero-valent iron/sulfite process under simulated sunlight irradiation, *Water Res.* 149 (2019) 169–178, <https://doi.org/10.1016/J.WATRES.2018.10.078>.
- [40] J.A. de Lima Perini, R. Fernandes Pupo Nogueira, Zero-valent iron mediated degradation of sertraline – effect of H₂O₂ addition and application to sewage treatment plant effluent, *J. Chem. Technol. Biotechnol.* 91 (2016) 276–282, <https://doi.org/10.1002/jctb.4705>.

SUPPORTING INFORMATION

Total dissolved iron and hydrogen peroxide determination using the PhotoMetrixPRO application: a portable colorimetric analysis tool for controlling important conditions in the solar photo-Fenton process

Elisabeth C. Lumbaque^a, Bruna A. da Silva^a, Fernanda C. Böck^a, Gilson A. Helfer^b, Marco F. Ferrão^{a,c*}, Carla Sirtori^{a*}

^aInstituto de Química- Universidade Federal do Rio Grande do Sul, Av. Bento Gonçalves, 9500, Porto Alegre-RS, Brazil.

^bDepartamento de Computação - Universidade de Santa Cruz do Sul, Avenida Independência, 2293, Santa Cruz do Sul-RS, Brazil.

^cInstituto Nacional de Ciência e Tecnologia-Bioanalítica (INCT-Bioanalítica), Cidade Universitária, Zeferino Vaz s/n, Campinas, SP, Brazil

*Authors to whom all correspondence should be addressed: marco.ferrao@ufrgs.br (Marco F. Ferrão) and carla.sirtori@ufrgs.br (Carla Sirtori)

S.1 PhotoMetrixPRO system

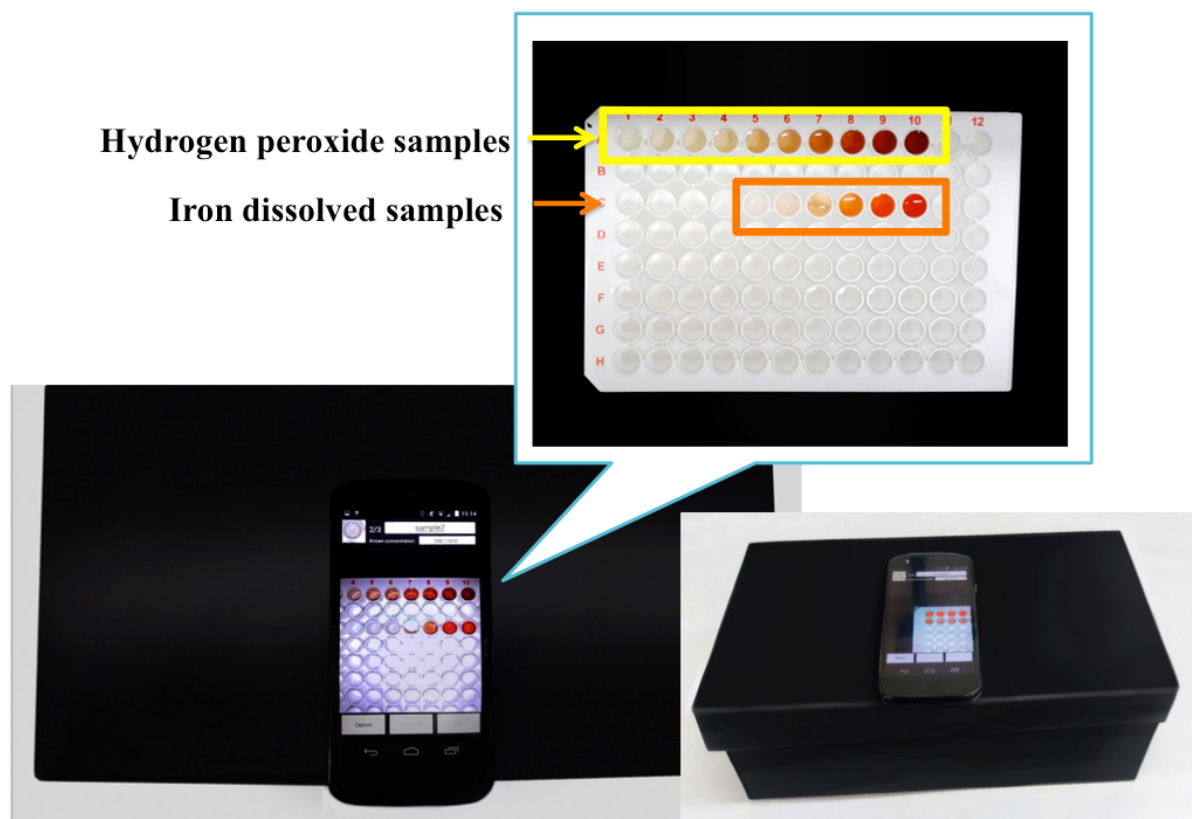
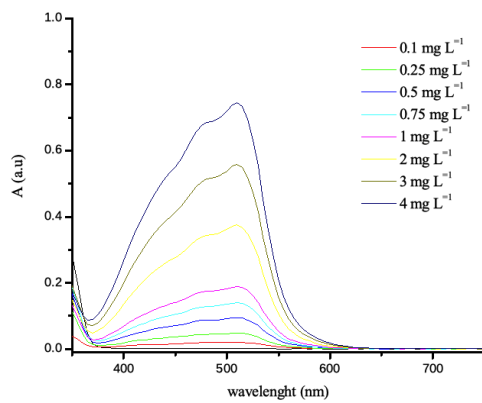


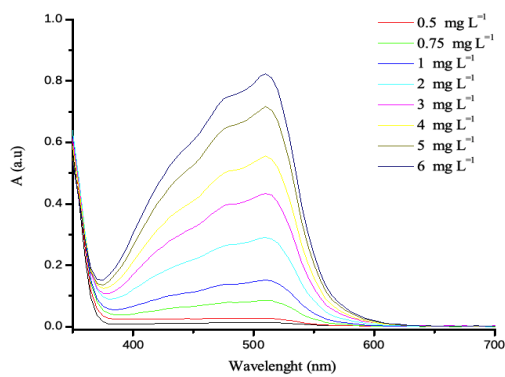
Figure S.1 Design of PhotoMetrixPRO system.

S.2 UV-visible absorption spectra

(a)



(b)



(c)

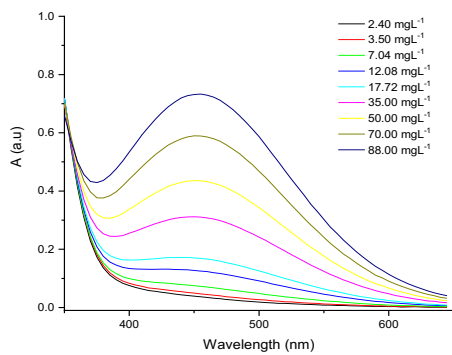


Figure S.2 UV-visible absorption spectra for (a) hydroquinone method (b) total dissolved iron modified ISO 6332 and (c) hydrogen peroxide.

S.3 Linearity test

S.3.1 Cochran test: Homoscedasticity

$$C = \frac{s^2}{\sum_{i=1}^k s_i^2} \text{ (Equation 2)}$$

k: represents the number of factor levels;

s_i^2 : represents the sample variance.

Table S.3.2: Evaluation of homoscedasticity using Cochran test.

Analyte	Method	DF	C calc	C _{max} α=0.05	Prediction
Total dissolved iron (Modified ISO 6332 methodology)	UV-vis	2	0.3683	0.6161	Homoscedasticity
	PhotoMetrixPRO	2	0.0396	0.6161	Homoscedasticity
Methodology of iron speciation	UV-vis	2	0.1773	0.6161	Homoscedasticity
	PhotoMetrixPRO	2	0.0092	0.6161	Homoscedasticity
H ₂ O ₂ low range	UV-vis	2	0.6040	0.6838	Homoscedasticity
	PhotoMetrixPRO	2	0.6284	0.6838	Homoscedasticity
H ₂ O ₂ high range	UV-vis	2	0.3328	0.6838	Homoscedasticity
	PhotoMetrixPRO	2	0.4655	0.6838	Homoscedasticity

DF: Degrees of freedom

S.3.2 Residual

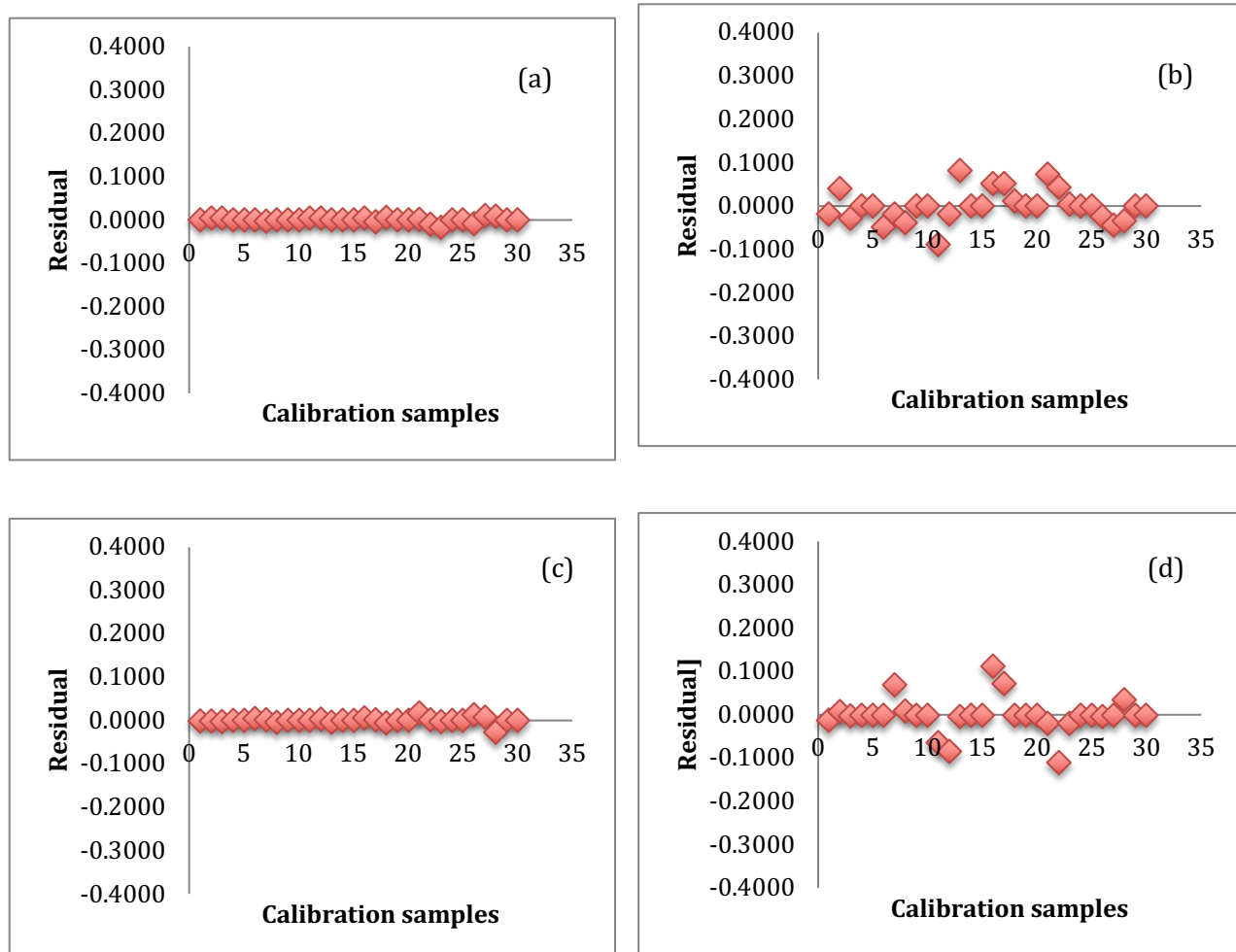


Figure S.3.2.1 Residual graphical analysis for (a) Total dissolved iron (Modified ISO 6332 methodology) UV-vis (b) Total iron dissolved (Modified ISO 6332 methodology) PhotoMetrixPRO, (c) Hydroquinone method UV-vis and (d) Hydroquinone method PhotoMetrixPRO.

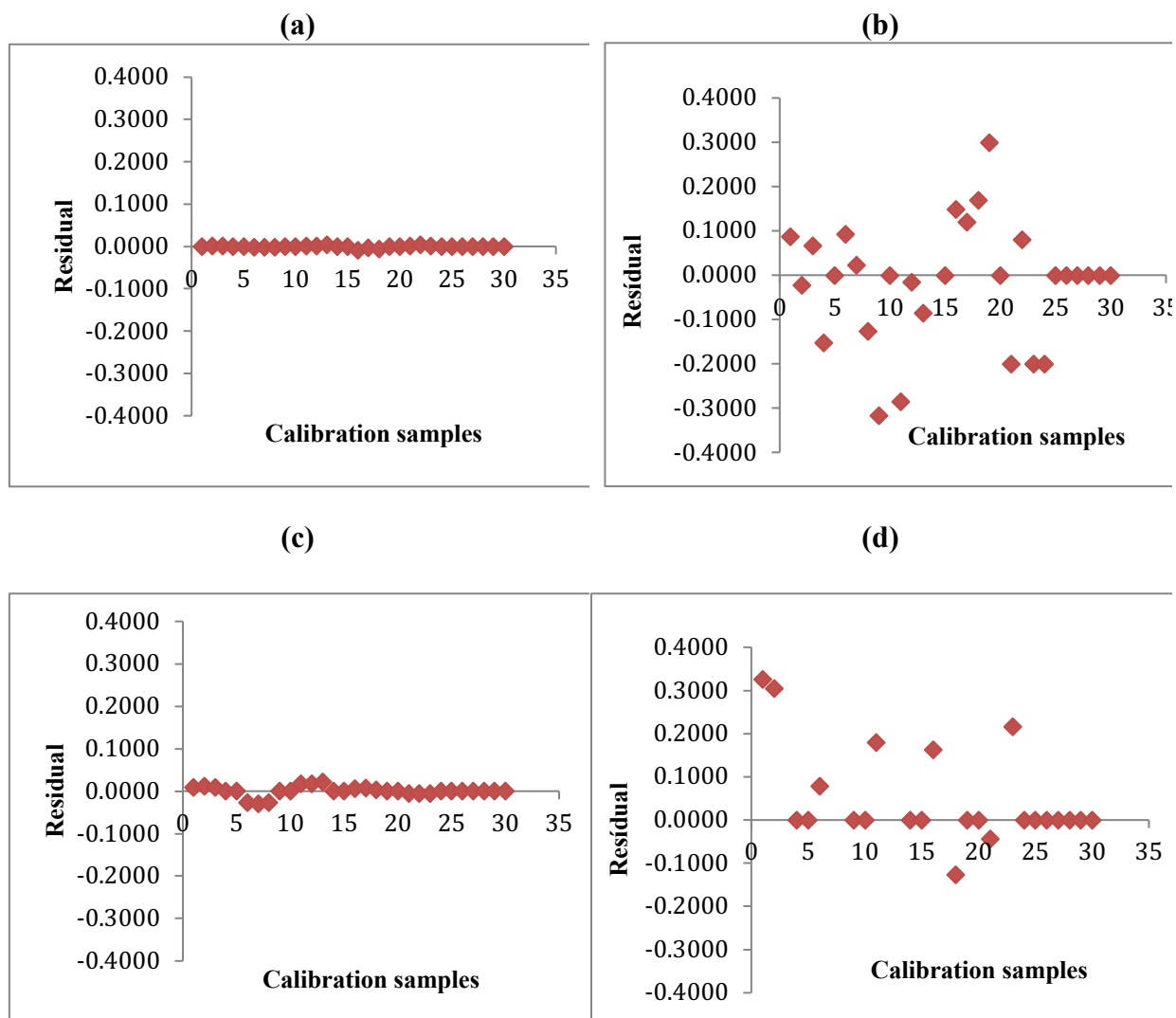


Figure S.3.2.2 Residual graphical analysis for (a) H₂O₂ low range UV-vis, (b) H₂O₂ low range PhotoMetrixPRO, (c) H₂O₂ high range UV-vis and (d) H₂O₂ high range PhotoMetrixPRO.

S.4 Student test and F test

S.4.1 Miniaturization effect analysis

$$t = \frac{\bar{x}_{DW} - \bar{x}_{SW}}{s \sqrt{\frac{1}{N_{DW}} + \frac{1}{N_{SW}}}} \quad (\text{Equation 3}) \quad F = \frac{s_{DW}^2}{s_{SW}^2} \quad (\text{Equation 4})$$

Table S.4.1: Main parameters for the comparison of the normal and miniaturized scale.

Method	Level	Mode	N	Mean	s ²	t _{calc}	t _{critical} α=0.05	F _{calc}	F _{critical} α=0.05
Total iron dissolved (Modified ISO 6332 methodology) PhotoMetrixPRO	Low	NS	7	0.75	0.00003	0.00	2.45	0.88	4.74
		MS	7	0.75					
	Medium	NS	7	2.05	0.003	-0.98	2.45	1.34	4.74
		MS	7	2.08					
	High	NS	7	5.04	0.003	1.02	2.45	1.24	4.74
		MS	7	5.01					
Methodology of iron speciation PhotoMetrixPRO	Low	NS	7	0.75	0.001	0.68	2.45	0.52	4.74
		MS	7	0.74					
	Medium	NS	7	2.02	0.002	-1.96	2.45	2.59	4.74
		MS	7	2.06					
	High	NS	7	2.98	0.001	-1.81	2.45	2.96	4.74
		MS	7	3.00					
H₂O₂ low range PhotoMetrixPRO	Low	NS	7	2.49	0.023	1.22	2.45	1.87	4.74
		MS	7	2.72					
	Medium	NS	7	7.05	0.076	-2.01	2.45	1.31	4.74
		MS	7	7.22					
	High	NS	7	17.22	0.378	0.49	2.45	0.28	4.74
		MS	7	17.05					
H₂O₂ high range PhotoMetrixPRO	Low	NS	7	17.22	0.378	0.49	2.45	0.28	4.74
		MS	7	17.05					
	Medium	NS	7	50.39	0.379	-0.75	2.45	0.35	4.74
		MS	7	50.59					
	High	NS	7	88.04	0.952	0.62	2.45	0.35	4.74
		MS	7	87.73					

n: replicates performed

NS: Normal scale

MS: Miniaturization scale

S.4.2 Matrix effect analysis

Table S.4.2.1: Matrix effect evaluation for both iron determination methods in distilled water (DW) and simulated wastewater (SW).

Method	Level	Matrix	N	Mean	s ²	t _{calc}	t _{critical} α=0.05	F _{calc}	F _{critical} α=0.05
Total dissolved iron (Modified ISO 6332 methodology) UV-vis	Low	DW	7	0.75	0.0024	-20.28	2.45	575.5	4.74
		SW	7	1.09					
	Medium	DW	7	2.05	0.0090	-3.66	2.45	13.37	4.74
		SW	7	2.37					
	High	DW	7	5.00	0.0148	-4.73	2.45	21.98	4.74
		SW	7	5.31					
Total iron dissolved (Modified ISO 6332 methodology) PhotoMetrixPRO	Low	DW	7	0.75	0.0024	0.001	2.45	0.03	4.74
		SW	7	0.75					
	Medium	DW	7	2.05	0.0069	4.67	2.45	-1.87	4.74
		SW	7	2.15					
	High	DW	7	5.04	0.0032	2.40	2.45	-1.46	4.74
		SW	7	5.09					
Methodology of iron speciation UV-vis	Low	DW	7	0.76	0.0007	-33.41	2.45	1543.9	4.74
		SW	7	1.04					
	Medium	DW	7	2.00	0.0006	-20.77	2.45	162.3	4.74
		SW	7	2.16					
	High	DW	7	2.99	0.0004	-27.14	2.45	1011.1	4.74
		SW	7	3.32					
Methodology of iron speciation PhotoMetrixPRO	Low	DW	7	0.77	0.0007	79.53	2.45	-11.56	4.74
		SW	7	0.89					
	Medium	DW	7	1.99	0.0044	17.20	2.45	-4.12	4.74
		SW	7	2.16					
	High	DW	7	2.94	0.0175	-1.41	2.45	2.82	4.74
		SW	7	3.07					

n: replicates performed

DW: distilled water

SW: simulated wastewater

Table S.4.2.2: Matrix effect evaluation for hydrogen peroxide method in distilled water (DW) and simulated wastewater (SW).

Method	Level	Matrix	N	Mean	s ²	t _{calc}	t _{critical} α=0.05	F _{calc}	F _{critical} α=0.05
H₂O₂ low range UV-vis	Low	DW	7	2.55	0.0010	10.42	2.45	61.04	4.74
		SW	7	2.45					
	Medium	DW	7	7.05	0.0047	-17.75	2.45	190.6	4.74
		SW	7	7.56					
	High	DW	7	17.25	0.0682	-0.95	2.45	0.88	4.74
		SW	7	17.39					
H₂O₂ low range PhotoMetrixPRO	Low	DW	7	2.49	0.0167	5.92	2.45	3.80	4.74
		SW	7	2.08					
	Medium	DW	7	7.05	0.0352	-7.53	2.45	4.76	4.74
		SW	7	7.80					
	High	DW	7	17.22	0.5802	0.32	2.45	0.68	4.74
		SW	7	17.09					
H₂O₂ high range UV-vis	Low	DW	7	17.25	0.0682	-0.95	2.45	0.88	4.74
		SW	7	17.39					
	Medium	DW	7	50.96	0.5235	-0.13	2.45	0.013	4.74
		SW	7	51.00					
	High	DW	7	88.12	3.1205	0.56	2.45	0.46	4.74
		SW	7	87.47					
H₂O₂ high range PhotoMetrixPRO	Low	DW	7	17.22	0.5802	0.56	2.45	0.68	4.74
		SW	7	17.09					
	Medium	DW	7	50.39	0.5235	-1.17	2.45	0.82	4.74
		SW	7	50.85					
	High	DW	7	88.04	0.3387	-2.73	2.45	0.28	4.74
		SW	7	88.89					

n: replicates performed
 DW: distilled water
 SW: simulated wastewater



CHAPTER 5

*“Nothing is absolute. Everything changes, everything moves, everything revolves,
everything flies and goes away.”*

Frida Kahlo



CONCLUSIONS AND FUTURE PERSPECTIVES

Some relevant aspects could be observed throughout the execution of the different studies that make up the present thesis.

Firstly, it can be considered that, solar photo-Fenton processes for the degradation of pharmaceutical products under circumneutral pH conditions is possible with a previous optimization of variables.

The study with steel scrap as source of iron (ZVI) reported level of catalyst leaching less than the maximum concentration for Brazilian legislation. However, some negative effects, such as increased salinity due to acidic pH required to perform the treatment was observed.

The homogeneous/heterogeneous alginate system has great advantages for catalyst dosage, allowing more than 3 times the use of Fe^{3+} -alginate beads. The disadvantages of this process are the possible adsorption/desorption that take place in the different reuse cycles and the partial depolymerization of alginate with H_2O_2 , which leads to an increase in the organic load of the matrix.

On the other hand, Fe^{3+} complexed with EDDS is a suitable alternative for the degradation of pharmaceuticals in homogeneous systems, achieving high degradation rates in short periods of time and being efficient in matrices with a higher organic load such as SW and RHW. Furthermore, EDDS is biodegradable and has high stability. Therefore, based on pharmaceutical and TPs mitigation efficiency, the Fe^{3+} -EDDS was the best reported treatment and the scale-up of this was carried out in the homemade *raceway ponds* reactor.

The scale up of the process presented percentage of degradation similar to those reported in the batch reactor. Additionally, it was confirmed that Fe^{3+} -EDDS (1:2) ratio favors the degradation of the TPs and principal component analysis (PCA) was performed to compare the toxicity of the TPs, it allows a consideration of two principal components which characterized 88% of the predicted dates. Most of the TPs did not show mutagenicity or bioaccumulation characteristics.

In relation to all solar processes, the importance of the PhotoMetrix PRO® application is highlighted, as experiments of this category are carried out in open areas where there is no possibility of accessing the UV-vis spectrophotometer. This application provides the option of monitoring Fe and H₂O₂ *in situ*. It also offers the opportunity to optimize the app for other colorimetric methods such as COD, among others.

Table 3 summarizes some generalities of the AOPs studied in this thesis and mentioned in this chapter.

In general, the most persistent pharmaceuticals were diazepam, fluoxetine, and progesterone. These pharmaceuticals do not have spontaneous reactions through an electron transfer mechanism with ROS due to the presence of strong electron-withdrawing groups in the structures.

The TPs identified in this thesis were assigned, as aforementioned, using a purpose built-database for the first time. On the basis of the TPs identified, it was observed that generally the breakdown of pharmaceuticals involved hydroxylation of the aromatic ring by an electrophilic attack from ROS, cleavage of C-O, C-N bonds, H-abstraction and free radical reactions of pharmaceuticals.

Mechanisms in the degradation of pharmaceuticals can be elucidated as follows: (i) free radical addition to the neutral pharmaceutical molecule (ii) free radical abstract one H atom from the neutral molecule (iii) hydroxylation through interaction of HO• with HO⁻, O₂ or H₂O (iv) ring-opening reactions that generate less aromatic TPs.

With respect to TPs and (Q)SAR tools, in addition to having low biodegradability, most of the structures generated in all processes represent high to medium toxicity for different trophic levels in ecosystems and for human health. The data obtained are only predictions since the effect of each TP on the environment depends on various factors, such as concentration, reactivity, matrix characteristics, etc. (Q)SAR predictions are indicators of the possible impact of each TP and, as such more research is needed in this area to expand the domain and applicability of these tools.

Table 3. Comparison of the processes studied for the degradation of some pharmaceuticals in RHW.

		Solar photo-Fenton		
Reactor				
Process		Fe-Alginate	Fe-EDDS (1:2)	ZVI
pH		5.0	7.0	3.0
Pharmaceuticals		8	8	6
Persistent Pharmaceuticals		PPN/NMD/FXT /DZP/PRG	PCT/PPN/DZP /PRG	PPN/FXT/DZP /PRG
TPs identified	Total	19	16	23
	High toxicity*	16	9	9
	Persistent	18	13	14
[H ₂ O ₂]	Final time	< LOQ	< LOQ	< LOQ
Treatment cost for 1 L of effluent**	Real R\$	0.0015	0.013	0.006
	Dollar US\$	0.0003	0.002	0.001
Observation		Alginate degradation by H ₂ O ₂ , which causes a higher organic load in the solution	Higher organic load in the solution due to EDDS	Due to the acidic pH, large amounts of iron are released into the solution

*High toxicity according to TOXTREE software - Cramer rules.

**Process cost per 1L of treated wastewater. The reagent values in "Real"(R\$ - official coin of Brazil) were taken from industrial prices <https://www.alibaba.com/>(Iron(II) sulfate hydrate: 1Kg R\$ 1.17; Hydrogen peroxide solution: 500 mL R\$ 2.29; Ethylenediamine-N,N'-disuccinic acid trisodium salt solution: 1 KgR\$ 18.68, and Sodium alginate: 1 Kg R\$ 5.59)

Source: Author.

The results of the solar process described in this thesis encourage further research in the area of AOPs as more sustainable processes. Operating conditions need to be optimized, low concentrations of reagents explored, charge recombinations suppressed and the quantum yield increased with more efficient catalytic systems. Similarly, major attention in the future should be dedicated to the identification of reaction mechanisms of TPs and criteria for cost effectiveness.

A further question to consider is whether the application of the chelate-assisted solar photo-Fenton process really addresses the problem of the cost of acidification and the basification of hospital effluents, considering the cost of some of these chelates compared to the cost of acids and bases used in neutralization. Cheaper and more accessible chelates could be investigated, for example, humic-like substances.

The coupling of AOPs to biological treatments at a pre-treatment or post-treatment stage should be considered as potential ways to improve biodegradability and reduce the toxicity of treated wastewater.

Studies are currently underway to investigate the potential use of enzymes (manganese peroxidase - EC 1.11.1.13) in pharmaceutical degradation with a focus on anti-cancer drugs (imatinib mesylate), these studies were started in January 2020 in collaboration with the University of Manitoba (Canada), through a six-month scholarship from the Canadian Government, and will be completed in Brazil at the UFRGS facilities, in the near future. This research aims to elucidate the mechanisms of enzyme-pharmaceutical degradation, transformation products, immobilization of enzymes, and toxicity studies. Additionally, this study hopes to assess whether there is a possibility of coupling AOPs and enzymatic degradation, in addition to investigating the best coupling strategy between both these systems.

Observance of current international and Brazilian legislation has shown that there is a lack of legislation for emerging pollutants. Be that as it may, Brazil may set maximum levels for hospital wastewater for some important pharmaceuticals (e.g. antibiotics) in the future. Therefore, the relationship between validated, sensitive, and rapid analytical methods together with analyses of toxicity, bacterial resistance, and transformation products are essential for providing solid evidence in order for this legislation to be established.

It is of crucial importance to promote activities or programs in which members of different sectors of society interact with professionals in scientific research and their efforts to reduce contamination of emerging pollutants. We cannot try to control a problem without intervening in its true cause, and it is here that science education and, scientific communication directed toward the population can make a difference in mitigating climate change and water pollution.

Forthcoming initiatives should include the promotion of youth participation and education in environmental science and decision-making as a means to help young people contribute to solving environmental problems in the future. This doctoral thesis has focused on treating an environmental problem based on scientific knowledge, but future research should include social and economic components, in order to improve scientific literacy in society.

5.1 Final disposal of wastes

All residues generated from the development of this work were separated, stored, identified in appropriate bottles, and taken to the UFRGS Chemical Waste Management and Treatment Center (CGTRQ), where specialized outsourced companies were allocated for their final destinate.

List of works developed during the PhD

1. LUMBAQUE, ELISABETH C; CARDOSO, RENATA M; SÁNCHEZ JOSÉ A; MALATO, SIXTO; SIRTORI, CARLA. Oxidation of the pharmaceutical mixture in real hospital wastewater by solar photo-Fenton with Fe (III): EDDS at neutral pH using a home-made Raceway Ponds Reactor: their transformation products and toxicity assessment (Manuscript in construction).
2. LUMBAQUE, ELISABETH C.; LÜDTKE DIOGO.; DIONYSIOU, DIONYSIOS.; SIRTORI, CARLA; VILAR, V. New Equipment to Boost Sulfate Radical Advanced Oxidation Processes (Manuscript submitted in the Chemical Engineering Journal).
3. LUMBAQUE, ELISABETH C; SCHWEIGERT, CALITA; DOS SANTOS, LEONARDO; LAVAYEN, VLADIMIR; DOS SANTOS, JOÃO H Z; SIRTORI, CARLA. Degradation of pharmaceuticals in wastewater matrices through solar light-driven photocatalyst prepared from petrochemical waste (Manuscript submitted in the Environmental Science and Pollution Research).
4. LUMBAQUE, ELISABETH C.; WILDE, MARCELO LUÍS; LOPEZ, F. A; DUARTE, E. S. A.; BARRETO-RODRIGUES, MÁRCIO; TIBURTIUS E; SIRTORI, C. Degradation of a mixture of pharmaceuticals in hospital wastewater by a zero-valent scrap iron (ZVSI) combined reduction-oxidation process. JOURNAL OF WATER PROCESS ENGINEERING, v. 37, p. 101410, 2020.
<https://doi.org/10.1016/j.jwpe.2020.101410>
5. LUMBAQUE, ELISABETH C.; SIRTORI, CARLA; VILAR, V. Heterogeneous photocatalytic degradation of pharmaceuticals in synthetic and real matrices using a tube-in-tube membrane reactor with radial addition of H₂O₂. SCIENCE OF THE TOTAL ENVIRONMENT, v. 743, p. 140629, 2020.
<https://doi.org/10.1016/j.scitotenv.2020.140629>
6. CUERVO LUMBAQUE, ELISABETH; SALMORIA ARAÚJO, DÉBORA; MOREIRA KLEIN, THÁGOR; LOPES TIBURTIUS, ELAINE R; ARGÜELLO, JACQUELINE; SIRTORI, CARLA. Solar photo-Fenton-like process at neutral pH:

Fe(III)-EDDS complex formation and optimization of experimental conditions for degradation of pharmaceuticals. CATALYSIS TODAY, v. 328, p. 259-266, 2019.

<https://doi.org/10.1016/j.cattod.2019.01.006>

7. CUERVO LUMBAQUE, ELISABETH; WIELENS BECKER, RAQUEL; SALMORIA ARAÚJO, DÉBORA; DALLEGRAVE, ALEXSANDRO; OST FRACARI, TIAGO; LAVAYEN, VLADIMIR; SIRTORI, CARLA. Degradation of pharmaceuticals in different water matrices by a solar homo/heterogeneous photo-Fenton process over modified alginate spheres. Environmental Science and Pollution Research, v. 26, p. 6532-6544, 2019.

<https://doi.org/10.1007/s11356-018-04092-z>

8. LUMBAQUE, ELISABETH C.; DA SILVA, BRUNA A.; BÖCK, FERNANDA C; HELFER, GILSON A.; FERRÃO, MARCO F.; SIRTORI, CARLA. Total dissolved iron and hydrogen peroxide determination using the PhotoMetrixPRO application: a portable colorimetric analysis tool for controlling important conditions in the solar photo-Fenton process. JOURNAL OF HAZARDOUS MATERIALS, v. 378, p. 120740, 2019.

<https://doi.org/10.1016/j.jhazmat.2019.06.017>

9. CUERVO LUMBAQUE, ELISABETH; LOPES TIBURTIUS, ELAINE R.; BARRETO-RODRIGUES, MÁRCIO; SIRTORI, CARLA. Current trends in the use of zero-valent iron (Fe^0) for degradation of pharmaceuticals present in different water matrices. Trends in Environmental Analytical Chemistry, v. 24, p. e00069, 2019.

<https://doi.org/10.1016/j.teac.2019.e00069>

10. LUMBAQUE, E. CUERVO; CARDOSO, R.M.; DALLEGRAVE, A.; DOS SANTOS, L.O.; IBÁÑEZ, M.; HERNÁNDEZ, F.; SIRTORI, C. Pharmaceutical removal from different water matrixes by Fenton process at near-neutral pH: Doehlert design and transformation products identification by UHPLC-QTOF MS using a purpose-built database. JOURNAL OF ENVIRONMENTAL CHEMICAL ENGINEERING, v. 6, p. 3951-3961, 2018.

<https://doi.org/10.1016/j.jece.2018.05.051>

Oral presentations in conferences

1. LUMBAQUE, E. CUERVO; LOPEZ, F. A.; DUARTE, E. S. A.; RODRIGUES, M. B.; TIBURTIUS, ELAINE REGINA LOPES; SIRTORI, C. Effect of solar photo-advanced Fenton on degradation of pharmaceuticals in real hospital wastewater. 2019.
2. LUMBAQUE, ELISABETH C.; SIRTORI, C.; TIBURTIUS E. Proposed reaction pathways for pharmaceuticals degradation by solar photo-advanced Fenton process. 2019.
3. KOSERA, V. S.; LUMBAQUE, ELISABETH C.; DALLEGRAVE, A; Felipe M; PAULA, V. C.; MARTINS DE FREITAS A; SIRTORI, C.; TIBURTIUS E. Degradação fotocatalítica do Triclosan *via* TiO₂/UV: Identificação dos produtos de transformação e ecotoxicidade. 2019.
4. LUMBAQUE, ELISABETH C.; SIRTORI, C.; TIBURTIUS E. Use of EDDS in solar photo-Fenton-like process to improve the efficiency of pharmaceutical degradation in real hospital wastewater at neutral pH. 2019.
5. LUMBAQUE, ELISABETH C.; SCHWEIGERT, C. E.; SANTOS, L. O.; LAVAYEN, V.; RODEMBUSCHI, F. S.; SANTOS, J. H.; SIRTORI, C. Degradation of pharmaceuticals through solar light-driven heterogeneous photocatalysis from petrochemical waste. 2019.
6. LUMBAQUE, E. C.; MARTINS, R.; DALLEGRAVE, A; FRACARI, T.; LAVAYEN, V.; SIRTORI, C. Pharmaceuticals Degradation using Solar Heterogeneous Photo-Fenton Process over Modified Alginate Spheres: Preliminary Evaluation. 2017.
7. LUMBAQUE, E. C.; SANTOS, L. O.; MARTINS, R.; DELLGRAVE, A.; SIRTORI, C. Pharmaceutical Removal from Hospital Wastewater by Homogeneous Fenton Process at Near Neutral pH. 2017.

8. LUMBAQUE, E. C.; SILVA, B. A.; SANTOS, L. O.; HELFER, G.; FERRAO, M.; SIRTORI, C. Total iron and hydrogen peroxide determination during AOPs using Photo-Metrix application: a mobile colorimetric analysis tool. 2017.

REFERENCES

1. Frédéric, O.; Yves, P. ;*Chemosphere* **2014**, *115*, 31.
2. Rahim Pouran, S.; Abdul Aziz, A. R.; Wan Daud, W. M. A. ;*J. Ind. Eng. Chem.* **2015**, *21*, 53.
3. Rivera-Utrilla, J.; Sánchez-Polo, M.; Ferro-García, M. Á.; Prados-Joya, G.; Ocampo-Pérez, R. ;*Chemosphere* **2013**, *93*, 1268.
4. Verlicchi, P.; Al Aukidy, M.; Galletti, A.; Petrovic, M.; Barceló, D. ;*Sci. Total Environ.* **2012**, *430*, 109.
5. Santos, L. H. M. L. M.; Gros, M.; Rodriguez-Mozaz, S.; Delerue-Matos, C.; Pena, A.; Barceló, D.; Montenegro, M. C. B. S. M. ;*Sci. Total Environ.* **2013**, *461–462*, 302.
6. von der Ohe, P. C.; Dulio, V.; Slobodnik, J.; De Deckere, E.; Kühne, R.; Ebert, R.-U.; Ginebreda, A.; De Cooman, W.; Schüürmann, G.; Brack, W. ;*Sci. Total Environ.* **2011**, *409*, 2064.
7. Barceló, D. ;*TrAC Trends Anal. Chem.* **2003**, *22*.
8. Carraro, E.; Bonetta, S.; Bertino, C.; Lorenzi, E.; Bonetta, S.; Gilli, G. ;*J. Environ. Manage.* **2016**, *168*, 185.
9. Marković, M.; Jović, M.; Stanković, D.; Kovačević, V.; Roglić, G.; Gojgić-Cvijović, G.; Manojlović, D. ;*Sci. Total Environ.* **2015**, *505*, 1148.
10. Mendoza, A.; Aceña, J.; Pérez, S.; López de Alda, M.; Barceló, D.; Gil, A.; Valcárcel, Y. ;*Environ. Res.* **2015**, *140*, 225.
11. Llorca, M.; Lucas, D.; Ferrando-Climent, L.; Badia-Fabregat, M.; Cruz-Morató, C.; Barceló, D.; Rodríguez-Mozaz, S. ;*J. Chromatogr. A* **2016**, *1439*, 124.
12. Dulio, V.; van Bavel, B.; Brorström-Lundén, E.; Harmsen, J.; Hollender, J.; Schlabach, M.; Slobodnik, J.; Thomas, K.; Koschorreck, J. ;*Environ. Sci. Eur.* **2018**, *30*, 1.
13. Bello, M. M.; Raman, A. A. A.; Asghar, A. ;*Process Saf. Environ. Prot.* **2019**, *126*, 119.
14. OECD Emerging policy instruments for the control of pharmaceuticals in water <https://www.oecd-ilibrary.org/sites/4781cb74-en/index.html?itemId=/content/component/4781cb74-en> (accessed Jul 9, 2020).
15. National Environment Council-CONAMA *Resolution N° 357, March 17, 2005*; Brazil (document in Portuguese).

16. Ministry of the Environment *Resolution No 430, May 13, 2011*; Brazil (document in Portuguese), 2011.
17. National Environment Council-CONAMA *Resolution N° 396*; Brazil (document in Portuguese).
18. Cunha, D. L. da; Silva, S. M. C. da; Bila, D. M.; Oliveira, J. L. da M.; Sarcinelli, P. de N.; Larentis, A. L. ;*Cad. Saude Publica* **2016**, *32*, e00056715.
19. Presidency of the republic of Brazil *Ordinance N° 5.472*; Brazil (document in Portuguese), 2005.
20. Ministry of health *Ordinance no. 2,914 December 12, 2011*; Brazil (document in Portuguese).
21. Ministry of Regional Development; National Secretariat of Sanitation *Diagnosis of Water and Sewage Services - 2017*; Brazil (document in Portuguese), 2017.
22. Wang, J.; Wang, S. ;*J. Environ. Manage.* **2016**, *182*, 620.
23. Bokare, A. D.; Choi, W. ;*J. Hazard. Mater.* **2014**, *275*, 121.
24. Kanakaraju, D.; Glass, B. D.; Oelgemöller, M. ;*J. Environ. Manage.* **2018**, *219*, 189.
25. Babuponnusami, A.; Muthukumar, K. ;*J. Environ. Chem. Eng.* **2014**, *2*, 557.
26. Miralles-Cuevas, S.; Oller, I.; Pérez, J. A. S.; Malato, S. ;*Water Res.* **2014**, *64*, 23.
27. Benitez, F. J.; Acero, J. L.; Real, F. J.; Roldan, G.; Rodriguez, E. ;*Water Res.* **2013**, *47*, 870.
28. Paredes, L.; Omil, F.; Lema, J. M.; Carballa, M. ;*J. Hazard. Mater.* **2018**, *342*, 670.
29. Starling, M. C. V. M.; Souza, P. P.; Le Person, A.; Amorim, C. C.; Criquet, J. ;*Chem. Eng. J.* **2019**, *376*, 120856.
30. Gallard, H.; de Laat, J.; Legube, B. ;*New J. Chem.* **1998**, *22*, 263.
31. He, J.; Yang, X.; Men, B.; Wang, D. ;*J. Environ. Sci.* **2016**, *39*, 97.
32. Mirzaei, A.; Chen, Z.; Haghghat, F.; Yerushalmi, L. ;*Chemosphere* **2017**, *174*, 665.
33. Heider, M. *Mineartigo*. 2017, pp. 9–11.
34. Rodríguez, R.; Espada, J. J.; Pariente, M. I.; Melero, J. A.; Martínez, F.; Molina, R. ;*J. Clean. Prod.* **2016**, *124*, 21.
35. Vermilyea, A. W.; Voelker, B. M. ;*Environ. Sci. Technol.* **2009**, *43*, 6927.
36. Papoutsakis, S.; Brites-gaNóbregas, F. F.; Pulgarin, C.; Malato, S. ;*J. Photochem. Photobiol. A Chem.* **2015**, *303–304*, 1.
37. Giannakis, S.; Gamarra Vives, F. A.; Grandjean, D.; Magnet, A.; De Alencastro,

- L. F.; Pulgarin, C. ;*Water Res.* **2015**, *84*, 295.
38. Malato, S.; Fernández-Ibáñez, P.; Maldonado, M. I.; Blanco, J.; Gernjak, W. ;*Catal. Today* **2009**, *147*, 1.
39. Bansal, P.; Verma, A.; Talwar, S. ;*Chem. Eng. J.* **2018**.
40. Jack, R. S.; Ayoko, G. A.; Adebajo, M. O.; Frost, R. L. ;*Environ. Sci. Pollut. Res.* **2015**, *22*, 7439.
41. Catastini, C.; Sarakha, M.; Mailhot, G.; Bolte, M. ;*Sci. Total Environ.* **2002**, *298*, 219.
42. Li, J.; Mailhot, G.; Wu, F.; Deng, N. ;*J. Photochem. Photobiol. A Chem.* **2010**, *212*, 1.
43. Huang, W.; Brigante, M.; Wu, F.; Hanna, K.; Mailhot, G. ;*J. Photochem. Photobiol. A Chem.* **2012**, *239*, 17.
44. Klammerth, N.; Malato, S.; Agüera, A.; Fernández-Alba, A.; Mailhot, G. ;*Environ. Sci. Technol.* **2012**, *46*, 2885.
45. Kowalczyk, M.; Hubicki, Z.; Kołodyńska, D. ;*Chem. Eng. J.* **2013**, *221*, 512.
46. Soriano-Molina, P.; García Sánchez, J. L.; Alfano, O. M.; Conte, L. O.; Malato, S.; Sánchez Pérez, J. A. ;*Appl. Catal. B Environ.* **2018**, *233*, 234.
47. Zhang, R.; Yang, Y.; Huang, C.-H.; Zhao, L.; Sun, P. ;*Water Res.* **2016**, *103*, 283.
48. Kirchhoff, V.; Echer, E.; Leme, N. P.; Silva, A. A. ;*Rev. Bras. Geofísica* **2000**, *18*, 63.
49. Kerr, J. B.; Fioletov, V. E. ;*Atmosphere-ocean* **2008**, *46*, 159.
50. Zhou, T.; Zou, X.; Wu, X.; Mao, J.; Wang, J. ;*Ultrason. Sonochem.* **2017**.
51. Du, J.; Guo, W.; Che, D.; Ren, N. ;*Chem. Eng. J.* **2018**, *351*, 532.
52. Luna, A. J.; Chiavone-Filho, O.; Machulek, A.; de Moraes, J. E. F.; Nascimento, C. A. O. ;*J. Environ. Manage.* **2012**, *111*, 10.
53. Zhang, Y.; Zhou, M. ;*J. Hazard. Mater.* **2019**, *362*, 436.
54. Nichela, D. A.; Donadelli, J. A.; Caram, B. F.; Haddou, M.; Nieto, F. J. R.; Oliveros, E.; Einschlag, F. S. G. ;*Appl. Catal. B Environ.* **2015**, *170*, 312.
55. Zhang, Y.; Zhou, M. ;*J. Hazard. Mater.* **2019**, *362*, 436.
56. Allabaksh, M. B.; Mandal, B. K.; Kesarla, M. K.; Kumar, K. S.; Reddy, P. S. ;*J. Chem. Pharm. Res.* **2010**, *2*, 67.
57. Ahile, U. J.; Wuana, R. A.; Itodo, A. U.; Sha'Ato, R.; Dantas, R. F. ;*Sci. Total Environ.* **2020**, *710*, 134872.
58. Clarizia, L.; Russo, D.; Di Somma, I.; Marotta, R.; Andreozzi, R. ;*Appl. Catal. B*

- Environ.* **2017**, *209*, 358.
59. Soriano-Molina, P.; Plaza-Bolaños, P.; Lorenzo, A.; Agüera, A.; Sánchez, J. L. G.; Malato, S.; Pérez, J. A. S. ;*Chem. Eng. J.* **2019**, *366*, 141.
 60. Soriano-Molina, P.; García Sánchez, J. L.; Malato, S.; Pérez-Estrada, L. A.; Sánchez Pérez, J. A. ;*Chem. Eng. J.* **2018**, *331*, 84.
 61. Lado Ribeiro, A. R.; Moreira, N. F. F.; Li Puma, G.; Silva, A. M. T. ;*Chem. Eng. J.* **2019**, *363*, 155.
 62. Sbardella, L.; Velo-Gala, I.; Comas, J.; Layret, I.; Rodríguez-Roda, A.; Gernjak, W. ;*J. Hazard. Mater.* **2019**, *380*, 120869.
 63. Yang, Y.; Pignatello, J. J.; Ma, J.; Mitch, W. A. ;*Water Res.* **2016**, *89*, 192.
 64. Devi, L. G.; Munikrishnappa, C.; Nagaraj, B.; Rajashekhar, K. E. ;*J. Mol. Catal. A Chem.* **2013**, *374*, 125.
 65. Shah, N. S.; He, X.; Khan, H. M.; Khan, J. A.; O’Shea, K. E.; Boccelli, D. L.; Dionysiou, D. D. ;*J. Hazard. Mater.* **2013**, *263*, 584.
 66. Ostra, M.; Ubide, C.; Zuriarrain, J. ;*Anal. Chim. Acta* **2007**, *584*, 228.
 67. Gago-Ferrero, P.; Schymanski, E. .; Hollender, J.; Thomaidis, N. . In *Applications of Time-of-Flight and Orbitrap Mass Spectrometry in Environmental, Food, Doping, and Forensic Analysis*; Comprehensive Analytical Chemistry, 2016; pp. 381–403.
 68. López, S. H.; Ulaszewska, M. M.; Hernando, M. D.; Bueno, M. J. M.; Gómez, M. J.; Fernández-Alba, A. R. ;*Environ. Sci. Pollut. Res.* **2014**, *21*, 12583.
 69. Agüera, A.; Bueno, M. J. M.; Fernández-Alba, A. R. ;*Environ. Sci. Pollut. Res.* **2013**, *20*, 3496.
 70. del Mar Gómez-Ramos, M.; Pérez-Parada, A.; García-Reyes, J. F.; Fernández-Alba, A. R.; Agüera, A. ;*J. Chromatogr. A* **2011**, *1218*, 8002.
 71. Sirtori, C.; Becker, R. *Using LC-HRMS to identify Transformation Products: conventional strategy vs. Expanded Databases, When and How to use them?*; Brazil , 2019.
 72. Idakwo, G.; Luttrell IV, J.; Chen, M.; Hong, H.; Gong, P.; Zhang, C. In *Advances in Computational Toxicology*; Springer, 2019; pp. 119–139.
 73. Chen, B.; Zhang, T.; Bond, T.; Gan, Y. ;*J. Hazard. Mater.* **2015**, *299*, 260.
 74. Jagwani, D.; Bhawsar, J. ;*J. Chem. Pharm. Res.* **2015**, *7*, 137.
 75. Becker, R. W.; Ibáñez, M.; Lumbaqué, E. C.; Wilde, M. L.; da Rosa, T. F.; Hernández, F.; Sirtori, C. ;*Sci. Total Environ.* **2019**, 134218.

76. Montagner, C. C.; Sodr , F. F.; Acayaba, R. D.; Vidal, C.; Campestrini, I.; Locatelli, M. A.; Pescara, I. C.; Albuquerque, A. F.; Umbuzeiro, G. A.; Jardim, W. F. ;*J. Braz. Chem. Soc.* **2019**, *30*, 614.
77. Benigni, R.; Bossa, C. ;*Mutagenesis* **2019**, *34*, 17.
78. Worth, A.; Lapenna, S.; Lo Piparo, E.; Mostrag-Szlichtyng, A.; Serafimova, R. ;*JRC Sci. Tech. reports. EC Jt. Res. Cent. Inst. Heal. Consum. Prot. Ispra* **2010**, 18.
79. EPA ;*Quant. Risk Assess. Calc.* **2012**, *13*, 1.
80. Martin, T. ;*Washingt. US-EPA* **2016**.
81. Mayo-Bean, K.; Moran-Bruce, K.; Nabholz, J. V; Meylan, W. M.; Howard, P. H.; Cassidy, L. ;*Risk Assess. Div. US EPA* **2012**.
82. OECD *Guidelines for Testing of Chemicals, Simulation Test-Aerobic Sewage Treatment 303^a*; 1999.
83. Contreras, S.; Rodr guez, M.; Momani, F. A.; Sans, C.; Esplugas, S. ;*Water Res.* **2003**, *37*, 3164.
84. Cruz-Morat , C.; Lucas, D.; Llorca, M.; Rodriguez-Mozaz, S.; Gorga, M.; Petrovic, M.; Barcel , D.; Vicent, T.; Sarr , M.; Marco-Urrea, E. ;*Sci. Total Environ.* **2014**, *493*, 365.
85. Segura, Y.; Mart nez, F.; Melero, J. A. ;*Appl. Catal. B Environ.* **2013**, *136–137*, 64.
86. Association, A. P. H.; Association, A. W. W.; Federation, W. P. C.; Federation, W. E. *Standard methods for the examination of water and wastewater*; American Public Health Association., 2012; Vol. 22.
87. Casierra-Martinez, H. A.; Madera-Parra, C. A.; Vargas-Ram rez, X. M.; Caselles-Osorio, A.; Torres-L pez, W. A. ;*Ecol. Eng.* **2020**, 105699.
88. Lancheros, J. C.; Madera-Parra, C. A.; Caselles-Osorio, A.; Torres-L pez, W. A.; Vargas-Ram rez, X. M. ;*Ecol. Eng.* **2019**, *135*, 89.
89. P rez-Estrada, L. A.; Malato, S.; Ag era, A.; Fern ndez-Alba, A. R. ;*Catal. Today* **2007**, *129*, 207.
90. Malato, S.; Blanco, J.; C ceres, J.; Fern ndez-Alba, A. R.; Ag era, A.; Rodr guez, A. ;*Catal. Today* **2002**, *76*, 209.
91. Malato, S.; Blanco, J.; Vidal, A.; Alarc n, D.; Maldonado, M. I.; C ceres, J.; Gernjak, W. ;*Sol. Energy* **2003**, *75*, 329.
92. Nogueira, R.; Oliveira, M.; Paterlini, W. ;*Talanta* **2005**, *66*, 86.

93. ISO 6332 *Water quality - Determination of iron - Spectrometric method using 1,10-phenanthroline*; 1988.
94. Atkins, R. C. ;*J. Chem. Educ.* **1975**, *52*, 550.
95. Chan, K. H.; Chu, W. ;*Chemosphere* **2003**, *51*, 305.
96. Hernández, F.; Ibáñez, M.; Bade, R.; Bijlsma, L.; Sancho, J. V. ;*TrAC Trends Anal. Chem.* **2014**, *63*, 140.
97. Diaz, R.; Ibáñez, M.; Sancho, J. V.; Hernández, F. ;*J. Chromatogr. A* **2013**, *1276*, 47.
98. Patlewicz, G.; Jeliaskova, N.; Safford, R. J.; Worth, A. P.; Aleksiev, B. ;*SAR QSAR Environ. Res.* **2008**, *19*, 495.
99. US EPA EPI Suite™-Estimation Program Interface <https://www.epa.gov/tsca-screening-tools/epi-suitetm-estimation-program-interface> (accessed Nov 3, 2019).
100. US EPA Ecological Structure Activity Relationships (ECOSAR) <https://www.epa.gov/tsca-screening-tools/ecological-structure-activity-relationships-ecosar-predictive-model> (accessed Oct 3, 2019).
101. Ortiz, I.; Rivero, M. J.; Margallo, M. Galanakis, C. M.; Agrafioti, E. B. T.-S. W. and W. P., Eds.; Elsevier, 2019; pp. 161–201.
102. Hamd, W. S.; Dutta, J. In *Micro and Nano Technologies*; Bonelli, B.; Freyria, F. S.; Rossetti, I.; Sethi, R. B. T.-N. for the D. and R. of W. P., Eds.; Elsevier, 2020; pp. 303–330.
103. Stefaniuk, M.; Oleszczuk, P.; Ok, Y. S. ;*Chem. Eng. J.* **2016**, *287*, 618.
104. Lumbaqué, E. C.; Wilde, M. L.; Lopes, F. A.; Duarte, E. de S. A.; Tiburtius, E. R. L.; Rodrigues, M. B.; Sirtori, C. ;*J. Water Process Eng.* **2020**, *37*, 101410.
105. Cuervo Lumbaqué, E.; Lopes Tiburtius, E. R.; Barreto-Rodrigues, M.; Sirtori, C. ;*Trends Environ. Anal. Chem.* **2019**, *24*, e00069.
106. Zhang, M.; Dong, H.; Zhao, L.; Wang, D.; Meng, D. ;*Sci. Total Environ.* **2019**, *670*, 110.
107. Kakavandi, B.; Takdastan, A.; Pourfadakari, S.; Ahmadmoazzam, M.; Jorfi, S. ;*J. Taiwan Inst. Chem. Eng.* **2018**.
108. Du, J.; Guo, W.; Li, X.; Li, Q.; Wang, B.; Huang, Y.; Ren, N. ;*J. Taiwan Inst. Chem. Eng.* **2017**, *81*, 232.
109. Quadrado, R. F. N.; Fajardo, A. R. **2017**.
110. Liu, T.; You, H.; Chen, Q. ;*J. Hazard. Mater.* **2009**, *162*, 860.
111. Cuervo Lumbaqué, E.; Wielens Becker, R.; Salmoria Araújo, D.; Dallegrove, A.;

- Ost Fracari, T.; Lavayen, V.; Sirtori, C. ;*Environ. Sci. Pollut. Res.* **2019**.
112. Cuervo Lumbaque, E.; Salmoria Araújo, D.; Moreira Klein, T.; Lopes Tiburtius, E. R.; Argüello, J.; Sirtori, C. ;*Catal. Today* **2019**.
113. Robert, D.; Malato, S. ;*Sci. Total Environ.* **2002**, 291, 85.
114. Miralles-Cuevas, S.; Oller, I.; Ruíz-Delgado, A.; Cabrera-Reina, A.; Cornejo-Ponce, L.; Malato, S. ;*J. Hazard. Mater.* **2018**, 1.
115. Böck, F. C.; Helfer, G. A.; da Costa, A. Ben; Dessuy, M. B.; Ferrão, M. F. ;*J. Chemom.* **2020**, e3251.
116. Lumbaque, E. C.; da Silva, B. A.; Böck, F. C.; Helfer, G. A.; Ferrão, M. F.; Sirtori, C. ;*J. Hazard. Mater.* **2019**, 378, 120740.

ANNEXES

Annex 1. Psychochemical characterization of RHW. W.

Parameter	2017											Method	LOD	LOQ
	Feb	Mar	Apr	May	Jun	Jul	Aug	Sep	Oct	Nov	Dec			
pH	8.02	7.52	7.8	8.06	7.98	8.21	8.86	8.51	8.98	8.47	8.53	*SMEWW 4500-H+ B	--	--
Conductivity ($\mu\text{S cm}^{-1}$)	944	326	956	539.3	471	781	1209	427	722	611	114	SMEWW 2510 B	1	0.2
COD ($\text{mg O}_2 \text{ L}^{-1}$)	203	211	473	277	273	706	571	350	217	209	365	SMEWW 5220 B	5	0.8
BOD ($\text{mg O}_2 \text{ L}^{-1}$)	132	45	236	108	83	319	103	117	69	70	82	SMEWW 5210 B	2	0.6
BOD/COD	0.65	0.21	0.50	0.39	0.30	0.45	0.18	0.33	0.32	0.33	0.22	≥ 0.5 biodegradable	--	--
TOC (mg L^{-1})	65	63.1	70.2	93.2	41.34	82.74	64.88	50.56	67.56	49.29	64.06	SMEWW 5310	1.68	3.99
Chloride (mg L^{-1})	72.9	27.9	4.3	37.7	41.6	9	98.8	33.9	49.1	44.5	61.7	SMEWW 4110 B	0.5	0.02
Phosphate (mg L^{-1})	21.36	3.93	22.07	8.56	2.99	0.45	52.37	5.39	9.45	5.9	14.58	SMEWW 4500 P E	0.03	0.006
TSS (mg L^{-1})	128	52	98	63	27	165	60	29	67	76	112	SMEWW 2540 D	10	5
TS (mg L^{-1})	525	222	521	244	225	611	654	218	261	317	177	SMEWW 2540 B	10	5

Parameter	2018							2019					
	Jan	Feb	Apr	Jun	Aug	Oct	Dec	Feb	Apr	Jun	Aug	Oct	Dec
pH	8.23	7.89	8.65	7.72	9.28	9.19	8.74	9.9	8	8	8.1	8.7	8
Conductivity ($\mu\text{S cm}^{-1}$)	812	753	530	1142	1239	697	554	1132	721	608	792	965	838
COD ($\text{mg O}_2 \text{L}^{-1}$)	616	166	863	563	570	332	206	173	143	309	465	195	246
BOD ($\text{mg O}_2 \text{L}^{-1}$)	312	46	670	475	300	143	89	92	57	197	216	49	96
BOD/COD	0.51	0.28	0.78	0.84	0.53	0.43	0.43	0.53	0.40	0.64	0.46	0.25	0.39
TOC (mg L^{-1})	198.7	--	--	882.5	--	--	--	--	--	--	--	--	105.4
DOC (mg L^{-1})	--	68.55	59.68		37.63	--	--	67.6	--	--	--	--	--
Chloride (mg L^{-1})	55.9	65.3	43.4	73.3	64.7	44.2	35.6	69.2	46	26.9	54.5	67.3	50.7
Phosphate (mg L^{-1})	21.85	22.02	7.49	5.55	52.68	23.47	58.67	22.27	18.04	14.27	21.09	20.32	18.5
TSS (mg L^{-1})	117	170	22	166	433	126	97	156	51	125	164	113	81
TS (mg L^{-1})	367	611	187	487	1040	383	265	415	231	396	538	410	313

*Standard Methods for the Examination of Water and Wastewater (SMEWW) - APHA 22nd edition, 2012⁸⁶.

Source: Author.